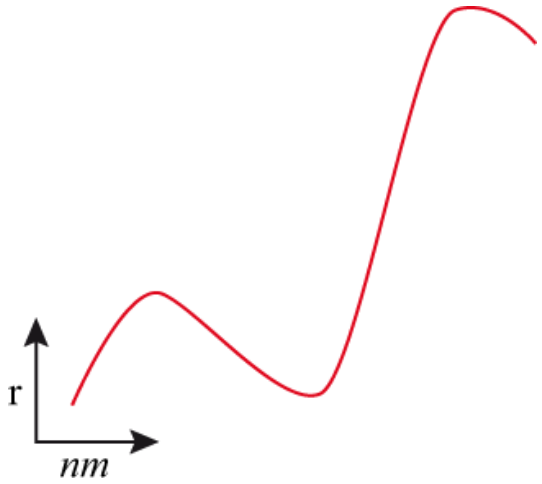

Printing Beyond Color:

Spectral and Specular Reproduction

Sepideh Samadzadegan
Technische Universität Darmstadt

delivered by
EUROGRAPHICS DIGITAL LIBRARY
www.eg.org diglib.eg.org

Printing Beyond Color: Spectral and Specular Reproduction

Vom Fachbereich Informatik
der Technischen Universität Darmstadt
genehmigte

DISSERTATION

zur Erlangung des akademischen Grades eines
Doktor-Ingenieurs (Dr.-Ing.)
von

M.Sc. Sepideh Samadzadegan

geboren in Mashhad, Iran

Referenten der Arbeit:	Prof. Dr. techn. Dieter W. Fellner Technische Universität Darmstadt
	Prof. Dr.-Ing. Edgar Dörsam Technische Universität Darmstadt
	Prof. Jon Yngve Hardeberg Gjøvik University College

Tag der Einreichung:	16.09.2015
Tag der mündlichen Prüfung:	30.11.2015

Darmstadt 2016
D17

Erklärung zur Dissertation

Hiermit versichere ich die vorliegende Dissertation selbständig nur mit den angegebenen Quellen und Hilfsmitteln angefertigt zu haben. Alle Stellen, die aus Quellen entnommen wurden, sind als solche kenntlich gemacht. Diese Arbeit hat in gleicher oder ähnlicher Form noch keiner Prüfungsbehörde vorgelegen.

Darmstadt, den 19.10.2015 Sepideh Samadzadegan

Zusammenfassung

Für eine akkurate drucktechnische Reproduktionen sind insbesondere zwei Eigenschaften von Bedeutung: Farbe und Glanz. Die Reproduktion dieser zwei Wahrnehmungsattribute sind die beiden Fokusthemen in dieser Dissertation: spektrale Reproduktion und Glanzdruck.

Der heute in der Druckindustrie verwendete metamere Workflow passt die Reproduktion an das Original lediglich für eine vordefinierte Lichtart an. In den meisten Fällen ist eine solche Reproduktion ausreichend. Im Bereichen wie der Kunstreproduktion, dem Sicherheitsdruck, in der industriellen Farbkommunikation, muss die Reproduktion mit dem Original unter einer Vielzahl von Lichtarten übereinstimmen (z.B. Tageslicht, Glühlampenlicht oder einer speziellen LED Beleuchtung) – eine Eigenschaft, die die metamere Reproduktion per Definition i.A. nicht leisten kann. Für diese Anwendungen müssen die Reflektionsspektren des Originals durcktechnisch Reproduziert werden. Wegen der Limitierungen existierender Drucksysteme, ist die Reproduktion gegebener Reflexionsspektren i.A. unmöglich. Daher müssen Strategien entwickelt werden, um nicht reproduzierbare in die Menge der reproduzierbaren Reflexionsspektren zu transformieren und um Druckeransteuerungswerte auszuwählen, die diese Reflektionsspektren artefaktfrei zu reproduzieren. In dieser Dissertation wurde hierfür ein Verfahren namens "Spatio-Spectral Gamut Mapping and Separation", SSGMS, vorgestellt, das nahezu artefaktfreie Ergebnisse liefert und die Reproduktion an das Original farbmetrisch für eine vorgegebene Menge an Lichtarten anpasst.

Heutzutage werden nur die farbmetrische Genauigkeit und strukturelle Bildartefakte in der Qualitätskontrolle überprüft. Eigenschaften die sich auf Glanz beziehen, wie zum Beispiel "gloss-differential" (inkonsistente Verteilung des Glanzes über das Bild hinweg, meistens erzeugt durch unregelmäßige Flächendeckung der verwendeten Tinten), werden nicht geprüft, da keine Strategie existiert um diese Fehler zu vermeiden. Zur Vermeidung solcher Glanzartefakte, und um die Glanzeigenschaften lokal anzupassen, werden in dieser Dissertation drei drucktechnische Verfahren vorgestellt.

Für eine perzeptuell akkurate Reproduktion von Farb- und Glanzeigenschaften, ist das Wissen über die Beziehung zwischen messtechnischen Werten und wahrgenommenen Größen Voraussetzung. Im Bereich der Farbe existieren bereits entsprechende Modelle sowie nahezu wahrnehmungsgleichabständige Farbräume, die für die Farbreproduktion erfolgreich eingesetzt werden. Solche Modelle fehlen jedoch für die drucktechnische Glanzreproduktion. Die meisten der existierenden Studien basieren auf Experimenten, die Glanz am Bildschirm simulieren (meistens mit unbunten Farben) und keine realen Objekte verwenden. In dieser Dissertation, wurden drei psychophysische Experimente durchgeführt, um die Beziehung zwischen gemessenen Glanz (objektiven Größen) und wahrgenommenen Glanz (subjektiven Größen) zu untersuchen. Hierfür wurden farbige reale Proben verwendet, die drucktechnisch mit den drei oben erwähnten Verfahren erstellt wurden. Das Ergebnis der Experimente zeigt, dass die Beziehung mit einer Potenzfunktion, gemäß des Stevensschen Potenzgesetzes, beschrieben werden kann.

In einem weiteren Experiment wurde die Beziehung zwischen wahrgenommenen Oberflächenglanz und Höhentextur untersucht. Hierbei wurden, 2,5D Proben mit zwei verschiedenen Texturtypen und unterschiedlichen Glanz- und Texturhöhenstufen verwendet. Das Ergebnis dieses Experiments zeigt, dass verschiedene makroskopische Textur-Typen und Höhenstufen einen leichten Einfluss auf die Glanzempfindung haben. Ein Einfluss des Oberflächenglanzes auf die beobachtete Texturhöhe konnte nicht festgestellt werden, was darauf hindeutet, dass die Texturwahrnehmung nicht von der Stärke des Oberflächenglanzes beeinflusst wird.

Das SSGMS Verfahren zur spektralen Reproduktion, die drei Druckstrategien für den Glanzdruck und die Ergebnisse der psychophysischen Experimente zur Untersuchung der Glanzwahrnehmung, können zur Verbesserung der Gesamtqualität der drucktechnischen Farb- und Glanzreproduktion benutzt werden.

Abstract

For accurate printing (reproduction), two important appearance attributes to consider are color and gloss. These attributes are related to two topics focused on in this dissertation: *spectral reproduction* and *specular (gloss) printing*.

In the conventional printing workflow known as the metameric printing workflow, which we use mostly nowadays, high-quality prints – in terms of colorimetric accuracy – can be achieved only under a predefined illuminant (i.e. an illuminant that the printing pipeline is adjusted to; e.g. daylight). While this printing workflow is useful and sufficient for many everyday purposes, in some special cases, such as artwork (e.g. painting) reproduction, security printing, accurate industrial color communication and so on, in which accurate reproduction of an original image under a variety of illumination conditions (e.g. daylight, tungsten light, museum light, etc.) is required, metameric reproduction may produce satisfactory results only with luck. Therefore, in these cases, another printing workflow, known as spectral printing pipeline must be used, with the ideal aim of illuminant-invariant match between the original image and the reproduction. In this workflow, the reproduction of spectral raw data (i.e. reflectances in the visible wavelength range), rather than reproduction of colorimetric values (colors) alone (under a predefined illuminant) is taken into account. Due to the limitations of printing systems extant, the reproduction of all reflectances is not possible even with multi-channel (multi-colorant) printers. Therefore, practical strategies are required in order to map non-reproducible reflectances into reproducible spectra and to choose appropriate combinations of printer colorants for the reproduction of the mapped reflectances. For this purpose, an approach called *Spatio-Spectral Gamut Mapping and Separation*, SSGMS, was proposed, which results in almost artifact-free spectral reproduction under a set of various illuminants.

The quality control stage is usually the last stage in any printing pipeline. Nowadays, the quality of the printout is usually controlled only in terms of colorimetric accuracy and common printing artifacts. However, some gloss-related artifacts, such as *gloss-differential* (inconsistent gloss appearance across an image, caused mostly by variations in deposited ink area coverage on different spots), are ignored, because no strategy to avoid them exists. In order to avoid such gloss-related artifacts and to control the glossiness of the printout locally, three printing strategies were proposed. In general, for perceptually accurate reproduction of color and gloss appearance attributes, understanding the relationship between measured values and perceived magnitudes of these attributes is essential. There has been much research into reproduction of colors within perceptually meaningful color spaces, but little research from the gloss perspective has been carried out. Most of these studies are based on simulated display-based images (mostly with neutral colors) and do not take real objects into account. In this dissertation, three psychophysical experiments were conducted in order to investigate the relationship between measured gloss values (objective quantities) and perceived gloss magnitudes (subjective quantities) using real colored samples printed by the aforementioned proposed printing strategies. These experiments revealed that the relationship mentioned can be explained by a *Power function* according to *Stevens' Power Law*, considering almost the entire gloss range. Another psychophysical experiment was also conducted in order to investigate the interrelation between perceived surface gloss and texture, using 2.5D samples printed in two different texture types and with various gloss levels and texture elevations. According to the results of this experiment, different macroscopic texture types and levels (in terms of texture elevation) were found to influence the perceived surface gloss level slightly. No noticeable influence of surface gloss on the perceived texture level was observed, indi-

cating texture constancy regardless of the gloss level printed.

The SSGMS approach proposed for the spectral reproduction, the three printing strategies presented for gloss printing, and the results of the psychophysical experiments conducted on gloss printing and appearance can be used to improve the overall print quality in terms of color and gloss reproduction.

Acknowledgements

First of all, I would like to thank everyone who participated in the Colour Printing 7.0: Next Generation Multi-Channel Printing (CP7.0) project through which I carried out my research during the last three years from August 2012 to July 2015. This was an amazing training and research project funded by Marie Curie Initial Training Networks (ITN) CP7.0 N-290154, which is gratefully acknowledged. This project was a collaborative project between full networks and associated partners from academia and industry across five countries in Europe: Norway, Germany, Sweden, France, and the United Kingdom. The project was led by Prof. Jon Yngve Hardeberg (the project leader) with the help of Aditya Sole (the project manager), at the Norwegian Colour and Visual Computing Laboratory at Gjøvik University College in Norway, whom I would like to thank. I would also like to thank all of the senior and junior researchers involved in this project, especially Dr. Maria V. Oritz Segovia at Océ Print Logic Technologies, Créteil, France, who gave me the opportunity of training at Océ in France. My friendly acknowledgements go also to Teun Baar and Jana Blahová with whom I worked closely. I would also like to thank Dr. Hans Brettel, an external researcher from Institut Mines-Télécom Télécom ParisTech, CNRS LTCI Paris, France, who collaborated on one of the papers published. My special thanks go to Dr. Philipp Urban, one of the senior researchers involved in the CP7.0 project and the head of Competence Center 3D Printing Technology, at Fraunhofer Institute for Computer Graphics Research IGD, in Darmstadt, Germany, who supervised me throughout my research and gave me helpful comments for the improvement of research outcomes both in terms of scientific ideas and scientific writing. I would also like to thank the Fraunhofer internal program which supported some part of the research carried out, under Grant No. Attract 008-600075.

I especially acknowledge the Technische Universität Darmstadt in Darmstadt, Germany, and two departments: Institut für Druckmaschinen und Druckverfahren IDD (English: Institute of Printing Science and Technology), where I started my PhD program, and Graphisch-Interaktive Systeme GRIS (English: Interactive Graphics Systems Group) where I accomplished my PhD studies. I would like to thank the heads of these two groups: Prof. Edgar Dörsam and Prof. Dieter W. Fellner who gave me helpful comments in occasional and annual meetings and access to measurement and printing equipment. I would also like to thank Christoph Godau, the head of the Color Research group at IDD, who helped me with some measurements. I acknowledge the ONYX Graphics, Inc - European Office Austria for providing an Academic License for the ProductionHouse RIP program that I used to control the printer.

I would also like to thank everyone in the GRIS community who helped me directly or indirectly to improve my research outcomes, especially Prof. Arjan Kuijper who commented helpfully on my dissertation, and Dr. Tatiana von Landesberger, the head of Junior Research Groups at GRIS, who gave me useful guidance on what needs to be included in a dissertation.

And finally, I would like to thank my family, especially my mother, who supported me all the way through, with best wishes and kindness. I dedicate my dissertation to my mother **Jaleh**, with much love ♡.

Darmstadt, September 2015

Contents

List of Figures

List of Tables

Glossary

Acronyms

AM	**A**mplitude-**M**odulated halftoning
AM-FM	**A**mplitude-**M**odulated-**F**requency-**M**odulated halftoning (i.e. hybrid halftoning)
ASTM	**A**merican **S**ociety for **T**esting and **M**aterials
BRDF	**B**i-directional **R**eflectance **D**istribution **F**unction
BSDF	**B**i-directional **S**cattering **D**istribution **F**unction
BSSRDF	**B**i-directional **S**ubsurface-**S**cattering **R**eflectance **D**istribution **F**unction
BTDF	**B**i-directional **T**ransmittance **D**istribution **F**unction
C-GMA	**C**olorimetric **G**amut **M**apping **A**pproach
CIE	**C**ommission **I**nternationale de l'**E**clairage (International Commission on Illumination)
C-LUT	**C**olor **L**ook-**U**p **T**able
CMF	**C**olor-**M**atching **F**unctions
CMYKRGB	**C**yan **M**agenta blac**K** **R**ed **G**reen **B**lue (i.e. printer colorants (inks))
CMYKW	**C**yan **M**agenta **Y**ellow blac**K** **W**hite (i.e. printer colorants (inks))
CPM	**C**olorimetric **P**rinter **M**odel
CS	**C**olor **S**pace
CYNSN	**C**ellular-**Y**ule-**N**ielsen-**S**pectral-**N**eugebauer spectral printer model
DBS	**D**irect **B**inary **S**earch
DIN	**D**eutsches **I**nstitut für **N**ormung (German Institute for Standardization)
DOI	**D**istinctness **O**f **I**mage
FM	**F**requency-**M**odulated halftoning
GBD	**G**amut **B**oundary **D**escriptor
G-JND	**G**loss-**J**ust **N**oticeable **D**ifference
GMA	**G**amut **M**apping **A**pproach
GU	**G**loss **U**nit
HVS	**H**uman **V**isual **S**ystem
ICC	**I**nternational **C**olor **C**onsortium
ICS	**I**nterim **C**onnection **S**pace
IDD	**I**nstitut für **D**ruckmaschinen und **D**ruckverfahren (Institute of Printing Science and Technology)
ISO	**I**nternational **O**rganization for **S**tandardization
JIS	**J**apanese **I**ndustrial **S**tandards Committe
JND	**J**ust **N**oticeable **D**ifference
LCD	**L**iquid **C**rystal **D**isplay
LUT	**L**ook-**U**p **T**able
MCMY	**M**att **C**yan **M**agenta **Y**ellow (i.e. a print mode)
MDS	**M**ulti-**D**imensional **S**caling
NCS	**N**atural **C**olor **S**ystem
PCA	**P**rinciple **C**omponent **A**nalysis
PCS	**P**rofile **C**onnection **S**pace
PMSGM	**P**aramer **M**ismatch-Based **S**pectral **G**amut **M**apping
RGB	**R**ed **G**reen **B**lue

RMS	Spectral **R**oot-**M**ean-**S**quare Error
S-GMA	**S**pectral **G**amut **M**apping **A**pproach
SGMS	Spatially Resolved Joint **S**pectral **G**amut **M**apping and **S**eparation
S-LUT	**S**pectral **L**ook-**U**p **T**able
SPD	**S**pectral **P**ower **D**istribution
SPEX	**SP**ecular **EX**cluded
SPIN	**SP**ecular **IN**cluded
SPM	**S**pectral **P**rinter **M**odel
SRCC	**S**pearman's **R**ank **C**orrelation **C**oefficient
SSGMS	**S**patio-**S**pectral **G**amut **M**apping and **S**eparation
VC	**V**arnish **C**overage
VH	**V**arnish **H**alftoning
WCMY	**W**hite **C**yan **M**agenta **Y**ellow (i.e. a print mode)
WWCMY	**W**hite **W**hite **C**yan **M**agenta **Y**ellow (i.e. a print mode)

Symbols

$\mathcal{G}$	Spectral printer gamut
Ω	All printable colorant combinations (i.e. printer colorant space)
o	Light encountered point to a surface / Center of a cross section of the spectral printer gamut
(α, β)	Tangent plane to a point on a given surface
$\widehat{N}$	Surface normal
ω_i	Incoming light (illumination) direction in the BRDF model
ω_r	Outgoing light (viewing) direction in the BRDF model
θ_i	The angle between incident light and the surface normal in the BRDF model
θ_r	The angle between reflected light and the surface normal in the BRDF model
ϕ_i	The angle between incident light and the tangent plane in the BRDF model
ϕ_r	The angle between reflected light and the tangent plane in the BRDF model
$d\omega_i = (\theta_i, \phi_i)$	Differential solid angle in the incoming light (illumination) direction in the BRDF model
$d\omega_r = (\theta_r, \phi_r)$	Differential solid angle in the outgoing light (viewing) direction in the BRDF model
$dL_r(\omega_r)$	Reflected radiance in the outgoing (viewing) direction in the BRDF model
$dE_i(\omega_i)$	Irradiance in the incoming (illumination) direction in the BRDF model
λ	Light wavelength in the visible range (approximately [380,730] *nm*)
LMS	Three types of cones (color receptors in the eye)
X, Y, Z	Tristimulus values
κ	Normalizing factor in an equation used for computing the XYZ tristimulus values
$\overline{x}$, $\overline{y}$, and $\overline{z}$	Color-matching functions (CMFs)
I	Arbitrary illuminant
n	Number of illuminants
$i = 1, ..., n$	Illuminant index
$I_i, i = 1, ..., n$	Different illuminants
$L_i, i = 1, ..., n$	Rendered colorimetric images from a spectral image for n illuminants
$\widehat{L}_i, i = 1, ..., n$	Gamut-mapped colorimetric images for n illuminants
R	Spectral image
(x, y)	Pixel position
r	Arbitrary reflectance
$r_(x, y)$	Each pixel's reflectance extracted from a spectral image
$l_(x, y)$	Each pixel's colorimetric values extracted from a colorimetric (e.g. LAB2000HL) image
$l_{Avg}(i)$	An Average LAB2000HL value computed for an image rendered under illuminant I_i

r^*	In-gamut reflectance
$\hat{r}$	Gamut-mapped reflectance
$\Upsilon(I,r)$	a vector containing XYZ tristimulus values computed for reflectance r and illuminant I
L^*	Lightness coordinate of the CIELAB color space
a^*	The opponent red-green color axis of the CIELAB color space
b^*	The opponent blue-yellow color axis of the CIELAB color space
G	Metameric or colorimetric printer gamut
CPM^{-1}	Inverted colorimetric printer model
SPM^{-1}	Inverted spectral printer model
S	Separation image
n'	Number of points sampled in the visible wavelength range
K'	A weighting parameter
E_{RMS}	Spectral root-mean-square error
$E_{RMS}(PCA)$	The RMS error occurred due to employment of PCA
$E_{RMS}(S-GMA)$	The RMS error occurred due to employment of a S-GMA
C	Color stimulus
C^*	Fundamental of color stimulus
E	Residual of color stimulus (metameric black)
PQR	Low dimensional spectral space computed from metameric blacks
$L:CS\ (I)\longmapsto CS\ (II)$	Color space transformation from $CS\ (I)$ to $CS\ (II)$
Γ_{Trad}	Traditional colorimetric gamut mapping
p_0	Actual under-process image pixel
$\zeta(p_0)$	Metameric set for pixel p_0
$\tau(p_0)$	Parameric set for pixel p_0
μ	Metamer-mismatch gamut
ρ	Paramer-mismatch gamut
χ	Printable colorant combination
ΔE_{00}	CIEDE2000 color-difference formula
Γ_{Meta}	Metamer-mismatch gamut mapping
Γ_{Para}	Paramer-mismatch gamut mapping
x'	Any CIELAB color that is aimed to be printed
y'	Any CIELAB color in any metamer-mismatch gamut
k_L, k_C, and k_H	Coefficients used in CIE94 and CIEDE2000 color-difference formulas
M	Number of used colorants (inks) in a printing system
N	Spectral image dimension
$N'\times M'$	Size of the spectral image R and separation image S
$CIED65$	CIE standard illuminant
$CIEA$	CIE standard illuminant
F_{cost}	Cost function
f_{col}	Colorimetric part of the cost function
$f_{spatial}$	Spatial part of the cost function
D	Just noticeable (color) difference (i.e. JND)
P_i	Color prediction of the printout under illuminant I_i
σ_1	Weighting parameter
σ_2	Weighting parameter
σ_3	Weighting parameter
$\wp$	Weighting parameter
p	A neighboring pixel
B	A set of neighboring pixels

$\omega(p)$	Spatial weight assigned to pixel p
ΔE^*_{ab}	CIE76 color-difference formula
$\Phi_{\theta,R^{Test}_{\lambda}}$	Emitted flux of a test sample
$\Phi_{\theta,R^{Reference}_{\lambda}}$	Emitted flux of the reference sample used in gloss meter
θ	Angles of the incident light and specularly reflected light with respect to the surface normal
g	Measured gloss value in gloss unit (GU)
Ψ	Predicted perceptual magnitude
γ	Measured stimulus intensity
γ_0	Perceptual threshold associated to a specific quantity
η	Constant
ν	Constant
φ	Spread of specular lobe in the Ward's light reflection model
ρ_d	Diffusely reflected light in the Ward's light reflection model
ρ_s	Specularly reflected light in the Ward's light reflection model
R^2	Coefficient of determination
$diff$	Diffuse illumination
ΔY	Difference between luminance factors
Y_{in}	Luminance factor of the SPIN case
Y_{ex}	Luminance factor of the SPEX case
ΔT	Drying time or computational time-difference
Std	Standard deviation
Max	Maximum value of a quantity
Avg	Average value of a quantity
x	Horizontal axis in the Cartesian space
y	Vertical axis in the Cartesian space
z	The axis perpendicular to the x-y axes in the Cartesian space
$(x_{i,j}, y_{i,j}, z_{i,j})$	A point in the Cartesian space
$\aleph[-1,1]$	A random number chosen from a uniformly distributed set of variables in the range from -1 to 1
$\hbar$	Texture level (elevation)
$R_{z_{i,j}}$	Radius in the z-direction
$H_{z_{i,j}}$	Surface height in the z-direction

Publications

I contributed to the following publications during the period of time (Aug 2012 - July 2015) as a research assistant at Technische Universität Darmstadt, Germany.

- Sepideh Samadzadegan and Philipp Urban, "Spatially Resolved Joint Spectral Gamut Mapping and Separation", 21st Color and Imaging Conference (CIC21), pp. 2-7, Albuquerque, New Mexico, USA., (2013).
  © 2013 Society for Imaging Science and Technology (IS&T/SID)

- Teun Baar, Sepideh Samadzadegan, Hans Brettel, Philipp Urban, and Maria V. Ortiz Segovia, "Printing gloss effects in a 2.5D system", SPIE Electronic Imaging Proceedings Vol. 9018: Measuring, Modeling, and Reproducing Material Appearance, San Francisco, USA., (2014).
  © 2014 The International Society for Optical Engineering (SPIE)

- Sepideh Samadzadegan, Jana Blahová, and Philipp Urban, "Color-Printed Gloss: Relating Measurements to Perception", 22nd Color and Imaging Conference (CIC22), pp. 207-211, Boston, Massachusetts, USA., (2014).
  © 2014 Society for Imaging Science and Technology (IS&T/SID)

- Sepideh Samadzadegan, Teun Baar, Philipp Urban, Maria V. Ortiz Segovia, and Jana Blahová, "Controlling colour-printed gloss by varnish-halftones", SPIE Electronic Imaging Proceedings Vol. 9398, Measuring, Modeling, and Reproducing Material Appearance, San Francisco, California, USA., (2015).
  © 2015 The International Society for Optical Engineering (SPIE)

- Sepideh Samadzadegan and Philipp Urban, "Spatio-Spectral Gamut Mapping and Separation", Journal of Imaging Science & Technology (JIST), Vol. 59, N. 4, pp. 40402-1-40402-12, (2015),
  23rd Color and Imaging Conference (CIC23), Darmstadt, Germany, (2015).
  © 2015 Society for Imaging Science and Technology (IS&T/SID)

- Teun Baar, Sepideh Samadzadegan, Philipp Urban, and Maria V. Ortiz Segovia, "Interrelation between gloss and texture perception of 2.5D-printed surfaces", SPIE Electronic Imaging Proceedings, Measuring, Modeling, and Reproducing Material Appearance, San Francisco, California, USA., (2016) – Accepted.
  © 2016 The International Society for Optical Engineering (SPIE)

1. Introduction

In general, for accurate printing (reproduction) of 2D images and 2.5D/3D objects, four main visual attributes have to be considered within a comprehensive printing pipeline: *color*, *gloss*, *opacity (translucency, or transparency)*, and *texture*. These are appearance attributes caused by the interaction of incident light and matter, perceived by the human observer. Therefore, the physical properties of the light encountered by a surface and light reflected from a surface as well as properties of the Human Visual System (HVS), have to be taken into account in any printing workflow that aims for accurate reproduction.

In this dissertation, reproductions of the first two appearance attributes (color and gloss) – related to diffusely and specularly reflected light – are considered, which correspond to the following two topics:

- *Spectral reproduction*, and
- *Gloss printing*.

These topics are addressed separately with the general aim of improving the print quality in mind.

1.1. Motivation

In the following sections, two examples are presented in order to explain briefly the main concepts of the aforementioned two topics and the necessity of carrying out research in these fields.

1.1.1. Example I

The main goal of a *proofing* system in a printing pipeline is to create an accurate prediction of the final printout, which will be printed by a printing press, so that the proof mimics the appearance of the printout and its visible effects. Proofing is a cost-efficient way used for customer verification and is based on a visual comparison between the original image and the proof, to ensure that the final printout will be satisfactory from the customer's perspective. According to this, contract proofs are signed between the provider and the customer prior to running the press – the most expensive stage of a printing pipeline. The critical question is: "Do the print and proof match?" If there is a noticeable mismatch between the print and the proof, then, besides the dissatisfaction of the customer, much money is wasted.

In a conventional, everyday printing workflow (e.g. printing a document using an office printer; printing high-quality prints with more sophisticated printing systems; or printing thousands of copies ordered by a customer via a huge press), the accurate reproduction of colors from the original image is considered only for a specific, predefined illuminant (i.e. an illuminant to which the reproduction is adjusted, such as daylight). Therefore, the proof-to-print mismatch and consequently customer dissatisfaction and waste of money may happen, when the comparison is made under another illumination condition, such as tungsten light. This conventional printing

workflow is known as the *metameric reproduction workflow*, and is based on the concept of *metamerism* [1].

To obtain the customer's verification and satisfaction regardless of changes in illumination conditions, *spectral proofing* must be used instead of conventional proofing (which is used in the metameric reproduction workflow). Spectral proofing leads to proof-to-print match independent of variations in illumination conditions. Spectral proofing is part of another printing workflow, known as the *spectral reproduction workflow*, which is based on the reproduction of spectral raw data, rather than the reproduction of colors only under a specific illumination condition.

Alongside spectral proofing, spectral reproduction has other applications including but not limited to: security printing, artwork (e.g. painting and cultural heritage) reproduction, accurate industrial color communication, aesthetic purposes, and so on. In general, for all cases in which accurate printing (reproduction) of an original (image) under a variety of illumination conditions (e.g. daylight, tungsten light, museum light, etc.) is required, spectral printing must be used. One aim of spectral printing is to obtain (ideally) an illuminant-invariant match between the original and the printout, which when using a traditional metameric printing workflow, is achievable only by chance. Although the spectral printing workflow is not yet commercially widespread, it is a printing workflow under research and development, with the aims of improving print quality and saving much expenditure.

As mentioned, in this workflow, the spectral raw data (reflectances in the visible wavelength range, roughly from 380 to 730 *nm*) rather than colorimetric values (colors) alone (determined for a predefined illuminant) are considered.

Due to the limitations of extant printing systems even those which are multi-channel (multi-colorant), there are always reflectances which are not printable. Thus, the non-reproducible reflectances have to be mapped into the set of reproducible spectra instead. This process is called *spectral gamut mapping* and is the first step required in a spectral reproduction workflow.

Choosing appropriate colorant combinations from the possibilities available in a printing system in order to print the mapped reflectances, is called *spectral separation* and is the second step required in a spectral reproduction pipeline.

The *spectral gamut mapping and separation* steps incorporated in a *spectral reproduction workflow* are investigated in the first topic focused on in this dissertation.

1.1.2. Example II

As mentioned previously, along with *color*, there are other important appearance attributes such as *gloss* which a comprehensive printing workflow should take into account if a reproduction as close as possible to the original is to be achieved.

We all know that customers always demand high-quality products, no matter what the target industry. The printing industry is not an exception. Clients request high-quality prints. The quality-control stage (see Fig. 1.1) in a printing pipeline is where the print job is controlled in terms of common printing defects both visually and by measurements. Nowadays, the print quality-control is mostly based on colorimetric accuracy between the original image and the printout. However, there are also gloss-related artifacts such as *bronzing* (see Fig. 1.2) and *gloss-differential* – visible in Fig. 1.1 (right image) as lustrous areas – which are not taken into account in the final quality-control stage in a printing pipeline, because there is no way to avoid them. Note that the bronzing artifact

[1] Two different reflectances – in the visible wavelength range – may produce the same visual response and consequently the same color under a specific illuminant. However, they may lead to different colors when another illuminant is taken into account. This is called metamerism and the corresponding spectra are known as metamers.

occurs due to ink aggregation in different spots, which may result in some hue shifts and an overall unevenness of glossiness appearance. Gloss-differential refers to an inconsistent gloss appearance across an image, which is caused by variations in deposited ink area coverage in different spots during the printing process. In order to avoid these gloss-related artifacts, controlling and printing local gloss effects independent of the amount of ink deposited is required, which can be incorporated in a printing pipeline. Gloss printing (reproduction) is the second topic of this dissertation.

Figure 1.1.: Print quality-control stage in a printing line. This figure has been taken at Heidelberger Druckmaschinen AG in Heidelberg, Germany. The *gloss-differential* artifacts are visible on the printout shown in the right image as lustrous areas.

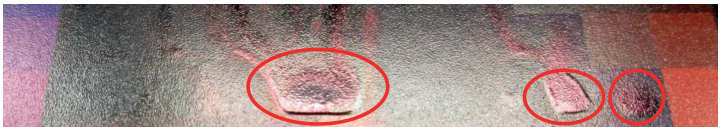

Figure 1.2.: A cutout of an image captured from a printout showing *bronzing* artifacts (visible in the marked ellipses), which have occurred due to aggregation of deposited inks.

One of the important applications of gloss printing can be found in the reproduction of masterpieces (paintings). Usually, masterpieces do not have uniform gloss appearance due to different painting materials used by the artist, which lead to different reflectance properties. In order to reproduce these masterpieces accurately, printing local gloss levels – covering different range of gloss values – is required, along with accurate color reproduction under a variety of illumination conditions.

As mentioned, the visual perception of the observer plays an important role in a printing pipeline both from the provider's side – by visually controlling the printout in the quality-control stage – and from the customer's side – in terms of verification of the print from the proof. Therefore, in any printing workflow the Human Visual System (HVS) must be taken into account if perceptually accurate reproduction is intended. Although different research has been conducted on reproduction of colors in perceptually uniform color spaces, few studies investigating the relationship between printable gloss values and perceived gloss magnitudes for the aim of perceptually accurate gloss reproduction have been carried out. As part of the second topic, we investigated this relationship based on color-printed samples produced according to the printing strategies outlined in this dissertation, with almost homogeneous appearance.

Additionally, the interrelation between perceived gloss and texture levels was studied using 2.5D-printed samples

[2] with two texture types and variations of gloss and texture levels (in terms of texture elevation). Understanding this interrelation is essential for perceptually accurate gloss reproduction in the presence of surface texture.

It should be noted that although different applications related to *spectral reproduction* and *gloss printing* – corresponding to the first and second addressed topics in this dissertation – were mentioned, we investigated the aforementioned fields of research separately and independent of any specific industrial application.

1.2. Research Questions

In this dissertation, the following four research questions in the areas of *spectral reproduction* and *gloss printing* were defined, with the general aim of improving printing quality.

- How might one control the printer in such a way as to achieve colorimetrically accurate reproduction across different illuminants without spatial artifacts? As mentioned in Section 1.1.1, this is the aim of spectral reproduction: to obtain an illuminant-invariant match between the original image and printout without introducing undesired artifacts. This research question is related to the first topic focused on in this dissertation.
- How can different glossiness levels be controlled and printed locally, in a wide range of gloss values, independently of the amount of deposited inks, in order to avoid gloss-related artifacts such as bronzing and gloss-differential? This is related to the second topic (gloss printing). As mentioned previously, nowadays, during the quality-control stage of a printing pipeline, the quality of the reproduction is controlled mostly according to colorimetric accuracy; however, gloss-related artifacts are usually ignored because there is not yet a solution (a printing strategy) available to control the glossiness appearance independent of the amount of deposited ink in local image areas. Thus, this research question was defined to address this issue.
- What is the relationship between measured printed-gloss values and visually perceived gloss magnitudes using color-printed samples with almost flat and homogeneous appearance? This is also related to the second topic in this dissertation. Understanding this relationship is important because it opens a door for controlling and printing perceptually accurate gloss levels.
- What is the interrelation between perceived surface gloss and texture levels considering 2.5D-printed samples? This is also related to the second topic in this dissertation. Understanding this interrelation is important because it opens a door for controlling and printing perceptually accurate gloss levels in the presence of surface texture.

1.3. Overview

This dissertation consists of eight chapters. In Chapter 1, the motivations for conducting this research (in the form of real examples) together with four research questions and an overview of chapters is presented.

In Chapter 2, the required fundamental knowledge of metameric and spectral printing workflows and their image processing steps, together with basic colorimetry, are introduced.

In Chapter 3, a survey of spectral gamut mapping approaches is presented.

In Chapter 4, the research conducted in this dissertation for the first topic (spectral reproduction) is explained

[2] In this context, 2.5D-print refers to a type of 3D-print with a flat-side which is printed without using any support material.

in detail, covering an approach proposed for spectral gamut mapping and separation (i.e. the answer to the first research question) together with a simple strategy for generating artificial targets and real spectral prints for security printing purposes.

In Chapter 5, fundamental knowledge and past research on gloss and gloss visual perception are presented.

In Chapter 6, the research conducted in this dissertation for the second topic (gloss reproduction) is explained in detail, including three printing strategies proposed for printing spatially varying gloss – in a wide range of gloss levels – independent of the amount of ink utilized (i.e. the answer to the second research question). Moreover, three perceptual experiments on gloss perception were conducted using the color samples printed via the aforementioned printing modes. These experiments were performed mainly in order to understand the relationship between gloss measurements and gloss perception (i.e. the answer to the third research question). Another perceptual experiment was also conducted in order to investigate the interrelation between perceived levels of surface gloss and texture using 2.5D prints (i.e. the answer to the fourth research question).

In Chapter 7, a summary followed by a conclusion to the work is presented.

In the last chapter (Chapter 8), my main contribution and ideas for further research are presented.

2. Metameric and Spectral Reproduction

In this chapter, a short introduction to printing technologies is presented. The basic of light and surface interaction, the BRDF[1] function and the geometries used in color measurement devices (according to BRFD model), and the basics of colorimetry are explained. Two printing workflows – *metameric* and *spectral* – together with their corresponding image processing steps are discussed. The limitation of the former reproduction workflow in terms of providing the colorimetric accuracy only for a specific predefined illumination condition is explained. To overcome this limitation, the latter printing workflow is introduced for the purpose of illuminant-invariant match between an original image and its printout. The challenges associated to this workflow are also briefly mentioned. In general, this chapter provides the fundamental knowledge required prior to detailed explanations given in Chapters 3 and 4. The content of this chapter is mostly inspired by [USD13] in which more details can be found.

2.1. Printing Technologies

Different printing technologies have been invented over the years, based on various application requirements such as speed, quality, individualization, and so on. There are varieties of so-called *relief printing* techniques such as *woodblock*, *letterpress*, and *flexographic printing* wherein the image areas are in relief and non-image areas are in recess. Although the first two mentioned relief-printing methods are very old, *flexographic printing* is still widely used, mostly in the packaging industry using cardboard, glass, paper, foil, and so on, as the substrate.

Another printing technology is called *gravure printing*, in which the image areas are in recess and non-image areas are in relief. This printing method is considered a high-speed printing technique with high quality and is used for very large print runs producing millions of copies.

There are also other printing methods such as *screen* and *offset printing* – the latter is widely used, especially in newspaper printing.

The printing techniques mentioned so far, are called *conventional* or *impact techniques* which require some sort of printing plate, either flat or cylindrical. *Offset printing* is the most common *conventional printing* method despite the high complexity of the printing unit. There are other printing methods known as *non-impact* where there is no direct contact between the substrate and inks. Most *digital printing* technologies are categorized in this group.

Inkjet printing is a digital printing technology in which the halftoned image is printed on the substrate by means of ink drops ejected from the nozzles of the print head.

Electrophotographic printing is another printing method used in laser and LED printers and copy machines, utilizing toner, light, and electrostatic charges [USD13].

In addition to the aforementioned printing technologies mostly used in the graphic arts industry, there is another printing technique called *functional printing*. In this printing method, functional materials are used instead of

[1] Bi-directional Reflectance Distribution Function

inks in order to print electronic circuits or devices such as batteries or transistors. For more information on the above-mentioned printing methods, please refer to [USD13] and [Kip01].

By the emergence of *2.5D/3D printing technology*, a revolution has occurred in the printing field. Unlike traditional printing methods in which the colorant combinations (inks) are printed (deposited) in a single layer, printing in multiple layers and passes is possible via 2.5D/3D printing technologies. More information on multi-layer and multi-pass printing is given in Section 6.1.1. Printing in different layers and passes eventually leads to either relief (2.5D) prints or 3D-printed objects. Note that in this context, 2.5D-print refers to a type of 3D-print with a flat-side which is printed without using any support material.

In this dissertation, two inkjet and three 2.5D printers were utilized for printing the required samples. The used inkjet printers were HP Designjet Z3100 and Canon iPF6450 with CMYKRGB[2] colorants. These printers are considered as multi-channel printers with more inks than the conventional 3 (CMY) or 4 (CMYK) channel printers. In general, using multi-channel printers leads to higher number of printable colorant combinations and consequently expansion of the set of reproducible colors. These printers were used for the research conducted in Chapter 4.

As 2.5D printers we used two prototypes performing wet-on-wet and wet-on-dry printing. The third 2.5D printer was an Océ Arizona 480 GT printer with multi-layer and multi-pass capabilities and CMYKW[3] ink set together with varnish[4] deposition possibility for printing 2.5D prints with glossy appearance. These printers were used for the research conducted in Chapter 6.

In general, "printing" is a multidisciplinary research field covering different research areas such as chemistry, physics, computer science, mechanical and electrical engineering, economics, computer graphics, and psychophysics.

In this dissertation, besides printing samples via inkjet and 2.5D printing technologies, we mostly focus on the computer science field (image processing), taking into account the physics of light interaction with the substrate and the psychophysics of human visual perception.

In the next section, the basic concept of light-matter interaction as well as the *Bi-directional Reflectance Distribution Function* (BRDF) – which is a *light reflection model* – are explained.

2.2. Light-Matter Interaction

Appearance can be defined as the overall look of an object perceived by a human observer based on the interaction of a light source and the object's material. This interaction can mainly be classified into four categories: absorption, reflection (diffuse and specular), scattering, and transmission (see Fig. 2.1). Based on these interactions – the results of the optical properties of light and matter – four underlying attributes are defined which affect the visual perception of materials [Hut99].

- Color
- Gloss
- Opacity, translucency, or transparency
- Texture

[2] C = Cyan, M = Magenta, Y = Yellow, K = Black, R = Red, G = Green, and B = Blue.
[3] W = White, the rest of abbreviations are as mentioned previously.
[4] Varnish is some sort of a liquid coating that can be deposited on printed surfaces to add some appearance effects such as matt or glossy to the finial finish. In the printing process used in this dissertation, using varnish deposition leads to a glossier surface appearance.

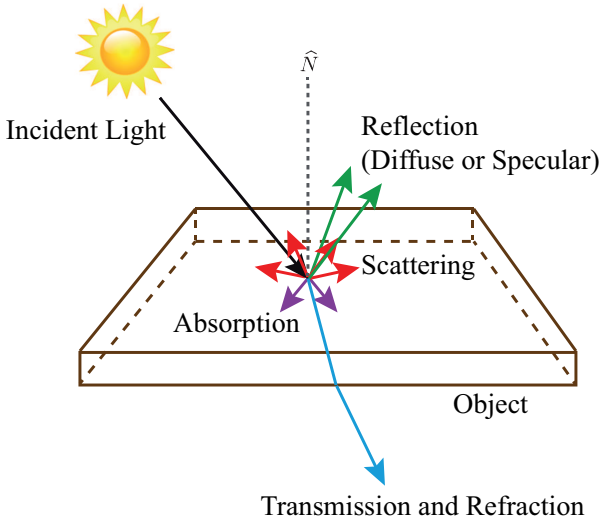

Figure 2.1.: Interactions between an incident light and an object.

There are different functions such as BSDF[5], BSSRDF[6], BTDF[7], and BRDF[8] used for modeling the aforementioned light-matter interactions [PMJ14, BDW81, Lee05].

The first three models consider the light scattering, reflectance, and transmittance phenomena. The last one (BRDF) is the simplified version of the BSSRDF model, and is based on a model of light reflection that assumes that light encounters and leaves the surface at the same point (i.e. no light scattering).

Since the first two listed attributes (color and gloss) – which are the two main focuses of this dissertation – are related to diffuse and specular reflection of the encountered light respectively, they can be described by the BRDF model. The flat samples used in this dissertation are printed via absorption inks and have almost homogeneous opaque appearances. Thus, the possibility of light scattering or transmittance can be neglected for these samples.

Since the color and gloss measurement devices have been designed based on rules of physics by taking the reflection of light from the surface into account, a brief explanation of the BRDF model is presented in the following section. These measurement devices are based on sampling the BRDF using different geometries. The geometries used in color and gloss measurement devices are explained in Sections 2.3.4.1, 2.3.4.2 and 5.1.

2.2.1. Bi-directional Reflectance Distribution Function (BRDF)

The BRDF model describes how much of the light encountering a surface is reflected. In general, the amount of reflected light from a surface depends on the position of the light source and the observer relative to the surface normal ($\widehat{N}$) and the tangent plane (defined by (α, β) coordinates)[9]. Consequently, the BRDF model is a function

[5] Bi-directional Scattering Distribution Function
[6] Bi-directional Subsurface-Scattering Reflectance Distribution Function
[7] Bi-directional Transmittance Distribution Function
[8] Bi-directional Reflectance Distribution Function
[9] In 3-dimensional space, the normal of a given surface at a fixed point *o* is defined as a vector which is perpendicular to the surface tangent at the same point. The tangent plane at point *o* is a plane which contains the tangent lines of all curves on the surface passing through that point.

of four input variables determined via the incoming light direction (ω_i) and outgoing viewing direction (ω_r) with respect to a local orientation at the light-encountered point (o).

We know that light is generally measured as energy per unit surface area. Therefore, instead of considering a single illumination and viewing direction, two small regions for both directions are considered and called *differential solid angles* ($d\omega_i$ and $d\omega_r$). As mentioned, the illumination and viewing directions are defined via the angles with respect to the surface normal (θ_i and θ_r) and the tangent plane (ϕ_i and ϕ_r) (i.e. $d\omega_i = (\theta_i, \phi_i)$ and $d\omega_r = (\theta_r, \phi_r)$, where i and r refer to the incident and reflected light respectively.). Figure 2.2 [Lee05] is a schematic representation of the BRDF.

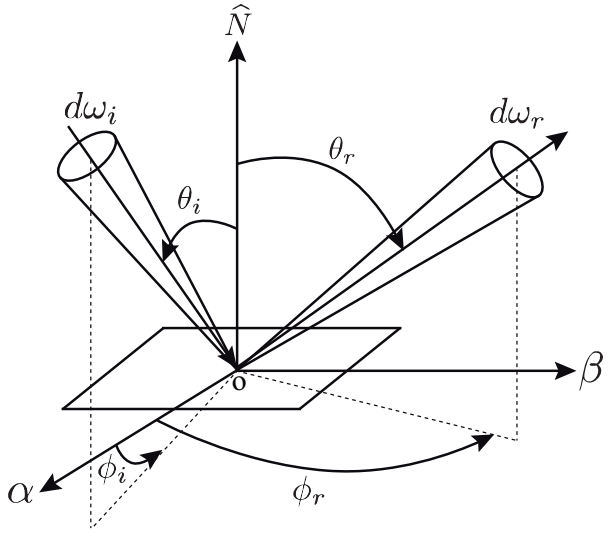

Figure 2.2.: Schematic representation of BRDF. This image has been taken from [Lee05] and re-sketched.

BRDF is defined as the ratio of the amount of the reflected radiance in the outgoing (viewing) direction ($dL_r(\omega_r)$) to the amount of irradiance in the incoming (illumination) direction ($dE_i(\omega_i)$) [Lee05]. As the result of light-surface interaction, different wavelengths (λ) of light in the visible range (approximately from 380 to 730 *nm*) may be absorbed, reflected, transmitted, and scattered in various degrees. Therefore, the BRDF also depends on the wavelength. Equation (2.1) [Lee05] represents the definition of BRDF.

$$BRDF_\lambda(\theta_i, \phi_i, \theta_r, \phi_r) = \frac{dL_r(\omega_r)}{dE_i(\omega_i)} \tag{2.1}$$

There are two different types of BRDFs, defined via the reflectance properties of materials with respect to their rotation around the surface normal. The BRDFs which are invariant are called *isotropic BRDFs* and those which exhibit variations in reflectance properties are called *anisotropic BRDFs*. For instance, brushed metal and satin are two materials with anisotropic BRDFs. The printed samples used in this dissertation have isotropic BRDFs.

2.3. Basic Colorimetry

The definition of color raises some challenges due to its dependence on various parameters such as *light Spectral Power Distribution* (SPD) and *Human Visual System* (HVS).

According to the definition used in International Lighting Vocabulary (ILV) [Fai05], color is an attribute of visual perception which depends on the spectral distribution of the color stimulus, i.e. the reflected light from an object in the visible wavelength range (roughly 380-730 *nm*), and contains chromatic and achromatic content. Thus, it can be described by chromatic color names such as blue, red, brown, pink, etc. or achromatic color names e.g. black, white, gray, etc. and quantified by light, dark, etc. or a combination of these terms.

Moreover, the size, shape, and surrounding background of an object as well as the state of adaptation of the observer's visual system have influence on the perception of color [Fai05].

2.3.1. Perceptual Color Attributes

Unlike the difficulty in definition of color, the perceptual color attributes can be more precisely defined as follows [Fai05]:

- **Hue:** "Attribute of visual sensation according to which an area appears to be similar to one of the perceived colors: red, yellow, green, and blue, or to a combination of two of them" [Fai05].
- **Brightness:** "Attribute of visual sensation according to which an area appears to emit more or less light" [Fai05].
- **Lightness:** "The brightness of an area judged relative to the brightness of a similarly illuminated area that appears to be white or highly transmitting", i.e. $Lightness = \frac{Brightness}{Brightness(White)}$ [Fai05].
- **Colorfulness:** "Attribute of a visual sensation according to which the perceived color of an area appears to be more or less chromatic" [Fai05].
- **Chroma:** "Colorfulness of an area judged as a proportion of the brightness of a similarly illuminated area that appears white or highly transmitting", i.e. $Chroma = \frac{Colorfulness}{Brightness(White)}$ [Fai05].

Although, five perceptual attributes are defined for color perception, it is mostly not necessary to consider all of them. Typically, the relative color attributes (hue, lightness, and chroma) have significant importance and are used for defining the perceived colors.

2.3.2. Perceiving Color

The light reflected from an object enters the human eye and is imaged on the *retina* where there are *light receptors*. The light receptors absorb a portion of the incoming light and send neural signals accordingly to the brain, for further processing.

There are two different light receptors, known as *rods* and *cones*. The rods are responsible for detecting small amount of lights such as starlight and have only one pigment type. Therefore, objects can only be seen as shades of gray using these receptors.

The cones are our color receptors and are less sensitive to the incident light. There are three types of cones (L, M, and S) responding differently to the incident light based on various wavelengths and consequently sending different signals to the brain.

Although the spectral sensitivities of L, M, and S cones overlap (see Fig. 2.3 [Ber00]), the peaks of their spectral

sensitivities are within the *long* (L: 560-580 *nm*), *middle* (M: 530-540 *nm*), and *short* (S: 420-440 *nm*) wavelengths. The mentioned overlaps are vital for distinguishing different colors [Ber00].

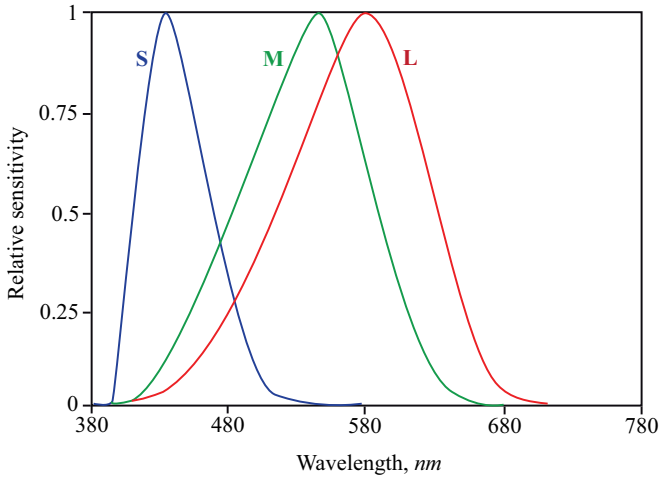

Figure 2.3.: Cones' spectral sensitivities. This figure has been taken from [Ber00] and re-sketched.

Therefore, in order to determine the object's color, three things must always be considered: the SPD of the light source, the reflected light from an object coming to the eye (i.e. the stimulus), and the cones' spectral sensitivities (see Fig. 2.4). In addition to these factors, the size and texture of the object as well as the background also influence the color perception [Ber00].

The International Commission on Illumination (CIE) has achieved some standardization in global communication. The committee defined standard illuminants – CIE illuminants – with specific SPDs simulating various light sources such as daylight and tungsten. Moreover, colorimetric standard observers (i.e. CIE 1931 2° and 1964 10°) were introduced with corresponding *Color-Matching Functions* (CMFs) obtained via conducting visual experiments. The CMFs are linearly related to the human cones' spectral sensitivities, LMS.

It should be mentioned that in the imaging industry, viewing booths are used to provide different simulated illuminants. The SPDs of these artificial illuminants usually vary from one device to another and also in comparison with both the real and standardized sources of illuminations. Usually, in the graphic arts industry, the CIE 2° standard observer and the CIED50 illuminant are used. Furthermore, for the sake of universal and device-independent color communication, standard color spaces such as CIEXYZ were defined. For more information regarding the CIE illuminants and colorimetric standard observers as well as universal color spaces, please refer to [Ber00] and [OR05].

2.3.3. CIEXYZ Tristimulus Values

Imagine there is an image observed under a particular viewing condition, i.e. an illuminant and an observer. In order to define a specific color for each image pixel, the human visual system (HVS) must be mimicked somehow. Equation (2.2) [Ber00] shows how this model results in a set of tristimulus values (X, Y, and Z) for any pixel of the image. This equation is considered to be the first step of color interpretation from raw spectral data, within the device-independent CIEXYZ color space. From the computed XYZ values, other transformations can also be employed for color representation within other color spaces.

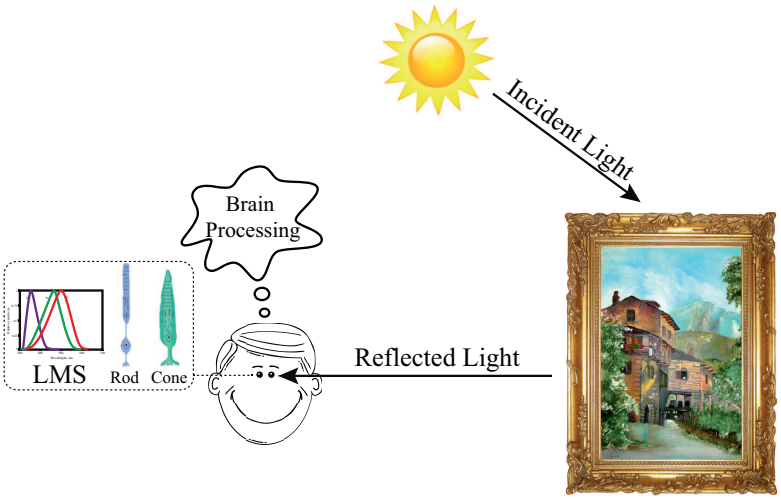

Figure 2.4.: Color perception.

$$\Upsilon(I,r) = \begin{bmatrix} X \\ Y \\ Z \end{bmatrix} = \kappa \int_{\Lambda} \begin{bmatrix} \bar{x}(\lambda) \\ \bar{y}(\lambda) \\ \bar{z}(\lambda) \end{bmatrix} I(\lambda) r(\lambda) d\lambda, \quad \kappa = \frac{100}{\int_{\Lambda} \bar{y}(\lambda) I(\lambda)\, d\lambda}, \tag{2.2}$$

where X, Y, and Z are the coordinates of CIEXYZ color, and Υ is a vector containing these tristimulus values. The reflected light from the observed image and the SPD of the considered illuminant are represented by r and I respectively. The visible wavelength range (roughly 380-730 *nm*) is denoted by Λ. The CIE color-matching functions (CMFs) of 2° or 10° colorimetric standard observers are shown by $\bar{x}$, $\bar{y}$, and $\bar{z}$. By convention, when there is a perfect reflecting diffuser material, i.e. $r(\lambda) = 1$, we assign: $Y = 100$. For this reason, in the above equation, κ is a constant that normalizes Y to 100 for the case given here [Ber00].

It should be noted that the CIEXYZ color space is related linearly to the stimulus intensity, i.e. $I(\lambda)r(\lambda)$, while human perception has a non-linear relation with the stimulus intensity according to Stevens' Power Law [Ste61]. This means that the CIEXYZ color space is perceptually non-uniform in the sense that equal perceptual color-differences do not necessarily correspond to equal distances in this space. Therefore, the color-differences computed based on these distances are not necessarily perceptually meaningful [SB02]. Hence, in order to calculate the perceptually meaningful color-differences between two stimuli, transformation from CIEXYZ color values to a perceptually uniform color space is required. As an example of a color space with improved perceptual uniformity, we can refer to the trichromatic opponent CIELAB color space [OR05]. In this color space, the lightness axis is denoted by the L^* coordinate. The opponent color axes are red-green (a^*) and blue-yellow (b^*). See Fig. 2.5.

The shortcoming of this color space is related to the hue linearity, i.e. the perceived hue changes across the predicted constant hue. This drawback is present mostly in the blue and red areas of the CIELAB color space. Hence, using another trichromatic opponent LAB2000HL color space [LU12] which is approximately perceptually uniform (for small color differences) and hue linear, is recommended when a more accurate result is desired.

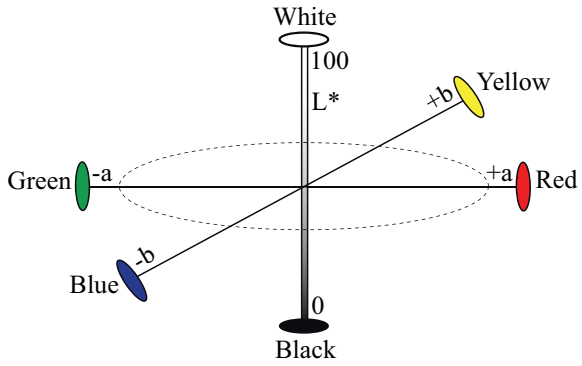

Figure 2.5.: Schematic representation of the CIELAB color space.

2.3.4. Color Measurement Devices and Geometries

As mentioned in Section 2.2, the diffuse reflection from an object's surface determines its color. There are two common types of geometries mainly used in color measurement devices considering the diffusely reflected light. These measurement geometries are $45^\circ/0^\circ$ and *Diffuse*$/8^\circ$ (Illumination/Viewing) which are explained in detail in two subsequent Sections 2.3.4.1 and 2.3.4.2.

The color measurement devices can be mainly divided in two groups: *colorimeter* and *spectrometer*, where the former is used for measuring the CIEXYZ tristimulus values for a stimulus, while the latter is utilized for measuring a specified optical property as a function of wavelength. If the spectrometer is used to measure the optical property of a source (spectral radiance or irradiance), it is called *spectroradiometer* and if it is utilized to measure the optical property of an object (reflectance or transmittance), it is called *spectrophotometer* [Ber00].

2.3.4.1. $45^\circ/0^\circ$ Geometry

The most commonly used color measurement devices in graphic arts industry have $45^\circ/0^\circ$ (illumination/viewing) geometry. Figure 2.6 is a schematic representation of the geometry used in these kinds of devices which can be described as an integral over the BRDF considering 45° angles of illumination (with respect to the surface normal) in a complete circle around the surface normal. According to the definition of BRDF (see Section 2.2.1), this means that $\theta_i = 45^\circ$, $\phi_i \in [0, 2\pi]$, $\theta_r = 0$, ϕ_r can be any angle (e.g. $\phi_r = 0$).

2.3.4.2. *Diffuse*$/8^\circ$ Geometry

There are other types of color measurement devices with diffuse$/8^\circ$ (illumination/viewing) geometry in which all incoming light directions (with respect to the surface normal) are considered in an encompassed sphere. According to the definition of BRDF (see Section 2.2.1), this means that $\theta_i \in [-\pi/2, \pi/2]$, $\phi_i \in [0, 2\pi]$, $\theta_r = 8^\circ$, and ϕ_r can be any angle (e.g. $\phi_r = 0$). Figure 2.7 shows the geometry used in these types of devices.

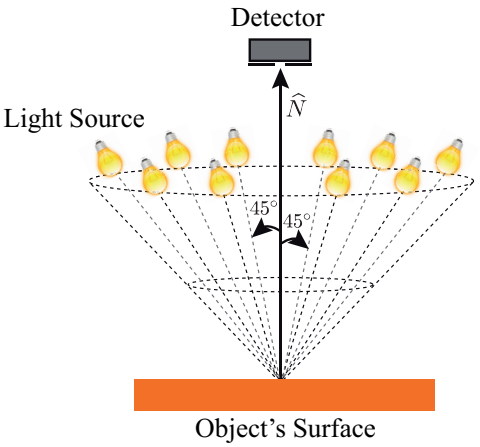

Figure 2.6.: Schematic representation of $45°/0°$ (illumination/viewing) geometry used in color measurement devices.

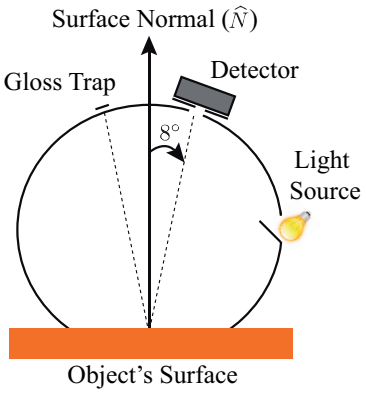

Figure 2.7.: Schematic representation of *diffuse*$/8°$ (illumination/viewing) geometry used in color measurement devices.

2.3.5. Color Space Transformations

For the sake of simplicity, in this dissertation, any transformation from a color space (CS) to another one is represented by the following notation:

$$L : CS\ (I) \longmapsto CS\ (II), \tag{2.3}$$

where $CS(I)$ and $CS(II)$ are two color spaces.

Thus, transformations from CIEXYZ to CIELAB and from CIELAB to LAB2000HL color space can be separately denoted by $L : CIEXYZ \longmapsto CIELAB$ and $L : CIELAB \longmapsto LAB2000HL$ respectively. Consequently, $L(\Upsilon(I,r))$ shows the corresponding colorimetric values of CIEXYZ coordinates (see Eq. (2.2)) in any color space specified by the L transformation.

Note that the Euclidean distances in the LAB2000HL color space are almost equal to the corresponding CIEDE2000 color-differences [SWD05] in the CIELAB color space. Thus, to calculate the color difference between each arbitrary pair of colors (e.g. $L(\Upsilon(I,r_1))$ and $L(\Upsilon(I,r_2))$, where $L : CIEXYZ \longmapsto LAB2000HL$) in the LAB2000HL color space, the 2-norm can be used (see Eq. (2.4)).

$$\| L(\Upsilon(I,r_1)) - L(\Upsilon(I,r_2)) \|_2, \tag{2.4}$$

where I represents the SPD of an arbitrary illuminant, and r_1 and r_2 are two different reflectances.

Although we used the aforementioned simplistic notation for the transformation from the CIEXYZ to LAB2000HL color space, in reality there is no direct transformation. The CIEXYZ values must first be transferred into the CIELAB color coordinates. Then, the transformation from CIELAB values to LAB2000HL coordinates (as well as the inverse transformation) is performed via look-up tables (LUTs)[10]. The supplementary material of the LAB2000HL paper [LU12] contains MATLAB scripts to encode look-up tables and color transformations.

For more information on color transformations and color-difference formulas, please refer to [Ber00] and [OR05]

2.4. Printing Workflows

There are two different major printing workflows, known as the *metameric* and *spectral reproduction workflows* which are discussed in detail in Sections 2.4.1 and 2.4.3 respectively. Their corresponding image processing steps are also explained. The limitation of metameric printing workflow and consequently the reason for using spectral reproduction workflow and the challenges associated to the latter case are also discussed.

2.4.1. Metameric Printing Workflow

In general, an image reproduction workflow consists of two parts: *capturing* and *printing*. The goal of a typical *metameric (colorimetric) image reproduction workflow* – from scene to print – is to provide a copy of an original sharing the same colorimetry for a specific viewing condition, i.e. an illuminant and an observer.

The ICC-based workflow is an example of a metameric reproduction workflow, based on the International Color Consortium (ICC) standard, and is commonly used in the graphic arts industry. In this workflow, for the purpose of color management and universal color communication between various input and output imaging devices, a device-independent color space known as *Profile Connection Space* (PCS), as well as device *input/output profiles* are used.

During the capturing stage, transformations from an RGB-camera response – used for capturing the scene – into a PCS (e.g. CIEXYZ/CIELAB) determine the *input profile*. Note that for building the input device profile, some image processing steps, such as linearization and color correction must be performed.

During the printing stage, transformations from a PCS to the printer digital counts, construct the *output profile*. Some image processing steps such as linearization, gamut mapping, separation, halftoning, and ink limitation are employed for building the output device profile. Consequently, the required colorant combinations and their fractional area coverages are determined from the output profile and are sent to the printer as digital counts for printing the output image. Please note that the input and output profiles are composed of various color look-up tables (C-LUTs).

[10] The nodes of the lookup tables represent a direct sampling of the transformation and intermediate values are interpolated from neighboring nodes.

Figure 2.8 shows a schematic representation of an ICC-based metameric image reproduction workflow.

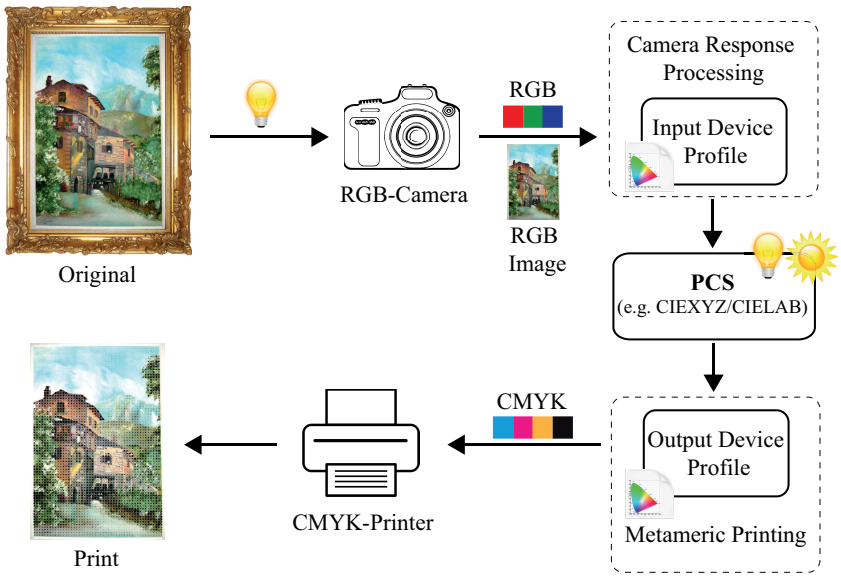

Figure 2.8.: Schematic representation of an ICC-based metameric image reproduction workflow.

Since the focus of this dissertation is on printing rather than capturing, more details about *printing workflows* and their required image processing steps will be presented.

The printing stage associated with the metameric image reproduction workflow is called the *metameric/colorimetric printing workflow*. Typically, in a *metameric printing workflow*, the aim is to make *metamers* of the original [DR06].

Two reflectances $r_1(\lambda)$ and $r_2(\lambda)$ are called *metamers* for a specific illuminant $I(\lambda)$ if their corresponding tristimuli match perfectly, i.e. their color difference is exactly zero for $I(\lambda)$. Equation (2.5) represents the definition of metamers where 2-norm is used for showing the color difference.

$$\| L(\Upsilon(I,r_1)) - L(\Upsilon(I,r_2)) \|_2 = 0, \tag{2.5}$$

where $L : CIEXYZ \longmapsto LAB2000HL$.

Therefore, the accuracy and print quality of the metameric printing workflow can only be discussed for a predefined specific illumination condition.

This workflow consists of four main image processing steps: *color gamut mapping*, *color separation*, *halftoning*, and *ink limitation*. Figure 2.9 is a block diagram representing the printing workflow in an overall view [USD13]. In this figure, a 4-channel (CMYK) printer is considered.

2.4.1.1. Gamut Mapping

As mentioned, the first step in a printing workflow is gamut mapping. The *colorimetric* or *metameric gamut* (denoted by G) of any printing system is defined as the whole set of printable colorimetric (e.g. CIELAB) values

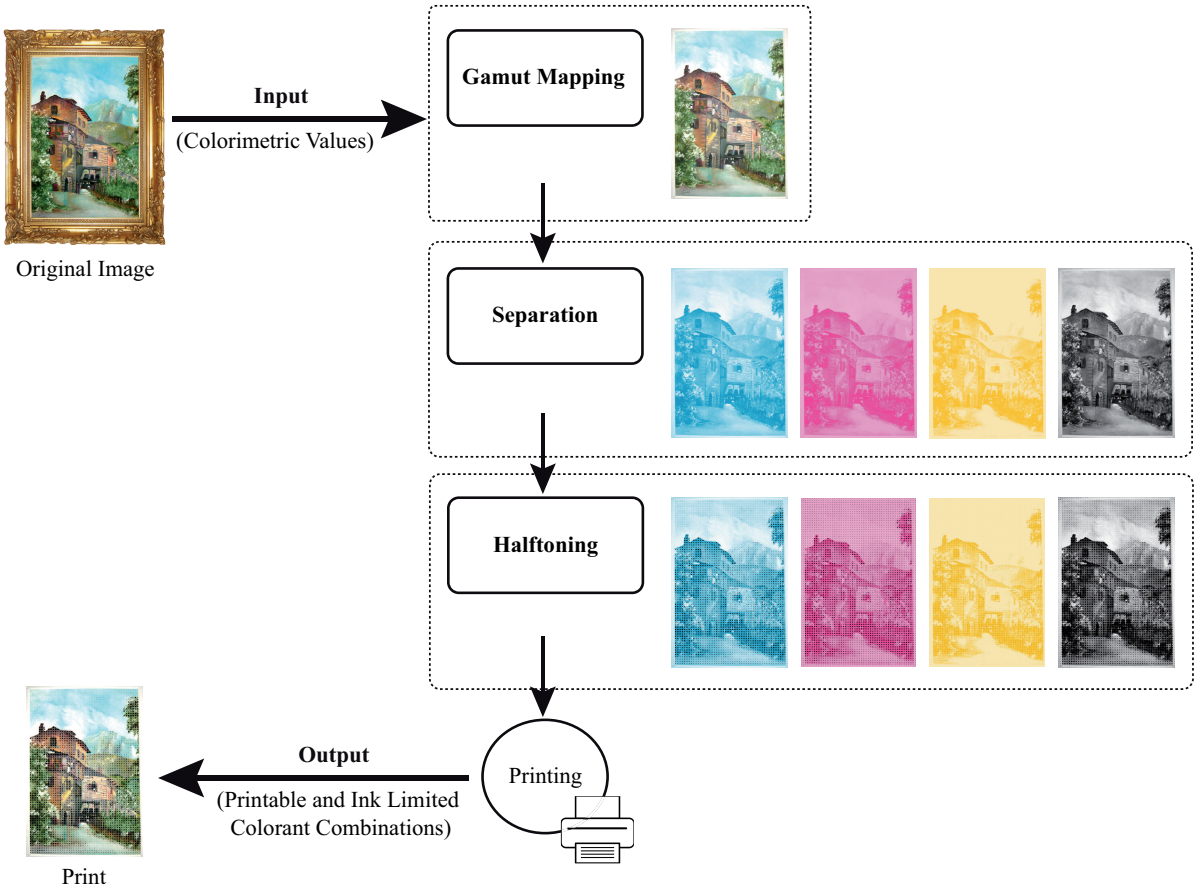

Figure 2.9.: Different image processing steps required in a printing workflow – considering a printing system with four channels (CMYK). This figure has been taken from [USD13], re-sketched and slightly modified.

under a specific viewing condition, i.e. an illuminant and an observer.

The colorimetric gamut of any printing system is always restricted to some extent, depending on the quality of the substrate used and the color and number of utilized colorants (inks). Although there are multi-channel printers with more inks, e.g. CMYKRGB, their gamut is still limited. Therefore, there are always colors which are not inside the printer colorimetric gamut. Hence, transformation of these out-of-gamut colors into the printer gamut is required. This transformation is called *colorimetric/metameric gamut mapping* which is based mostly on minimizing perceived color differences between the original and the printable colors.

For the purpose of colorimetric gamut mapping, it is important to have quick access to the printer's color-gamut boundaries. This can be done by employing a *Gamut Boundary Descriptor* (GBD) method used for describing approximately the extent of the gamut (i.e. gamut boundary) [Mor08]. In general, these approaches are classified into two main groups: *empirical* and *model-based* [USD13]. The former is based on a large number of printed and measured color patches which is a time-consuming process. In order to compute the printer gamut via a smaller

number of printed patches, model-based GBD methods are utilized. For more information about the empirical and model-based GBD approaches, please refer to [BF97, CL99, ML00] and [Mah96, Mah97, Mah98, URR02] respectively.

In general, *Colorimetric Gamut Mapping Approaches* (C-GMAs) are classified into two groups: *clipping* and *compression*. In clipping methods, only the out-of-gamut colors are affected and mapped onto the printer colorimetric gamut, while the in-gamut colors remain unaffected. The clipping gamut mapping approaches are usually more useful for printing systems with larger gamuts. However, for smaller gamuts where lots of colors are non-reproducible, smoother transitions are required in order to avoid visible banding artifacts. Therefore, compression algorithms are usually recommended for these cases in order to map both the in-gamut and out-of-gamut colors by compression methods [USD13].

Most of the clipping- and compression-based GMAs use pixel-wise transformations. In recent years, *spatial gamut mapping* algorithms have been also developed. These, aim to preserve the local color contrast in an image by considering the spatial neighborhood. Please refer to [McC01, MW03, BdEW01, ZS07] for more information on spatial gamut mapping approaches. Figure 2.10 is a schematic representation of the colorimetric gamut mapping.

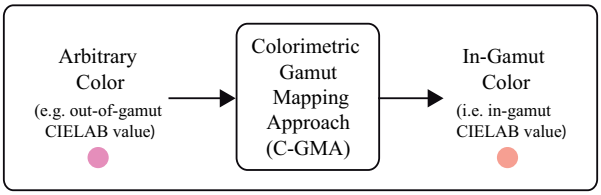

Figure 2.10.: Schematic representation of colorimetric gamut mapping.

2.4.1.2. Separation

The result of gamut mapping methods is in-gamut colors printable by the utilized printing system. In order to print each in-gamut color, the required printer's colorant combinations and their corresponding fractional area coverages must be determined. This process is called *separation* and can be performed mainly in two ways [USD13]:

1. Inverting the *colorimetric printer model* (CPM), i.e. $CPM^{-1} : G \rightarrow \Omega$, where G is the colorimetric printer gamut and Ω is the set of all printable colorant combinations defining the printer colorant space.
2. Solving a constraint optimization problem in case where the CPM is not analytically invertible.

It is noteworthy that the CPM predicts colorimetric (e.g. CIELAB) values from printer colorant combinations (e.g. CMYK) and their corresponding fractional area coverages, i.e. $CPM : \Omega \rightarrow G$.

Figure 2.11 is a schematic representation of the separation process as an inversion of the forward colorimetric printer model.

Usually, there are colorimetric redundancies in the printer colorimetric gamut, especially for printing systems with more than three conventional colorants (CMY), e.g. CMYK or CMYKRGB. As a simple example, we can refer to printing gray color using the black (K) ink or the combination of cyan (C), magenta (M), and yellow (Y) inks. Randomly choosing a colorimetric combination out of several different choices might lead to unwanted visually disturbing *banding artifacts* in areas where the original image has smooth color transitions. Therefore,

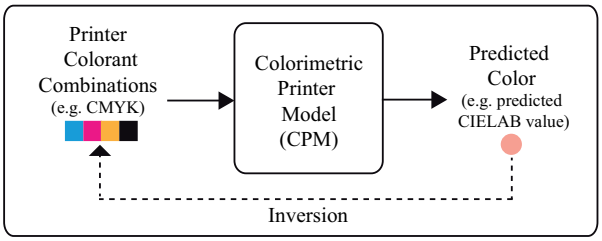

Figure 2.11.: Schematic representation of the separation process as an inversion of the forward colorimetric printer model (CPM^{-1}).

the accuracy of the printer model and the consequent selection of appropriate colorant combinations play an important role in a printing workflow.

By employing the separation process on a gamut-mapped image, a so-called *separation image* (denoted by *S*) with multi-bands is generated. The number of channels in this image is based on the number of inks utilized in a printing system. Usually, each band is encoded by 8 bits representing the area coverages of the used colorants (inks). This image contains the printable colorant combinations.

2.4.1.3. Halftoning

The final step in a printing workflow is *halftoning*. In the halftoning process, the corresponding value of each encoded 8-bit is transformed to either 0 or 1, where the former means no ink deposition at all, while the latter shows a droplet. Since the image has already been converted into multi-bands during the separation process, the arrangement of dots (specifically in multi-channel printers, e.g. CMYKRGB) is crucial for determining the quality of the printout. Moreover, for developing halftoning algorithms, the specification of the human visual system (HVS) and capabilities of the printing technology utilized are two important factors to consider [USD13].

Typically, there are three types of halftoning methods known as: *Amplitude-Modulated* (AM), *Frequency-Modulated* (FM), and *hybrid* (AM-FM) halftones. In AM halftoning procedure, dot clusters, with different sizes but similar distances with respect to each other, are generated. In contrast, in FM halftoning, similar-sized dots with varying intermediate spaces are printed. In the hybrid AM-FM halftoning approach, both the size of the dots and their relative distances vary. The AM, FM, and AM-FM halftoning approaches are shown in Fig. 2.12 from (a) to (c). More information on the halftoning process can be found in [Uli87], [Kan99], and [LA08].

2.4.1.4. Ink Limitation

It should be noted that there is another important step in any printing workflow, known as *ink limitation*. In general, each substrate has a specific physical threshold in terms of tolerating the amount of superimposed inks. If the total area coverages of deposited inks in a single spot exceed the maximum threshold, *ink bleeding* artifacts occur (see Fig. 2.13). Therefore, an ink limitation process must be performed in order to avoid undesired printing artifacts by transforming the theoretical printer control values into printable ones.

The ink limitation process can be performed either directly after the separation as a single stage, or during the printer characterization and modeling[11] procedure. Due to this flexibility, it is not mentioned explicitly in the

[11] In general, printer characterization refers to the process that determines which colors or reflectances can be printed via a specific printing system and from which colorant combinations. The printer characterization can be performed either completely manually by printing

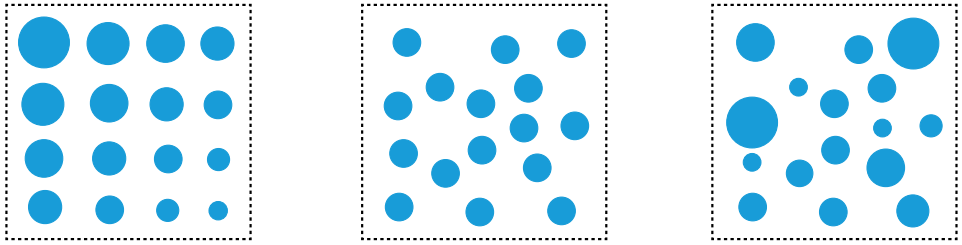

(a) (b) (c)

Figure 2.12.: Halftoning approaches: (a) AM, (b) FM, and (c) AM-FM Hybrid halftoning. This figure has been taken from [USD13] and re-sketched.

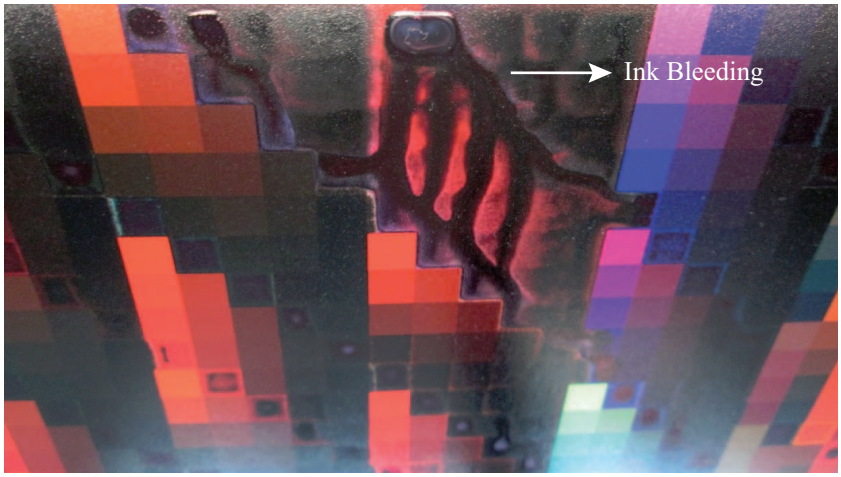

Figure 2.13.: Ink bleeding.

printing workflow shown in Fig. 2.9. However, the output of this workflow represents the printable and ink limited colorant combinations.

2.4.2. Limitations of Metameric Printing Workflow

The image reproduction workflow discussed in Section 2.4.1, is based on *metameric matches* between the original image and the printout under a specific viewing condition (i.e. an illuminant and an observer). This is the reason for naming it the *metameric* reproduction workflow – the most commonly used printing workflow nowadays. Although it is useful in applications with a predefined viewing condition, it is very likely that *metameric mismatches* occur for other cases in which illuminants and observers may vary. This occurs mostly due to limitations of the capturing devices, such as cameras and scanners, which are utilized. The result of the capturing process in

a large number of patches, or via a smaller number of printed samples and using a colorimetric or spectral printer model that predicts reproducible colors or reflectances from printable colorant combinations. The printer characterization has to be performed after the printer calibration process which restricts the amount of superimposed and deposited inks, in order to avoid printing artifacts such as ink bleeding.

a metameric image reproduction workflow, is often an RGB image specified by a standardized RGB color space. Thus, the information derived from the original scene has already been reduced to only three values per pixel using these devices. This means that these devices compute the CIEXYZ tristimulus values under a predefined viewing condition (see Eq. (2.2)). The RGB values are then obtained via transformation $L : CIEXYZ \longmapsto RGB$.

In order to have a more accurate reproduction which avoids *illuminant-* and *observer-metamerism*[12] (see Fig. 2.14 and 2.15), the spectral raw data must be captured and reproduced rather than only colorimetric values.

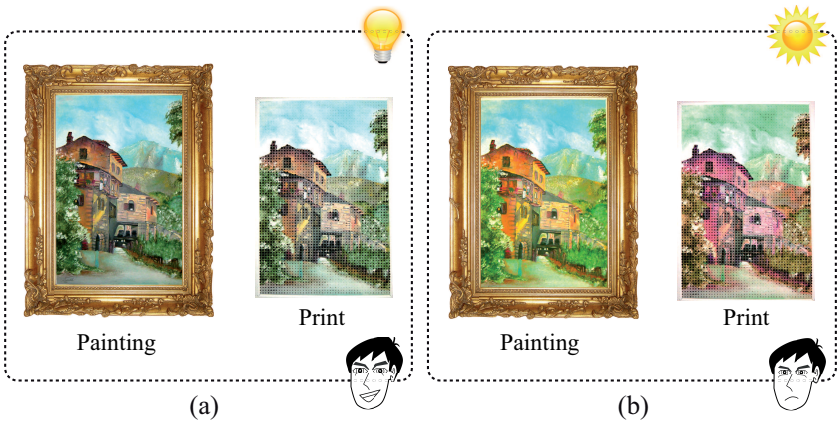

Figure 2.14.: A comparison between (a) illuminant-match and (b) illuminant-mismatch (*illuminant-metamerism*) in a metameric image reproduction workflow. In this example the illuminant is changed, however the painting is observed by the same observer.

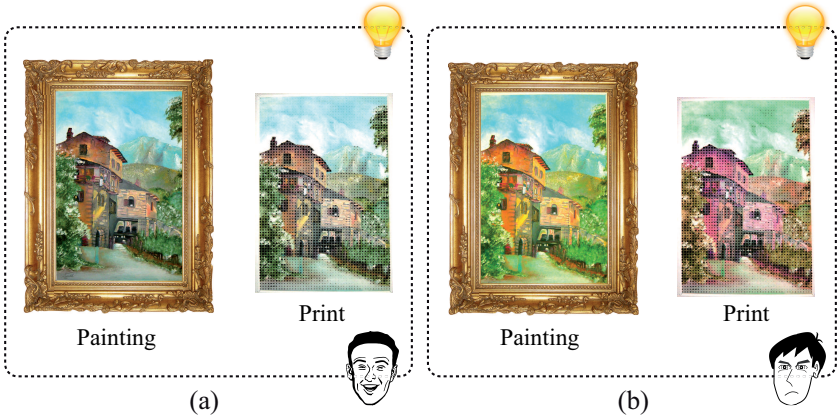

Figure 2.15.: A comparison between (a) observer-match and (b) observer-mismatch (*observer-metamerism*) in a metameric image reproduction workflow. In contrast to Fig. 2.14, in this example, the illuminant is constant; however, the painting is observed by two different observers.

[12] Spectrally dissimilar stimuli may nonetheless lead to the visual perception of similarity. In this case, the corresponding reflectances are called *metamers*. The *illuminant* and *observer-metamerism* are defined for cases where a shift in visual perception occurs due to changes in illumination and observer respectively [Ber00].

More research has been carried out on the capturing stage in the past decade. Nowadays, spectral cameras and scanners are commercially available. The captured spectral image from these devices can be used as input to a spectral-based printing procedure known as *spectral printing workflow*.

2.4.3. Spectral Printing Workflow

Similar to the metameric image reproduction pipeline, a spectral image reproduction workflow consists of two stages: *capturing* and *printing*. This workflow has the general aim of illuminant- and observer-invariant match between the original scene and final reproduction.

There are major and minor differences between the input/output devices used in spectral reproduction and those utilized in the metameric workflow. During the capturing stage, a multi-spectral camera must be used instead of a typical RGB-camera in order to capture the spectral raw data (spectral image R) – rather than only RGB values – from the scene. For doing this, multi-spectral cameras use filters or other instruments which are sensitive to different wavelengths. The dimension of the captured spectral image is determined via the number of sampled values in the visible wavelength range; e.g. by sampling from 400 to 700 *nm* by steps of 10 *nm*, the spectral image has 31 dimensions per pixel.

A multi-channel printer (e.g. CMYKRGB) must be utilized during the printing stage rather than a conventional 3- or 4-channel printer. This is required in order to expand the *spectral gamut* of the printer which is denoted by $\mathcal{G}$ and is defined as the set of all printable reflectances reproducible by a printing system (consisting of the printer, used halftone, employed inks, and media). Note that the spectral printer gamut is independent of the illumination condition. Equation (2.6) represents the relationship between the spectral and colorimetric printer gamuts, $\mathcal{G}$ and G.

$$G(I,\mathcal{G}) = L(\Upsilon(I,\mathcal{G})), \tag{2.6}$$

where I is an arbitrary illuminant, and L is a transformation from the CIEXYZ tristimulus values (see Eq. (2.2)) to e.g. CIELAB or LAB2000HL color space.

There are two main approaches for spectral reproduction:

- Pre-Built Transformations
- Direct Computations

The former is similar to the metameric (e.g. ICC-based) workflow in which *input* and *output profiles* are built via transformations between the input/output devices and a *Profile Connection Space* (PCS) required for device-independent spectral communication. Since the spectral space has a high number of dimensions (in comparison to three-dimensional color spaces), building spectral look-up tables (S-LUT) such as ICC-based LUTs is not practical in this space. Different research has been done to reduce the high-dimensional spectral space (roughly 31-dimensions if sampled in the [400,700] *nm* visible wavelength range by steps of 10 *nm*) to a low-dimensional space known as *Interim Connection Space* (ICS) such as: LabPQR (6-d) [DR06, RD06, TRB07], synthetic illuminants-based space (e.g. XYZXYZ (6-d)) [ZWL*12], and LabAB (5-d) [LU14] (d refers to dimension).

The latter approach, used in spectral reproduction workflow, is based on direct computations from the high dimensional space to the printer's final colorant combinations.

Different strategies and algorithms from those employed in metameric workflows must be used in a spectral reproduction pipeline. These methods are required for both the capturing and the printing stages to be able to

process the multi-spectral camera response and to perform spectral printing. Figure 2.16 is a block diagram representing the spectral image reproduction workflow.

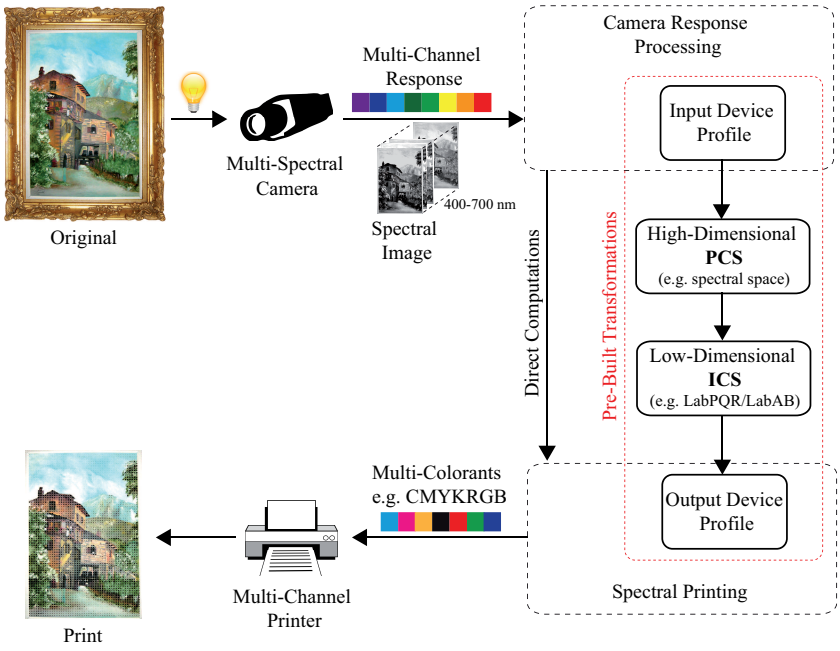

Figure 2.16.: Spectral image reproduction workflow.

To discern the advantage of spectral reproduction compared to metameric workflow, multiple illuminants must be considered. One aim of the *spectral printing workflow* is to be as good as metameric reproduction for a specific illumination condition and to be better (than the metameric reproduction) for the rest of the illuminants in question.

There are many different applications of spectral printing workflow including, but not limited to: security printing, spectral prepress proofing[13], accurate industrial color communication, and the accurate reproduction of artwork and cultural heritage.

The main steps required in this workflow are similar to those used in metameric reproduction (see Fig. 2.9). A general definition of these steps is given as follows:

2.4.3.1. Spectral Gamut Mapping

Spectral gamut mapping is defined by a process for mapping out-of-spectral gamut reflectances into the spectral gamut of the printer, $\mathcal{G}$ (see Fig. 2.17).

[13] In general, *prepress proofing* is used for customer verification prior to running the main press. In metameric reproduction workflows, this depends on the used illuminant. The aim of *spectral proofing* is the client verification invariant to changes in illumination condition.

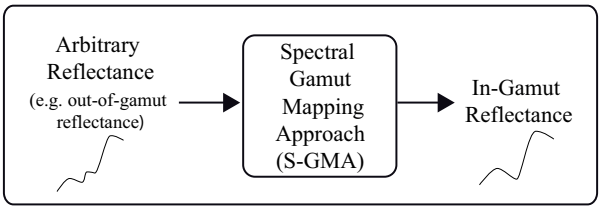

Figure 2.17.: Schematic representation of spectral gamut mapping.

2.4.3.2. Spectral Separation

Spectral separation is defined by a process for choosing appropriate colorant combinations for printing the gamut-mapped spectra. Similar to the colorimetric separation, there are two main ways in which spectral separation can be performed:

1. Inverting the *spectral printer model* (SPM), i.e. $SPM^{-1} : \mathcal{G} \rightarrow \Omega$, where $\mathcal{G}$ is the spectral printer gamut and Ω is the set of all printable colorant combinations defining the printer colorant space.
2. Solving a constrained optimization problem in cases where the SPM is not analytically invertible.

It is noteworthy that the SPM predicts reflectances from the printer colorant combinations (e.g. CMYKRGB) and their corresponding fractional area coverages, i.e. $SPM : \Omega \rightarrow \mathcal{G}$.

Figure 2.18 is a schematic representation of the spectral separation process as an inversion of the forward spectral printer model.

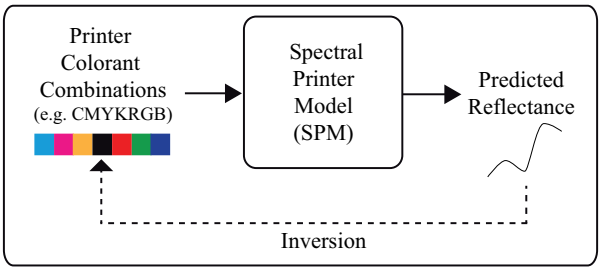

Figure 2.18.: Schematic representation of spectral separation process as an inversion of the forward spectral printer model (SPM^{-1}).

2.4.3.3. Multi-Channel Halftoning

Multi-channel halftoning is defined by a process for arranging multi-ink droplets (e.g. CMYKRGB) on the substrate used.

2.4.3.4. Multi-Channel Ink Limitation

Multi-channel ink limitation is defined by a process of restricting the amount of deposited inks depending on the used substrate and the superimposed colorants in a multi-channel printer (e.g. CMYKRGB). Various ink

limitation algorithms have been designed and developed for metameric printing workflow, which can also be used in spectral reproduction. These algorithms can be used either as part of the process of printer characterization and modeling [CBT04], or as a separate stage following the separation procedure [Urb07], [Urb09].

2.4.4. Challenges in Spectral Printing Workflow

Employing three- or four-ink printers (e.g. CMY or CMYK), which is common in metameric reproduction, seems to be impractical in spectral printing. This is due to the small spectral gamuts they provide. When using these kinds of printers, it is very likely that reflectances of spectral images lie outside the printer's spectral gamut. Therefore, utilizing multi-channel printers, e.g. CMYKRGB, is highly recommended in a spectral printing workflow. This is essential for expanding the printer spectral gamut and, consequently, the probability of in-gamut reflectances.

There are different challenges associated with the spectral printing workflow:

1. One of the challenges related to multi-ink printers is their *spectral characterization* and *modeling*. A spectral printer model (SPM) is a prediction function from the printer colorant space (Ω) to spectral space (printer spectral gamut $\mathcal{G}$). The available spectral printer models use a number of printed and measured color patches to predict spectra from the fractional area coverages of the printer colorants. As an example of these models, we can refer to Cellular-Yule-Nielsen-Spectral-Neugebauer (CYNSN) models [YN51, YC51, Vig85, Vig90] in which the required number of training samples is exponentially related to the number of utilized inks [USD13]. New models are needed if the number of training patches required is to be reduced. For more information regarding spectral printer models please refer to [CBT04], [WB00], [TB01], [Bal99], [RBH10], [BBH08], [HC05], and [HH14].

2. Another challenge in spectral printing is related to *spectral gamut mapping* which is much more complex than conventional metameric gamut mapping due to the high-dimensionality of the spectral space. Since the spectral printer model only provides the spectral printer gamut implicitly, having access to its boundaries is a further challenge requiring new strategies and methods [USD13]. It is noteworthy that spectral gamut mapping is always required even for multi-channel printers. This is due to the fact that the spectral gamut of any printing system is always much smaller than all natural reflectances. If only the reproduction of in-gamut reflectances is desirable, any spectral gamut mapping procedure can be ignored [USD13], [TB98], and [TB99].

3. Another challenge is related to the metrics used in the spectral space, which are not well correlated with human color perception. Therefore, even small spectral differences based on spectral metrics may lead to large perceived color differences between the original image and the printout under different viewing conditions. Hence, considering the properties of human color vision is essential. For more information on *spectral metrics*, please refer to [Vig04] and [IRB02].

4. Another challenge in spectral reproduction is *spectral separation*. Each pixel of any spectral image is represented by a N-dimensional array where N depends on the sampling step (which is usually 10 *nm*), in the visible wavelength range: 400-700 *nm*. In order to find the fractional area coverages of colorant combinations, the forward *spectral printer model* (SPM) that goes from M-dimensional colorant space (Ω) to N-dimensional spectral space ($SPM : \Omega \rightarrow \mathcal{G}$) usually has to be inverted for each image pixel ($SPM^{-1} : \mathcal{G} \rightarrow \Omega$). Please note that M refers to the number of utilized inks in a printing system. Therefore, the dimensionality of the problem is much greater than that in metameric reproduction. This high-dimensionality is a critical issue for encoding the aforementioned transformation, using multi-dimensional look-up tables [USD13]. As mentioned in Section 2.4.3, some attempts have been made to transfer the high-dimensional spectral data to a low-dimensional space called *Interim Connection Space* (ICS). This transformation is practical bacause spectral reflectances are smooth. This allows them

to be shown in a lower-dimensional space by reducing the number of components [PHJ89, Dan92, Har02]. The number of dimensions required in order to represent any spectral reflectance with reasonable precision, is still not clearly determined; however, reducing the number of components to 3-21 sample points is suggested [Har02]. So far, few Interim Connection Spaces (ICSs), such as LabPQR (6-d) [DR06, RD06, TRB07], synthetic illuminants-based space (e.g. XYZXYZ (6-d)) [ZWL*12], and LabAB (5-d) [LU14], have been introduced (d refers to dimension).

2.5. Summary

In this chapter, a brief introduction to printing technologies followed by basics of colorimetry was presented as the required fundamental knowledge prior to more in detail explanations.

Two printing workflows known as metameric and spectral reproduction workflows together with their image processing steps (gamut mapping, separation, halftoning, and ink limitation) were introduced. The dependency of the metameric reproduction workflow to a predefined viewing condition, i.e. a specific illuminant and an observer, was discussed as a limitation associated with this workflow.

The spectral printing workflow was introduced and recommended to be used for applications in which the colorimetric accuracy is required under a variety of viewing (specifically illumination) conditions in order to obtain an (ideally) illuminant-invariant match between the original image and the printout.

The challenges associated with the spectral reproduction, which are mostly related to the high-dimensionality of the spectral space, were also discussed. This high-dimensionality specifically increases the complexity of the spectral gamut mapping compared to traditional colorimetric gamut mapping. In the following chapter, the current state-of-the-art spectral gamut mapping approaches (S-GMAs) are discussed prior to presenting the proposed spectral gamut mapping method in Chapter 4.

3. Spectral Gamut Mapping - a Survey

As mentioned in the previous chapter, in order to have an invariant match (across a variety of illuminants) between the original image and the printout, the spectral reproduction workflow is considered. This printing workflow has applications in (for example) security printing, spectral proofing, accurate universal and industrial color communication, and artwork and cultural heritage reproduction.

In this workflow, the aim is to reproduce the original so that the resulting spectral print will be as good as metameric reproduction under a specific chosen illumination condition, and will be better than the metameric reproduction for the rest of considered illuminants.

The first step in a spectral printing workflow – which is the focus of Chapters 3 and 4 – is *spectral gamut mapping*, required for mapping any out-of-gamut reflectance into the spectral gamut of the printer, i.e. $r \rightarrow \hat{r}$, where r is any out-of-gamut reflectance which is mapped into an in-gamut spectrum $\hat{r}$.

We denoted the printer spectral gamut by $\mathcal{G}$ which is defined as the whole set of reflectances printable by a specific printing system (consisting of the printer, the halftone used, the inks employed, and the medium). Thus, the spectral printer gamut is defined independent of the illumination condition.

In general, *spectral gamut mapping approaches* (S-GMAs) can be divided into three main categories:

- *Spectral Space-Based Approaches*
- *Perceptual and Spectral Space-Based Approaches*
- *Multi-Illuminant Perceptual Space-Based Approaches*

The methods of the first group (spectral space-based approaches) merely operate within the spectral space. Such approaches are usually based on minimizing spectral differences using spectral metrics. One of the advantages of spectral metrics is that they are independent of the viewing condition because they are directly applied to spectral reflectances. However, a noticeable shortcoming associated to these metrics is that they do not take into account the properties of the human visual system (HVS). Therefore, even small spectral differences may result in large perceptual color errors [BFH05]. For a comprehensive overview on spectral metrics please refer to [IRB02] and [SPGH14].

The spectral gamut mapping methods of the second category operate within both the perceptual color and spectral spaces.

Whilst the approaches belonging to the aforementioned two groups are only or partially performed in the spectral space, the methods of the third group operate mainly in perceptual color spaces defined via a hierarchy of application-dependent illuminants, sorted from most to least important in an underlying application. These approaches compute the color accuracy of the reproduction across all considered illuminants using color-difference formulas (e.g. CIEDE2000 [CIE01]) which are more correlated with human perceived color differences.

Although wide research has been conducted in metameric gamut mapping, few attempts have been made from the spectral point of view. In Sections 3.1 to 3.3, some of the methods proposed for spectral gamut mapping –

belonging to the aforementioned categories – are briefly explained and discussed.

It is worth mentioning that there are some other spectral gamut mapping approaches (e.g. [KTH*99]) which are directly related to the halftoning process and are not considered in this dissertation.

3.1. Spectral Space-Based Approaches

In general, the performance of gamut mapping approaches (GMAs) that rely on detection of gamut boundaries, largely depends on the *Gamut Boundary Descriptor* (GBD) methods used. These methods are used for approximately describing the extent of the gamut (i.e. gamut boundary) [Mor08] and are defined mostly for metameric workflows. A common approach used for determining the metameric gamut boundary of a printer is *convex hull*[1]. This approach has also been used for finding the spectral gamut boundary of a printing system [HS01]. It is mostly in spectral space-based approaches that the spectral gamut boundary needs to be determined. In the next section, one of these methods is presented.

3.1.1. Spectral Gamut Mapping in Spectral Space - Approach I

The spectral gamut mapping approach (S-GMA) proposed by Bakke et al. [BFH05] is an example of a spectral space-based method where the concept of convex hull is used as a spectral GBD. Using spectral measurements as the initial points, they found the approximation of the spectral gamut boundary using a convex hull algorithm such as *quickhull* [Bar96]. It is essential to make an assumption that the measurements that define the spectral gamut, compose an object which is convex.

The captured spectral data is almost always described in a high-dimensional space, usually 31 samples in the range of 400 to 700 *nm* in 10 *nm* steps. It has been shown that spectral reflectances usually tend to be smooth, with some recurring patterns [PHJ89, Dan92, Har02]. This fact enables their representation in a lower-dimensional space. The number of dimensions required in order to represent any spectral reflectance with reasonable precision is still not clearly determined; however, reducing the number of dimensions to 3-21 sample points is suggested [Har02].

Principal Component Analysis (PCA) [And63] is an approach used to alleviate the number of samples in a high-dimensional data-set such as spectral measurements [Har02, ITHM96].

Bakke et al. [BFH05] utilized the PCA to represent the measured spectral reflectances in a low dimensional space in order to reduce the complexity of spectral gamut boundary determination by means of convex hull.

If an arbitrary point (reflectance) is inside the convex hull, it is considered to be an in-gamut reflectance; otherwise, it is an out-of-gamut spectrum [BFH05]. This definition is useful for conducting the spectral gamut mapping. It should be mentioned that any arbitrarily given reflectance must be transformed into the same PCA-based space utilized for dimension-reduction of the spectral gamut. Then, for each reflectance which is inside the PCA-based space, an individual 2D plane is built (as a cross section) based on two vectors: a vector from the gamut center to the given reflectance, and another line which represents the medium gray component.

If the reflectance is on the outside of the boundary of the relevant gamut cross section, clipping is applied towards an inner point, i.e. an in-spectral gamut reflectance. This transformation continues until the gamut surface is encountered. Bakke et al. [BFH05] suggested using the center of the gamut cross section as the inner-point. This is similar to applying clipping towards the center of a color space (e.g. CIELAB) in conventional metameric gamut

[1] The convex hull of a specific set of points is the smallest convex set containing all those points.

mappings [BFH05]. The in-spectral gamut reflectances remain unaffected. Figure 3.1 is a schematic representation of a spectral gamut cross section together with in- and out-of-gamut reflectances and the clipped spectrum.

The result of the proposed S-GMA by Bakke et al. [BFH05] is influenced by the inaccuracies introduced by employing the PCA and spectral GMA, i.e. clipping in a PCA-based spectral space. These errors occurred due to the deviations of the PCA-based and gamut mapped reflectances from the original out-of-spectral gamut reflectance. They used spectral RMS differences in order to calculate these errors (E_{RMS}).

The spectral RMS difference is a spectral metric defined as the spectral root-mean-square error computed between two spectra (see Eq. (3.1)).

$$RMS = \sqrt{\frac{1}{n'}\sum_{i=1}^{n'}[r_1(\lambda_i) - r_2(\lambda_i)]^2}, \tag{3.1}$$

where r_1 and r_2 are two arbitrary reflectances, and λ is the visible wavelength range (approximately [380,730] *nm*) which is sampled in n' separate values.

The comparisons between the original reflectance, the PCA-based, and the gamut mapped reflectances were conducted considering different PCA spaces ranging from 2 to 8 dimensions. As Bakke and co-workers [BFH05] mentioned, one of the issues related to choosing an appropriate number of dimensions is the lack of a precise metric for determining whether two reflectances are sufficiently equal.

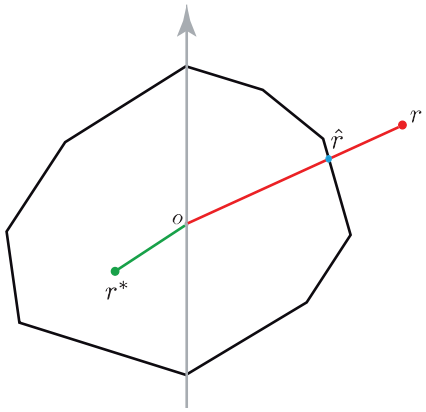

Figure 3.1.: A spectral gamut cross section together with (o) the center, (r^*) in-gamut, (r) out-of-gamut, and ($\hat{r}$) spectrally gamut-mapped (clipped) reflectances. The gray line represents the medium gray component. This figure has been taken from [BFH05] and re-sketched.

According to their reported results, the E_{RMS} after applying PCA, i.e. $E_{RMS}(PCA)$, decreases by increasing the number of dimensions, while, the inaccuracy imposed by the clipping strategy, i.e. $E_{RMS}(S-GMA)$, increases. Therefore, for PCA spaces with more dimensions it is important to enlarge the approximation of the spectral gamut using an appropriate number of spectral measurements [BFH05].

3.1.2. Shortcoming

One drawback associated with the spectral gamut mapping method proposed in [BFH05], and with spectral space-based spectral gamut mapping approaches in general, is related to the metrics (e.g. RMS error) used in the spectral space. These metrics are not well correlated with human visual perception. Therefore, even small spectral differences may lead to large perceptual color errors and, consequently, an inaccurate reproduction.

3.2. Perceptual and Spectral Space-Based Approaches

In contrast to the spectral gamut mapping method presented in Section 3.1.1, which merely operates in the spectral space, there are other approaches which are based on joint perceptual-spectral spaces. In the next two subsections, two of these methods are presented. Both methods operate in the LabPQR [DR06] space. Therefore, prior to explaining them, a short introduction to LabPQR space is presented. For more information, please refer to [DR06].

3.2.1. LabPQR Interim Connection Space

LabPQR is a six-dimensional *Interim Connection Space* (ICS) where the first three components, Lab, are the colorimetric CIELAB values calculated for a specific viewing condition. These values construct the perceptual colorimetric space. The next three coordinates, PQR, describe the *metameric black* space.

According to the Wyszecki hypothesis [Coh01], the human color vision processing system only considers a portion of the color stimulus available, while ignoring the rest. The part of the stimulus that gets considered is called the *fundamental color stimulus*, and includes information required for color sensation. The remaining part is termed *residual* or *metameric black* and does not carry any data for color sensation. However, it evokes the black which is interpreted as null color sensation. This can be formulated simply via Eq. (3.2) [Coh01] using three vectors containing tristimulus (CIEXYZ) values.

$$C = C^* + E, \tag{3.2}$$

where C represents any color stimulus, C^* is the *fundamental* of color stimulus C, and E is its *residual* or *metameric black* part.

Referring to Eq. (2.2), identical color sensation is experienced by metameric reflectances (e.g. r_1 and r_2). In this case, their computed tristimulus values are exactly equal for a certain viewing condition (an illuminant and observer), i.e. $X_1 = X_2$, $Y_1 = Y_2$, and $Z_1 = Z_2$. A reflectance is called *metameric black* when it results in: $X = Y = Z = 0$ [vT94]. Theoretically, *metameric black* refers to any reflectance that does not evoke color sensation [Coh01].

For composing the LabPQR ICS, the first step is building the colorimetric space. For this purpose, each reflectance given (r) needs to be converted to CIEXYZ tristimulus values (see Eq. (2.2)) and thence to CIELAB colorimetric coordinates for a specific viewing condition, i.e. $L : CIEXYZ \longmapsto CIELAB$ (for exact transformation from the CIEXYZ tristimulus values to CIELAB coordinates, please refer to [Ber00]).

The next step is finding the metameric black space for each CIELAB value, in order to construct the spectral space. The spectral differences between the original and a set of metameric reflectances reconstructed from each CIELAB value are calculated thereby. These spectral differences yield the metameric black space. By applying the PCA to the resulting spectra, and choosing the first three components (eigenvectors), a spectral PQR space is

constructed for each CIELAB value [TRB07].

Therefore, we can refer to the LabPQR space as a 6-dimensional hybrid ICS obtained from the transformation of the spectra into three explicit colorimetric coordinates (Lab) and three spectral reconstructed axes (PQR). In this ICS, there is a nested 3-dimensional spectral gamut (PQR) for each CIELAB value, providing an easy strategy for reducing the complexity of the spectral gamut, in terms of visualization (see Fig. 3.2).

3.2.2. Spectral Gamut Mapping in LabPQR - Approach I

Rosen and Derhak [RD06] proposed a spectral gamut mapping approach based on the LabPQR space. In this method, there are two main steps: *colorimetric* and *spectral*.

After converting any spectral request for printing to LabPQR values, e.g. L*a*b* = (75, 65, 60) and PQR = (0.161, 0.01, 0.004), it must be determined whether the calculated CIELAB values are inside the colorimetric gamut of the printer. In case they are out-of-gamut, a traditional colorimetric gamut mapping approach (C-GMA) [Mor08] is used to obtain in-gamut colorimetric values. This process is performed in the first (i.e. colorimetric) step. Figure 3.2 [TRB07] represents an approximation of a nested PQR gamut (via sampled points) for an in-gamut CIELAB value. This figure has been taken from [TRB07] and re-sketched. Although an approximation of the entire colorimetric gamut of an arbitrary printing system is illustrated in this figure via sampling, only one of the sampled PQR-nested gamuts associated with one of the colorimetric values, is shown.

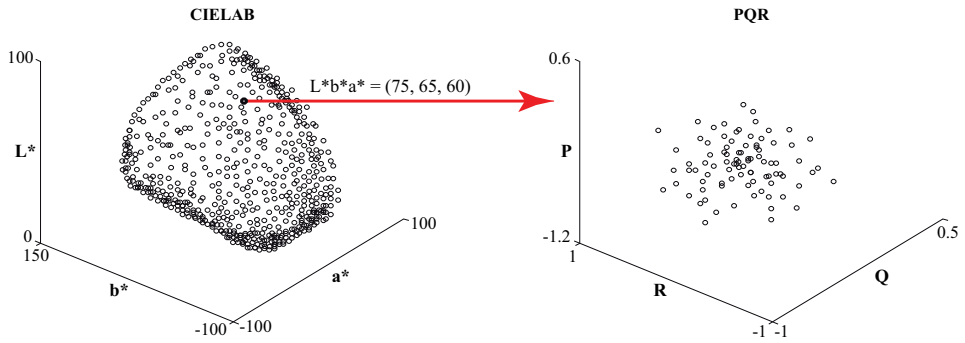

Figure 3.2.: Simplistic representation of the LabPQR ICS. This figure has been taken from [TRB07] and re-sketched.

In the second (i.e. spectral) step, a nested PQR spectral gamut associated with the in-gamut CIELAB value, i.e. L*a*b* = (75, 65, 60) in our example, must be found. Then, it must be determined whether the initial PQR values, i.e. PQR = (0.161, 0.01, 0.004) in our example, are inside the extracted nested PQR gamut. If they are out-of-gamut, spectral PQR gamut mapping must be performed.

Different spectral PQR gamut mapping strategies were employed by Rosen and Derhak [RD06], which are called: *closest PQR, closest (scaled PQR) = (normalized PQR), closest P, closest Q, closest R*, and *furthest PQR*. All of these techniques are based on the spectral PQR distance, i.e. the Euclidean distance between the requested PQR values and those inside the spectral PQR gamut. In the first two methods as well as the last one, all of the three PQR coordinates were considered for the comparison, while in the rest, only one of them (P or Q or R) took part in the gamut mapping strategy.

According to their experiments, minimizing the PQR distances leads to lower spectral RMS errors. Since the

PQR values are calculated by applying the PCA to the spectral error, it is expected that spectral minimization would be achieved by minimizing the PQR values, which is in accordance with their reported result. However, the lowest spectral RMS error does not necessarily ensure the lowest CIEDE2000 color-difference for all illuminants. This result is also predictable because spectral RMS differences are not well correlated with human color perception and colorimetric errors.

3.2.3. Spectral Gamut Mapping in LabPQR - Approach II

It is noteworthy that the spectral gamut mapping strategy used by Rosen and Derhak [RD06] was tested only in the PQR space, while no evaluation was performed in the entire LabPQR ICS. Moreover, their methodology considers the colorimetric and spectral mappings in two separate steps. Therefore, Tsutsumi and co-workers [TRB07] conducted research in order to investigate the feasibility of spectral gamut mapping in the entire LabPQR space, considering the *colorimetric* and *spectral* criteria dependently and in a single stage. Their objective, defined as follows, was to minimize the weighted sum of spectral and colorimetric parameters [TRB07].

$$Minimize(\Delta E_{00} + K'\Delta PQR), \tag{3.3}$$

where ΔE_{00} is the CIEDE2000 [LCR01] color-difference formula, ΔPQR is the normalized Euclidean distance in the PQR space which is proportional to the spectral RMS error [TRB07], and K' is a weighting parameter that is set empirically.

This objective can be used in any case, regardless of whether the requested reflectance is inside the printer colorimetric or spectral gamut. If the reflectance requested is within the colorimetric gamut, the first parameter of this objective is discarded and only the second part remains active (see Fig. 3.3 [TRB07]). If the spectrum requested is outside the colorimetric gamut, both parts are considered in the gamut mapping process. A traditional colorimetric gamut mapping strategy followed by a spectral gamut mapping method based on the spectral RMS error, are employed in this scenario (see Fig. 3.4 [TRB07]).

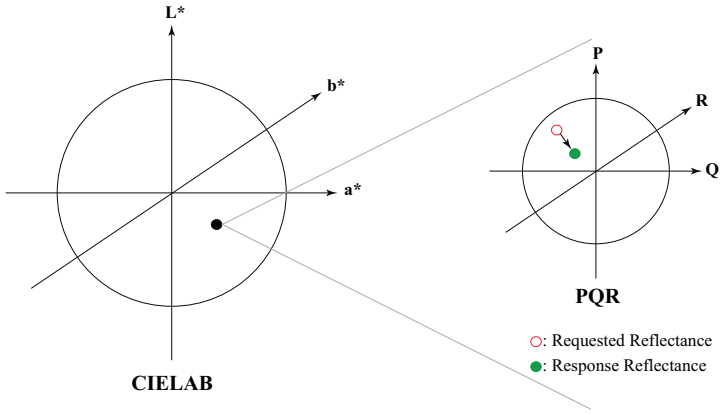

Figure 3.3.: Spectral gamut mapping when the requested reflectance is inside the colorimetric gamut. This figure has been taken from [TRB07] and re-sketched.

A compromise between colorimetric and spectral accuracy can be achieved by tuning the weighting parameter K'. Larger values of K' lead to higher relative importance of spectral accuracy, while smaller K' values result in

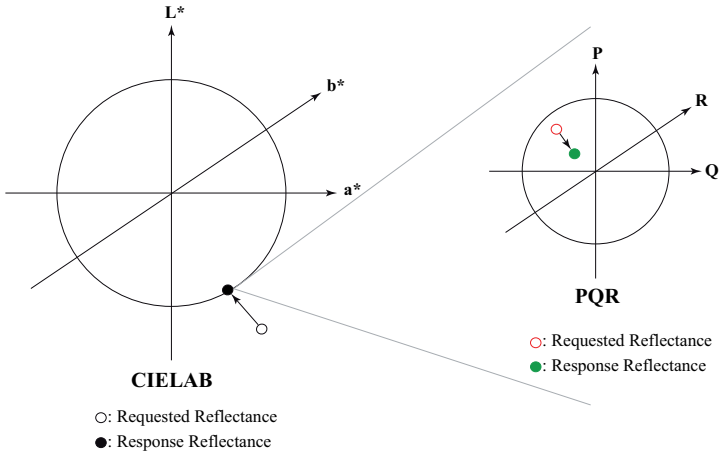

Figure 3.4.: Spectral gamut mapping when the requested reflectance is outside the colorimetric gamut. This figure has been taken from [TRB07] and re-sketched.

higher colorimetric accuracy. The best performance was found by setting $K' = 50$. However, this value is based only on a set of experiments conducted by Tsutsumi et al. [TRB07].

They explored the feasibility of the proposed spectral gamut mapping approach in comparison with two other cases: 1) Using the high-dimensional (31-d) (d refers to dimension) spectral space instead of 6-d LabPQR ICS. 2) Employing only the colorimetric part of the objective shown in (3.3) by ignoring the weighting parameter ($K' = 0$). The full 31-d and colorimetric-only approaches are expected to show better results in terms of spectral and colorimetric accuracy respectively.

In order to compare their method to the first case mentioned, the proposed objective shown in (3.3) was also considered in the 31-d spectral space. Instead of normalized PQR distances, spectral RMS differences were used. They conducted experiments using different arbitrary spectral data-sets containing the patches generated by a spectral printer model using a CMYKRG printer, GretagMacbeth ColorChecker, and Munsell samples.

In their results, the LabPQR and full-spectral approach showed equivalency in terms of spectral accuracy (spectral RMS error). No significant difference was found between the reconstructed reflectance from the LabPQR values and 31-d spectra. In comparison with the colorimetric-only approach, the LabPQR method showed noticeable improvements at longer wavelengths and where the original spectral curve had high fluctuations.
From the colorimetric point of view, no significant CIEDE2000 color differences were obtained for the CIED50 illuminant and 2° colorimetric standard observer. However, no information was reported regarding the colorimetric accuracies for other illuminants.

It is worth mentioning that in the spectral gamut mapping approaches mentioned in Sections 3.2.2 and 3.2.3, before applying the gamut mapping strategy the printing system needs to be spectrally characterized either by an empirical approach or a spectral printer model. This process is required in order to predict reflectances from fractional area coverages of the inks utilized in a printing system. Afterward, another conversion from the high-dimensional spectral space to the low-dimensional LabPQR ICS, is required. Finally, a mapping from the fractional area coverages of the colorants to LabPQR values must be performed. These three steps are illustrated in Fig. 3.5 [TRB07]. After conducting the gamut mapping process and obtaining the in-gamut LabPQR values,

an inversion of the aforementioned steps must be performed in order to find the fractional area coverages of the colorants required for printing the gamut-mapped LabPQR values.

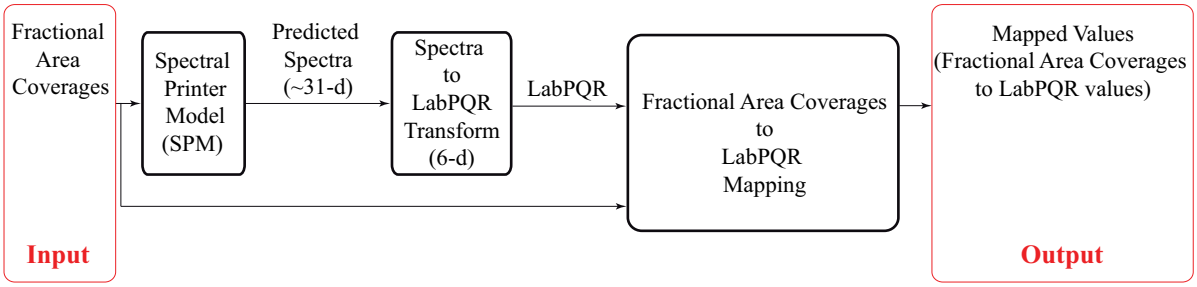

Figure 3.5.: Simple diagram representing the forward mapping from fractional area coverages to LabPQR values. This figure has been taken from [TRB07], re-sketched and slightly modified.

3.2.4. Shortcoming

The explained approaches in Sections 3.2.2 and 3.2.3, and the spectral gamut mapping methods which are partially performed in spectral (e.g. PQR) space in general, still have the tendency for large perceptual color errors. Although this probability has been reduced in comparison to fully spectral space-based approaches, via mappings in colorimetric spaces, the usage of spectral metrics (e.g. RMS errors, etc.) in the spectral space (e.g. nested PQR gamuts) may be the source of perceptual colorimetric errors.

3.3. Multi-Illuminant Perceptual Space-Based Approaches

Unlike the approaches explained in Sections 3.1 and 3.2, which totally or partially operate in spectral space, there are two other spectral gamut mapping methods, which only operate in perceptual (color) spaces, by taking different illumination conditions into account. In the following two subsections, these approaches are presented.

3.3.1. Metamer Mismatch-Based Spectral Gamut Mapping (MMSGM)

Urban et al. [URB08] proposed a framework for spectral gamut mapping which is based on human color vision. A hierarchy of application-dependent illuminants sorted from the most to the least important one, $I_1, I_2, \ldots, I_n$, is considered in this framework. The result of final reproduction using this framework varies by changing either the considered set of illuminants or their order.

Interestingly, if the reproduction matches the original image under all of the considered illuminants, it also matches the original image under any mixture of these illuminants [Urb05]. Therefore, this multi-illuminant structure is especially useful for environments where the illumination condition is blending between pre-set illuminants [URB08].

In this framework, the metameric/colorimetric gamut G[2] of the printer has to be determined for the first illuminant in question. This can be done in different ways depending on the implementation strategy. However,

[2]The metameric/colorimetric printer gamut G is the set of all colors printable via a printing system considering a specific illuminant.

the most straight-forward way is to go from the printer colorant space Ω[3] to the colorimetric printer gamut G in two steps: 1. Applying the spectral printer model (SPM) to the whole set of printable colorant combinations Ω to approximately predict the spectral printer gamut $\mathcal{G}$[4], 2. Computing the corresponding tristimulus CIEXYZ values of all in-gamut spectra via Eq. (2.2) for the first considered illuminant I_1. The colorimetric values and consequently the colorimetric gamut G of the printer are then determined via another transformation from CIEXYZ values to coordinates of a hue-linearized color space, e.g. CIELAB [HB95] (i.e. $L : CIEXYZ \longmapsto CIELAB$). The printer colorant space Ω, the spectral printer gamut $\mathcal{G}$, and the metameric printer gamut G for the first illuminant I_1 are shown as schematic representations in Fig. 3.6.

The input to this framework is the spectral image R[5]. In the first step, this image must be rendered in colorimetric (CIELAB) images for all n illuminants, $I_1,...,I_n$. The result of this rendering process is n CIELAB images denoted by $L_1,...,L_n$.

In the next step, the rendered CIELAB image for the first illuminant, L_1, must be transformed into the metameric printer gamut G using a *traditional metameric gamut mapping* algorithm [ML01, Mor08] denoted by Γ_{Trad}. It is noteworthy that in addition to the pixel-wise traditional gamut mapping methods, *spatial gamut mapping* approaches [BSBB06] can also be employed in this stage. The result of the aforementioned process is an in-gamut CIELAB image denoted by $\widehat{L}_1$.

The same procedure, i.e. applying Γ_{Trad}, cannot be performed for the CIELAB image rendered for the second illuminant, L_2. This is because the traditional gamut mapping strategy cannot ensure the reproduction of gamut-mapped CIELAB colors for both illuminants (first and second) by in-gamut spectra. Therefore, the reproduction must be adjusted for the second illuminant.

Due to the colorimetric printer redundancy, there are probably different colorant combinations that can be used to print each in-gamut CIELAB value. Therefore, for each image pixel p_0, a *metameric set* $\zeta(p_0)$ is defined. Each pixel- and device-dependent metameric set contains all printable colorant combinations χ which result in exactly the same colorimetric (CIELAB) value for the first considered illuminant I_1. Equation (3.4) represents the definition of a metameric set.

$$\zeta(p_0) = \left\{ \chi \in \Omega \;\middle|\; \Delta E_{00}(P_1(\chi), \widehat{L_1}(p_0)) = 0 \right\}, \tag{3.4}$$

where χ is any colorant combination in the printer's colorant space Ω, ΔE_{00} is the CIEDE2000 color-different formula [SWD05], $P_1(\chi)$ is the color prediction of the printout under illuminant I_1 given the colorant combination χ, i.e. $P_1(\chi) = L(\Upsilon(I_1, SPM(\chi)))$ for a spectral printer model SPM (e.g. Cellular-Yule-Nielsen-Spectral-Neugebauer (CYNSN) model [YN51, YC51, Vig85, Vig90]) and color transformation $L : CIEXYZ \longmapsto CIELAB$, $\widehat{L_1}(p_0)$ is the CIELAB value at pixel p_0 extracted from the gamut mapped CIELAB image for the first illuminant, I_1.

Each metameric set $\zeta(p_0)$ leads to metameric reflectances (metamers)[6] for the first illuminant I_1. These device- and pixel-dependent metamers have to be intersected with the spectral gamut of the printer $\mathcal{G}$ to ensure in-spectral gamut metamer spectra.

Consequently, a device- and pixel-dependent *metamer-mismatch gamut*, μ, is defined for each image pixel p_0 by

[3] The printer colorant space Ω is defined as the whole set of colorant combinations printable by a printing system.

[4] The spectral printer gamut $\mathcal{G}$ is the set of all reflectances printable via a printing system and is independent of the illumination condition.

[5] The spectral image R is captured via a multi-spectral camera and has high dimensions. The number of dimensions (per image pixel) is defined via the number of sampled values in the visible wavelength range, e.g. 31-dimensions if the sampling is performed in steps of 10 *nm* in the range of [400,700] *nm*.

[6] The metameric reflectances (metamers) are reflectances resulting in exactly the same colorimetric (e.g. CIELAB) value for a specific viewing condition.

converting the corresponding metameric spectra – determined for I_1 and p_0 – to CIELAB values for the second illuminant, I_2. Note that since these CIELAB values may not be equal, the term "mismatch" is used.

The CIELAB values of the image rendered for the second illuminant, L_2, have to be mapped into their corresponding metamer-mismatch gamuts. Using this strategy, one ensures almost similar metameric reproduction of the gamut-mapped CIELAB image for the first illuminant, $\widehat{L}_1$, with non-noticeable changes. This is required since the aim of spectral reproduction is to be as good as metameric reproduction for at least one illuminant considered (here I_1) and be superior for the rest (here $I_2,...,I_n$).

Different strategies can be used for pixel-wise metamer-mismatch gamut mapping (denoted by Γ_{Meta}) in order to choose an appropriate CIELAB color – within each metamer-mismatch gamut μ – and consequently to select a colorant combination χ for reproduction of this color which belongs to the metameric set $\zeta(p_0)$.

These strategies include minimizing color differences or hue angle preservation. The pixel-wise equations (3.5)-(3.7) represent three strategies for metamer mismatch-based gamut mapping Γ_{Meta} used in [URB08].

$$\Gamma_{Meta}(x') = \underset{y' \in \mu}{\arg\min} \ \Delta E^*_{ab}(x', y') \tag{3.5}$$

$$\Gamma_{Meta}(x') = \underset{y' \in \mu}{\arg\min} \ \Delta E^*_{94(2:2:1)}(x', y') \tag{3.6}$$

$$\Gamma_{Meta}(x') = \underset{y' \in \mu}{\arg\min} \ \Delta E_{00(2:2:1)}(x', y'), \tag{3.7}$$

where x' refers to a CIELAB color to be printed, which is extracted from the rendered CIELAB image for the second illuminant. The metamer-mismatch gamut, μ, differs depending on the CIELAB value for each image pixel. ΔE^*_{ab}, ΔE^*_{94}, and ΔE_{00} are CIE76, CIE94 [CIE95], and CIEDE2000 [CIE01] color-difference formulas respectively. In equations (3.6) and (3.7), the k_L, k_C, and k_H coefficients used in CIE94 and CIEDE2000 color-difference formulas are set to 2, 2, and 1 respectively in order to provide hue accuracy with double the accuracy of lightness and chroma [URB08]. Generally, by setting $k_L, k_C > k_H$, distances in the hue direction are weighted more [BB83], [CBTI03].

Urban et al. [URB08] employed the "hue and lightness preserving, chroma clipping" approach as the strategy for traditional gamut mapping, Γ_{Trad}. Minimizing CIEDE2000 (ΔE_{00}) color differences was utilized for the metamer mismatch-based gamut mapping, Γ_{Meta}, within metamer-mismatch gamuts.

The procedure applied to the second illuminant, I_2, must also be performed for any additional illuminant, $I_3, I_4, ..., I_n$, in a similar way. The CIELAB color of each pixel of the image rendered for any remained illuminant, can only be mapped into the corresponding specific device- and pixel-dependent metamer-mismatch gamut μ derived from the associated metamers and metameric set ζ.

Each set of metameric reflectances for the remaining illuminants is obtained via the intersection of two things: 1) the spectral printer gamut $\mathcal{G}$, 2) the intersected set of metameric spectra related to the previously gamut-mapped CIELAB values for all of the previous illuminants. These intersections are required firstly to ensure that each set of metameric reflectances is within the spectral gamut of the printer and, secondly, to protect the previous gamut mappings from noticeable changes. The intersection process is individually performed for each image pixel [URB08].

The results of the mappings performed proceed to the next stage as parameters leading to other transformations along with the corresponding illuminant. In this way, the reproduction is adjusted to a hierarchical set of application-dependent illuminants.

Finally, a separation image S[7] is generated as the result of hierarchical mappings and choosing appropriate in-gamut colorimetric (CIELAB) values and their corresponding printable colorant combinations.

Figure 3.6 is a simplified representation of the *metamer mismatch-based spectral gamut mapping* MMSGM framework proposed in [URB08]. For the sake of brevity, only two illuminants are considered in this figure.

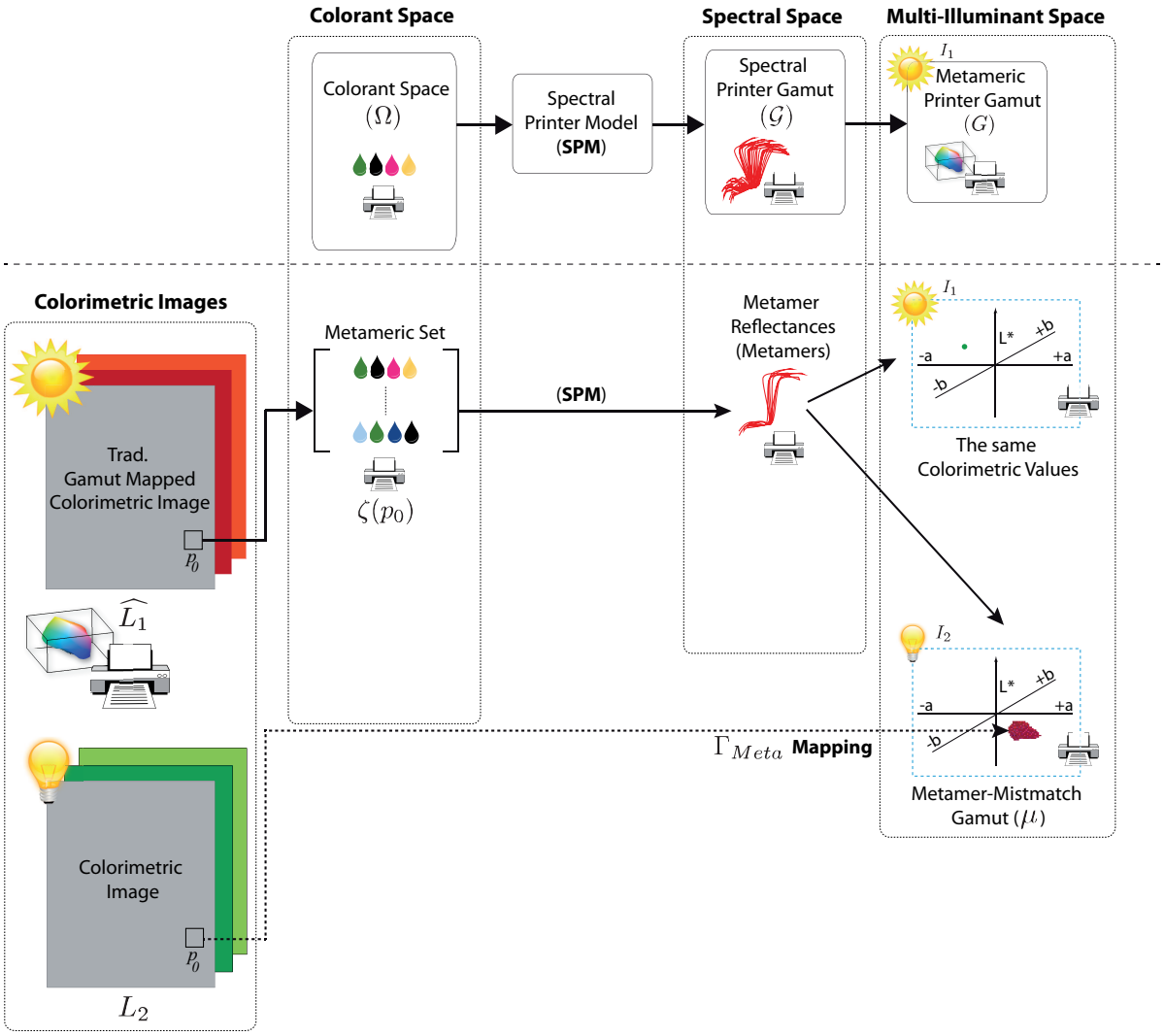

Figure 3.6.: Simplified representation of the *metamer mismatch-based spectral gamut mapping* (MMSGM) framework proposed by Urban et al. [URB08], considering two illuminants.

Note that the spectral image can be reconstructed from the gamut mapped CIELAB images across all illuminants considered. This spectral image will be in the spectral gamut of the printer.

[7] The separation image S is an image containing the printable colorant combinations for all image pixels.

In general, performing a traditional gamut mapping strategy Γ_{Trad} for the first illuminant decreases the degree of freedom possible for subsequent hierarchical mappings. This is due to the restriction applied by mapping merely in metamer-mismatch gamuts. Urban and Berns [UB11] extended the aforementioned spectral gamut mapping framework in such a way that it theoretically leads to expansion of mismatch-gamuts. The corresponding approach is explained in the next section.

3.3.2. Paramer Mismatch-Based Spectral Gamut Mapping (PMSGM)

The main concept of the PMSGM approach is based on the MMSGM method; the only difference is that in this approach, Urban and Berns [UB11] extended the MMSGM method by expanding the degree of freedom for gamut mappings inside mismatch-gamuts for the second and subsequent illuminants.

For this purpose, they defined and computed device- and pixel-dependent *parameric sets* τs and their corresponding parameric reflectances (paramers), instead of metameric sets ζs and metameric reflectances (metamers). Consequently, they determined *paramer-mismatch gamuts*, ρs, instead of metamer-mismatch gamuts, μs.

As mentioned previously, two reflectances are called *metamers* when they result in exactly the same color for a certain viewing condition (an illuminant and an observer), i.e. their corresponding color difference is exactly zero. Two reflectances are called *paramers* when they represent a non-noticeable color difference (below the Just Noticeable Difference (JND)) for a specific viewing condition. This definition is in accordance with Urban and Berns [UB11]. No other definition of paramers, determining a specific threshold value for distinguishing them from metamers, was found in the literature.

Based on this definition, each pixel-dependent parameric set $\tau(p_0)$ is defined as all printable colorant combinations which lead to parameric reflectances (paramers) and consequently almost the same colorimetric (e.g. CIELAB) values – with color differences below the JND – for the first considered illuminant, I_1.

The paramer-mismatch gamuts, ρs, are determined by transforming the pixel-dependent parameric reflectances (paramers) to colorimetric (CIELAB) values for the second illuminant, I_2. These paramer-mismatch gamuts, ρs, are defined instead of metamer-mismatch gamuts, μs, in order to increase the spectral variability of mismatch-gamuts, by utilizing the properties of the human visual system (HVS). Figure 3.7 is a schematic representation of a comparison between metamer- and paramer-mismatch gamuts, μ and ρ.

Similar to equations (3.5)-(3.7), *paramer mismatch-based gamut mapping* Γ_{Para} can be performed by minimizing color differences or hue angle preservation, in order to choose appropriate colorimetric (CIELAB) values within paramer-mismatch gamuts and, consequently, the corresponding printable colorant combinations. For the sake of brevity, only the first adjusted equation (analogous to Eq. (3.5)) is presented here. Equations (3.6) and (3.7) are similarly modified.

$$\Gamma_{Para}(x') = \underset{y' \in \rho}{\arg\min} \ \Delta E^*_{ab}(x', y'), \tag{3.8}$$

where all notations are as defined previously.

Urban and Berns [UB11] employed the "hue and lightness preserving, chroma clipping" approach as the strategy for traditional gamut mapping, Γ_{Trad}. Minimizing ΔE^*_{ab} color differences was utilized for the paramer mismatch-based gamut mapping, Γ_{Para}, within paramer-mismatch gamuts.

For each illuminant, a procedure similar to the one given in Section 3.3.1 must be performed in the 3-dimensional and hue-linearized [HB95] CIELAB color space using the concept of parameric sets, paramers, and paramer-mismatch gamuts. The results of the mappings performed proceed to the next stage as parameters, leading to

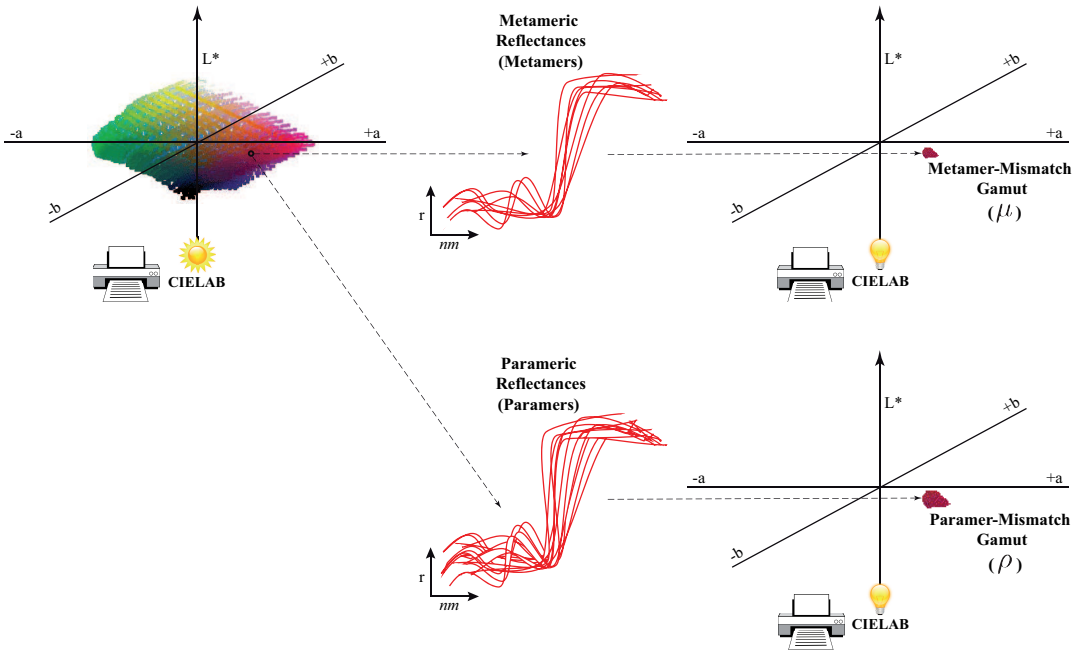

Figure 3.7.: Metamer-mismatch gamut (μ) vs. paramer-mismatch gamut (ρ).

other transformations along with the corresponding illuminant. In this way, the reproduction is adjusted to a hierarchical set of application-dependent illuminants.

Figure 3.8 is a simplified representation of the *paramer mismatch-based spectral gamut mapping* PMSGM framework proposed by Urban and Berns [UB11]. For the sake of brevity, only two illuminants are considered in this figure.

A separation image S is generated as the result of hierarchical mappings and choosing appropriate in-gamut colorimetric values and their corresponding printable colorant combinations.

Note that the spectral image can be reconstructed from the gamut mapped CIELAB images across all illuminants considered. This spectral image will be in the spectral gamut of the printer.

3.3.3. Shortcoming

The PMSGM method was shown to be a promising approach for spectral gamut mapping, since it is performed in multi-illuminant perceptual color spaces using color-difference formulas which are better correlated with the human perceptual color difference than the metrics used in the spectral space. However, this method generates unwanted *banding artifacts*. This is because, in this approach, the gamut mapping is performed pixel-wisely and independently of the spatial neighborhood. Therefore, neighboring pixels with almost similar colors (in the original rendered images) may be printed by completely different colorant combinations, which leads to discontinuities in the generated separation image S – even where the original image is smooth. Through the halftoning process, abrupt changes in dot placement may occur as a result of these discontinuities in the separation image which eventually lead to banding artifacts.

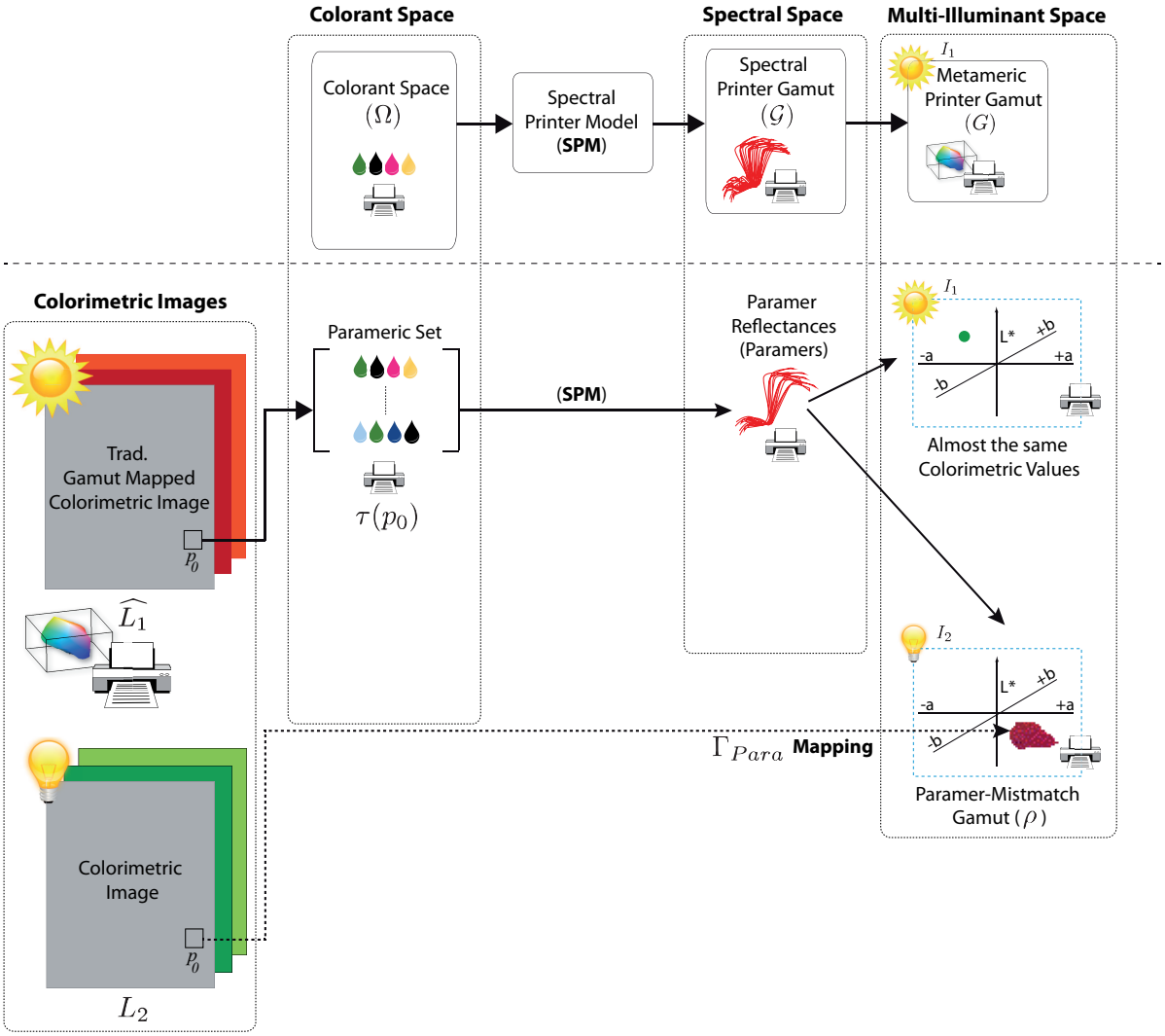

Figure 3.8.: Simplified representation of the *paramer mismatch-based spectral gamut mapping* (PMSGM) framework proposed by Urban and Berns [UB11] in a multi-illuminant perceptual space, considering two illuminants.

For avoiding such artifacts, Urban and Berns [UB11] suggested adding noise to the a* and b* channels of the CIELAB image rendered for the first illuminant prior to gamut mapping. Although this could solve the banding problem, it would also increase the *graininess* of the separation image and the printout. Figure 3.9 shows this problem. In this figure, a cutout of the METACOW spectral image [FJ04] is shown in (a). This cutout was taken as the input to the PMSGM framework.

It should be noted that the artificially-made METACOW [FJ04] image is a spectral image composed of 24 cows which has two specific aspects: 1. The rear part of each cow has the spectral reflectance of the GretagMac-

beth Color Checker, while the front part is the metameric black computed so that it shows metameric effect under CIED65 illuminant with maximum color difference under CIEA illuminant, 2. It is completely noise-free. Therefore, the METACOW [FJ04] image is considered as a challenging spectral image in terms of its spectral reproduction.

The aforementioned cutout of this image was rendered for CIED65 and CIEA illuminants. The corresponding colorimetric images are shown in Fig. 3.9 (b) and (c) respectively. By applying the PMSGM method, the separation image shown in (d) is generated. As can be seen, the banding artifacts are visible in this image. The separation image obtained as the result of adding noise to the a* and b* channels of the CIELAB image – rendered for the first illuminant – prior to gamut mapping, is shown in (e). In this image, the banding artifacts are diminished; however, the image graininess is increased. Please note that for the sake of brevity, only one channel of the 7-channel (CMYKRGB) image is shown in this figure where the increased amount of colorant combinations – per image pixel – is represented by a gradient from white (no ink = 0%) to black (full ink = 100%).

In the next chapter, we propose an approach based on the PMSGM framework for minimizing its associated banding and graininess artifacts.

3.4. Summary

In this chapter, five spectral gamut mapping approaches (S-GMAs) were explained which are categorized in three main groups based on their working space: fully spectral space-based methods, approaches which are employed partially in perceptual and spectral spaces and methods which are conducted only in multi-illuminant perceptual spaces.

In general, there is a major shortcoming associated with methods fully or partially performed in spectral space. This drawback is related to the metrics (e.g. RMS error) used in this space, which are not very well correlated with human color perception. Consequently, they can be the source of inappropriate mappings. The multi-illuminant perceptual space-based approaches are more promising. This is because they use color-difference formulas for gamut mappings which are better correlated with the human color perception compared to spectral metrics.

The second explained approach from this category, PMSGM [UB11] (which is the extended version of the first approach MMSGM [URB08]), leads to colorimetric accuracy across a hierarchy of application-dependent illuminants. However, due to its pixel-wise strategy, the local spatial content of the image is not considered which leads to unwanted banding artifacts.

In the next chapter, an approach is proposed as an improvement of this method for minimizing its associated artifacts by taking the colorimetric and spatial content of the image into account.

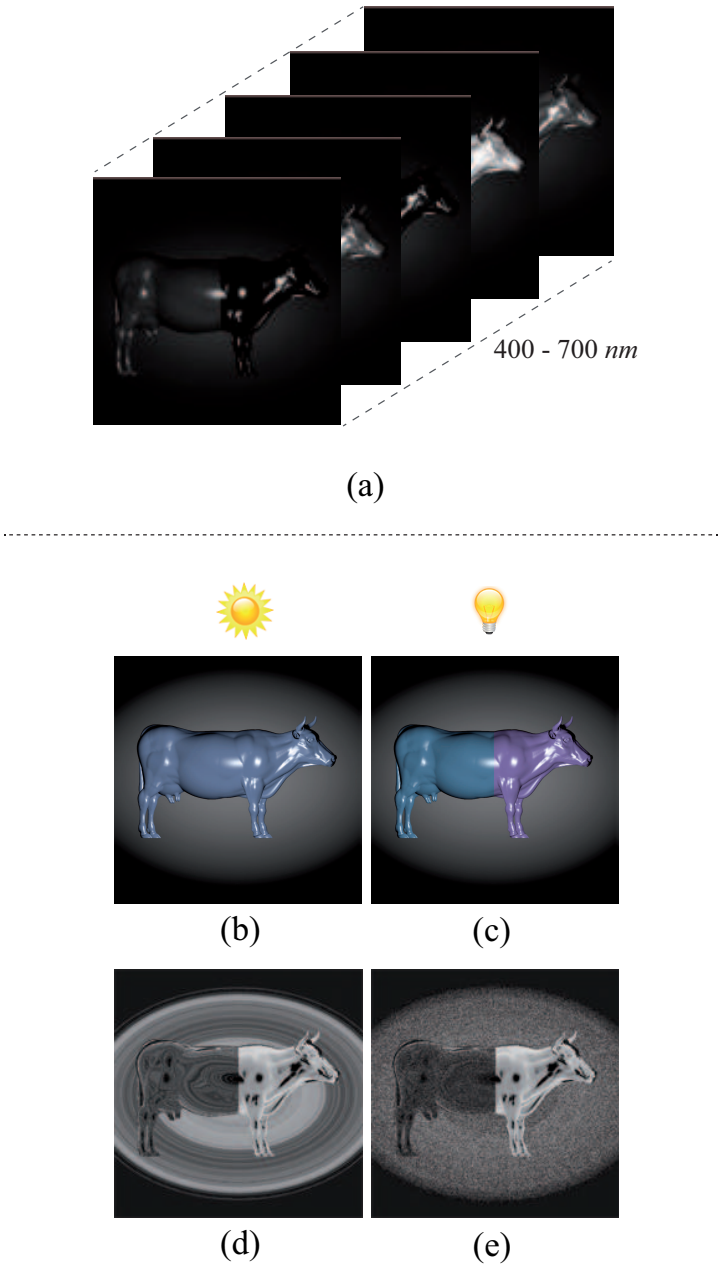

Figure 3.9.: A cutout of the METACOW [FJ04] spectral image (a), the rendered colorimetric images under CIED65 (b) and CIEA (c) illuminants, the separation images generated by applying the PMSGM method without addition of noise (d) and with noise addition to the a* and b* channels of the CIELAB image – rendered for the first illuminant – prior to gamut mapping (e). The *banding* and *graininess* artifacts are visible in (d) and (e) respectively. For the sake of brevity, only one channel of multi-channel separation images is shown where white = 0% ink and black = 100% ink deposited.

4. Spatio-Spectral Gamut Mapping and Separation

In this chapter, a novel approach called *Spatio-Spectral Gamut Mapping and Separation* SSGMS [SU15a,SU15b] is presented. This approach is considered an improvement of our previously proposed and published method called *Spatially Resolved Joint Spectral Gamut Mapping and Separation* SGMS [SU13] which to our knowledge is the first attempt to combine spectral gamut mapping and separation. The SGMS and its improved version SSGMS are based on the multi-illuminant PMSGM framework [UB11] – explained in Section 3.3.2 – which aim to minimize its associated drawback of generating *banding* artifacts. Prior to detailed explanation of SSGMS method, the SGMS approach is briefly explained and discussed in the next section.

The content of this chapter is mostly based on the following publications:

- Sepideh Samadzadegan and Philipp Urban, "Spatially Resolved Joint Spectral Gamut Mapping and Separation", 21st Color and Imaging Conference (CIC21), pp. 2-7, Albuquerque, New Mexico, USA., (2013).

- Sepideh Samadzadegan and Philipp Urban, "Spatio-Spectral Gamut Mapping and Separation", Journal of Imaging Science & Technology (JIST), Vol. 59, N. 4, pp. 40402-1-40402-12, (2015),
  23rd Color and Imaging Conference (CIC23), Darmstadt, Germany, (2015).

4.1. SGMS Approach

As mentioned in Section 3.3.3, the drawback associated with the *paramer mismatch-based spectral gamut mapping* PMSGM [UB11] method is related to its pixel-wise strategy. Since the spatial neighborhoods of image pixels are not considered in this approach, the adjacent pixels with almost similar colors in the original rendered colorimetric (e.g. CIELAB) images may be printed with completely different colorant combinations. This leads to discontinuities in the generated separation image S[1] even in areas in which the original image is smooth. Consequently, through the halftoning process abrupt changes in dot placements occur, which eventually result in *banding* artifacts visible in the spectral print. As Urban and Berns [UB11] suggested, adding noise to the a* and b* channels of the image rendered for the first illuminant prior to gamut mapping, solves the banding problem. However, adding noise adversely increases the image *graininess* (see Fig. 3.9).

In order to avoid these banding and graininess artifacts, we proposed an approach called *spatially resolved joint spectral gamut mapping and separation* SGMS [SU13] taking into account the local spatial neighborhoods of image pixels in incomplete 3×3 windows. In this approach, the image is traversed from the top-left to the bottom-right pixel. A cost function is applied through image traversal for selecting a colorant combination from

[1] The separation image S is an image containing the printable colorant combinations for all image pixels.

the parameric set $\tau(p_0)$[2] – previously defined in Section 3.3.2 – associated with the under-process pixel p_0, considering the colorimetric criteria (as in [UB11]) and the colorant combinations of already processed pixels in a local spatial neighborhood.

4.1.1. Shortcoming

Although the SGMS [SU13] approach leads to a smoother separation image S and spectral printout, it suffers from another sort of artifact called *smearing*. The smearing artifacts occur due to the accumulation of spatial errors in the image traversal direction (top-left to bottom-right) as the result of the incomplete spatial neighborhoods (windows) considered in this approach. Figure 4.1 shows a comparison between the *banding* (c), *graininess* (d), and *smearing* (e) artifacts generated via PMSGM [UB11] and SGMS [SU13] approaches. In this figure, a cutout of the METACOW [FJ04] spectral image was used and rendered under CIED65 (a) and CIEA (b) illuminants. For the sake of brevity, only one channel of the 7-channel (CMYKRGB) separation images is shown in (c) - (e) where the amount of colorant combinations (per image pixel) is represented by a gradient from white (no ink = 0%) to black (full ink = 100%).

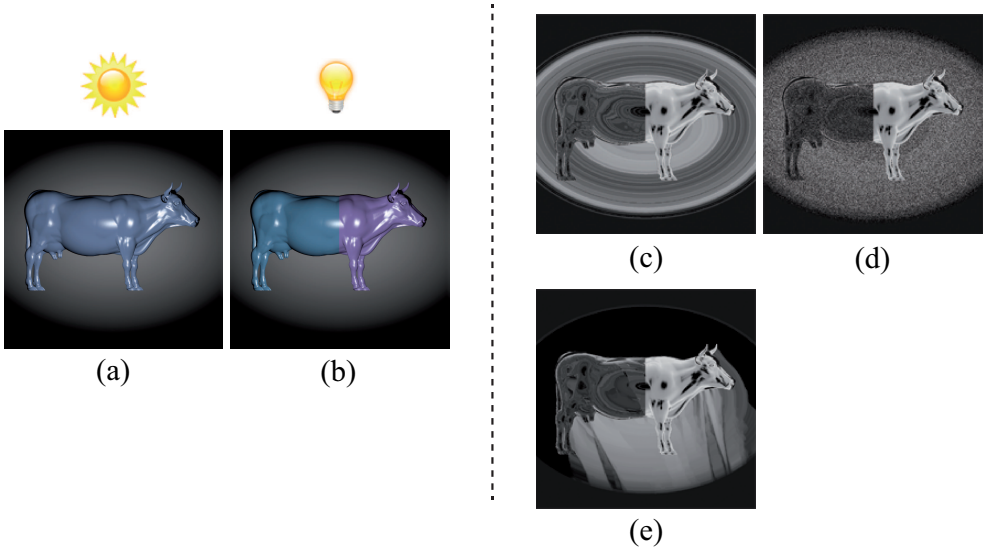

Figure 4.1.: A cutout of the METACOW [FJ04] spectral image rendered under CIED65 (a) and CIEA (b) illuminants. The *banding*, *graininess*, and *smearing* artifacts generated via PMSGM [UB11] and SGMS [SU13] methods are shown in (c), (d), and (e). For the sake of brevity, only one channel of the 7-channel separation images is shown in (c)-(e) where white = 0% ink and black = 100% ink deposited. This figure has been taken from [SU15a].

[2] A parameric set is defined as all printable colorant combinations which lead to parameric reflectances (paramers) and, consequently, almost the same colorimetric (e.g. CIELAB or LAB2000HL) values – with color differences below the JND – for the first considered illuminant (I_1) in a multi-illuminant framework.

4.2. SSGMS Approach

As mentioned, there are some drawbacks associated with the PMSGM [UB11] method and our previously published approach, SGMS [SU13]. These drawbacks are related to the generation of undesired *banding*, *graininess*, and *smearing* artifacts visible in separation images (see Fig. 4.1) and printouts.

In this section, the improved version of the SGMS [SU13] approach – based on the PMSGM multi-illuminant framework – is presented in order to minimize the aforementioned artifacts, resulting in smoother separation images and spectral prints. This approach is explained in detail in the following section.

4.2.1. Methodology

As mentioned, the *spatio-spectral gamut mapping and separation* SSGMS [SU15a] method is based on the concept of the PMSGM [UB11] framework shown in Fig. 3.8. However, in the SSGMS approach, the paramer mismatch-based gamut mappings, Γ_{Para}, are replaced by an improved strategy which takes the *colorimetric* and the *spatial* criteria into account. The steps required for applying the SSGMS method to an arbitrary spectral image are presented in the following subsections.

4.2.1.1. Step 1: Rendering the Spectral Image

Suppose there is a set of application-dependent illuminants $I_1(\lambda),...,I_n(\lambda)$ sorted based on their priority (from the most to the least important one) in an underlying application. In the first step, the spectral image R – with the size of $N' \times M'$ – must be rendered (transformed into colorimetric (e.g. LAB2000HL) values) for all of the illuminants considered and a CIE standard observer. Please note that although this approach is not dependent on any specific color space, using a perceptually-uniform and hue-linear color space such as LAB2000HL [LU12] is recommended. As the result of the rendering/transformation process, n LAB2000HL images $L_1,...,L_n$ are generated (see Fig. 4.2).

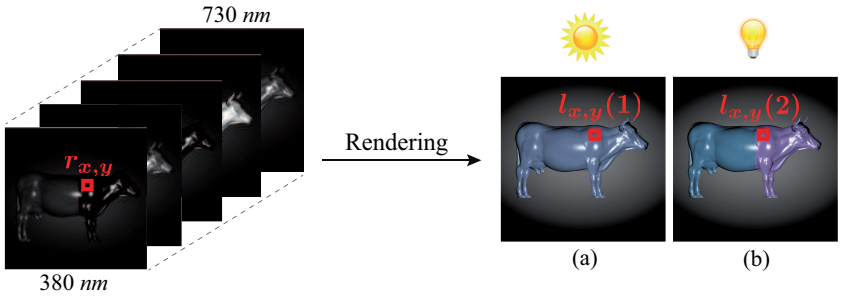

Figure 4.2.: Rendering a spectral image R into LAB2000HL images. In this example, two illuminants are considered: (a) CIED65 and (b) CIEA.

Each pixel of the spectral image R is rendered into n LAB2000HL pixels via Eq. (4.1).

$$l_{x,y}(i) = L(\Upsilon(I_i, r_{x,y})), \tag{4.1}$$

where the illuminant index is represented by $i = 1,...,n$, Υ is a vector of tristimulus values (see Eq. (2.2)), L is a transformation from the CIEXYZ to LAB2000HL [LU12] color space ($L : CIEXYZ \longmapsto LAB2000HL$), and each

pixel position is shown by x and y coordinates. Thus, $r_{x,y}$ represents any pixel of the spectral image R and $l_{x,y}(i)$ is referred to the corresponding pixel of the LAB2000HL image rendered for illuminant I_i. Consequently, the i^{th} rendered LAB2000HL image can be defined by Eq. 4.2.

$$L_i : \begin{cases} \underline{N'} \times \underline{M'} \rightarrow LAB2000HL \\ (x,y) \quad \rightarrow l_{x,y}(i), \end{cases} \tag{4.2}$$

where $\underline{N'} = 1,...,N'$ and $\underline{M'} = 1,...,M'$.

4.2.1.2. Step 2: Initialization by Averaging

In this step, an average LAB2000HL value is computed for all pixels of each rendered LAB2000HL image via Eq. (4.3).

$$l_{Avg}(i) = \frac{\sum_{x=1}^{N'} \sum_{y=1}^{M'} l_{x,y}(i)}{N' \times M'}, \tag{4.3}$$

where $i = 1,..,n$ represents the illuminant index, and $l_{Avg}(i)$ is an averaged LAB2000HL value computed for all image pixels of the LAB2000HL image rendered for illuminant I_i.

By employing the PMSGM [UB11] method – explained in Section 3.3.2 – on these n averaged LAB2000HL colors, one colorant combination is computed. An *initial separation image* S – with the size of $N' \times M'$ – is created by assigning this colorant combination to all image pixels.

4.2.1.3. Step 3: Traditional Gamut Mapping

Since our goal is to be as good as metameric reproduction at least for the first considered illuminant I_1, and to be superior to the metameric reproduction for the rest of the illuminants considered, $I_2,...,I_n$, we apply a traditional colorimetric gamut mapping algorithm (C-GMA) Γ_{Trad} to the LAB2000HL image L_1 rendered for the first illuminant, I_1. This process is represented via Eq. (4.4).

$$\Gamma_{Trad}[G(I_1, \mathcal{G})] : L_1 \mapsto \widehat{L_1} \tag{4.4}$$

The input to this transformation is the metameric printer gamut, G[3], determined for the first illuminant I_1 via the spectral printer gamut, $\mathcal{G}$[4]. The relationship between the metameric and spectral printer gamuts is represented via Eq. (2.6). The result of this transformation is the gamut-mapped image $\widehat{L_1}$ – with the smallest perceptual color difference from the original image, L_1. Note that any colorimetric, as well as, spatial gamut mapping can be used.

4.2.1.4. Step 4: Cost Function

In this approach (similar to the SGMS [SU13] method (see Section 4.1)), by traversing the image from the first top-left to the final bottom-right pixel, we select the appropriate printable colorant combinations for all image

[3] The metameric printer gamut G is defined as a set of all colors reproducible by a printing system considering a specific illuminant, here I_1.
[4] The spectral printer gamut $\mathcal{G}$ is defined as a set of all reflectances printable by a printing system. Thus, it is independent of the illumination condition.

pixels. From the colorant combinations chosen, the *final separation image* is computed. Please note that since the final separation image is generated by updating the initial separation image, it is also denoted by S.

Unlike the pixel-wise PMSGM [UB11] method, in the SSGMS approach, both the *colorimetric* and *spatial* content of the rendered LAB2000HL images are taken into account. In the spatial part, a local neighborhood of pixels in a complete 3×3 spatial window (except for any bordering pixel) is considered for each image pixel, p_0. Figure 4.3 is a schematic representation of image traversal. The actual under-process pixel and its direct neighbors are denoted by p_0 and $p_1, ..., p_8$ respectively. Note that, for bordering pixels, the number of direct neighbors in a spatial window is less than eight.

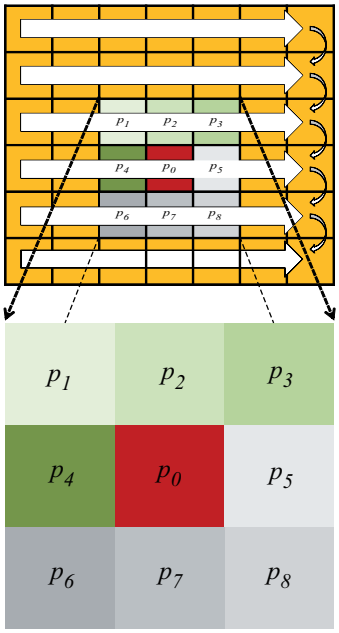

Figure 4.3.: Image traversal from the top-left to the bottom-right pixel. The actual under-process pixel is denoted by p_0, and its direct pre-processed neighbors are denoted by $p_1, ..., p_8$ in a 3×3 spatial window. This figure has been taken from [SU13] and slightly modified.

To compute the final colorant combinations for each image pixel, i.e. $S(p_0)$, the following optimization problem has to be solved:

$$S(p_0) = \underset{\chi \in \tau(p_0)}{\arg\min} \; F_{cost}(\chi), \tag{4.5}$$

where S is the separation image, F_{cost} is a cost function explained in Eq. (4.7) and below, χ is a printable colorant combination, and $\tau(p_0)$ is the parameric set for actual pixel p_0.

As mentioned previously, a parameric set $\tau(p_0)$ is defined, for each image pixel p_0, as all printable colorant combinations which lead to parameric reflectances (paramers) and consequently almost the same colorimetric (LAB2000HL) values – with color differences below the JND – for the first considered illuminant, I_1. Equation (4.6) represents the definition of a parameric set.

$$\tau(p_0) = \left\{ \chi \in \Omega \mid \| P_1(\chi) - \widehat{L_1}(p_0) \|_2 \leq D \right\}, \tag{4.6}$$

where Ω is the printer colorant space composed of all printable colorant combinations, $P_1(\chi)$ is the color prediction of the printout under illuminant I_1 given the colorant combination χ, i.e. $P_1(\chi) = L(\Upsilon(I_1, SPM(\chi)))$ for a spectral printer model *SPM* (e.g. Cellular-Yule-Nielsen-Spectral-Neugebauer (CYNSN) model [YN51, YC51, Vig85, Vig90]) and color space transformation $L : CIEXYZ \longmapsto LAB2000HL$, $\widehat{L_1}(p_0)$ is the LAB2000HL value at pixel p_0 extracted from the gamut-mapped LAB2000HL image for the first illuminant, and D is the JND. Note that using the 2-norm for computing the color differences in the LAB2000HL color space can almost be interpreted as utilizing the CIEDE2000 color-difference formula in the CIELAB color space.

The cost function $F_{cost} : \Omega \mapsto [0,1]$ is defined via Eq. (4.7) and composed of two parts: *colorimetric* and *spatial*.

$$F_{cost}(\chi) = 1 - f_{col}(\chi) f_{spatial}(\chi), \tag{4.7}$$

where χ is a printable colorant combination, and f_{col} and $f_{spatial}$ are the colorimetric and spatial parts of the cost function used to balance the colorimetric and spatial accuracy which are explained in detail in sections 4.2.1.4.1 and 4.2.1.4.2. Note that $f_{spatial}$ and consequently F_{cost} depend on each actual under-process pixel p_0 and its direct neighbors in a local 3×3 spatial window.

4.2.1.4.1. Step 4.1: Colorimetric Part – In the colorimetric part of the cost function, the color differences between the colorimetric values extracted from the rendered LAB2000HL images $L_i(p_0)$ and the predicted LAB2000HL values ($P_i(\chi) = L(\Upsilon(I_i, SPM(\chi))), \chi \in \tau(p_0), L : CIEXYZ \longmapsto LAB2000HL$) for the second and subsequent illuminants, $I_2, ..., I_n$ are computed as follows:

$$f_{\text{col}}(\chi) = \prod_{i=2}^{n} \exp\left(-\frac{1}{\sigma_1} \| P_i(\chi) - L_i(p_0) \|_2 \right) \qquad \chi \in \tau(p_0), \tag{4.8}$$

where χ is any colorant combination within the parameric set $\tau(p_0)$ associated with each actual under-process pixel p_0, $i = 2, ..., n$ is the illuminant index, $P_i(\chi)$ is the color prediction of the printout under illuminant I_i given the colorant combination χ, and $\sigma_1 > 0$ is a weighting parameter.

If the given pixel reflectance $r(p_0)$ is within the spectral gamut $\mathcal{G}$ of the printer, then the aforementioned computed color differences across all illuminants will be zero and, consequently, the result of the colorimetric part of the cost function will be one. However, for other (most likely) cases where $r(p_0)$ is not within the spectral printer gamut $\mathcal{G}$, the color differences become larger than zero; thus, the result of the colorimetric part will be smaller than one, but still remain positive.

As mentioned previously, the L_1 image was mapped into the colorimetric gamut of the printer G defined for the first illuminant, I_1. Thus, this illuminant is not considered in Eq. (4.8). This is because, by computing each parameric set $\tau(p_0)$, we already knew that all available colorant combinations, χ, belonging to this set will eventually lead to nearly the same colorimetric (LAB2000HL) values for the first illuminant I_1 with unnoticeable color changes.

4.2.1.4.2. Step 4.2: Spatial Part – In the spatial part of the cost function, all direct neighbors of any image pixel p_0 in a 3×3 spatial window are considered. Their corresponding colorant combinations, which are computed through the initialization process (see Section 4.2.1.2), are also used to determine the colorant combination

of the actual under-process pixel p_0 and, eventually, to update the separation image S. Equation (4.9) represents the spatial part of the cost function:

$$f_{spatial}(\chi) = \exp\left(-\frac{1}{\wp}\left\|\sum_{j\in B}\omega(p_j)S(p_j)-\chi\right\|_2\right) \qquad \chi \in \tau(p_0), \tag{4.9}$$

where χ is any colorant combination within the parameric set $\tau(p_0)$, B is a set of all direct neighboring pixels of any actual pixel p_0 within a 3×3 spatial neighborhood (window), $S(p_j), j \in B$ is the actual colorant combination for the neighboring pixel p_j, $\omega(p_j) \geq 0, j \in B$ is a *spatial weight* (defined via Eq. (4.10)) assigned to pixel p_j, and $\wp$ is a *weight* used to make a balance between the *colorimetric* and *spatial* parts of the cost function which is explained via Eq. (4.11).

The colorant combinations of neighboring pixels are weighted in order to facilitate edge-preserving which is adopted from bilateral filtering. However, the color differences across all illuminants, $I_1,...,I_n$, are considered instead of spatial distances and range differences. The following equation represents the spatial weights:

$$\omega(p) = \frac{\prod_{i=1}^{n}\exp\left(-\frac{1}{\sigma_2}\parallel L_i(p_0)-L_i(p)\parallel_2\right)}{\sum_{j\in B}\prod_{i=1}^{n}\exp\left(-\frac{1}{\sigma_2}\parallel L_i(p_0)-L_i(p_j),\parallel_2\right)}, \tag{4.10}$$

where p is a neighboring pixel, and $\sigma_2 > 0$ is a weighting parameter.

The spatial weights are assigned to the neighboring pixels based on the degree of color deviations considering all illuminants. If the computed color differences between the actual pixel $L_i(p_0)$ and its neighbor $L_i(p)$ across all illuminants are small, the associated spatial weight to that neighboring pixel is larger than the case where there are large color differences – representing a sharp edge. The denominator is used to ensure that all spatial weights sum up to 1, i.e. $\sum_{j\in B}\omega(p_j) = 1$.

In Eq. (4.9), if the weighted average of the neighboring pixels' colorant combinations is equal to χ, the spatial part of the cost function becomes 1. If the weighted average deviates from χ, the spatial part becomes smaller than 1 but still remains positive.

According to the optimization process defined in Eq. (4.5), the minimization of the cost function leads to a separation image S which follows the colorimetric and spatial content of the original image in terms of preserving the metameric and parameric edges[5], avoiding banding artifacts, and maintaining the local spatial correlations.

As mentioned, the weighting parameter $\wp$ is required in order to balance the colorimetric (f_{col}) and spatial ($f_{spatial}$) parts of the cost function, based on the image content. Making this trade-off is essential for generating a separation image S so that it mimics the content of the original image. If the spatial part becomes dominant, the local spatial correlation of the original image will be preserved at the expense of possibly large colorimetric errors under the second and subsequent illuminants, $I_2,...,I_n$. In contrary, if the colorimetric part becomes dominant, the colorimetric errors will be reduced at the expense of banding artifacts, which is similar to the result obtained via the PMSGM [UB11] method – explained in Section 3.3.2. In the PMSGM [UB11] approach, only the colorimetric criterion is considered, leading to colorimetric accuracy, but also causing unwanted banding artifacts.

Therefore, in smooth image regions, the contribution of the spatial part must be increased in order to avoid bandings, while in areas with low spatial correlation, the colorimetric part should be dominant. Thus, we defined the following weighting parameter $\wp$, adapted to the image content.

[5] Metameric and parameric edges are referred to edges which appear under one illumination condition, but are invisible under another one.

$$\wp = \sigma_3 + \min_{j \in B} \left(\sum_{i=1}^{n} (\| L_i(p_0) - L_i(p_j) \|_2)^2 \right), \tag{4.11}$$

where $\sigma_3 > 0$ is a weighting parameter.

The contribution of the spatial part in the cost function is controlled by the magnitude of $\wp$ so that more dominant $f_{spatial}$ is obtained via smaller $\wp$ values. If there is a neighboring pixel which has a similar color to pixel p_0 across all considered illuminants $I_1, ..., I_n$ (a smooth area), the maximum impact of the spatial part is achieved with $\wp \approx \sigma_3$ in order to avoid banding artifacts. It should be noted that the spatial weights used in $f_{spatial}$ and defined via Eq. (4.10) alleviate the influence of other neighboring pixels with non-similar color considering all illuminants. In non-smooth regions (such as edges), the contribution of $f_{spatial}$ decreases via larger $\wp$ values, resulting in higher impact of f_{col} and the consequent preservation of metameric and parameric edges.

By traversing all image pixels, the optimal colorant combinations and, as a result, the final separation image S are computed by minimizing the cost function (see Eq. (4.5)). For controlling the printer and eventually printing the spectral sprints, this separation image is further processed (ink limited and halftoned) and then sent to the printer.

4.2.2. Remarks

4.2.2.1. Additional (Optional) Step 1: Initialization by Segmentation

In order to improve the colorimetric accuracy – specifically for preserving the metameric and parameric edges – initialization of the separation image S by segmentation, can be replaced with initialization by averaging (see Section 4.2.1.2).

In this process, the colorimetric (LAB2000HL) images rendered for all considered illuminants are segmented into different clusters using e.g. a color-based segmentation method such as K-means clustering [CK10]. Afterwards, for each segmented image, an average LAB2000HL value must be computed for all pixels within each cluster.

Note that the segmentation process may not necessarily lead to the same number of clusters for all LAB2000HL images. For instance, we applied the aforementioned segmentation method to a cutout of the METACOW [FJ04] image, rendered for CIED65 and CIEA illuminants, which led to two and three clusters respectively. Figure 4.4 shows the result of this segmentation as well as the cluster-wise averaging process.

The initial colorant combinations for all image pixels and, consequently, the *initial separation image S* are then computed by applying the PMSGM [UB11] method – explained in Section 3.3.2 – to the segmented and cluster-wise averaged LAB2000HL images.

The colorant combination from each parameric set $\tau(p_0)$ with the highest colorimetric accuracy across all considered illuminants, is more likely to be similar to the weighted average of colorant combinations of the neighboring pixels (used in $f_{spatial}$ (see Eq. (4.9))) if the initialization is performed by averaging within the actual cluster rather than the whole image. Therefore, using segmentation, such colorant combinations are more likely to be selected by the optimization process (defined in Eq. (4.5)), leading to improved colorimetric accuracy and preservation of metameric and parameric edges between the clusters, while avoiding banding artifacts within the segmented parts.

Please note that this is an optional step and not necessarily required for all images. This is because we didn't find metameric or parameric edges in natural images; however, we cannot exclude the images which may contain

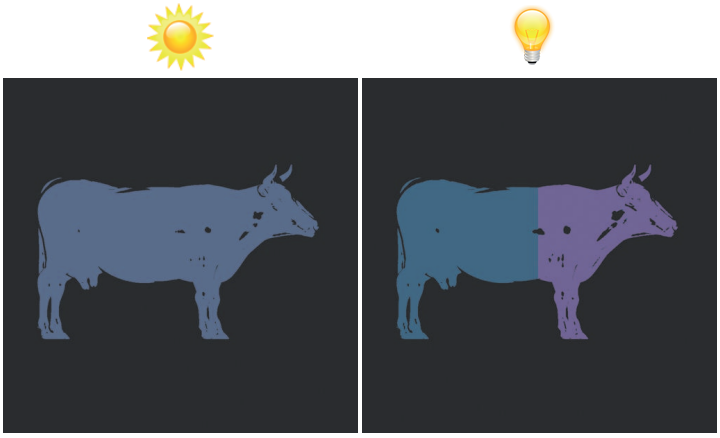

(a) (b)

Figure 4.4.: Segmented and cluster-wise averaged LAB2000HL images for two illuminants: (a) CIED65 and (b) CIEA. A cutout of the METACOW [FJ04] image was used. This figure has been taken from our published article [SU15a].

such edges in general. For instance, the METACOW [FJ04] image is one of the special cases containing sharp metameric edges.

4.2.2.2. Additional (Optional) Step 2: Noise Addition

This step is also optional and need not be applied to all spectral images. This is because most spectral images taken from natural scenes and paintings, contain some sort of noise such as short and thermal noise. However, for completely noise-free artificially-made images such as the METACOW [FJ04] image, employing this step leads to an improved reproduction.

Adding a small amount of noise to the colorimetric image rendered for the first illuminant (L_1) adds high frequency components into the separation image S. These high frequency components break up the unwanted remaining low frequency patterns (bandings) in the separation image and eventually the final spectral printout.

We added zero-mean Gaussian noise with a standard deviation of 2.55 to all channels of a cutout of the completely noise-free CIELAB METACOW [FJ04] image – rendered for the first illuminant – prior to gamut mapping. This amount of added noise does not affect the printout's graininess in a visually detectable way. The black channel of the obtained multi-channel separation image is illustrated in Fig. 4.8, (e).

Figures 4.5 and 4.6 represent the methodology, using a pseudocode and a block diagram.

4.2.3. Experiments

4.2.3.1. Printing System and Implementation

For conducting our experiments, we used a HP Designjet Z3100 printer controlled by the ONYX Production-House RIP Version 7. The CMYKRGB standard inks and the HP Premium Instant-dry Gloss Photo paper were

```
Rendering the spectral image into LAB2000HL images                                  Sec. 4.2.1.1
IF (no metameric/parameric edge) THEN
  Averaging each LAB2000HL image into a single LAB2000HL value                     Sec. 4.2.1.2
  Initialization of the separation image by averaging
ELSE
  Segmentation of each LAB2000HL image and then averaging within each cluster      Sec. 4.2.2.1
  Initialization of the separation image by segmentation and averaging
END IF
IF (completely noise-free images) THEN
  Adding a small amount of noise to the image rendered for the first illuminant    Sec. 4.2.2.2
END IF
Traditional gamut mapping for the first illuminant                                  Sec. 4.2.1.3
Applying the cost function (colorimetric and spatial parts)                         Sec. 4.2.1.4
```

Figure 4.5.: Pseudocode implementation of the method. This figure has been taken from [SU15a].

utilized.

We restricted the number of overprints to four obtained via different combinations of the black (K) ink together with three other colorants from the CMYRGB set, assuming that these colorant combinations approximately covered the spectral gamut of the printer. This restriction was also employed previously, in [TB00, UB11, SU13].

In order to spectrally characterize and model the printer, 20 Cellular-Yule-Nielsen-Spectral-Neugebauer (CYNSN) spectral printer sub-models [YN51, YC51, Vig85, Vig90] were used for all combinations composed of four inks including the black: CMYK, CMKR, CMKG, CMKB, CYKR, CYKG, CYKB, CKRG, CKRB, CKGB, MYKR, MYKG, MYKB, MKRG, MKRB, MKGB, YKRG, YKRB, YKGB, and KRGB.

The 4-dimensional colorant space of each of these 20 printer sub-models were sampled in steps of 1%. Thus, $100 \times 100 \times 100 \times 100 = 10^8$ colorant combinations were considered within each sub-model. In total $20 \times 2^8 = 2$ billion colorant combinations were computed to approximately define the printer colorant space Ω. Consequently, the spectral gamut of the printer $\mathcal{G}$ was defined implicitly by applying the aforementioned 20 spectral printer models (SPM) to the colorant combinations within the printer colorant space, i.e. the $\Omega \xrightarrow{SPM} \mathcal{G}$. The colorimetric printer gamut G was defined for the first considered illuminant I_1, by computing the tristimulus values (by applying the Eq. (2.2) to the spectral gamut of the printer $\mathcal{G}$) and then employing two consecutive transformations from the CIEXYZ to CIELAB and from the CIELAB to LAB2000HL [LU12] color space.

For computing the parameric sets (τs) – defined in Eq. (4.6), the LAB2000HL color space [LU12] was divided into cubes with side length of approximately 0.4 CIEDE2000, which is below the JND considering the office viewing condition. The colorant combinations which their corresponding predicted LAB2000HL values (predicted by the printer model under the first illuminant I_1) fell into the same cube, were considered as parameric colorant combinations (defining a parameric set) and stored in a list for later quick access. Thus, separate lists were created representing different parameric sets. The optimization process – defined in Eq. (4.5) – was applied to each individual colorant combination within each parameric set, in order to finally select a colorant combination (from each set) that would minimize the cost function – defined in Eq. (4.7). From the chosen colorant combinations, the separation image S was generated.

Note that we considered two illuminants: $I_1 = CIED65$ and $I_2 = CIEA$.

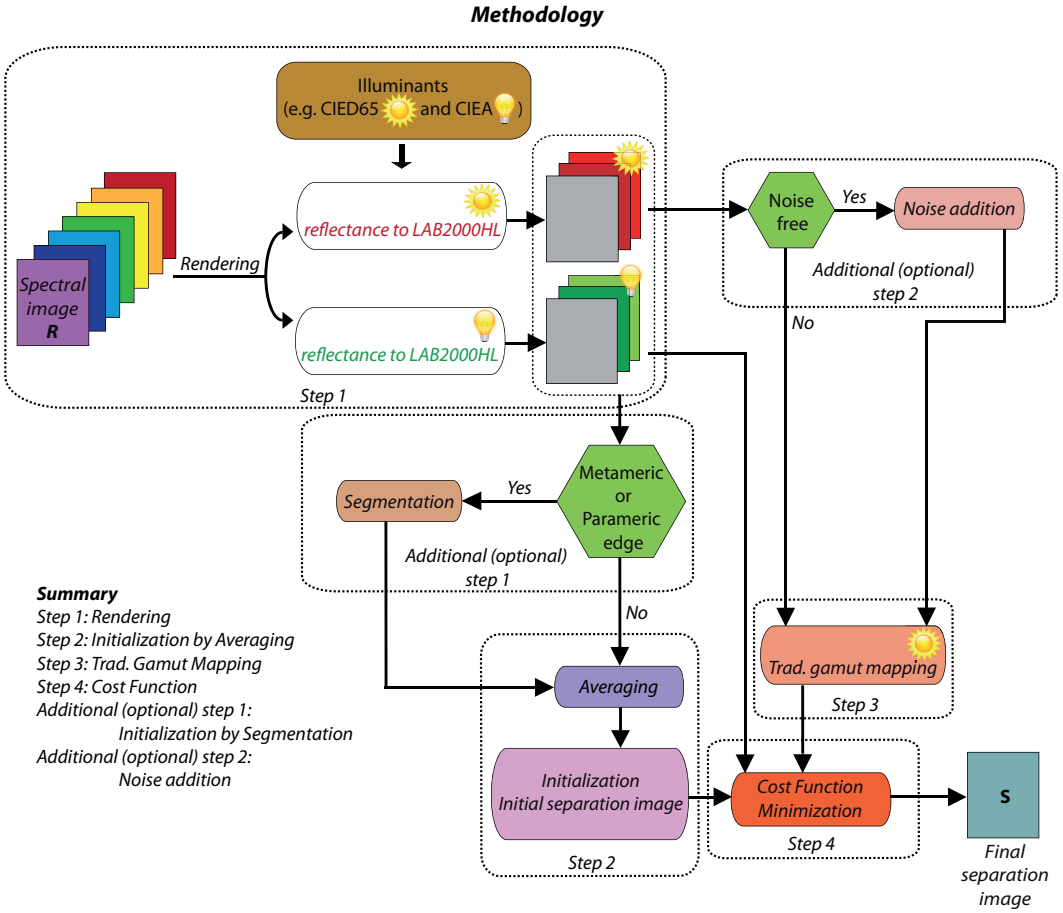

Figure 4.6.: An overview of the proposed methodology, using a block diagram. This figure has been taken from [SU15a].

4.2.3.2. Test Images

We used the following 11 spectral images to test the proposed SSGMS [SU15a] method and adjust the weighting parameters (σ_1, σ_2, and σ_3) defined in equations (4.8), (4.10), and (4.11).

- A cutout of the METACOW [FJ04] spectral image (containing metameric edges).
- Eight captured spectral images of natural scenes taken from the Foster database [FANF06].
- Two spectral images captured from two paintings.

We applied the proposed method to each of the aforementioned spectral images in order to obtain the corresponding separation images S. These images were further processed via ink limitation and halftoning and then sent to the utilized printing system. The resulting spectral printouts were captured using a Canon EOS 5D Mark III camera. No chromatic adaptation or white balancing was used in capturing the prints.

4.2.3.3. Adjustment of the Cost Function's Parameters

In order to adjust the weighting parameters (σ_1, σ_2, and σ_3) used in the cost function (see equations (4.8), (4.10), and (4.11)), we used a cutout of the completely noise-free METACOW [FJ04] spectral image in order to preserve the metameric edges and avoid banding artifacts by visually inspecting the 7-channels of the generated separation images. Note that banding artifacts occurred due to abrupt changes in dot placements through the halftoning process as a result of severe discontinuities in the separation image. Therefore, in order to avoid these cases, spatial correlations in local 3×3 windows of surrounding neighbors were considered independently of the image resolution.

The following table represents the cost function's weighting parameters together with their adjusted values. We are aware that these parameters were suboptimally adjusted.

Table 4.1.: Weighting parameters of the proposed SSGMS method together with their adjusted values. This table has been taken from [SU15a].

Parameter	Value
σ_1	3
σ_2	2
σ_3	9

4.2.4. Results and Evaluation

The obtained results via applying the proposed SSGMS [SU15a] method on 11 spectral images mentioned in Section 4.2.3.2, were evaluated by visually inspecting the printouts. The colorimetric error and the computational time (associated with each image) were computed also.

4.2.4.1. Printouts

As mentioned in Section 4.2.3.2, in order to test the proposed SSGMS [SU15a] method, we used 11 spectral images. From these images, two of them – a cutout of the METACOW [FJ04] image and a natural image (House image) from the Foster [FANF06] database – were selected in order to compare the spectral prints generated by the proposed SSGMS [SU15a] method and PMSGM [UB11] and SGMS [SU13] approaches. The other images also showed the same result.

Figures 4.7 and 4.8 show the separation images obtained via the PMSGM [UB11] method (a) without addition of noise, and (b) with addition of a zero-mean Gaussian noise with a 2.55 standard deviation, to all channels of the CIELAB image, rendered for the first illuminant (CIED65) prior to gamut mapping, (c) the SGMS [SU13] approach, and (d) the SSGMS [SU15a] method. The banding, graininess, and smearing artifacts are visible in (a) to (c), while (d) shows the improved result.

Please note that for obtaining the separation image shown in Fig. 4.8 (d), the segmentation process was used and led to two and three clusters for the CIED65 and CIEA illuminants respectively. In this figure, (e) shows the separation image achieved by applying both optional steps so that the same number of clusters as (d) was defined; the same amount of aforementioned Gaussian noise was also added. As can be seen, (e) shows a smoother separation image than (d).

In figures 4.7 and 4.8, for the sake of brevity, only one channel of the 7-channel (CMYKRGB) separation images is shown, where the increased amount of colorant combinations utilized (per image pixel) is represented via a gradient from white (= 0% ink) to black (= 100 % ink).

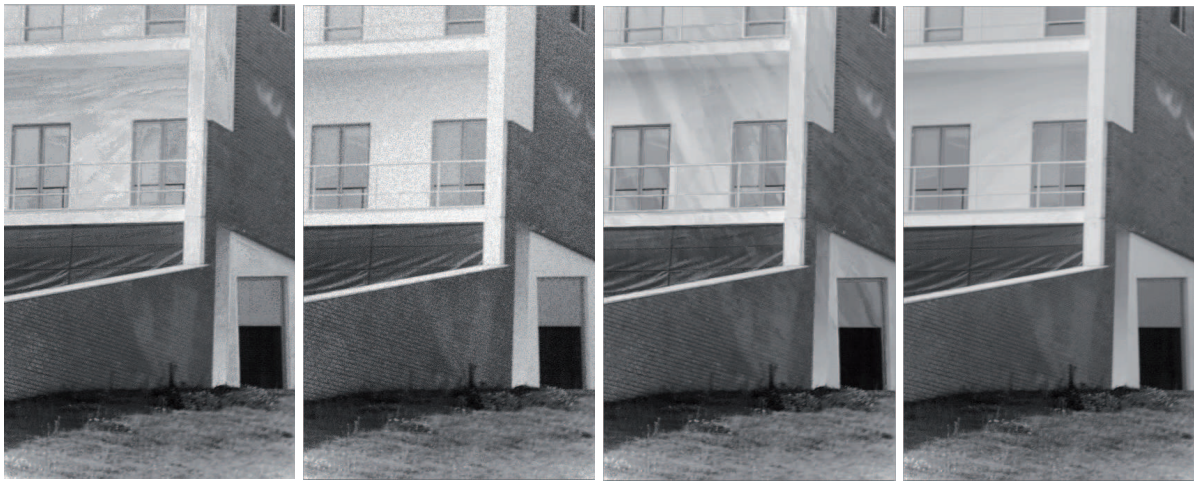

Figure 4.7.: Separation images of a natural scene [FANF06] (House image) generated by these approaches: PMSGM [UB11]: (a) without, and (b) with addition of a small amount of noise, (c) SGMS [SU13], and (d) SSGMS [SU15a]. Note that only one channel (K) of the separation images is shown where white = 0% ink- and black = 100% ink-deposition. This figure has been taken from [SU15a].

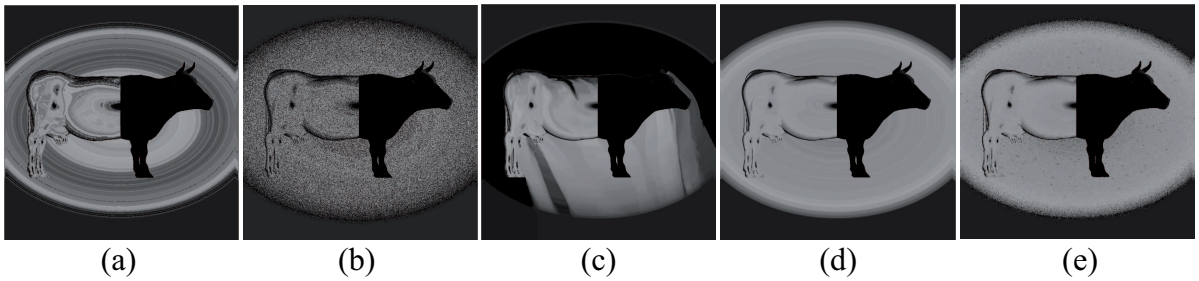

Figure 4.8.: Separation images of a cutout of the METACOW [FJ04] image generated by these approaches: PMSGM [UB11]: (a) without, and (b) with addition of a small amount of noise, (c) SGMS [SU13], and SSGMS [SU15a]: (d) with additional step 1 (using 2 and 3 clusters for CIED65 and CIEA illuminants respectively), and (e) with additional step 1 (as (d)) and additional step 2 (addition of a small amount of noise). Note that only one channel (R) of the separation images is shown where white = 0% ink- and black = 100% ink-deposition. This figure has been taken from [SU15a].

Figure 4.9 shows cutouts of captured images of real spectral prints obtained via the separation images shown in Fig. 4.7. The capturing was performed under two illuminants: (first row) CIED65 and (second row) CIEA.

The banding, graininess, and smearing artifacts are visible in (a) to (c) specifically inside the areas of marked rectangles; while, (d) shows the improved reproduction.

Please note that the capturing process can lead to color errors. The images are reliable in the zoomed-in electronic version of this dissertation and not its printed version. Note that we used a printing system (composed of a printer, halftone, set of inks, and a paper type) for printing these images, which is different from the printing system that may be used for printing this dissertation.

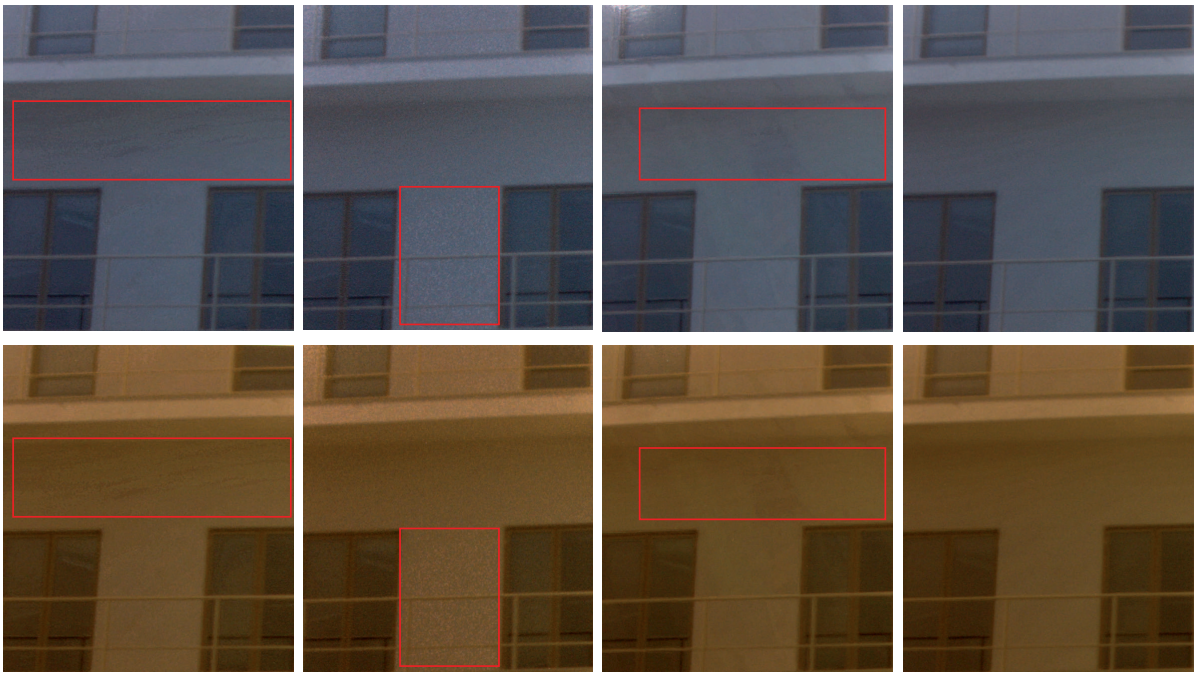

Figure 4.9.: Cutouts of captured images (under illuminants: CIED65 (first row) and CIEA (second row)) from spectral prints obtained via separations shown in Fig. 4.7. The banding, graininess, and smearing artifacts are visible in (a)-(c). (d) represents an improved reproduction. Please note that the capturing process can lead to color errors. The results are reliable on the zoomed-in electronic version of this dissertation. This figure has been taken from [SU15a].

The separation images shown in Fig. 4.8 (a) and (e) were also printed in order to compare the PMSGM [UB11] method and the novel approach, SSGMS [SU15a]. The corresponding captured images under CIED65 (a) and CIEA (b) illuminants are shown in Fig. 4.10, in the middle and bottom rows respectively. In order to show the advantage of spectral printing, the same cutout of the METACOW [FJ04] image was printed via an ICC-based metameric workflow and then captured under the same illuminants. These captured images are shown in the top row. As can be seen, the metameric edge apparent under the CIEA illuminant is preserved via PMSGM [UB11] and SSGMS [SU15a] methods, and it has vanished in the print generated via the ICC-based metameric reproduction workflow. The colors of original images (see Fig. 4.1 (a) and (b)), are mimicked by the spectral prints. The banding artifacts generated by the PMSGM [UB11] method (middle row) are minimized by the

SSGMS [SU15a] approach (bottom row).

It should be mentioned that for natural images and paintings used for testing the proposed SSGMS [SU15a] method, we didn't find apparent colorimetric improvements in comparison to the metameric reproduction.

4.2.4.2. Colorimetric Error

In order to investigate whether the spatial part ($f_{spatial}$) of the proposed cost function in the SSGMS [SU15a] approach adversely affects the colorimetric accuracy of the result in comparison with the PMSGM [UB11] method which is based merely on the colorimetric criterion, the average and 95th percentile CIEDE2000 color differences were computed for all 11 tested spectral images: 8 natural images from the Foster database [FANF06], 2 paintings, and a cutout of the METACOW [FJ04] image shown in Fig. 3.9 (a), (b), and (c). These 11 spectral images are listed in Table 4.2.

The color differences between the original colorimetric images – rendered for CIED65 and CIEA illuminants – and the predicted colorimetric values from the printouts obtained via the PMSGM [UB11] and SSGMS [SU15a] approaches were calculated pixel-wisely. Figures 4.11 and 4.12 show the deviations between the colorimetric errors caused by employing the PMSGM [UB11] and SSGMS [SU15a] methods.

As can be seen in these figures, the deviations corresponding to the average and 95th percentile CIEDE2000 color differences are smaller than 0.2 and -1 CIEDE2000 units respectively. Note that the negative values indicate the higher accuracy of the proposed SSGMS method in comparison to the PMSGM approach; the positive values indicate lower accuracy. According to these results, avoiding (minimizing) banding artifacts by considering the spatial criterion ($f_{spatial}$) does not lead to a significant drop in terms of colorimetric accuracy across considered illuminants (blue bars: CIED65 and red bars: CIEA).

4.2.4.3. Computational Time

As mentioned previously, we applied the proposed SSGMS [SU15a] method to 11 spectral images. In order to calculate the extra amount of computational time (ΔT) required by the spatial computation in comparison with the colorimetric-only strategy used in the PMSGM [UB11] method, we also employed the PMSGM approach on the same set of spectral images. Table 4.2 represents the elapsed time associated with applying the SSGMS and PMSGM approaches – implemented in C++ – to 11 spectral images using an *Intel®Core^{TM}i7-3820 CPU @ 3.60 GHz* processor.

According to the results obtained based on the spectral images used in our experiments (see Table 4.2), the maximum computational time of the SSGMS method was 17.15 *min* which corresponds to the image *Painting 1*. The maximum computational time difference (ΔT) between the PMSGM and SSGMS approaches was 7.69 *min* (showing approximately 65% computational percentage difference) which corresponds to the *METACOW (cutout)* [FJ04] image.

4.3. Spectral Prints for Light Indicators and Security Prints

As mentioned previously, spectral printing can be used for different applications and purposes. Here, our aim is to use spectral printing for generating light indicators[6] and security prints. For this, we need to find metameric

[6] Here, light indicators refer to printed samples which have almost the same color when viewed under one illuminant, and different colors when viewed under another illuminant. Using these light indicators, one can determine which illuminant is using based on the observed color.

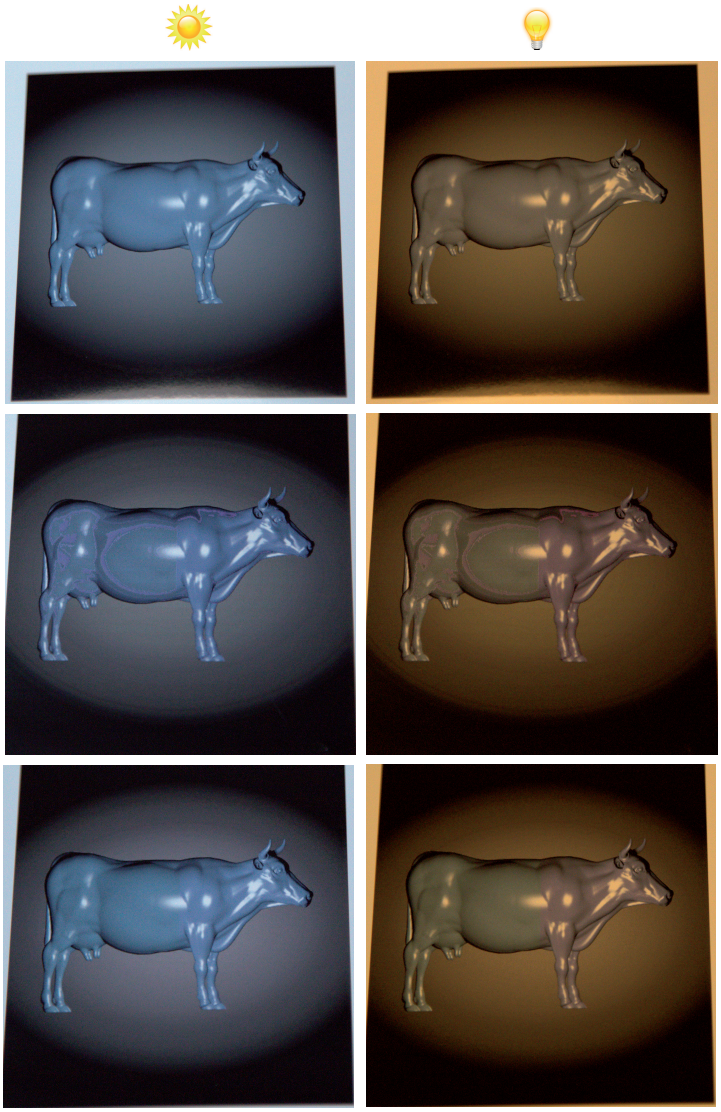

Figure 4.10.: Captured images of real prints generated by an ICC-based metameric reproduction workflow (top row), the PMSGM [UB11] approach (middle row), and the SSGMS [SU15a] method (bottom row). The capturing process was performed under CIED65 (a) and CIEA (b) illuminants. Please note that the capturing process can lead to color errors. The results are more reliable on the zoomed-in electronic version of this dissertation. This figure has been taken from [SU15a].

pairs[7] and, consequently, metameric colorant combinations[8] printable by a printing system. For this purpose, a

[7] Here, each metameric pair refers to colorimetric (LAB2000HL) values that are metamers under one illuminant, but showing the maximum color difference under another one.

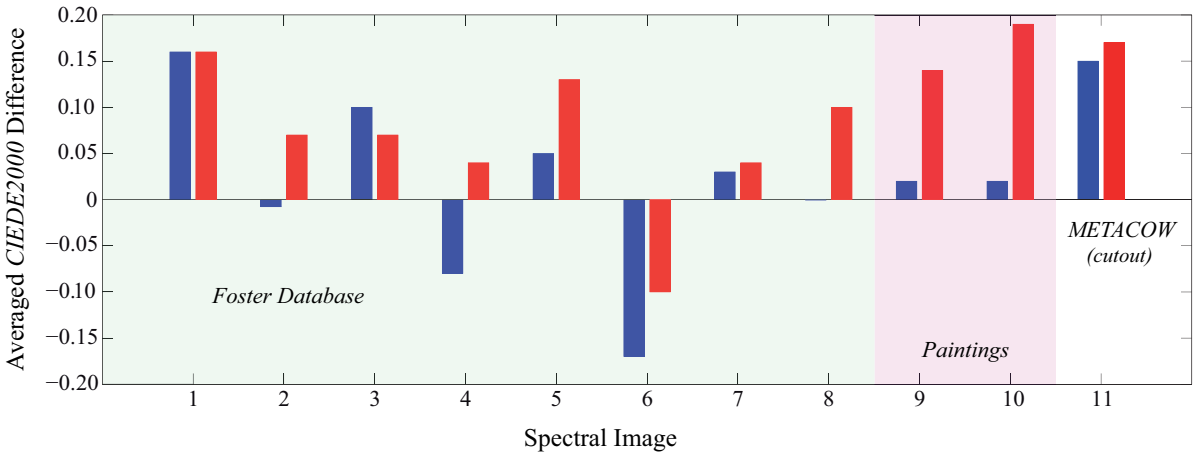

Figure 4.11.: Deviations between average CIEDE2000 errors computed between the original colorimetric images and the predicted colorimetric values from the printouts obtained via the proposed SSGMS approach and the PMSGM method for CIED65 (blue bars) and CIEA (red bars) illuminants. Negative values indicate a higher colorimetric accuracy for the proposed method. Positive values indicate a lower accuracy. This figure has been taken from [SU15a].

simple strategy for generating and printing some targets is presented and explained in detail in the subsequent sections.

4.3.1. Generating the Targets

To generate the artificial targets for finding metameric pairs and, consequently, printable metameric colorant combinations, a set of grid points was considered by sampling the LAB2000HL [LU12] color space in lightness ($L^* \in [0,70]$) and color-opponent dimensions ($a^* \in [-50,50]$ and $b^* \in [-50,50]$) in steps of 5 units. Thus, the LAB2000HL [LU12] color space was characterized by $15 \times 21 \times 21 = 6615$ sampled LAB2000HL values (grid points).

We considered two arbitrary illuminants (I_1 and I_2), and we planned to find the printable colorant combinations which are metamers under the first illuminant I_1, but showing the maximum color difference under the second illuminant I_2.

All of the aforementioned sampled LAB2000HL values were stored in two matrices with size 6615×9, where the rows of these matrices referred to all 6615 different cases (sampled LAB2000HL values) and the columns referred to sampled values within metamer- or paramer-mismatch gamuts (see Fig. 3.7) corresponding to 6615 LAB2000HL colors. Note that 9 is an arbitrary number used for sampling these spaces. The first matrix relates to the first illuminant I_1. The columns within each row of this matrix are equal LAB2000HL values; consequently, their color differences are exactly zero, indicating metamers. This matrix was stored as an image called $Image_1$ (see Fig. 4.13 (a)).

[8] Metameric colorant combinations are referred to colorant combinations resulting in metameric reflectances (metamers) under a specific illumination condition.

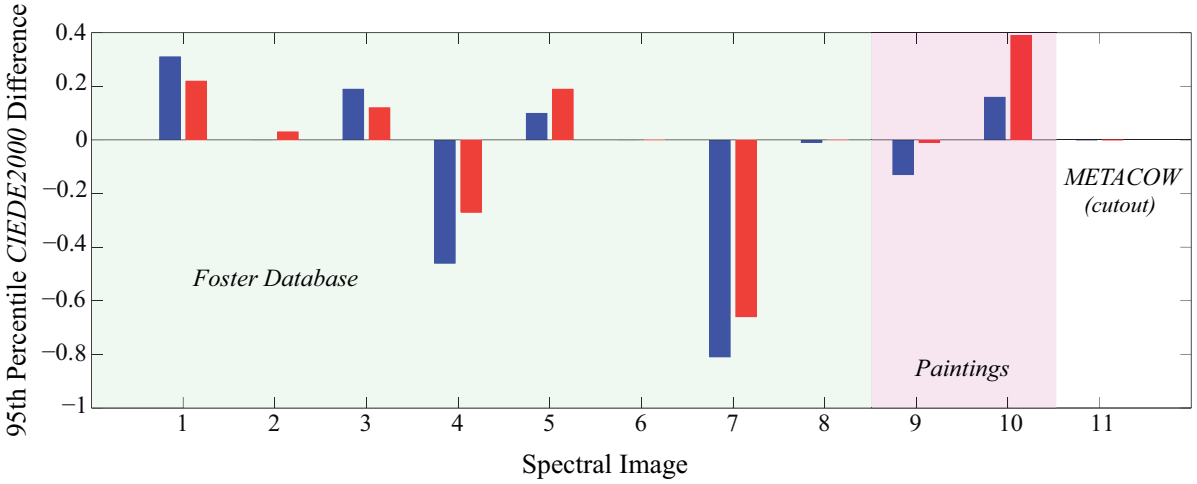

Figure 4.12.: Deviations between 95th percentile CIEDE2000 errors computed between the original colorimetric images and the predicted colorimetric values from the printouts obtained via the proposed SSGMS approach and the PMSGM method for CIED65 (blue bars) and CIEA (red bars) illuminants. Negative values indicate a higher colorimetric accuracy for the proposed method. Positive values indicate a lower accuracy.

The colorimetric values of the columns of the second matrix were obtained by applying a mask to colorimetric values of each row within the first matrix. This mask is considered as a vector of 9 elements with these LAB2000HL values: $(0,0,0),(0,-d,+d),(0,0,d),(0,d,d),(0,-d,0),(0,d,0),(0,-d,-d),(0,0,-d),(0,d,-d)$, where $d = 20$. Thus, the color differences between the LAB2000HL values of columns within each row of the second matrix are no longer zero. This matrix was also stored, as another image called *Image*$_2$ (see Fig. 4.13 (b)).

It should be noted that the generation of the artificial targets (*Image*$_1$ and *Image*$_2$) is completely independent of any illumination condition. Thus, we may assume that these images are obtained by rendering a spectral image R under any arbitrary pairs of illuminants.

Figure 4.13 shows a small number of sampled grid points (LAB2000HL values) extracted from these images. As can be seen in (a), all nine columns within each row have the same LAB2000HL value, representing metamers. However, this is not the case for (b).

These two images are used as inputs to the proposed SSGMS [SU15a] approach – explained in Section 4.2 – in such a way that only the colorimetric part of the cost function is activated. This is because these artificial images should be treated exclusively in a pixel-wise manner. Since we are not considering the spatial neighborhood, applying the SGMS [SU13] approach – explained in Section 4.1 – also leads to the same result, by taking only the colorimetric part of the cost function into account. Moreover, the pixel-wise PMSGM [UB11] method proposed by Urban and Berns (see Section 3.3.2) can also be used.

As a result of applying one of the aforementioned approaches to the artificial images considering a pair of illuminants (see Table 4.3) and 2° CIE colorimetric standard observer, a separation image S containing printable colorant combinations was generated. We predicted (simulated) the colorimetric (LAB2000HL) values of the

Spectral Image	Size ($h \times w$)	PMSGM	SSGMS	ΔT	Percentage Difference
METACOW (cutout) [FJ04]	1024 × 1024	7.92	15.61	**7.69**	**65%**
Natural Scene 1	745 × 820	5.22	6.10	0.88	15%
Natural Scene 2	700 × 820	5.57	6.55	0.98	16%
Natural Scene 3	737 × 820	5.74	6.65	0.91	15%
Natural Scene 4	663 × 721	7.01	9.46	2.45	30%
Natural Scene 5	819 × 810	5.82	6.23	0.41	7%
Natural Scene 6	755 × 467	6.26	6.51	0.25	4%
Natural Scene 7	681 × 418	6.13	7.55	1.42	21%
Natural Scene 8	700 × 608	5.41	5.56	0.15	3%
Painting 1	1941 × 1410	11.79	**17.15**	5.36	37%
Painting 2	1410 × 1941	11.39	17.00	5.61	39%

Table 4.2.: Computational time and time difference ΔT in minutes (*min*) together with computational percentage difference associated with running the PMSGM [UB11] and SSGMS [SU15a] approaches on different spectral images. The sizes of the images are given in pixels (h and w refer to height and width respectively). The natural scenes are taken from the Foster [FANF06] database.

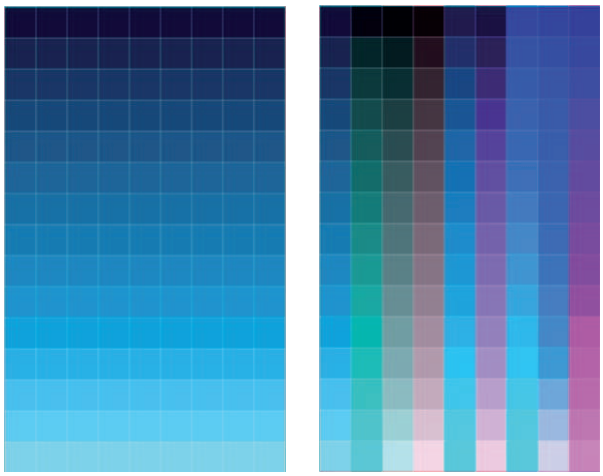

(a) (b)

Figure 4.13.: A small number of grid points (LAB2000HL values) extracted from the artificial images ($Image_1$ and $Image_2$). As can be seen in (a), all columns within each row have the same LAB2000HL values representing metamers. However, this is not the case for (b). We assume that these LAB2000HL values are obtained by rendering a spectral image under an arbitrary pair of illuminants: I_1 and I_2.

printout for the same considered pair of illuminants. These predicted values for illuminants I_1 and I_2 were stored as two other images: $Pred_1$ and $Pred_2$.

Assuming that all nine columns (representing LAB2000HL values) within each row of the $Image_1$ image led to printed metamers under the first considered illuminant I_1, we were aiming to find the metameric pairs indicating

the largest color differences under the second considered illuminant I_2. Therefore, for each row within the $Pred_2$ image – simulated from the printout under the second illuminant I_2 – we computed eight color differences (based on Euclidean norm) between the predicted (simulated) LAB2000HL values extracted from the first column and the other eight columns. Consequently, eight pairs (each consists of LAB2000HL values extracted from the first column and one of the eight remaining ones) were defined within each row, representing different color differences under the second illuminant I_2. In total, $6615 \times 8 = 52920$ pairs were considered, with different color differences.

We know that these pairs are values simulated from the printout of $Image_2$ under the second illuminant I_2. This means that the colorimetric values used in the $Image_2$ target will approximately lead to these simulated colorimetric values – under the illuminant I_2 – when the target is printed. In order to understand which colorimetric values will eventually result in these simulated pairs, 52920 different cases (pairs) were determined from the $Image_2$ target, where each pair corresponds to a simulated pair showing metamers under illuminant I_1 and non-metamers under illuminant I_2. These pairs were then sorted in descending order from the first one representing the largest color difference to the last one with the lowest colorimetric error under the second illuminant.

From the 52920 different cases, we selected the first 1350 metameric pairs representing the largest predicted color differences under the second illuminant I_2. Their corresponding LAB2000HL colors were extracted from the $Image_1$ and $Image_2$ images, and were stored as other images called $SubImage_1$ and $SubImage_2$. Figure 4.14 shows a small number of metameric pairs belonging to these images.

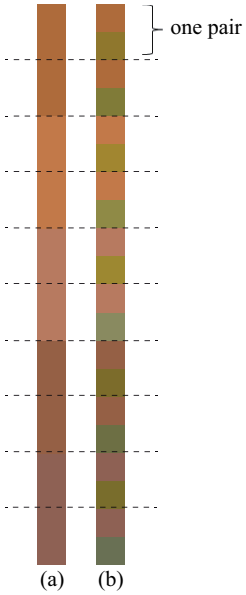

Figure 4.14.: A small number of metameric pairs extracted from the images ($SubImage_1$ and $SubImage_2$) representing the LAB2000HL colors that lead to (a) metamers under the first considered illuminant and (b) non-metamers under the second considered illuminant, indicating possibly the largest color differences.

4.3.2. Printing the Targets

In order to print the $SubImage_1$ and $SubImage_2$ images, four illuminants were considered in two pairs (see Table 4.3 and Fig. 4.15). For each pair, we planned to find the printable colorant combinations which are metamers under the first illuminant I_1, and non-metamers under the second illuminant I_2.

Type of Light Sources (Pairs)	Illuminant I_1	Illuminant I_2
Flashlights	Halogen-Based	LED-Based
Caddon Viewing Booth Illuminants	3200K	D65

Table 4.3.: Two types of light sources representing two pairs of illuminants used for generating the artificial targets for finding the printable metameric colorant combinations.

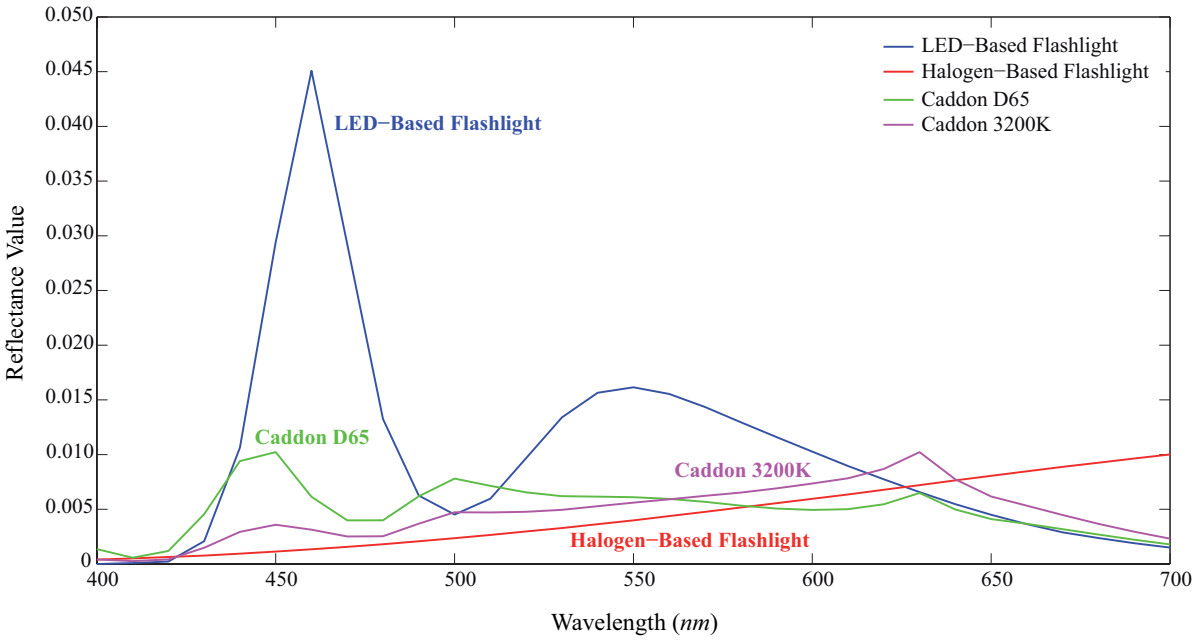

Figure 4.15.: Spectral power distribution (SPD) of four illuminants: LED-based and halogen-based flashlights as well as D65 and 3200K light sources embedded in the Caddon viewing booth. The SPDs were sampled in the range of 400 to 700 *nm*, by steps of 10 *nm*.

We used the $SubImage_1$ and $SubImage_2$ images – computed for a pair of illuminants indicated in Table 4.3 and 2° CIE standard colorimetric observer – as inputs to one of the spectral gamut mapping approaches mentioned in Section 4.3.1. The generated separation image S was then used to print the corresponding real spectral printout with HP Designjet Z3100 and Canon iPF6450 printers with seven inks (CMYKRGB). It should be noted that the HP Designjet Z3100 printer was controlled by the ONYX ProductionHouse RIP Version 7, while the Canon iPF6450 printer was controlled by a self-written raster image processor (RIP). Both printers were spectrally characterized via 20 spectral printer sub-models as previously mentioned in Section 4.2.3.1. Two paper types were

utilized: HP Premium Instant-dry Gloss Photo paper and Caddon can:proof MaxGamut 200 cd semimatt.

We visually inspected the spectral printout under both illuminants considered, in order to find those pairs representing the largest visible color differences under the second illuminant I_2 that match under I_1. Based on the colorimetric (LAB2000HL) values of the chosen pairs, we printed the spectral print samples under the two pairs of illuminants mentioned in Table 4.3. It should be noted that, although we expected to have almost no color difference between colors within each pair when viewed under the first illuminant I_1, we found cases (pairs) with color differences even above the just noticeable difference (JND). This was caused because of the inaccuracy of the employed spectral printer sub-models used to characterize the printing system.

It should be noted that since we controlled the HP Designjet Z3100 printer via an RIP, each generated 7-channel separation image S was sent directly to the printer. The halftoning process of the separation image was performed by the printer as an internal process. However, in order to print each sample via the Canon iPF6450 printer, we halftoned the generated 7-channel separation image S, using a halftoning strategy combining a tonal-value-adaptive error-diffusion algorithm [Ost01] with a threshold modulation method [BF03]. The halftoned channels were then sent individually to the printer in the form of 1-bit files (per channel).

Figure 4.16 shows one of the spectral print samples captured by a Canon EOS 5D Mark III camera. As can be seen, the rear and front of the logo are metamers under the 3200K illumination provided by the Caddon viewing booth. However, they (the rear and front of the logo) represent a noticeable color difference under the D65 light source embedded in the same viewing booth. No white balancing or chromatic adaptation was used for displaying the images.

(a) (b)

Figure 4.16.: A captured spectral print representing metamers and non-metamers under the 3200K and D65 illuminations respectively. The embedded light sources of the Caddon viewing booth were utilized. Please note that the printing and capturing process can lead to color errors. The results are more reliable in the zoomed-in electronic version of this dissertation.

Figure 4.17 shows other captured spectral prints (without white balancing or chromatic adaptation) under two light sources: (a) halogen-based and (b) LED-based flashlights. As can be seen, noticeable color differences are visible in the samples of the second row. Please note that the printing and capturing process can lead to color errors. The results are more reliable in the zoomed-in electronic version of this dissertation.

Figure 4.17.: Captured spectral prints under two light sources: (a) halogen-based and (b) LED-based flashlights. Noticeable color changes are visible in the samples of the second row. Please note that the printing and capturing process can introduce color errors. The results are more reliable in the zoomed-in electronic version of this dissertation.

4.4. Summary

In this chapter, an approach called *Spatio-Spectral Gamut Mapping and Separation* (SSGMS) [SU15a] is presented for spectral printing leading to almost an artifact-free reproduction. This method is an improvement of the PMSGM [UB11] and SGMS [SU13] approaches, because it minimizes their associated banding and smearing artifacts.

This approach is performed within a multi-illuminant framework composed of a hierarchy of application-dependent illuminants sorted from the most to the least important in the underlying application, with the aim of being as good as metameric reproduction for the most important illuminant and superior to the metameric reproduction for the rest of the illuminants considered.

To achieve this aim, a traditional metameric gamut mapping is performed for the first illuminant. For each remaining illuminant, all image pixels are traversed and gamut mappings are performed into paramer-mismatch gamuts. The paramer-mismatch gamuts are determined via parameric sets consisting of printable colorant combinations leading to paramers under the first illuminant, and different colorimetric values under the second and subsequent illuminants. The gamut mappings within paramer-mismatch gamuts ensure that color changes under the first illuminant will be unnoticeable.

For choosing appropriate colorant combinations within these parameric sets, an optimization process is performed by minimizing a cost function considering the *colorimetric* and *spatial* content of the image. The colorimetric part is used to optimize the colorimetric accuracy of the reproduction under the set of illuminants

considered, and to preserve the metameric and parameric edges. The spatial part is considered to avoid banding and smearing artifacts. A locally-adaptive trade-off between the colorimetric and spatial parts, leads to high colorimetric accuracy across considered illuminants, and reduced artifacts.

As a result of the aforementioned optimization process, a separation image, containing printable colorant combinations, is obtained. This image mimics the content of the original image, by preserving the metameric and parameric edges while avoiding banding and smearing artifacts in smooth image regions.

We tested the proposed SSGMS method using 11 spectral images. The spectral prints obtained via generated separation images by applying this approach, showed improved results in comparison with the PMSGM [UB11] and SGMS [SU13] methods. We computed the colorimetric errors between the colorimetric images rendered from spectral images under a pair of illuminants, and those obtained via simulation of the printouts using the PMSGM and SSGMS approaches. The average and 95^{th} percentile CIEDE2000 color deviations between these two methods were found to be small (below 0.2 and 1 CIEDE2000 unit respectively). This means that minimizing artifacts is not obtained at the expense of a noticeable drop in colorimetric accuracy across considered illuminants.

According to the images used in our experiments, the average and maximum extra time required by the spatial part, for computation of the SSGMS method in comparison to the colorimetric-only PMSGM approach, were found to be 2.37 and 7.69 minutes which correspond to approximately 23% and 65% percentage difference respectively.

In this chapter, we also present a simple strategy for generating artificial targets, in order to find printable colorimetric values (colors) that lead to metamers under one illuminant, but noticeable color differences under another illumination condition. These printable colorimetric values were used to generate spectral printouts representing a light indicator and security prints.

5. Specular (Gloss) Reproduction - Background and Related Work

As mentioned in the introduction (Chapter 1), four main attributes affect the visual perception of an object's material, called *color*, *gloss*, *opacity* (*translucency or transparency*), and *texture*. In Chapters 2, 3, and 4 the first attribute (color), which is related to the *spectral reflectance properties*, was discussed in colorimetric and spectral image reproduction workflows. The second attribute (gloss), which is associated with *directional reflectance properties*, is considered as the focus of this chapter and the next one. Printing gloss effects in a wide range of gloss values, gloss measurement and its relationship to gloss perception, the effect of color on perceived gloss, and the interrelation between perceived surface gloss and texture, are discussed in these chapters.

Printing masterpieces (paintings) is one of the application areas in which gloss reproduction is required. The gloss appearances of paintings are usually non-homogeneous, as a result of different painting materials used by the artist which lead to different reflectance properties. Printing these masterpieces so that they perfectly resemble the original paintings, requires accurate measurement and reproduction of perceived local surface glossiness, alongside the reproduction of other appearance attributes such as color.

Other areas in which the reproduction of gloss effects is required, include cultural heritage, aesthetic purposes, packaging, improving overall print quality (avoiding gloss-related artifacts), and security printing.

In this chapter, the general information on definition of gloss, gloss measurement and perception, together with basics of psychophysics used to study the human visual perception are presented in Section 5.1. More detailed explanation of related work conducted to understand different cues affecting the visual gloss perception and the relationship between gloss measurements and gloss perception are given in Sections 5.2 and 5.3. In Section 5.4 a summary of the chapter is presented.

5.1. Gloss Perception and Measurement

Gloss is an attribute of an object's material related to the directional-oriented specular reflection of light from the object's surface. A surface is perceived as shiny if it has a high specular reflection, while it is perceived as matt in the case of low specular reflection. Figure 5.1 represents a comparison between diffuse and specular reflections and the most common specular angles: 20°, 60°, and 85°.

There is a relationship between the amount of specular reflection and the perceived surface glossiness. The former can be determined based on rules of physics, developed standards, and measurement devices. However, determining a surface's perceived glossiness requires conducting visual experiments. Finding the relationship between these two concepts (measured gloss values and perceived gloss magnitudes) is essential for perceptually accurate reproduction of gloss.

Gloss Perception – Gloss-related studies began in 1914, when Ingersoll [Ing14] made investigations of the appearances of glossy papers. Later, in 1936, Hunter and Harold [HH87] conducted studies of gloss perception and found six visual phenomena determining the perceived glossiness of different surfaces. These visual gloss

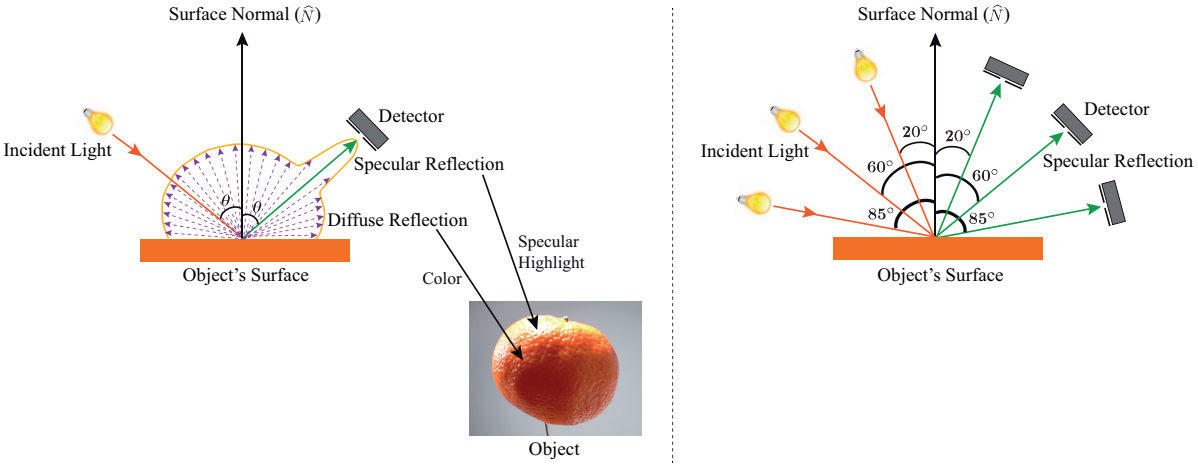

Figure 5.1.: Specular vs. diffuse reflection (left). The most common specular angles used by gloss meters (20°, 60°, and 85°) (right).

dimensions are listed as follows, with their intuitive definitions [FFTR13], [FPG01]. Figure 5.2 represents a scene in which different visual gloss dimensions can be viewed and compared.

- **Specular gloss**: It is the specular reflection at specular angles with respect to the surface normal. In other words, it is the perceived brightness determined by specular reflection from an object's surface.
- **Sheen**: It is the specular reflection at grazing angles[1] to the surface. In other words, it is the perceived shininess at grazing angles to the surface (e.g. 85°).
- **Contrast gloss**: It is the perceived difference between highlighted and adjacent areas. In other words, it is the perceived relative brightness as a result of the specularly and diffusely reflecting areas on an object's surface.
- **Haze**: It is related to the spread of the specular reflection. In other words, it is the perceived cloudiness or milky appearance of the areas adjacent to the specular reflection.
- **Distinctness-of-image (DOI)**: It is related to the potential of a material to reflect a background image on its surface. In other words, DOI is the perceived sharpness of a reflected image on a material's surface.
- **Surface uniformity**: It refers to the absence of any visible texture or defects (e.g. orange peel[2] or scratches). In other words, it is the perceived smoothness of a material's surface.

Gloss Measurement – Many attempts to measure the glossiness of surfaces have been carried out by ASTM[3], ISO[4], DIN[5], and JIS[6]. Specular gloss is defined by ASTM D523 [AST14], ASTM D2457 [AST13], ISO 2813 [ISO14a], ISO 7668 [ISO10], DIN 67530 [DIN82], and JIS Z 8741 [JIS97]. Distinctness-of-image (DOI)

[1] Grazing angle refers to the angle between the incident beam and the encountered surface. It is more common to use the grazing angle instead of the angle between the incident beam and the surface normal in cases where the incident light is nearly parallel to the surface.
[2] Orange peel refers to bumpiness on the object's surface, which is usually caused by the coating process. It resembles the surface of an orange skin.
[3] American Society for Testing and Materials
[4] International Organization for Standardization
[5] Deutsches Institut für Normung/German Institute for Standardization
[6] Japanese Industrial Standards Committee

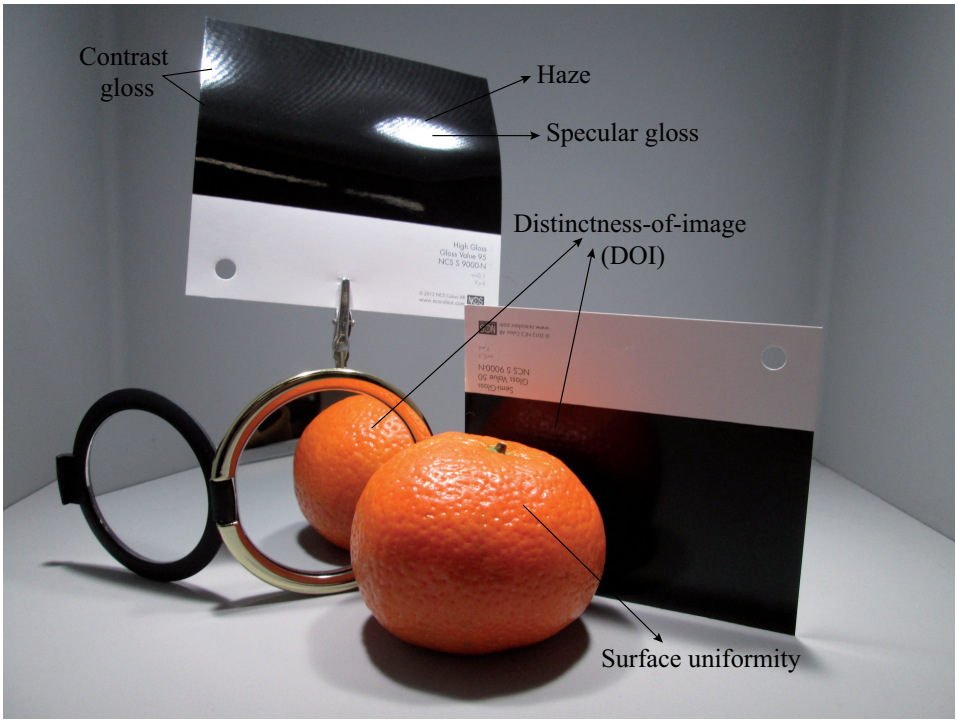

Figure 5.2.: A representation of different visual gloss dimensions according to Hunter [HH87].

gloss is defined by ASTM D5767 [AST12], and Haze gloss is determined by ASTM E430 [AST11], and ISO 13803 [ISO14b]. There are some measurement instruments available for the direct measurement of some of the aforementioned visual gloss attributes such as: gloss meters (for measuring specular/sheen gloss), haze meters (for measuring haze gloss), and orange peel/DOI meters (for measuring orange peel artifacts and distinctness-of-image (DOI) gloss).

In this dissertation, we focus mainly on *specular gloss* and use gloss meters to measure it. Gloss meters obey a physical concept [NT00] generalized by the aforementioned universal standardizations. According to these standards, the glossiness of surfaces is measured based on the illumination angle and relative to a standard mirror-like black glass with a refractive index of 1.567. The illumination angles include 20, 30, 45, 60, 75, and 85 degree of specular gloss. Among them, 20°, 60°, 75°, and 85° are the most popular specular angles in the printing industry. In general, 20°, 60°, and 85° are the most commonly used specular gloss angles. The Gloss Unit (GU) of 100 is defined for the black glass independently of the incident illumination angle [NT00], [NT00].

In general, the measurement of gloss using gloss meters is approximated by sampling the BRDF function (see Section 2.2.1) where the incident and reflected angles with respect to the surface normal are equal ($\theta_i = \theta_r$), and correspond to the aforementioned specular angles. By rotating either the gloss meter or the underlying substrate around the surface normal, different gloss values may be obtained. This occurs only for materials with anisotropic BRDFs such as brushed metal, satin, or wood. However, for materials with isotropic BRDFs, the rotation does not result in noticeable changes in measurements. Please note that the flat samples used in this dissertation have isotropic BRDFs.

According to gloss meters, specular gloss is measured as the ratio of the *luminous flux*[7] reflected from a test sample in the specular angle, to the luminous flux reflected from a black glass reference sample (embedded in gloss meters) in the same specular direction (see Eq.(5.1)) [NZM*03, SPM08]:

$$Specular\ Gloss = 100 \times \frac{\Phi_{\theta,R_\lambda^{Test}}}{\Phi_{\theta,R_\lambda^{Reference}}}, \tag{5.1}$$

where $\Phi_{\theta,R_\lambda^{Test}}$ and $\Phi_{\theta,R_\lambda^{Reference}}$ are the emitted flux of the test and reference samples respectively. The specular angles of incident and reflected light are equal and represented by θ.

In order to distinguish different samples based on their measured gloss values, it is necessary to consider an appropriate measuring geometry (illumination/viewing angle) [JPLD06].

As mentioned, many developments of gloss measurement were designed and performed by taking into account different geometries. According to the ASTM D523 [AST14] standard, three angles (20°, 60°, and 85°) were considered for the specular gloss measurement. Three gloss regions and two gloss thresholds were determined approximately via a visual gloss experiment conducted by Byk-Gardner [HH87]. In this experiment, 13 samples of black glass were ranked visually, from matt to high gloss.

The visual gloss ranks were then compared to the gloss values measured at the aforementioned specular gloss angles. Three gloss regions (low, medium, and high gloss) were determined based on parts of graphs representing higher slopes (see Fig. 5.3 taken from [JPLD06]). The measured gloss values (g in GU) related to these gloss regions are: $g < 10$, $10 \leq g \leq 70$, and $g > 70$, representing two gloss thresholds at 10 and 70 GU, which distinguish three gloss regions. The higher slopes in low, medium, and high gloss regions are associated with the curves plotted as a function of perceived gloss levels and measured gloss values at 85°, 60°, and 20° specular angles respectively. Therefore, any sample is usually measured at 60° geometry at first. If the corresponding gloss value is higher than 70 GU (high gloss), it is then re-measured at 20°. In cases where the gloss value is smaller than 10 GU (low gloss), the sample is re-measured at 85°.

However, according to Fig. 5.3, in a wide range of gloss values from 10 to 70 GU, gloss measurements at 20°, 60°, and 85° lead to corresponding curves with almost identical slopes.

In Sections 5.1.1 and 5.2, useful information about human visual perception and specifically visual gloss perception is presented.

5.1.1. Basic Psychophysics Used to Study Human Visual Perception

The term "Psychophysik" (in German) (English translation: "Psychophysics") was introduced by Fechner, with the aim of establishing a scientific approach for studying the relationship between the physical (objective) and perceptual (subjective) worlds. The former is based on measuring a physical quantity, while the latter comes from the sensorial/perceptual abilities of the human. There are also other pioneers in the field of sensory research such as Weber and Stevens, who discovered the fundamentals of sensory mechanisms [EE99].

Measuring Human Perception – A problem arises in psychophysics research, which is how to objectively measure humans' subjective/sensorial perception, for the sake of understanding their relationship. To solve this problem, *psychophysical methods* for relating human perception and physical stimuli, were defined. The basic principle of these methods is to use a physically measurable stimulus as a consistent source for multiple subjective comparisons. The parameters of the stimulus are adjusted precisely, and observers are asked to report their

[7] Luminous flux is the energy radiated from a source over visible wavelengths, resulting in visual sensation.

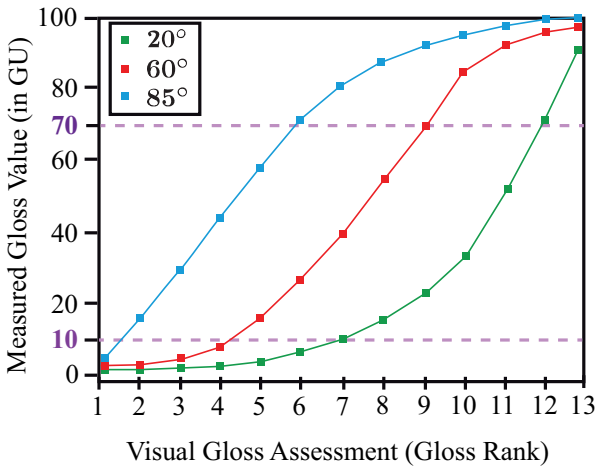

Figure 5.3.: Fundamental of the specular gloss measurement based on the specular angle. This figure has been taken from [JPLD06] and re-sketched.

perceptions with respect to the modifications. Fechner suggested using variations in observers' judgements to determine the minimum required difference for sensing the modifications made in the magnitude of the underlying stimulus. This minimum difference is called Just Noticeable Difference (JND) [EE99].

Different psychophysical methods, such as *method of adjustment*, *method of limits*, *method of constant stimuli*, *category judgment*, *pair comparison*, *rank order*, *scaling methods*, and so on, were defined. In general, in psychophysical scaling methods, observers are asked to assign numbers (scales) to the stimuli presented. The main aim is to assign magnitudes to perceptual sensations. There are different types of scaling methods, such as *category scaling* and *magnitude estimation*. For more detailed explanation of each of these methods, please refer to [EE99] and [Ges84].

Before conducting any psychophysical experiment, a method (or a combination of methods) must be chosen carefully determined by the aim of the experiment. The number of subjects (observers) and test and/or reference stimuli required, must be chosen depending on the task selected and the experimental design, to ensure the fidelity of the experiment and reliability of the result. It is important to test the color vision and/or visual acuity of the observers prior to the main experiment, using color vision and/or visual acuity tests.

Determining Psychophysical Functions – After conducting an appropriate psychophysical experiment, a set of perceptual values is obtained. The relationship between these sensorial values and psychical measurements can almost never be determined by a simple straight line in a 2-D space representing the perceptual and physical coordinates. However, the function representing the aforementioned relationship becomes steeper as it approaches the JND defining the threshold of sensation [EE99].

In 1975, Stevens suggested subtracting the JND from the measured physical value of a specific quantity. His suggestion was based on reasoning that, after passing the threshold corresponding to each specific quantity, the relationship between sensorial (perceived) values and physical measurements might be defined by a power function. Equation (5.2) represents his explanation [EE99].

$$\Psi = \eta(\gamma - \gamma_0)^{\nu}, \tag{5.2}$$

where Ψ is the perceptual magnitude predicted, γ is the stimulus intensity measured (physical value), Υ_0 is the perceptual threshold (just noticeable difference (JND)) associated with a specific quantity, and η and ν are constants.

However, a power function may not be appropriate for describing any physical-perceptual relationship. Thus, fitting different functions to the obtained data points is generally necessary in order to estimate the aforementioned relationship in different cases.

Psychophysical Methods Used in this Dissertation – Because, two of the aforementioned psychophysical methods are used in the next chapter, a brief explanation of these methods (in such a way that they are used in our experiments) follows.

- Rank order method: In this experiment, some stimuli (in our case: printed samples) are presented to the observers. Their task is to rank or sort the stimuli based on a specified criterion.
- Scaling method: In this experiment, the observers are provided with some reference and test stimuli (in our case: printed samples). The reference samples presented to the observers have some predefined scales. The observers are asked to give a scale (magnitude) to each test stimulus, based on the degree of similarity or difference they perceive between the reference and test samples.

Please refer to [Ges84], [EE99], and [Keh13] for more information about the methods, theories, and applications used in psychophysics and psychophysical experiments.

5.2. Different Cues Affecting the Visual Gloss Perception

Based on the visual gloss dimensions suggested by Hunter [HH87], different studies have been conducted in order to understand the influence of different cues on gloss perception. Interactions between surface gloss and texture [HLM08], shape [FTA04, NTO04, VLD07, WFEM10], color [WFEM10, XB08, MvV03, DNH99], and illumination geometry [LPDH11] have all been reported in the literature, mostly based on display-based experiments.

For example, Ho and co-workers [HLM08] conducted a display-based psychophysical experiment (using an LCD[8] monitor) to study how surface 3D (relief) texture affects perceived surface glossiness and vice versa. In their experiment, samples with variation in 3D texture ("bumpiness") and specularity ("glossiness") were presented to observers. The observers were asked to judge the "bumpiness" and "glossiness" of the samples. According to the obtained results, they found that these two appearance attributes affect the perception of each other so that the samples with physically glossier appearance are perceived as bumpier and the samples with physically bumpier appearance are perceived as glossier.

Marlow et al. [MKA12] extended the above display-based study and included another variable: illumination angle with respect to the surface normal. Two illumination orientations were considered: frontal and oblique. Surfaces with different reliefs yet the same gloss value were considered. Although all of the surfaces had the same reflectance properties, most of the observers perceived the surface with lowest reliefs and illuminated with the frontal light source, as glossier than the others. This visual gloss confusion or misperception occurred due to the non-linear and complex interactions between the different variables considered. Based on a hypothesis made by Marlow and co-workers, this gloss misperception can be justified by the fact that both relief and illumination conditions affect specular highlights in terms of their size, contrast, distinction (sharpness), and so on (see Fig. 5.4).

[8] Liquid Crystal Display

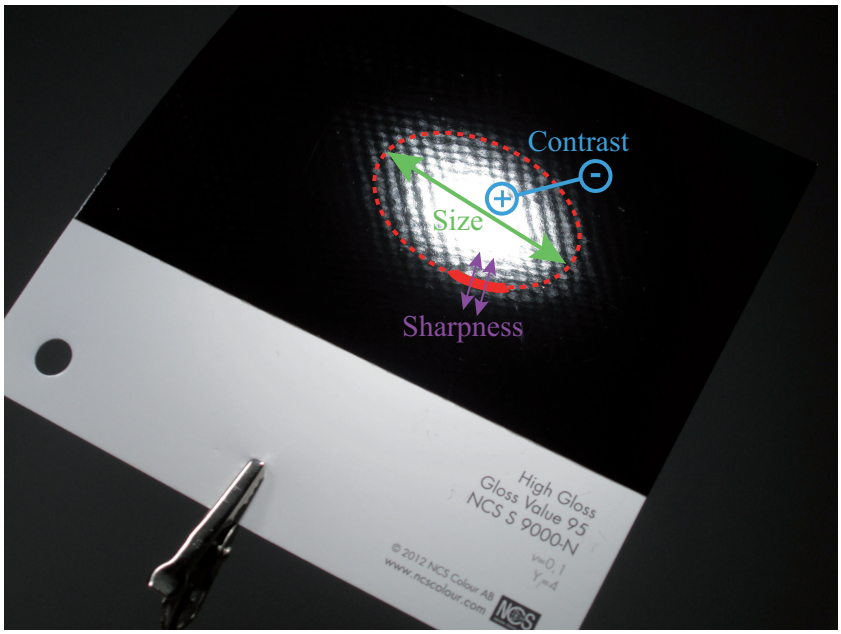

Figure 5.4.: Some of the proximal gloss cues related to specular highlights according to Marlow et al. [MKA12].

Therefore, they conducted another experiment with different observers, and asked them to scale only properties related to perceived highlights such as the size of the highlighted area, contrast, and distinctness. The new set of observers was not asked to judge surfaces based on the perceived gloss per se, or any intrinsic properties of the surfaces. They had only to focus on the part of the image representing the highlights.

Interestingly, Marlow and colleagues found that a weighted combination of the judgments based on simple and proximal attributes has almost the same trend as the glossiness judgment considering the non-linear effects of relief depths and illumination angles. According to their result, it seems that when observers are asked to judge the glossiness of surfaces, they automatically focus on the perceived "highlights" as a "proxy" for the surface glossiness and related physical properties. Based on the simple and proximal features related to those highlights, such as size, contrast, and sharpness, they judge the glossiness of the surface. Simply speaking, the brain interprets the surfaces representing large and sharp highlights to have a glossy appearance. In contrary, surfaces with blurred and small highlights are observed to have a less glossy look. This brain interpretation might be in contrast with the intrinsic physical properties of materials leading to some so-called *gloss misperceptions*.

Marlow and colleagues were not certain that only the size, contrast, and sharpness of the highlights determine the perceived glossiness; there probably exist some other attributes affecting the highlights and, as a result, affecting human gloss perception. Broadly speaking, it seems that material perception by the human visual system (HVS) is not based on complex computations of the physical properties of materials per se. What the brain seems to carry out is an exploration process for collecting some proximal imperfect cues (heuristics) from images. Then, by performing statistical analysis on the information extracted, the brain finally judges the material's appearance. Therefore, along with the correct perceptions of the materials, human visual perception might also fall into some misperceptions depending on various circumstances [Fle12]. Figure 5.5 is an example representing perception and misperception of surface glossiness. However, we may assume that in those cases which lead to visual

misperception (e.g. Fig. 5.5), it is very likely that the information received from the observer is not accurate. For instance, in Fig. 5.5, the BRDF-related information is transported to the observer based on three different viewing angles ((a), (b), and (c)). Therefore, visual gloss misperception occurs.

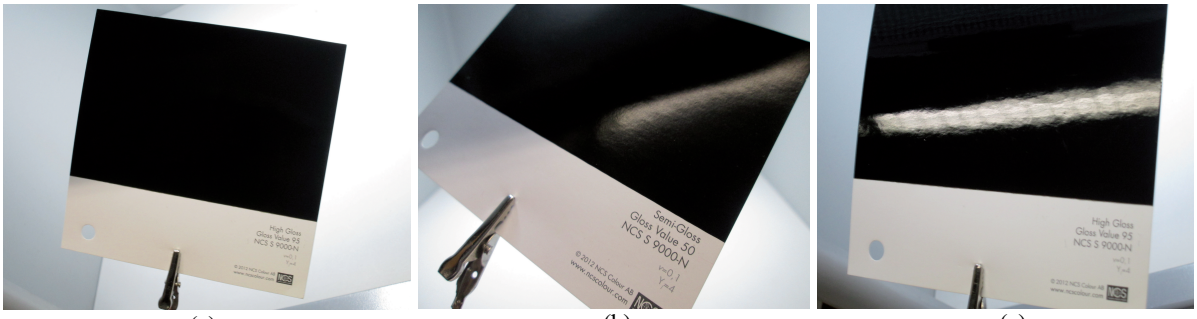

(a) (b) (c)

Figure 5.5.: Perception and misperception of gloss: As can be seen, the glossiness of the surfaces seems to increase from left to right. This gloss perception is correct in comparing the samples denoted (b) and (c). However, gloss misperception may be occurring in the other comparisons. Samples (a) and (c) have the same measured gloss level (95 GU). The gloss value of the left sample (95 GU) is higher than that of the middle one (50 GU). Although all the images were captured under CIED65 illumination with an equal ambient light source, changes in the viewing angle lead to these gloss misperceptions. It should be noted that these samples have been taken from the NCS Gloss Scale fan deck. Their gloss values have been measured at 60° specular gloss angle.

In accordance with the aforementioned study, Fleming [Fle14] suggested a general theory of material perception, based on *statistical generative models* rather than *physically-based models*. His suggested theory – which is based on computer graphics and visual research – is as follows:

"When we look at an object and experience a vivid subjective impression of its material properties, we are not actually perceiving its physical properties at all. Instead, we have learned a set of appearance characteristics–i.e., properties of the way the material tends to appear in the image–that capture its distinctive 'look' [Fle14]."

Based on the aforementioned statement, the brain does not predict the properties of the BRDF in order to estimate the glossiness of objects. However, it does use some proximal image measurements in order to understand the extent to which the material represents specular reflections (highlights). Based on this information, it generates a statistical appearance model for gloss perception automatically.

However, we believe that although the brain may not compute the properties of the BRDF (according to its equation), the perception or misperception of material appearance attributes such as *gloss* depends on the BRDF-related information received by the observer. This illumination- and viewing-angle-dependent information is a key factor of the stimulus received, for detecting the proximal cues used for building the *generative models* proposed by Fleming [Fle14] and, eventually, for judging the attributes of object's appearance, e.g. their surface glossiness.

It is noteworthy that the proximal cues (heuristics) mentioned in [MKA12] and [Fle12], representing the features of highlights used for gloss discrimination, can be mapped approximately to some of the visual gloss dimensions defined by Hunter [HH87], e.g. *contrast* and *contrast gloss*, *sharpness* and *specular gloss*, and *haze*.

There are also some discussions based on the visual gloss dimensions defined by Hunter [HH87] in the context of their real usability from the observer's point of view, in the form of a single or multiple cue(s) used for gloss perception determining the observer's gloss sensation strategy.

Leloup and co-workers [LHPD12] conducted a psychophysical experiment on real black samples in order to understand the observers' strategy for gloss evaluation. According to their result, a dichotomy was realized between the observers. Some of them considered the distinctness-of-image (DOI) as the main feature for gloss evaluation, while another group was concentrated primarily on differences in brightness of highlights (which is mostly associated with specular and contrast gloss). Therefore, they inferred that in conflicting situations (e.g. when a sample has a higher DOI gloss yet lower specular or contrast gloss in comparison to another one), the observers do not have the same criteria for gloss evaluation. Therefore, some discrepancies in terms of cue selection for gloss perception may occur. They suggested conducting more research to investigate whether gloss characterization can be performed more precisely using only a single feature or a combination of multiple cues.

Ferwerda and colleagues [FPG01] also argued that although the visual gloss dimensions proposed by Hunter [HH87] can be measured and observed, few attempts have been carried out to really understand whether they are really used by people for gloss evaluation. Therefore, they conducted an experiment using achromatic (white, gray, and black) glossy synthetic images shown on a display, to re-study the dimensionality of gloss perception. Their work was based mainly on computer graphics modeling, using a physically-based *Monte Carlo path-tracer model* –which works based on a version of *Ward's light reflection model* [War92]– to generate the computer-based images. They utilized the *multidimensional scaling* (MDS) technique to understand the dimensionality of perceptual gloss. The MDS is a statistical method that takes some distances measured between the pairs of stimuli used in a dataset. From the distances measured, the MDS predicts the overall structure of the database under consideration by revealing the hidden potential dimensions. Based on this method, a psychophysical experiment was designed, in which two synthetic, display-based images were shown at each time to each observer. The task was to determine the apparent perceptual gloss difference from 0 (small difference) to 100 (large difference), by adjusting a slider below the images.

According to their results (via display-based experiment) for glossy synthetic images, apparent gloss has two dimensions similar to distinctness-of-image (DOI) and contrast gloss, defined by Hunter [HH87] earlier. From the visual gloss dimensions suggested, they established a two-dimensional visual gloss space with perceptually meaningful axes.

They conducted two scaling psychophysical experiments known as *magnitude estimation* for DOI and contrast gloss separately. Magnitude estimation is a scaling method used for determining the relationship between the physical properties of a stimulus and its perceptual features. They found that the DOI gloss is related inversely to the spread of the specular lobe denoted by φ in Ward's light reflection model, i.e. $DOI = 1 - \varphi$.

Moreover, they realized that contract gloss can be defined as the relationship between the diffusely and specularly reflected lights denoted as ρ_d and ρ_s in Ward's light reflection model respectively, i.e. $Contrast\ Gloss = \sqrt[3]{\rho_s + \rho_d/2} - \sqrt[3]{\rho_d/2}$.

Based on the aforementioned equations, they found that DOI and contrast gloss are independent of each other. Thus, they considered them to be orthogonal axes forming the perceptually meaningful gloss space.

The relationship between the observers given gloss scales (magnitudes) and the DOI, as well as contrast gloss values – predicted via the aforementioned equations – was found to be linear. They used the linear regression to fit the data points achieved by the observers' scales and the computed magnitudes, based on the suggested equations.

In order to establish a perceptually uniform gloss space, they had to define distance metrics based on the Gloss Just Noticeable Differences (G-JNDs) for DOI and contrast gloss separately. According to Torgerson [Tor58],

the Just Noticeable Differences can be computed based on the disparities in the ratings given to any stimulus in a scaling experiment. Ferwerda et al. [FPG01] also used this concept to determine the G-JNDs. They computed the average standard deviations between the gloss scales given by the observers and the gloss values predicted by the linear regression lines mentioned. Based on their results, two G-JNDs were acquired separately for DOI and contrast gloss, which are 0.031 and 0.017 respectively.

The limitation of their method is the usage of Ward's light reflection model which cannot describe all BRDFs. Ward's model was defined in 1992 for anisotropic BRDFs, and does not take the isotropic BRDFs into account.

Obein et al. [OLKV03] argue that gloss is a second-order feature of visual sensation, which is obtained by the brain's interpretation of first-order signals (images). According to their point of view, this is the reason why subjects usually need to observe an object from different viewing angles to obtain enough first-order information (images) to finally make a conclusive judgment of the object's glossiness [OLKV03]. This point of view is very similar to the basic idea used in [MKA12], [Fle12], and [Fle14].

In the next section, the related studies conducted to investigate the relationship between gloss measurements and gloss perception, are presented.

5.3. Specular Gloss Measurements and Gloss Perception Relationship

In order to understand the relationship between specular gloss measurements and gloss perception, Billmeyer and O'Donnell [BJO87] prepared painted panels in a wide range of gloss values and in three achromatic (white, middle gray, and black) colors. They conducted a gloss scaling psychophysical experiment for estimating the visual gloss dissimilarities between each pair of panels. The surface glossiness of the samples was also measured using a gloss meter. According to their results, the aforementioned relationship does not obey a simple linear function. However, they reported that a *cubic equation* could describe this relationship better.

By conducting a psychophysical experiment using painted black samples, Obein et al. [OLKV03] also showed that the visual gloss scales and measured gloss values (using a gloss meter) are not linearly correlated.

In another study by Obein and colleagues [OKV04] using black samples, a nonlinear relationship between gloss perception and specular gloss measurements was also found. Greater sensitivity of the human observer in terms of gloss perception in both gloss extremes (i.e. matt and high gloss) was also reported. Moreover, they defined the term *gloss constancy* in a manner analogous to *color constancy*. This means that the observers are able to understand the glossiness level of surfaces approximately, regardless of the illumination geometry (e.g. 20° or 60° of specular angle). The same concept applies to color, so that the perceived color of an object remains relatively constant, regardless of variations in the illumination condition (e.g. a green apple is perceived as green during the day, afternoon and midnight). However, based on a display-based psychophysical experiment, Fleming [Fle14] realized that the observers' gloss perception is unstable under artificial and unnatural illuminants. Therefore, they argued that the human observer has partial gloss constancy which can be affected by changes in illumination conditions.

A psychophysical scaling experiment known as *magnitude estimation* was conducted by Ji and co-workers [JPLD06] to understand the relationship between gloss measurements and perception. The test samples used in their experiment contained both neutral (white, gray, and black) and colored real flat patches. A neutral (gray) patch was utilized as the reference sample. Two instruments (a gloss meter and a sphere-based spectrophotometer) were utilized for measuring the glossiness of the samples. A value of approximately 50 GU (measured at 60° specular angle) was defined for the reference sample. The observers were asked to assign a scale (magnitude) to each of the randomly-given test samples, based on a side-by-side comparison with the reference sample. The

lowest acceptable given gloss value was defined as zero (i.e. no perceived glossiness), while no upper limit was chosen, because of the principles of the magnitude estimation task. Observers were allowed to hold the reference and each of the given test samples at arm's length and tilt the samples in order to find the best viewing angle for gloss perception.

According to their result, the graph obtained from the visually scaled data and gloss measurements using a gloss meter (for 60° specualr angle), does not show a linear relationship. Two breakpoints at approximately 20 and 80 gloss units (GU), can be seen. Their result shows a similar trend to that presented by Obein et al. [OLKV03]. Ji and co-workers [JPLD06] have shown that the data can be fitted either by *three-part, linear least-square curves* considering three separate parts (i.e. $g \leq 20$ (matt gloss), $20 < g < 80$ (medium gloss), and $g \geq 80$ (high gloss), where g is a measured gloss value in GU); or by a *cubic function* with higher coefficient of determination (R^2). This result agrees with two other related studies [BJO87] and [OLKV03]. Figures 5.6 and 5.7 show the three-part linear and cubic function used by Ji et al. [JPLD06] to fit the data points. Please note that these figures are re-sketched from the original images shown in [JPLD06]; thus, the number and position of data points as well as the fitted functions are approximately represented the original images.

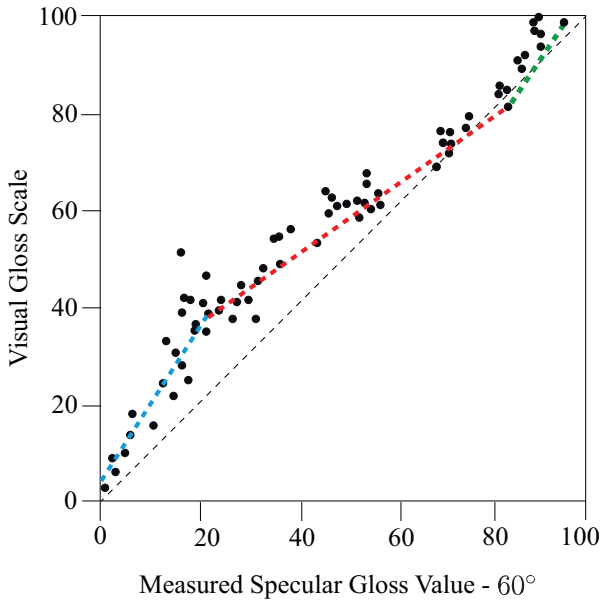

Figure 5.6.: Three-part linear function used by Ji et al. [JPLD06] to represent the relationship between measured gloss values and visual gloss scale magnitudes. There are two breakpoints in this graph, at approximately 20 and 80 GU.

As mentioned, Ji and co-workers [JPLD06] also utilized a sphere-based spectrophotometer. This instrument is based on $diff/8°$ geometry, where $diff$ refers to the diffuse illumination inside an integrating sphere and 8° represents an angle to the surface normal considered for detection of the reflected light. With this instrument, it is possible to include (SPIN[9]) or exclude (SPEX[10]) the reflected light at a specular angle via a so-called gloss trap. They conducted two sets of measurements without and with the gloss trap, to measure the reflected light

[9] Specular included
[10] Specular excluded

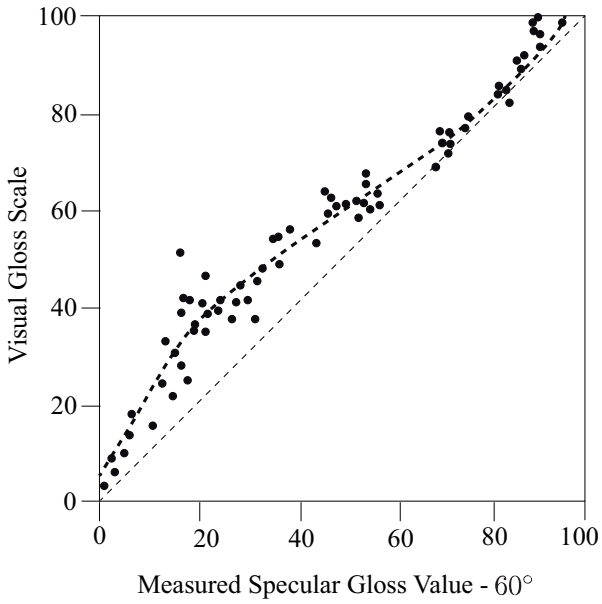

Figure 5.7.: Cubic function used by Ji et al. [JPLD06] for representing the relationship between measured gloss values and visual gloss scale magnitudes. According to Ji and co-workers [JPLD06], the data points can be better fitted via cubic equation rather than three-part linear function with higher coefficient of determination (R^2).

considering SPIN and SPEX cases respectively. The CIEXYZ values were computed from the measured reflection data. The difference between the luminance factor ΔY of the SPIN and SPEX cases (i.e. $\Delta Y = Y_{in} - Y_{ex}$) was calculated to find the light reflection at the specular angle approximately. Based on these measurements, they reported an almost linear relationship between the visual gloss scales and differences in the luminance factor, ΔY.

There is another study by Fores et al. [FFTR13] in which three psychophysical experiments were conducted using black samples to compare the sensitivity of the human observer in terms of gloss perception when viewing real prints, when viewing synthetic images shown on a LCD display, and when viewing joint real-synthetic images (i.e. the cross-media experiment).

According to their result, significant differences in the sensitivity of gloss perception were found to be dependent on the medium used. The highest gloss sensitivity was reported when real samples were used in the assessment. Slightly less sensitivity was found in the experiment where the synthetic images on the display were utilized. A large sensitivity difference was found for the cross-media experiment where the glossiness of real vs. synthetic display-based images was compared.

Although no specific fitting function was suggested by the authors, to represent the relationship between visual gloss perception and gloss measurements, the graphs plotted in the related paper represent a *three-linear* or a *cubic function*, at least for the experiment conducted with the real samples. It should be mentioned that the glossiness of the samples used in this study was limited, at most, to the medium gloss range (i.e. $20 < g < 80$ according to [JPLD06], where g is the measured gloss value in GU).

In another study, Ng et al. [NZM*03] conducted a psychophysical experiment with printed black samples to investigate the relationship between the measured gloss and Gloss Just Noticeable Difference (G-JND). In their experiment, two adjacent samples were shown simultaneously to each observer. The task was to select a sample with higher perceived glossiness from each comparison. According to their statistical analysis of the observers' judgments, the aforementioned relationship can be represented by the *Power Law*[11], i.e. G-JND $= 0.14 \times g^{0.96} \sim 0.14 \times g$, where g is the measured gloss value in GU at 60° specular angle. Based on this result, they wrote that the differences in gloss perception are analogous to differences in light intensity perception so that they both can be described via the *Weber's Law*[12].

As mentioned, in order to understand the relationship between gloss measurements and gloss perception, in almost all studies, either achromatic real samples or achromatic synthetic computer-based images were utilized, with some exceptions such as [JPLD06]. In the next chapter, we propose three printing strategies for printing colored flat samples with different gloss levels covering a wide range of gloss values, from full matt to high gloss. Afterwards, three psychophysical experiments (based on rank order and scaling methods) are conducted in order to investigate the relationship between measured gloss values and perceived gloss magnitudes, utilizing the colored-gloss printed samples. Moreover, another psychophysical experiment is conducted using 2.5D-printed samples (in gray color) varying in gloss and texture levels in order to investigate the interrelation between perceived surface gloss and texture levels.

5.4. Summary

In this chapter, the definition of gloss (specifically specular gloss), the strategies used for its measurement, and useful information on visual gloss perception, were presented. Related studies, concerning the dimensions of visual gloss perception and the latest hypothesis on how the human visual system (HVS) interprets image cues with respect to gloss, were discussed. Related investigations of the relationship between gloss measurements and gloss perception were briefly explained also.

According to these studies and the current state of the art, perception of gloss is complicated. There are some subsets of attributes – mentioned by researchers in different ways, yet sharing the same fundamental concept – which determine the observer's final judgments of a material's glossiness level. On the other hand, there are various parameters, such as the illumination conditions and geometry, the object's shape, the color, and the texture, which can influence gloss perception. In general, reliable gloss perception requires adequate BRDF-related information. If observers receive limited BRDF-related information, large variance between observer's judgments of the glossiness level may result. Thus, gloss misperceptions may occur.

The related studies found a non-linear relationship between gloss measurements and gloss perception. In these studies, which were mostly based on neutral samples, the majority of researchers inferred that the relationship could be explained either by a *three-linear* function, or by a *cubic* curve.

It should be noted that visual gloss perception and specular gloss measurements have a non-functional relationship intrinsically. This is because although a single measured gloss value might be obtained for different materials, the observer's gloss perception may lead to different visual gloss magnitudes. In this dissertation, we focus only on printed, flat, and almost homogeneous samples with isotropic BRFDs.

In the next chapter, printing local gloss levels in a wide range of gloss values and independent of the amount

[11] The Power Law defines a relationship between two quantities where the variation of one of them is influenced as the power of another. i.e $f(x) = ax^K$

[12] The Weber's Law states that an increment threshold to a background intensity is defined via a constant value (i.e. $\frac{\Delta I}{I} = K$).

of deposited inks is investigated using three printing strategies in order to avoid gloss-related artifacts that may occur during the printing process. Moreover, the relationship between measured gloss values and perceived gloss magnitudes is studied using color-printed and flat samples. The influence of samples' colors on perceived gloss levels was also studied. Moreover, the interrelation between perceived surface gloss and texture levels was investigated using 2.5D-printed samples (in gray color) varying in gloss and texture levels.

6. Printing Gloss Effects and Conducting Psychophysical Experiments

In this chapter, three main printing strategies for printing different gloss levels in a wide range of gloss values are presented which are based on varnish deposition, multi-layer, and multi-pass capabilities of the 2.5D printing systems used. These printing strategies are controlled independent of the amount of ink deposited in order to avoid gloss-related artifacts. Two groups of samples in different colors with almost flat and homogeneous appearances are printed using these printing strategies and used in psychophysical experiments to investigate the relationship between measured gloss values and perceived gloss magnitudes. The reliability of gloss meters in terms of sorting printed samples according to their measured gloss values compared to perceptual gloss ranks, is studied. Moreover, the gloss-varnish relationship and the influence of gloss (varnish) on color and vice versa are investigated. Another group of samples in two texture types and different gloss and texture levels is also printed using another 2.5D prototype printing system. A psychophysical experiment is conducted – using this set of samples – in order to investigate the interrelation between perceived gloss and texture levels of 2.5D prints.

Prior to detailed explanations, it should be mentioned that much of the content of this chapter has been published previously, in the following papers (Ref. [BSB*14], [SBU14], and [SBU*15]):

- Teun Baar, Sepideh Samadzadegan, Hans Brettel, Philipp Urban, and Maria V. Ortiz Segovia, "Printing gloss effects in a 2.5D system", SPIE Electronic Imaging Proceedings Vol. 9018: Measuring, Modeling, and Reproducing Material Appearance, San Francisco, USA., (2014).

- Sepideh Samadzadegan, Jana Blahová, Philipp Urban, "Color-Printed Gloss: Relating Measurements to Perception", 22nd Color and Imaging Conference (CIC22), pp. 207-211, Boston, Massachusetts, USA., (2014).

- Sepideh Samadzadegan, Teun Baar, Philipp Urban, Maria V. Ortiz Segovia, and Jana Blahová, "Controlling colour-printed gloss by varnish-halftones", SPIE Electronic Imaging Proceedings Vol. 9398, Measuring, Modeling, and Reproducing Material Appearance, San Francisco, California, USA., (2015).

- Teun Baar, Sepideh Samadzadegan, Philipp Urban, and Maria V. Ortiz Segovia, "Interrelation between gloss and texture perception of 2.5D-printed surfaces", SPIE Electronic Imaging Proceedings, Measuring, Modeling, and Reproducing Material Appearance, San Francisco, California, USA., (2016) – Accepted.

6.1. Printing Gloss Effects

One aspect important in assessment of print quality is the appearance of gloss across the printout. We know that the materials' optical surface properties and their surface roughness have a large impact on overall measured/perceived glossiness. This is because of the interaction between the incident light and the surface encountered. The result of this interaction determines the diffusely and specularly reflected lights associated with *color* and *gloss* respectively. For instance, a coated metallic surface is intrinsically and perceptually glossier than a piece of coarse wood. Different factors affect surface roughness/glossiness in a printing procedure, such as the substrate, colorants (inks), the printing technology/method, and the printing parameters [NZM*03].

Different printing parameters influence the printout's surface roughness. Controlling these parameters gives us local control of surface glossiness and consequently allows us to avoid some common printing artifacts, such as bronzing[1] and gloss-differential[2] (see Fig. 6.1 and 6.2). Besides improving the print quality via locally controlled gloss, printing gloss effects also has other applications, in areas such as artwork (e.g. painting) reproduction, aesthetic purposes, packaging, security printing and so on [Hod05].

Figure 6.1.: A cutout of an image captured from a printout representing *bronzing* artifacts (visible in the marked ellipses) occurred due to aggregation of deposited inks.

Figure 6.2.: A cutout of an image captured from a printout representing *gloss-differential* artifacts (visible banding in the marked ellipse) occurred due to variations in deposited ink area coverage.

In this chapter, three color-gloss printing strategies for controlling surface roughness are presented. By using these printing strategies, we printed color samples which varied in their gloss levels from "Very Matt" to almost "High Gloss" using three 2.5D (also called relief) printing systems. In this context, the 2.5D printing refers to a simplified version of 3D printing in which a flat surface always exists. Relief printing is performed on a layer-by-layer basis, rising to different heights (per voxel) on the flat side of the printout, laid on the print bed. Unlike 3D printing, usually no support material is used in 2.5D printing. The aforementioned proposed printing strategies are explained in detail in Sections 6.1.1 and 6.1.2.

It should be noted that all of the printing strategies used in this chapter dependent on the printing systems utilized and their corresponding control values/parameters. Other results might therefore be obtained when using other printing systems.

[1] Bronzing refers to some sort of metallic lustrous appearance visible on some image areas when viewed at specific viewing angles. This undesirable effect is mostly due to aggregation of ink in different spots. Some hue shifts as well as overall unevenness of glossiness appearance may occur, as a side effect of this artifact.

[2] Gloss-differential refers to inconsistent gloss appearance across an image, caused mostly by variations in deposited ink area coverage in each single spot during the printing process.

6.1.1. Gloss Control via Multi-Layer and Multi-Pass Printing

We conducted a simple preliminary experiment using a printing system with three inks: CMY (C = Cyan, M = Magenta, and Y = Yellow). In this experiment, a number of patches with different total ink area coverages, ranging from 0% to 300%, were printed on a substrate in the *traditional* (*standard*) way[3]. The glossiness levels of the printed patches were measured at a 60° specular angle using a *BYK Gardner Micro-Tri-Gloss* gloss meter. We found an almost monotonously direct relationship between the ink area coverages, from 0% to 170%, and the gloss values measured. Our results showed some slight fluctuations for the area coverages in between 170% and 300%; however, their glossiness levels were still among the highest measured gloss values (see Fig. 6.3).

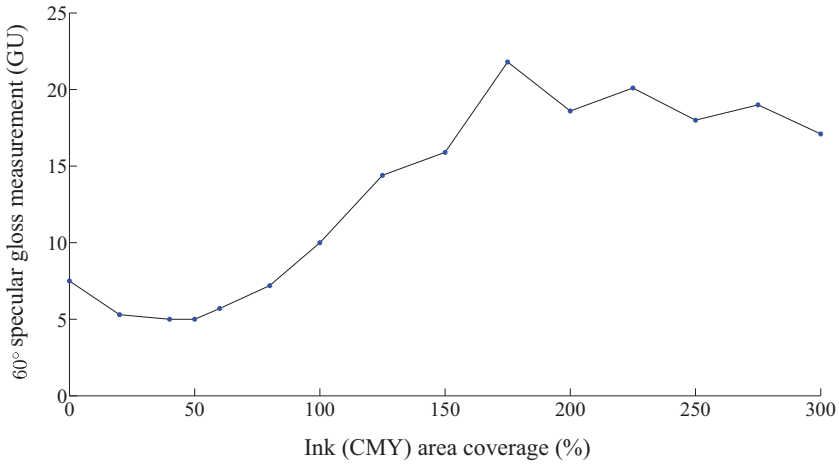

Figure 6.3.: Relationship between ink area coverages and 60° specular gloss measurements. In this experiment, the samples printed with the *traditional* printing method were utilized. This figure has been taken from [BSB*14].

This result shows that gloss-differential artifacts are very likely in *traditional* printing because the glossiness of the printout dependents on the local ink area coverage. These artifacts occur due to interactions between inks and the substrate surface roughness with the result that the inks fill microscopic holes within the substrate, resulting in smoother (glossier) appearance. In order to avoid this and achieve a printout with almost uniform gloss appearance, we devised *multi-layer* and *multi-pass* printing strategies using two prototype 2.5D printing systems (a wet-on-wet and a wet-on-dry).

Unlike the *traditional* printing strategy in which all colorant combinations are printed on the substrate in a single layer, a *multi-layer* printing strategy can print different layers, resulting in a so-called relief print. Printing of each layer can be performed either only at once or via a sequence of passes (steps) controlled by the print head's movement. This is called *multi-pass* printing, and it leads to variations in the print surface's topography (roughness). It should be noted that the *traditional*, *multi-layer*, and *multi-pass* printing strategies are terminologies have specific definitions in this dissertation, in order to clarify the work. Since there is no general agreement on these terminologies, one might find other definitions in different literatures.

In Sections 6.1.1.1 and 6.1.1.2, two printing strategies are proposed using the aforementioned *multi-layer* and

[3]The *traditional* or *standard* printing way is a term exclusively defined in this dissertation to refer to ordinary type of printing where colorant combinations (inks) are all deposited/printed in a single layer on a substrate.

multi-pass printing capabilities which lead to color-printed samples with surface roughness in the range of "Very Matt" to "Semi Matt". The gloss levels of these samples can be controlled almost independently of the ink area coverage, in order to avoid gloss-differential and bronzing artifacts.

6.1.1.1. WCMY and WWCMY Print Modes

In order to control the substrate surface roughness, we used an ink as a coating material. We chose the white ink (W) because it maximizes the reflectances achievable by a color-subtracting printing system, which eventually leads to a larger printer color gamut. Thus, the white ink (W) was deposited on the substrate to make an intermediate layer between the substrate surface and the image to be printed on top as the finish color layer, using a combination of cyan (C), magenta (M), and yellow (Y) inks.

As expected, the printout showed a glossier appearance with a more homogenous surface structure. We denoted this printing strategy by **WCMY** (**W** = White, **C** = Cyan, **M** = Magenta, and **Y** = Yellow). To control the surface gloss appearance better, we deposited another base layer of white ink (W) as a coating layer between the substrate surface and the top color layer. Consequently, glossier printouts with more uniform appearance were created. Printing another base white layer did not lead to noticeable changes; thus, two white layers were considered as the basic structure used for smoothing the roughness of the substrate surface to be covered by the finish color layer. We called this printing strategy **WWCMY** (**W** = White, **W** = White, **C** = Cyan, **M** = Magenta, and **Y** = Yellow). Figure 6.4 is a schematic representation of three print modes: *standard* (*traditional*), **WCMY**, and **WWCMY**.

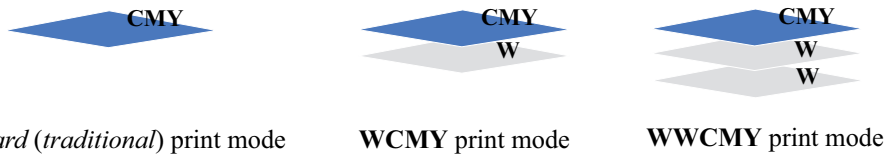

Figure 6.4.: Schematic representation of three print modes: *standard*, **WCMY**, and **WWCMY**. Here, (W) refers to base white layers and CMY represents the top color layer achieved via combinations of C, M, and Y inks. This figure has been taken from [BSB*14].

From initial printing experiments, we realized that changing the printing time (in other word, drying time (ΔT)) between two base layers of white ink, leads to variations in the substrate surface structure (roughness) and consequently the gloss appearance.

In order to control the drying time (ΔT) between applying the two base layers of white ink, we used the multi-pass capability of a 2.5D printing system. In the initial **WWCMY** print mode, 1 second passes between printing the two base layers of white ink (W) and 1 second passes between printing the second white layer and printing the top finish color (CMY) layer. By changing the strategy of the printing process for printing white layers using multi-pass printing, we are able to change the ink deposition time (drying time (ΔT)) between the white layers locally, in steps of 1 second as the result of print head's movement. The time between the second white layer and the top CMY color layer was kept constant (1 second), to ensure the minimal effect of ink area coverage on the gloss appearance.

We conducted a preliminary experiment to understand the effect of ΔT on surface glossiness. Thus, we considered 10 different cases where the time between two white layers was varied from 1 to 10 seconds in steps of 1 second. For printing the base white layers, 100% ink area coverage was utilized in all cases. Three different ink area coverages (0%, 50%, and 100%) of C, M, and Y inks were used for printing the color layer via randomly

distributed dots on halftoning screens. In total, $10 \times 3 \times 3 \times 3 = 270$ samples were printed using the **WWCMY** print mode.

The glossiness of printed samples was measured at 60° specular gloss angle using the *BYK Gardner Micro-Tri-Gloss* gloss meter. We found that, in the **WWCMY** print mode, the time delay (ΔT) between the depositions of two base white layers and the final glossiness appearance have an indirect relationship (see Fig. 6.5).

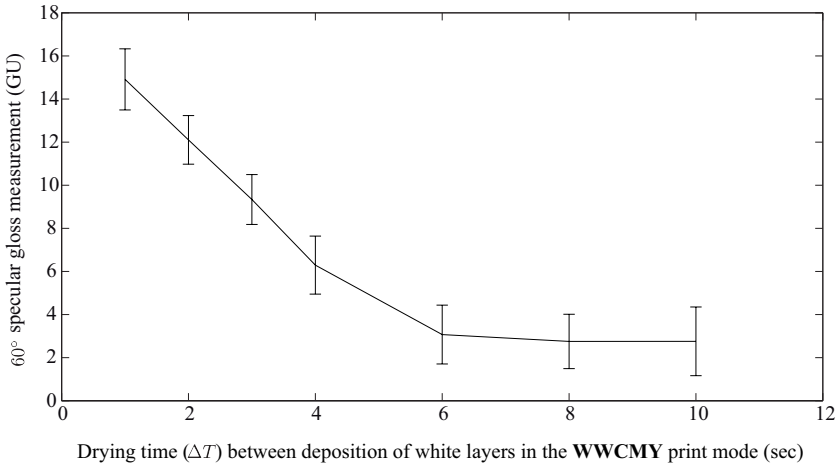

Figure 6.5.: Surface gloss measurements as a function of drying time (ΔT) variations in seconds (sec) between deposition of two base white layers in the **WWCMY** print mode. This figure has been taken from [BSB*14].

As can be seen in Fig. 6.5, increasing the drying time (ΔT) generally leads to less glossy surface appearance. We realized that this indirect relationship is dominant mostly for time variations from 1 to 6 seconds. However, no noticeable gloss differences were found between the samples printed by the **WWCMY** print mode and $6 < \Delta T \leq 10$. Some deviations from the general trend were observed, which might be due to the properties of the inks utilized or banding artifacts visible on some of the printed samples affecting the gloss measurements.

Figure 6.6 represents the 60° specular gloss measurements of the samples printed with different ink area coverages (from 0% to 300%) and various drying times (ΔTs) (from 1 to 5 seconds), using the **WWCMY** print mode. As can be seen, the measured glossiness of the printed samples is generally decreased by increasing the drying time (ΔT) from 1 to 5 seconds. However, the gloss values seem to be almost constant and independent of the ink area coverage (see separate graphs in Fig. 6.6). There are still some fluctuations in the gloss appearance that might be due to the influence of banding artifacts – occurred during the printing process – on the gloss measurements. However, the graphs represent much smoother results in comparison with the result achieved by employing the *standard* printing method (see Fig. 6.3). Therefore, applying the aforementioned printing strategy leads to a high independence of gloss appearance from variations of the ink area coverage. Consequently, avoiding or minimizing gloss-related artifacts such as bronzing and gloss-differential, is possible using the proposed **WWCMY** multi-layer and multi-pass print mode with adjustable drying time ($\Delta T \in [1,5]$ sec).

So far, our aim had been to print colored samples varying in their gloss levels, so that they represent glossier surfaces in comparison with those printed via the *traditional* (*standard*) printing method. Since we were also interested in printing surfaces with more matt appearance, we defined another printing strategy that is explained in the next section.

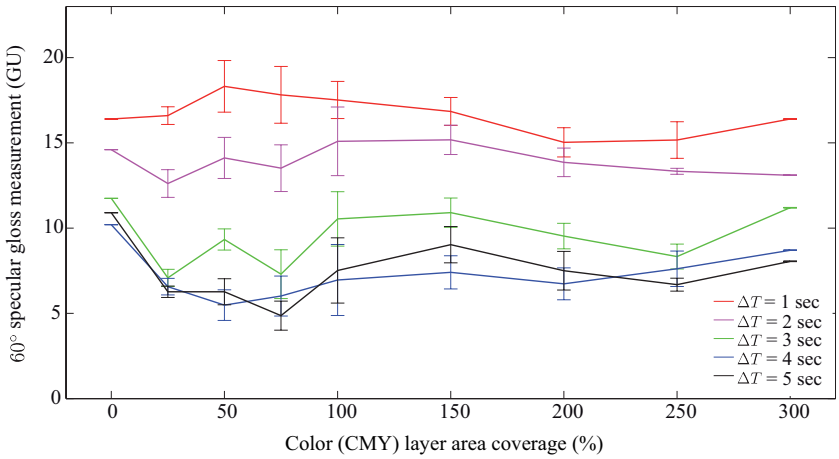

Figure 6.6.: Surface gloss measurements as a function of CMY area coverages and adjustable drying times ($\Delta T \in [1,5]$) using the **WWCMY** print mode. This figure has been taken from [BSB*14].

6.1.1.2. MCMY Print Mode

The printing strategy explained in this section is denoted by **MCMY** (**M** = Matt, **C** = Cyan, **M** = Magenta, and **Y** = Yellow) and is based on the *multi-pass* printing capability of a 2.5D printing system that was previously defined.

In **MCMY** print mode, adjacent neighboring pixels in the halftone screens are printed at different times (orders). We divided the image to be printed into 6 passes, so that each 2 passes were dedicated to one of the utilized colorants (C, M, or Y) and represented the "odd" and "even" pixels of the halftone screens separately. As a result, the odd and even pixels of each halftone screen were printed at different times (orders) leading to some variations in the drying time and, consequently, a more matt appearance. Figure 6.7 is a schematic representation of the **MCMY** print mode.

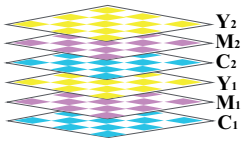

MCMY print mode

Figure 6.7.: Schematic representation of the **MCMY** print mode. This figure has been taken from [BSB*14].

Figures 6.8 and 6.9 represent a comparison between the *standard* (*traditional*) printing strategy and the proposed print modes (**WWCMY** and **MCMY**) presented in Sections 6.1.1.1 and 6.1.1.2.

As can be seen in Fig. 6.8, in contrast to the *standard* printing method, the surface glossiness achieved using the **WWCMY** and **MCMY** print modes, is almost independent of the ink area coverage. This helps to avoid bronzing and gloss-differential artifacts. On the other hand, higher and lower gloss levels can be controlled and printed via the **WWCMY** and **MCMY** print modes respectively. Moreover, as can be seen in Fig. 6.9, different

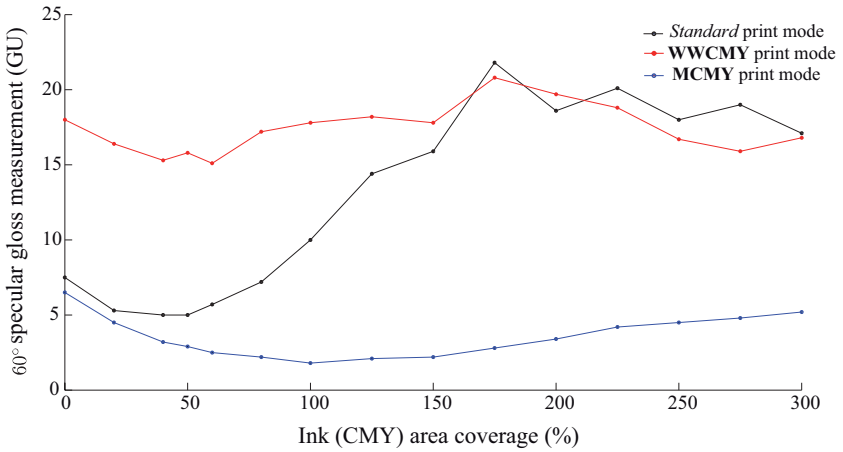

Figure 6.8.: A comparison between three print modes (*standard*, **WWCMY**, and **MCMY**) in terms of the relationship between gloss measurements and ink area coverages as well as different achieved gloss levels. This figure has been taken from [BSB*14].

levels of glossiness can be achieved via the **WWCMY** print mode with variations in the drying time (ΔT) from 1 to 5 seconds ($\Delta T \in [1,5]$ *sec*).

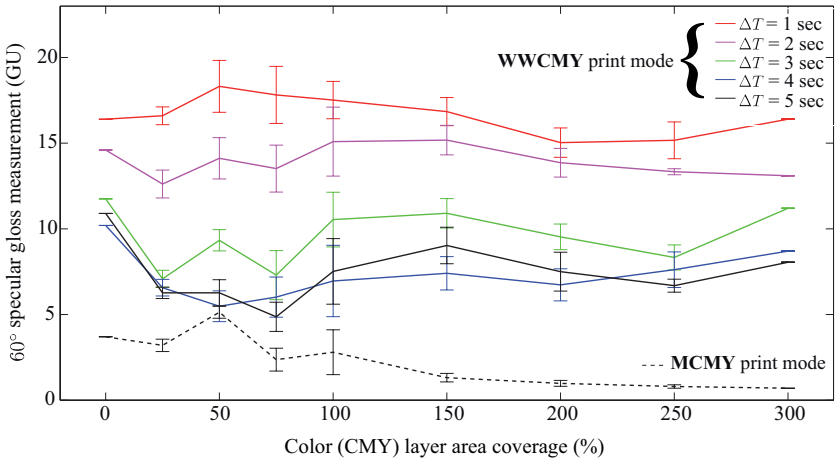

Figure 6.9.: A comparison between the **WWCMY** ($\Delta T \in [1,5]$ *sec*) and **MCMY** print modes. The comparison was made based on the relationship between gloss measurements and ink area coverages as well as different achieved levels of glossiness represented in separate graphs. This figure has been taken from [BSB*14].

It is noteworthy that using the aforementioned printing modes (**MCMY** and **WWCMY**), printing samples with "Very Matt", "Matt", and "Semi Matt" surfaces – covering a range of gloss values approximately from 0.70 to 18.10 GU – is possible. Another printing strategy for printing samples with more variations in surface glossiness, covering a wider range of gloss values from "Semi Matt" to almost "High Gloss," is proposed in the next section.

6.1.2. Gloss Control via Varnish Halftoning (VH)

Although some research into how to generate surfaces with different glossiness levels using spatially-varying varnish[4] [FFTR13] has been already done, only black samples were utilized in those studies. Here, we are interested in using varnish halftones to achieve different levels of glossiness appearance of color-printed patches.

Varnish is usually applied either in full (100%) coverage or not at all (0%). By using a halftoning method such as *Direct Binary Search* (DBS) [5] [BA03], the varnish deposition can be controlled not only in these two extremes but also in intermediate levels. By conducting some preliminary experiments, we realized that the deposition of varnish at a level of more than 60% does not lead to noticeable differences in terms of surface glossiness in the printing system utilized. Thus, 60% was considered as the maximum amount of varnish coverage (VC). Therefore, 13 different varnish coverages from 0% (no varnish at all) to 60% (maximum varnish coverage (VC)) in steps of 5% were printed. The *IJM611 Océ outdoor paper* (140 g/m^2) and the *Océ Arizona 480 GT printer* were utilized for printing the samples. This is a 2.5D printer with *multi-layer* and *multi-pass* printing capabilities. It has a varnish option together with five inks: cyan (C), magenta (M), yellow (Y), black (K), and white (W).

In order to understand the range of gloss values producible (printable) via varnish deposition in the printing system utilized, the gloss-varnish relationship, and the influence of varnish on color, an experiment was conducted. We considered 9 different sets of colorant combinations: C, M, Y, K, W, R = (M+Y), G = (C+Y), B = (C+M), and CMY = (C+M+Y). For each of them, a color ramp made of 8 different ink area coverages from 12.5% to 100% in steps of 12.5% was printed. As earlier mentioned, the printer employed enables us to use the *multi-layer* functionality. First, each color ramp was printed (in thirteen-times) generating the base "color" layer. Then, the varnish-halftoned screens (in 13 different varnish coverages from 0% to 60% by steps of 5%) were superimposed on the color layer, leading to the finish "varnish" layer. In total, 9 (colorant combinations) $\times$ 8 (ink area coverages) $\times$ 13 (varnish coverages ~ gloss levels) = 936 different patches were printed. Figure 6.10 is a schematic representation of the color-varnish printing process.

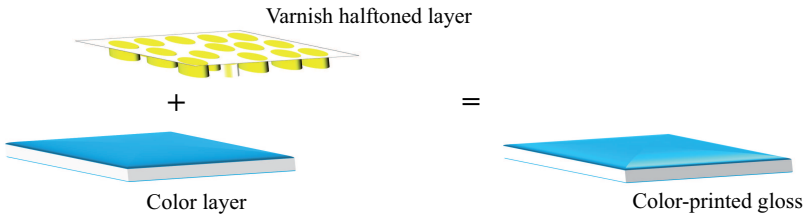

Figure 6.10.: Schematic representation of generating color-printed gloss via *Varnish Halftoning* (**VH**) strategy.

A *KSJ MG628-F2* multi-angle gloss meter was utilized to measure the gloss values of the aforementioned printed samples. For the 60° specular angle, different gloss levels from approximately 13.10 to 89.50 GU were found. This gloss range covers a wide range of gloss values from "Semi Matt" to almost "High Gloss," according to the NCS Gloss Scale[6] naming and product description.

[4] Varnish is some sort of a liquid coating that can be deposited on printed surfaces to add some appearance effects such as matt or glossy to the final finish. In our printing process, using varnish deposition leads to a glossier surface appearance.

[5] Direct Binary Search (DBS) is an iterative halftoning method. The process starts with an initial halftoned image. Many iterations are required for refining the halftone image based on a distortion metric used for calculating the perceptual error between the original and halftoned images. In each iteration and for each image pixel, either a *swapping* (the pixel with one of its 8 nearest neighbors) or a *toggling* (the pixel to the opposite color) process is conducted, based on the minimization of the considered distortion metric. The iterations proceed to the next one until obtaining the last halftoned image produced without any changes (swapping or toggling).

[6] NCS Gloss Scale is a tool composed of 28 samples in a pocket-sized fan deck format in four neutral colors: white (NCS S 0500-N), light grey (NCS S 2500-N), medium grey (NCS S 5000-N) and black (NCS S 9000-N). Each color set consists of 7 samples differing in

In the following section, the relationship between the varnish deposition amount (varnish coverage (VC)) and the corresponding measured gloss value is discussed.

6.1.2.1. Gloss-Varnish Relationship

In order to study the relationship between the amount of varnish deposited (varnish coverage (VC)) and the corresponding gloss level achieved, we selected a subset of 117 color-printed patches out of the 936 samples printed and mentioned in the previous section.

By visual inspection of the 936 printed samples, we realized that some artifacts occurred during the varnish halftoning process on samples printed with non-full ink area coverage. Therefore, we considered only the patches printed with full (100%) ink area coverage and discarded other cases (samples and their corresponding gloss measurements) possibly affected by these artifacts. Thus, 9 (colorant combinations: C, M, Y, K, W, R = (M+Y), G = (C+Y), B = (C+M), and CMY = (C+M+Y)) $\times$ 1 (ink area coverage = 100%) $\times$ 13 (gloss levels = varnish coverages (from 0% to 60% in steps of 5%)) = 117 patches were chosen. Their gloss values were measured using the *KSJ MG628-F2* gloss meter.

As can be seen in Fig. 6.11, an almost monotoniccally increasing relationship was found between varnish coverages and gloss measurements for all 9 different color sets, represented by different graphs. This means that by using of a greater amount of varnish, a glossier surface appearance can be achieved as expected.

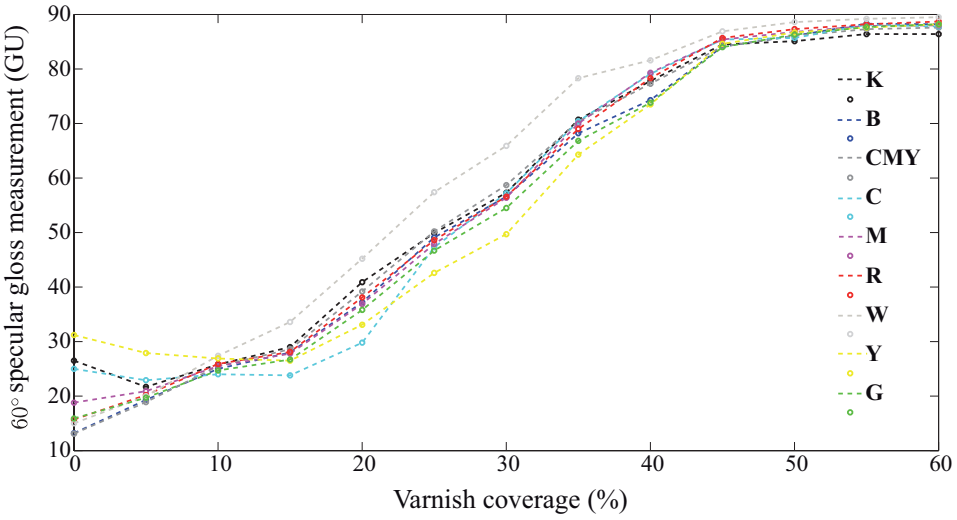

Figure 6.11.: Relationship between gloss measurements and varnish coverages. This figure has been taken from [SBU*15].

To understand the variations between the measured gloss values of the samples printed with the same amount of varnish coverage (VC), we computed 13 standard deviations (Stds) corresponding to 13 different varnish coverages. Each Std is related to a set encompassing samples with the same varnish coverage but in 9 different colors (colorant combinations). Table 6.1 shows the computed Stds for all varnish coverages.

their levels of glossiness from "Full Matt" to "High Gloss" (i.e. 2 to 95 GU measured at 60° specular angle according to the ISO 2813

VC	0%	5%	10%	15%	20%	25%	30%	35%	40%	45%	50%	55%	60%
Std (in GU)	**6.57**	2.78	1.05	2.61	**4.41**	**3.92**	**4.22**	**3.81**	2.80	0.96	1.00	0.77	0.84

Table 6.1.: Standard deviations (Stds) calculated between the 60° specular measurements of all color-printed samples in each set. Each set contains samples printed in 9 different colors but with the same amount of varnish coverage (VC). This table has been taken from [SBU*15].

As can be seen in Table 6.1, the highest value of Std (6.57) is for the case where there is no varnish deposition at all (VC = 0%). This high Std can be explained by the fact that gloss-differential or bronzing artifacts are very likely for prints without any deposited varnish or any other finishing coating. However, there are also relatively high Stds (e.g. 4.41, 4.22, 3.92, and 3.81) associated with other varnish coverages (VC > 0%). These high Stds might be due to interactions between different inks and the top varnish layer. In order to find a precise reason for these cases, investigation on the microscale level is required, which is beyond the scope of this dissertation.

6.1.2.2. Influence of Varnish on Color

To investigate the influence of varnish deposition on a sample's color, we considered all of the 117 color-printed patches used in the previous section. The color of these samples was measured via a spectrophotometer with 45°/0° (illumination/viewing) geometry. The CIEDE2000 (ΔE_{00}) color differences between each pair within each color set (each color set consists of printed patches with the same colorant combination yet 13 different varnish coverages) were computed. Table 6.2 shows the maximum ($Max_{\Delta E_{00}}$), average ($Avg_{\Delta E_{00}}$), and standard deviation ($Std_{\Delta E_{00}}$) of the computed color differences.

Test Set	C	M	Y	K	W	R	G	B	CMY
$\boldsymbol{Max}_{\Delta E_{00}}$	0.71	2.21	0.31	1.66	3.66	1.29	1.25	2.94	1.89
$\boldsymbol{Avg}_{\Delta E_{00}}$	0.28	0.61	0.15	0.62	0.92	0.55	0.40	1.09	0.69
$\boldsymbol{Std}_{\Delta E_{00}}$	0.19	0.57	0.07	0.39	1.10	0.30	0.28	0.87	0.46

Table 6.2.: The maximum ($Max_{\Delta E_{00}}$), average ($Avg_{\Delta E_{00}}$), and standard deviation ($Std_{\Delta E_{00}}$) of CIEDE2000 (ΔE_{00}) color differences computed for each color set composed of samples printed with the same colorant combination but 13 different varnish coverages. This table has been taken from [SBU*15].

Table 6.2 shows that although the maximum color differences are mostly above the Just Noticeable Difference (JND)[7], they are small. On the other hand, all of the averaged color differences are below or almost equal to the JND. Therefore, according to our results, the influence of varnish deposition on samples' colors is rather small; however, this influence is not negligible for critical printing applications in which color accuracy (around JND)

standard. The samples within each color set have visually equal gloss steps assessed by human visual experiments in terms of perceived level of glossiness.

[7] In general, Just Noticeable Difference (JND) refers to the required difference between two measured values of the same attribute so that the difference is perceivable. In color science, this definition applies to the color attribute. Thus, it refers to the minimum required amount of color difference between two measured colorimetric values before observers can reliably detect them [Bra03]. This required color difference is denoted as Just Noticeable (color) Difference (JND) in relevant literature. The amount of the JND depends on different color-difference formulas developed and the viewing condition. However, for office-based viewing condition, the value of "1" is mentioned as a rule of thumb.

is desired. For these applications, the color separation needs to be taken into account for varnish deposition.

In the following section, two examples of real color-printed gloss, based on two images and desired local gloss levels, are presented.

6.1.3. Printing Local Gloss Effects

In order to drive the printer locally via the local color and gloss values, we used a model. Based on the desired local gloss value (in the possible printable gloss range) a print mode (either **WWCMY** or **MCMY**) is chosen which is dependent either on the ink deposition (drying) time or the pixels' printing order in halftone screens. See Sections 6.1.1.1 and 6.1.1.2 for detailed explanations of these printing modes.

Figure 6.12 shows two real examples of color-printed gloss. In this figure, (a) and (d) (denoted by *color images*) represent the colors used in the original images. The gray-scale (b) and (e) images (termed *gloss masks*) illustrate the local gloss values intended to be printed. In these images, the glossiness level, from matt to glossy appearance, is represented by a tonal value from white to black.

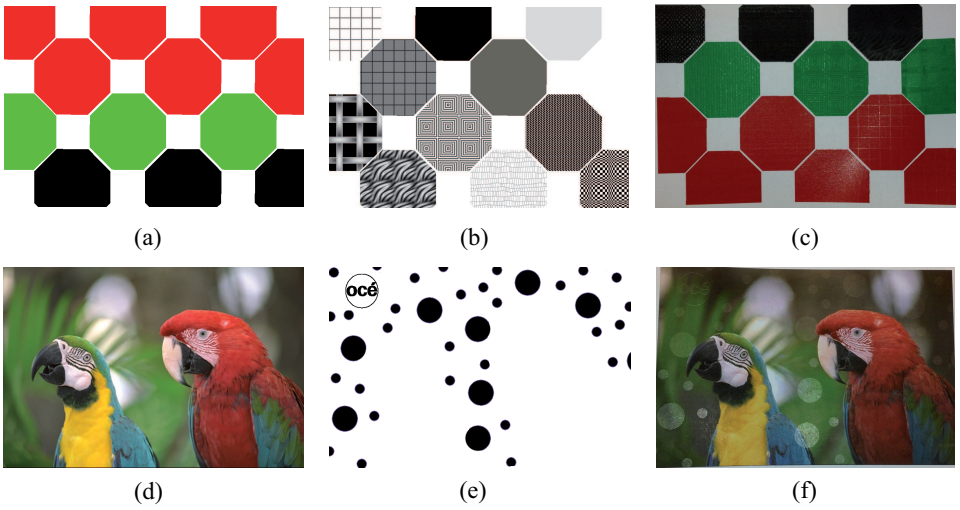

Figure 6.12.: Two examples of real color-printed gloss. The *color images* – representing the color information – are illustrated in (a) and (d). The *gloss masks* – carrying the desired printable local gloss values – are shown in (b) and (e). Eventually, the results of color-printed gloss captured from the real printouts are illustrated in (c) and (f). This figure has been taken from [BSB*14].

For printing the final printouts ((c) and (f)), a combination of printable color and gloss values has to be chosen for each image pixel. The choice of printable color is independent of the gloss value and can be performed via traditional gamut mapping methods in case of out-of-gamut colors. A print mode (either **WWCMY** or **MCMY**) is selected based on the desired local and pixel-dependent gloss level. It is worth remembering that it is possible to print and control different gloss levels by adjusting the drying time (ΔT) within the range of 1 to 5 seconds ($\Delta T \in [1,5]$ *sec*) in the **WWCMY** printing strategy. However, the **MCMY** print mode is useful for printing more matt surfaces. Eventually, the gloss level expected can be printed approximately within the range of gloss values printable using either the **WWCMY** or the **MCMY** print mode.

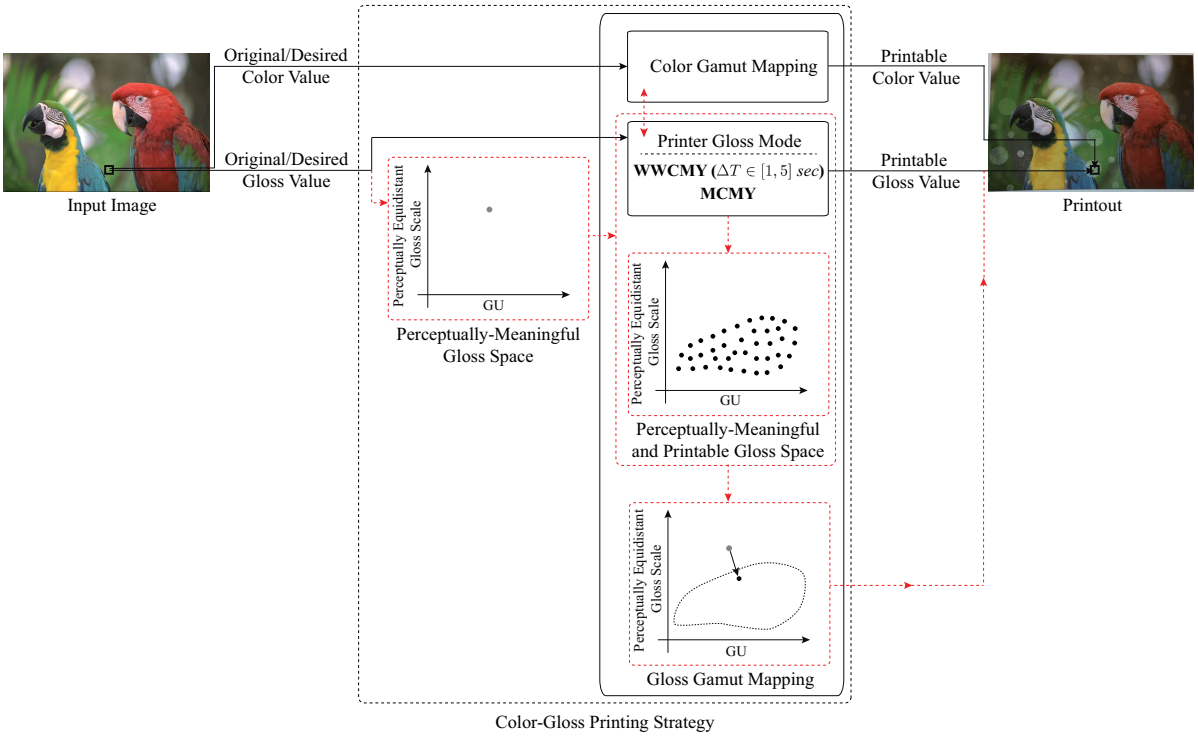

Figure 6.13.: A schematic representation of a color-gloss printing strategy (model).

Figure 6.13 is a schematic representation of the aforementioned color-gloss printing strategy. Although we treated the color and gloss separately, for more accurate reproduction, the interaction between these two appearance attributes (represented by a dashed double-headed arrow) must be taken into account. Moreover, using the spectral data rather than colorimetric values can lead to reproductions adjusted for multiple illumination conditions.

It should be noted that we didn't consider the varnish halftoning technique described in Section 6.1.2 for driving the printer and controlling the local gloss levels. This is considered a future objective, resulting in a more comprehensive color-gloss printing strategy considering a wider range of gloss values.

It is noteworthy that generating the *gloss mask* based on the local gloss values desired is not an easy, straightforward task. For a gloss reproduction from the intended gloss values which are perceptually meaningful, a perceptual gloss scale has to be defined and related to the instrumental gloss measurements and must be embedded in the color-gloss printing model. The red-dashed blocks and arrows in Fig. 6.13 represent the steps that can be added to the model used to obtain perceptually meaningful gloss reproduction. More information in this regard, relating gloss measurements to gloss perception through psychophysical experiments, is presented in the next section.

6.2. Psychophysical Experiments

As mentioned, it is very important to understand the relationship between gloss values (objective physical gloss measurements in GU) and gloss perception[8] (subjective evaluation of surface glossiness). Understanding this relationship gives us the fundamental knowledge required for gloss gamut mapping (see Fig. 6.13). Moreover, by taking the color information into account, color-gloss gamut mapping is also possible, which is left for the future work.

Therefore, we conducted three psychophysical experiments (see Sections 6.2.3, 6.2.4, and 6.2.5) based on ranking and scaling color-printed test samples according to their perceived gloss levels. Using these experiments, we investigated the relationship between measured and perceived surface glossiness. The *validity of gloss meters*[9] in terms of sorting printed flat samples (with absorption inks) based on their measured gloss values, in comparison with perceptual gloss ranking, was also studied. Moreover, the interrelation between perceived macroscopic surface texture and surface glossiness was investigated by conducting another psychophysical experiment based on gloss scaling, texture rank order and scaling strategies (see Section 6.2.6). The details of these experiments (the test and reference samples utilized, experimental setup, observers, and the tasks assigned) are explained in the subsequent sections.

6.2.1. Printed Test Samples

In Section 6.1.1, two different print modes (**WWCMY** and **MCMY**) were explained using the multi-layer and multi-pass capabilities of 2.5D printing systems to generate surfaces with different gloss levels, ranging from "Very Matt" to "Semi Matt". In Section 6.1.2, another printing method, known as *Varnish Halftoning* (**VH**), was explained and employed to print surfaces in a wider gloss range from "Semi Matt" to almost "High Gloss". Using these three printing strategies, we printed two sets of samples (**Group I** and **Group II**) defined in the next two sections (6.2.1.1 and 6.2.1.2). The gloss levels of these samples covered approximately the entire gloss range. The samples of **Group I** and **II** were used in psychophysical experiments conducted in Sections 6.2.3 to 6.2.5 in order to investigate the relationship between measured gloss values and perceived gloss magnitudes. Another set of samples (**Group III**) was also printed and used in another psychophysical experiment, conducted in Section 6.2.6, to investigate the interrelation between perceived macroscopic surface texture and gloss level.

6.2.1.1. Group I

For printing the first set of samples, the **WWCMY** and **MCMY** print modes were applied in a 2.5D printing system with three inks: cyan (C), magenta (M), and yellow (Y). We utilized three different area coverages per ink: 0%, 50%, and 100%. Thus, $3 \times 3 \times 3 = 27$ colorant combinations were considered. For each colorant combination, five patches were printed via the **WWCMY** print mode with five variations in the drying time (ΔT) between two layers of white ink (W) from 1 to 5 seconds ($\Delta T \in [1,5]$ *sec*). Another sample was also printed for each colorant combination using the **MCMY** print mode, representing a more matt surface appearance. In total, 27 (colorant combinations) $\times$ 6 (gloss levels) = 162 patches were printed in the size of approximately 9×4 *cm*.

Due to the time constraint in conducting psychophysical experiments, using all of the printed patches was not

[8] According to Hunter [HH87], there are six visual (perceptual) gloss attributes: specular gloss, sheen, contrast gloss, haze, distinctness-of-image (DOI), and surface uniformity.

[9] Note that the *validity of gloss meters* – in the sense that is explained in this dissertation – depends on the surface/material used. This is due to the fact that the gloss meters capture only a very limited amount of information. However, the observers judge the gloss level based on the total surface appearance. Thus, this was studied only within the scope of common printing systems with absorption inks.

practical. Therefore, a subset of 42 samples out of the available 162 printed patches was selected for usage in the experiments.

The samples were selected based on their *surface uniformity*[10]. This criterion was chosen due to the fact that banding artifacts (see Fig. 6.14), which had occurred during the printing process, were visible on some of the samples printed with non-full ink area coverage. Therefore, only the samples printed with full coverage were considered for the experiments. Consequently, 7 colorant combinations in 6 gloss levels were selected. The chosen colorant combinations in percent were: 1. (C =)(C,M,Y) = (100,0,0), 2. (M =)(C,M,Y) = (0,100,0), 3. (Y =)(C,M,Y) = (0,0,100), 4. (K = C+M+Y =)(C,M,Y) = (100,100,100), 5. (R = M+Y =)(C,M,Y) = (0,100,100), 6. (G = C+Y =)(C,M,Y) = (100,0,100), and 7. (B = C+M =)(C,M,Y) = (100,100,0).

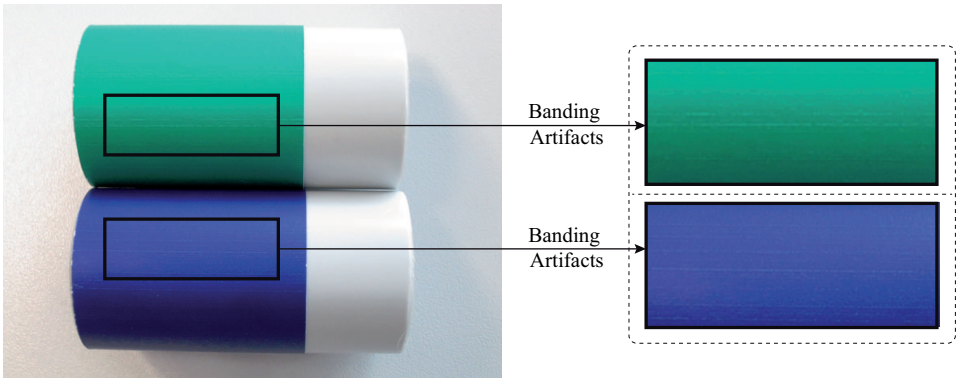

Figure 6.14.: Banding artifacts visible on some of the samples printed via **WWCMY** and **MCMY** print modes. These artifacts are more visible on the electronic version of this dissertation.

We denoted this subset of samples by **Group I** (see Fig. 6.16 as an example of the printed cyan (C) samples). Gloss values from 0.70 to 18.10 GU were found for the samples of this group via gloss measurements at 60° specular gloss angle using the *BYK Gardner Micro-Tri-Gloss* gloss meter. These gloss values cover a range of gloss levels from "Very Matt" to "Semi Matt".

6.2.1.2. Group II

Another set of samples was printed with another 2.5D printer (Océ Arizona 480 GT) using five inks (cyan (C), magenta (M), yellow (Y), black (K), and white (W)) and the *Varnish Halftoning* (**VH**) printing strategy. Nine different sets of color ramps (C, M, Y, K, W, R = (M+Y), G = (C+Y), B = (C+M), and CMY = (C+M+Y)) were generated using 8 different ink area coverages from 12.5% to 100% in steps of 12.5%. Thus $9 \times 8 = 72$ colorant combinations were printed. For each colorant combination, 13 gloss levels were generated using varnish deposition amounts in the range of 0% to 60% in steps of 5%. In total, 9 (color ramps) $\times$ 8 (ink area coverages) $\times$ 13 (varnish coverages ~ gloss levels) = 936 different samples were printed in the size of approximately 6.6×3.5 *cm*.

As mentioned previously, due to time constraint, using all of the printed patches was not practical in a psy-

[10] According to Hunter [HH87], *surface uniformity* is one of the six visual (perceptual) gloss dimensions, which is related to the degree of surface smoothness.

chophysical experiment. Because *orange peel artifacts*[11] were visible on some of the printed patches (see Fig. 6.15), we again selected a subset of samples according to the *surface uniformity* criterion. Thus, a group of patches in 9 color ramps, with total 100% ink area coverage and 6 different gloss levels generated via 6 varnish coverages (0%, 5%, 15%, 25%, 45%, and 60%), were selected. The chosen colorant combinations, in percentages, were: 1. (C =)(C,M,Y,K,W) = (100,0,0,0,0), 2. (M =)(C,M,Y,K,W) = (0,100,0,0,0), 3. (Y =)(C,M,Y,K,W) = (0,0,100,0,0), 4. (K =)(C,M,Y,K,W) = (0,0,0,100,0), 5. (W =)(C,M,Y,K,W) = (0,0,0,0,100), 6. (R = M+Y =)(C,M,Y,K,W) = (0,50,50,0,0), 7. (G = C+Y =)(C,M,Y,K,W) = (50,0,50,0,0), 8. (B = C+M =)(C,M,Y,K,W) = (50,50,0,0,0), and 9. (CMY = C+M+Y =)(C,M,Y,K,W) = (33,33,33,0,0).

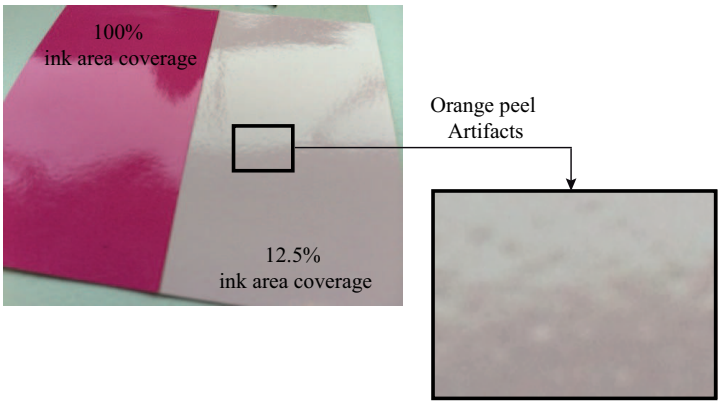

Figure 6.15.: Orange peel artifacts visible on some of the samples printed using the *Varnish Halftoning* (**VH**) printing strategy. These artifacts are more visible on the electronic version of this dissertation. This figure has been taken from [SBU*15].

In total, 9 (color ramps) $\times$ 1 (total ink area coverage = 100%) $\times$ 6 (varnish coverages ~ gloss levels) = 54 patches were chosen, with more homogeneous appearance.

We denoted this subset of samples by **Group II** (see Fig. 6.16 as an example of the printed cyan (C) samples). The gloss values from 13.10 to 89.50 GU were found for the samples in this group via gloss measurements at 60° specular gloss angle using the *KSJ MG628-F2* gloss meter. These gloss values cover a range of gloss levels from "Semi Matt" to almost "High Gloss".

Table 6.3 represents an overview of the aforementioned two subsets of samples (**Group I** and **Group II**) together with their colorant combinations, the utilized printing strategies, the number of generated gloss levels, the gloss range values, as well as the number of samples in each group.

Figure 6.16 is an example where the printed cyan (C) samples of both groups are illustrated. As can be seen in this figure, the surface glossiness of printed samples increases from left to right (**Group I** to **II**).

6.2.1.3. Group III

Unlike the flat samples of **Group I** and **II**, another set of samples (**Group III**) was printed in two different texture types: "Bumpy" ellipsoids and macroscopic "Facet"s. These samples were printed via an Océ 2.5D prototype

[11] Orange peel artifacts are some sort of bumpiness resembling the texture of an orange peel. These artifacts can occur during the coating or finishing processes. In our case, the orange peel artifacts occurred due to the varnish halftoning procedure and they were related to the surface topography of the varnish-halftoned layer.

#	Group I	Group II
1	C	C
2	M	M
3	Y	Y
4	K = (C+M+Y)	K
5	R = (M+Y)	R = (M+Y)
6	G = (C+Y)	G = (C+Y)
7	B = (C+M)	B = (C+M)
8		W
9		CMY = (C+M+Y)
Printing Strategy	**WWCMY** and **MCMY** Print Modes	*Varnish Halftoning* (**VH**)
# of Gloss Levels	6	6
Gloss Range Values	0.70-18.10 GU	13.10-89.50 GU
Type of Substrate	Océ LFM090 Top Color Paper (90 g/m^2)	Océ IJM611 Outdoor Paper (140 g/m^2)
# of Samples	42	54

Table 6.3.: Two groups of printed samples: **Group I** and **Group II**.

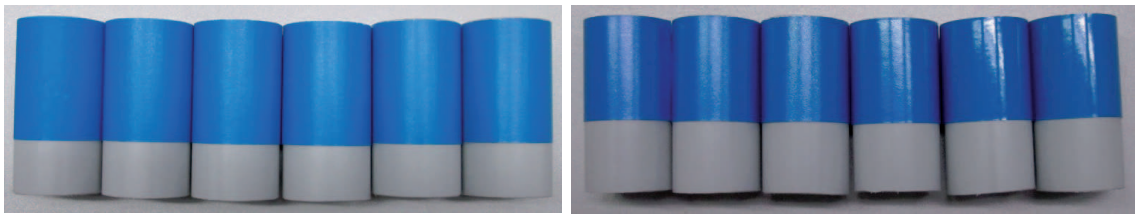

Group I **Group II**

Figure 6.16.: Printed cyan (C) samples of both sets of patches: **Group I** and **Group II**. The surface glossiness increases from left to right.

printing system – with multi-layer and multi-pass capability – only in gray color, as squares of $7 \times 7cm$. For ease of handling, each sample was surrounded by light gray and matt borders of $1cm$ both in horizontal and vertical directions, denoted by x and y respectively.

The glossiness of each texture type was controlled using the *Varnish Halftoning* (**VH**) printing strategy (explained in Section 6.1.2) in five different gloss levels generated by deposition of varnish in a range of [0,40] percent area coverages in steps of 10%.

In addition to five gloss levels, six different levels of texture – in terms of texture elevation (height) – were created for each texture type which are explained as follows:

"Bumpy" Ellipsoids – The textures of "Bumpy" patches were created based on surfaces used by Ho et al. [HLM08] and were adjusted to fit the samples' dimensions. A grid of 14×14 points was applied to each sample. The points of each grid were randomly displaced in x and y directions, so that:

$$x_{i,j} = 0.5i + 0.1\aleph[-1,1]$$
$$y_{i,j} = 0.5j + 0.1\aleph[-1,1],$$

where $\aleph[-1,1]$ is a random number chosen from a uniformly distributed set of variables in the range from -1 to 1. The "Bumpy" ellipsoids were centered on each point $(x_{i,j}, y_{i,j})$ with the radii of $0.5cm$ in the direction of x and y axes, according to the Cartesian coordinates. The amount of texture elevation of each ellipsoid was determined by its corresponding radius in the z direction ($R_{z_{i,j}}$) as follows:

$$R_{z_{i,j}} = 0.03(\hbar + 4)\aleph[-1,1], \tag{6.1}$$

where $\hbar = [0,2,3,4,5,6]$ represents texture levels corresponding to the six different texture elevations mentioned in Table 6.4 in *mm*.

The radius in the z direction $R_{z_{i,j}}$ was chosen from the uniformly distributed random variables between 0 and the maximum texture height based on the texture level $\hbar$. Although Ho et al. [HLM08] used quadratic spacing to obtain intermediate texture elevations, we employed linear spacing to create different texture heights ($R_{z_{i,j}} \sim \hbar$). It should be noted that, because the ellipsoids were intersected on each printed sample, the texture elevation of each particular position was determined based on the maximum height of the intersected ellipsoids.

Macroscopic "Facet"s – Similar to "Bumpy" patches, the macroscopic "Facet"s were created based on the surfaces used by Ho et al. [HLM08] and adjusted to fit the samples' dimensions. A grid of 14×14 points was applied to each sample. The points of each grid were displaced randomly in x and y directions, so that:

$$x_{i,j} = 0.5i + 0.24\aleph[-1,1]$$
$$y_{i,j} = 0.5j + 0.24\aleph[-1,1],$$

where $\aleph[-1,1]$ is as defined previously.

The "Facet" samples were made of connected triangular facets with random orientations. The surface height of each triangular facet in the z direction (i.e. $H_{z_{i,j}}$) was determined randomly for each location $(x_{i,j}, y_{i,j})$ according to the texture level $\hbar = [0,2,3,4,5,6]$, so that:

$$H_{z_{i,j}} = 0.0375(\hbar + 2)\aleph[-1,1], \tag{6.2}$$

where all notations are as defined previously.

The surface texture height in each local area composed of four grid points $((i,j), (i+1,j), (i,j+1)$, and $(i+1,j+1))$, was determined based on the interpolation of these points so that two triangular facets were defined. The separating edge between these triangular facets was chosen as a diagonal connecting either (i,j) and $(i+1,j+1)$ or connecting $(i,j+1)$ and $(i+1,j)$.

The edges of the elevated surfaces for both texture types ("Bumpy" and "Facet") were smoothed so that no vertical lengths were visible on the sides.

Using the aforementioned gloss and texture printing strategies, (5 = gloss variations) $\times$ (6 = texture variations) = 30 different samples varying in surface gloss level and texture elevation were printed for each texture type. Figure 6.17 and Table 6.4 represent the printed samples of **Group III**.

In the following section, the general conditions required for conducting the psychophysical experiments are explained.

Figure 6.17.: Textured samples of **Group III**: (left) "Bumpy" ellipsoids and (right) macroscopic "Facet"s.

Type	"Bumpy"	"Facet"
Color	gray	gray
Gloss Variation	5 varnish coverages: 0, 10, 20, 30 and 40%	
Texture Variation	6 texture levels, max. height: 1.2, 1.8, 2.1, 2.4, 2.7, 3 *mm*	6 texture levels, max. height: 0.75, 1.5, 1.875, 2.25, 2.625, 3 *mm*
# of Samples	30	30

Table 6.4.: Printed gloss and texture samples of **Group III**.

6.2.2. General Experimental Conditions

Since all of the psychophysical experiments conducted shared approximately the same general conditions, in this section, an overview of these conditions (observer selection, reference samples, and experimental setup) is provided.

6.2.2.1. Observers

Different numbers of color-normal or corrected-to-normal observers participated in the psychophysical experiments that will be explained in Sections 6.2.3 to 6.2.6. The exact number of participants in each psychophysical experiment is reported specifically in the corresponding section. Regardless of the number of observers, the color-vision of all of them was tested prior to the experiments via two tests: Ishihara Color Vision[12] [Ish17] and Farnsworth Munsell Dichotomus D-15[13] [Far43]. Moreover, for conducting the last psychophysical experiment, explained in Section 6.2.6, the visual acuity of observers were also examined using the Snellen test [Sne62]. This was required in order to ensure that observers could see different levels of surface gloss and texture clearly.

[12] The Ishihara Color Vision test is a color-blindness test designed for verifying red-green color-vision deficiencies, the most common kind of congenital color vision deficit.

[13] The Farnsworth Munsell Dichotomus D-15 test is a color-blindness test composing of 15 color hues of the Munsell color system. This test is used mainly for verifying red-green and blue-yellow color-vision deficiencies. It is the shortened version of the Farnsworth-Munsell 100-hue and dichotomous test [Far43].

Figure 6.18 shows the tests conducted prior to the main experiments. Only color normal or corrected-to-normal observers participated in the psychophysical experiments.

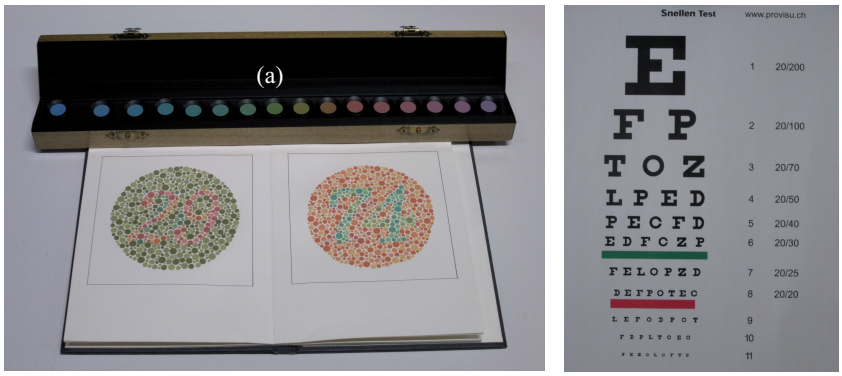

(b) (c)

Figure 6.18.: Color vision and visual acuity tests: (a) Farnsworth-Munsell Dichotomous D-15 [Far43], (b) Ishihara [Ish17], and (c) Snellen [Sne62] test.

6.2.2.2. Reference Samples

The reference samples were used only in the *gloss scaling*, *texture rank order* and *texture scaling* psychophysical experiments.

NCS[14] Gloss Scale – Either 5, 6, or 7 reference samples (depending on the corresponding gloss scaling experiments explained in Sections 6.2.4 to 6.2.6) were chosen out of the available 28 samples of the NCS Gloss Scale. All of these samples had medium gray (NCS S 5000-N) color. Their measured gloss values at 60° specular gloss angle covered the gloss range from 2 to 95 GU ("Full Matt" to "High Gloss"). They had visually equal gloss steps. We assigned some gloss scales (from 1 to 7) to these reference samples in ascending gloss order. Table 6.5 and Fig. 6.19 show these reference samples together with their associated names (according to the NCS Gloss Scale naming), their measured gloss values at 60° specular angle, and the corresponding assigned gloss scales.

Name	Full Matt	Matt	Semi Matt	Satin Matt	Semi Gloss	Glossy	High Gloss
Gloss value (in GU)	2	6	12	30	50	75	95
Gloss scale	1	2	3	4	5	6	7

Table 6.5.: NCS Gloss Scale reference samples used in the gloss scaling psychophysical experiments. This table has been taken from [SBU*15].

2.5D Textured Prints – As mentioned previously, the textured samples of **Group III** (see Section 6.2.1.3) were printed in 6 different texture levels (according to their texture height) and 5 gloss levels (using varnish halftoning in different area coverages). Two sets of textured samples (printed in only "Facet" type), with minimum (= 0% varnish coverage) and maximum (= 40% varnish coverage) printed-gloss were selected as the second group of

[14] Natural Color System

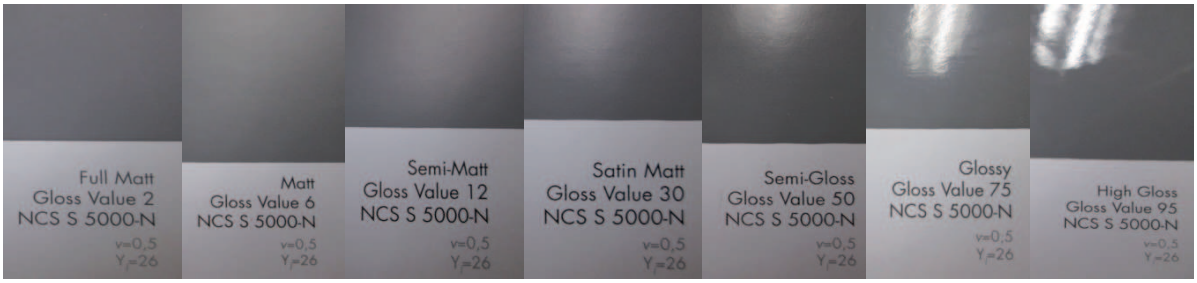

Figure 6.19.: NCS Gloss Scale reference samples used in the gloss scaling psychophysical experiments.

reference samples. Each set composed of 6 different texture levels (see Fig 6.20). These reference samples were used in the texture ranking and scaling psychophysical experiment explained in Section 6.2.6.

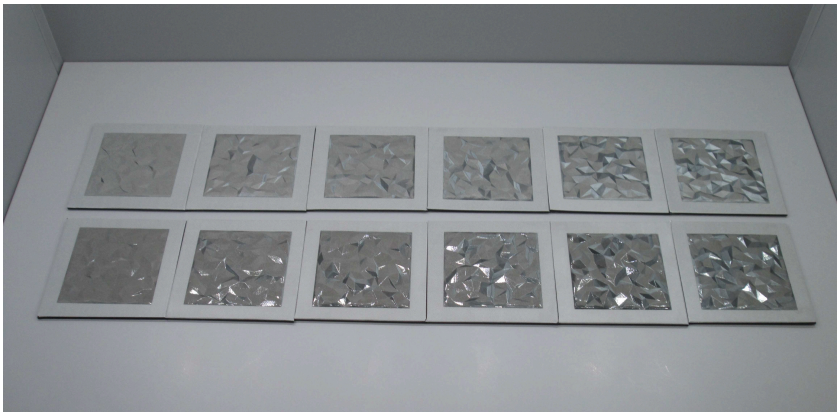

Figure 6.20.: Two sets of 2.5D textured reference samples with "Facet" texture type printed with minimum (first set = top row) and maximum (second set = bottom row) gloss, using 0% and 40% varnish deposition respectively. The six samples within each set have different texture levels, yet the same printed-gloss. These reference samples were used in the texture ranking and scaling psychophysical experiment.

6.2.2.3. Experimental Setup

All of the psychophysical experiments were conducted in a darkened room and inside a viewing booth with D65 illumination. All of the other light sources were switched off to avoid the interference of any unwanted stray light on the perception of observers.

All of the observers were asked to use a chinrest to ensure a fixed and stable condition for conducting the experiments so that the distance from the observers' eyes to the test and reference samples was approximately 60 *cm*. The observers were also asked to hold the test samples at their arm's length.

The test samples of **Group I** and **II** and the NCS Gloss Scale reference samples were attached to gray cylinders (with diameter of approximately 3 *cm*) allowing the perception of gloss in multiple viewing angles at the same

time. A small margin was left on each tube for ease of handling. When used, the NCS Gloss Scale reference samples were interconnected and placed at a fixed position inside the viewing booth to avoid their movement either unintentionally or on purpose.

Figure 6.21 illustrates some of the test samples of **Group I** and **II** together with all of the NCS Gloss Scale reference samples used in the gloss scaling experiments.

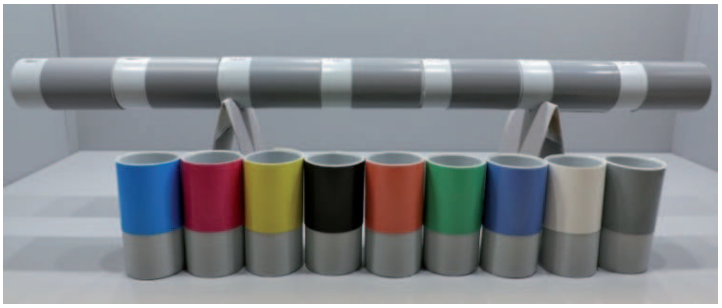

Figure 6.21.: Some of test samples of **Group I** and **II** together with the NCS Gloss Scale reference samples. This figure has been taken from [SBU*15].

Figure 6.22 shows the general psychophysical experimental setup.

Figure 6.22.: Psychophysical experimental setup. This figure has been taken from [SBU*15].

6.2.3. Psychophysical Experiment 1

The aims of conducting this psychophysical experiment are mentioned as follows.

- To study the validity of gloss meters in terms of sorting surfaces according to their measured gloss values (in a gloss range from "Very Matt" to "Semi Matt"), in comparison with perceived gloss ranks and based on the printed flat samples used in this dissertation.
- To study the influence of gloss on printed samples' perceived colors.

In this experiment, only the test samples of **Group I** (explained in Section 6.2.1.1) were considered. These samples were printed via **WWCMY** and **MCMY** print modes (see Sections 6.1.1.1 and 6.1.1.2) in 7 colorant combinations: C, M, Y, R = (M+Y), G = (C+Y), B = (C+M), and K = (C+M+Y). They covered a range of gloss values from 0.70 to 18.10 GU ("Very Matt" to "Semi Matt").

Ten color-normal observers (5 male and 5 female) participated in the experiment. Three of the participants were staff of the IDD printing lab[15] and the rest were from other groups and basically naive to the concept of the experiment.

6.2.3.1. Task: Gloss Ranking

The main experiment was based on a *gloss rank order* task. The observers were asked to sort the given test samples in the ascending order from the least glossy to the glossiest one. The gloss rank order task was conducted for separate color sets, each encompassing 6 samples printed with the same colorant combination yet different gloss levels. Figure 6.23 shows an image taken during the experiment's run-time. As can be seen, the cyan (C) color set (i.e. a mixture of 6 cyan (C) samples printed in 6 different gloss levels) was given to the observer.

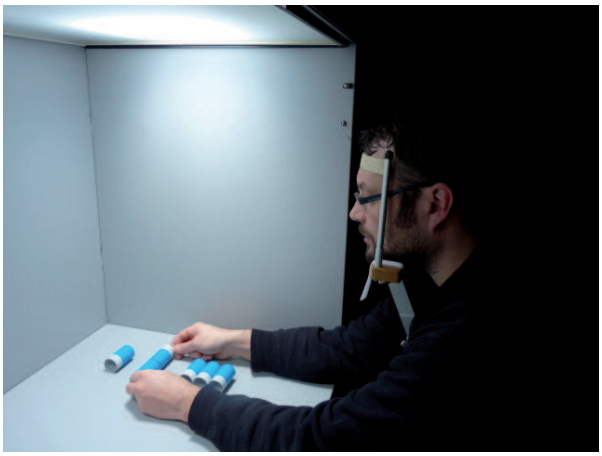

Figure 6.23.: Gloss rank order psychophysical experiment. This figure has been taken from [BSB*14].

Based on the comparisons made by the observers, they ranked the given samples of each color set according to their perceived level of glossiness. The experiment took approximately 20 minutes per observer.

Prior to conducting the psychophysical experiment, the gloss values of the test samples were measured at 20°, 60°, and 85° specular angles using the *BYK Gardner Micro-Tri-Gloss* gloss meter. Afterwards, the gloss values were sorted from the least glossy to the glossiest one.

It has been assumed that the perceptual and instrumental gloss rankings are directly correlated to each other; however, their correlation is not perfect. In order to investigate this correlation, we computed the Spearman's rank correlation coefficients (SRCCs) explained in the next section.

[15] Institut für Druckmaschinen und Druckverfahren (English: Institute of Printing Science and Technology), Darmstadt, Germany

6.2.3.2. Spearman's Rank Correlation Coefficient (*SRCC*)

To understand the relationship between the ranked gloss measurements – covering the range of gloss values between 0.70 and 18.10 GU ("Very Matt" to "Semi Matt") – and the perceptual gloss rankings of the printed test samples, the Spearman's rank correlation coefficients (SRCCs) were computed. For finding these correlations, the perceptual gloss ranks given to the samples within each color set, were averaged across all of the observers participated in the experiment. Table 6.6 shows the corresponding SRCCs for 20°, 60°, and 85° specular gloss measurements. As mentioned, these SRCCs were computed separately for different color sets.

Color Test Set	SRCC (20°)	SRCC (60°)	SRCC (85°)
C	0.6514	0.6514	0.4400
M	0.8057	0.8057	0.7829
Y	0.8800	0.8800	0.8514
R = (M+Y)	0.9314	0.9314	0.0857
G = (C+Y)	0.6800	0.6800	0.3086
B = (C+M)	0.8457	0.8457	0.3714
K = (C+M+Y)	0.9029	0.9029	0.0743

Table 6.6.: Spearman's rank correlation coefficients (SRCCs) computed between the instrumental and averaged perceptual gloss ranks. This table has been taken from [BSB*14].

As can be seen in Table 6.6, the computed SRCCs for 20° and 60° specular gloss measurements are quite identical (comparing the same color sets) and vary from 0.6514 to 0.9029. The averaged SRCC across all sets of color samples for these two specular angles, is 0.8139 which represents a high correlation between instrumental and perceptual gloss rankings. However, the SRCCs computed for the 85° specular angle show much lower correlations. These low correlations might be due to the fact that the 85° specular angle was not supported by the experimental setup used in this experiment.

In order to understand the influence of each sample's surface glossiness on its perceived color, a small study was conducted, which is explained in the next section.

6.2.3.3. Influence of Gloss on Perceived Color

Following the completion of the gloss rank order experiment for each color set, each observer was asked to answer the following two questions:

- "Was it a difficult task to order the test samples (in each color set)?"
- "Do you see any color change among the samples (in each color set)?"

Table 6.7 shows the "Yes" and "No" answers (in percent) given by the observers to the first question and for different color sets. According to these results, an average of 46% of observers found the gloss rank order task to be difficult. Since more than 50% agreed upon non-difficulty of the assigned task, and the SRCCs (considering the 20° and 60° specular angles) were high, we may assume that the gloss differences between the printed test samples were mostly above the Gloss Just Noticeable Distance (G-JND).

An average of 57% of observers reported some color changes between the samples within each color set. Since this result shows that approximately half of the observers were not agreed on the samples' color changes within each color set, we may assume that the color changes were small. This also follows the same behavior we

Hard Task?	Color Test Sets						
	C	M	Y	K	R	G	B
Yes	70%	60%	40%	50%	40%	20%	40%
No	30%	40%	60%	50%	60%	80%	60%

Table 6.7.: Observers' responses to the level of difficulty of the assigned gloss rank order task. This table has been taken from [BSB*14].

noticed in deposition of different amounts of varnish on color-printed samples which was previously discussed in Section 6.1.2.2. However, for critical printing applications – where very high color accuracy is required – color and gloss cannot be treated separately.

6.2.4. Psychophysical Experiment 2

In this section, a *gloss scaling* psychophysical experiment on the same printed patches (**Group I**) used in the previous experiment (see Sections 6.2.3 or 6.2.1.1) was conducted, with the following aims.

- To investigate the relationship between a perceptually equidistant gloss scale and measured gloss values in the range of "Very Matt" to "Semi Matt".
- To study the effect of printed samples' colors on perceived surface glossiness.

The samples' colors (CIE-L*a*b* values) were measured via a spectrophotometer with 0°/45° (illumination/viewing) geometry. Table 6.8 shows the average of the color coordinates per color set. Each set contains 6 printed patches with the same colorant combinations yet different gloss levels. The last column of this table represents the averaged pairwise CIEDE2000 (ΔE_{00}) color differences computed for each color set. As can be seen, the color variations are rather small.

Color Test Set	CIEL*	CIEa*	CIEb*	ΔE_{00}
C	54.38	-27.84	-44.79	0.98
M	41.46	69.45	-10.17	1.03
Y	88.10	-15.40	93.80	0.56
R = (M+Y)	41.57	57.01	33.32	1.83
G = (C+Y)	48.78	-71.24	30.76	1.44
B = (C+M)	21.60	24.59	-35.94	2.29
K = (C+M+Y)	22.68	-0.38	0.26	3.82

Table 6.8.: The averaged CIE-L*a*b* values together with the averaged CIEDE2000 (ΔE_{00}) color differences calculated for samples within each color set. This table has been taken from [SBU14].

In this experiment, we used 5 samples of the NCS Gloss Scale as the reference samples (see the first five samples shown in Fig. 6.19 from left to right). As mentioned previously in Section 6.2.2.2, these samples had medium gray (NCS S 5000-N) color. Their gloss values – measured at 60° specular angle – varied between 2 and 50 GU (from "Full Matt" to "Semi Gloss").

Since this experiment was based on a gloss scaling task, we assigned some gloss scales from 1 to 5 to the ref-

erence samples in ascending gloss order. Table 6.5 shows the reference samples utilized together with their names (according to the NCS Gloss Scale naming), their measured gloss values at 60° specular angle, and the corresponding assigned gloss scales. Please note that only the first five reference samples mentioned in this table (from left to right) were used in this experiment.

To conduct the experiment, 15 color-normal or corrected-to-normal observers (9 male and 6 female) participated in the experiment. Their color-vision was tested prior to the experiment using two tests mentioned in Section 6.2.2.1. The experimental condition was similar to the previous experiment (see Section 6.2.2.3). Figure 6.24 illustrates the experimental setup.

Figure 6.24.: Gloss scaling experimental setup. This figure has been taken from [SBU14].

6.2.4.1. Task: Gloss Scaling

The test samples were given to the observers randomly and one-by-one, in order to avoid the influence of observers' color adaptation on their gloss perception. The observers were asked to hold each given sample at arm's length and tilt it merely in the direction of the reference samples to judge the glossiness level of the sample's surface.

They were asked to compare the test samples to the reference samples and give a gloss scale to each of them, based on the similar gloss scales perceived from the reference samples. For higher observers' flexibility, they were also allowed to give gloss scales in steps of 0.5. Thus, the observers gave gloss scales in the range of 0.5 to 5.5, in steps of 0.5, i.e. 0.5, 1, 1.5, ..., 5, 5.5.

The gloss scales given to each test sample were averaged across all observers, in order to investigate the relationship between perceptual gloss scales and measured gloss values. Figure 6.25 shows the data points as the result of averaged visual gloss scales vs. 60° specular gloss measurements. In order to find the relationship between these two coordinates in the gloss range from 0.70 to 18.10 GU ("Very Matt" to "Semi Matt"), six functions were fitted to these data points. The employed functions and the achieved results are explained in detail in the following section.

6.2.4.2. Coefficient of Determination (R^2)

To investigate the relationship between the perceptually equidistant gloss scale and gloss measurements, an averaged perceptual gloss scale across all observers was computed for each test sample. The maximum and

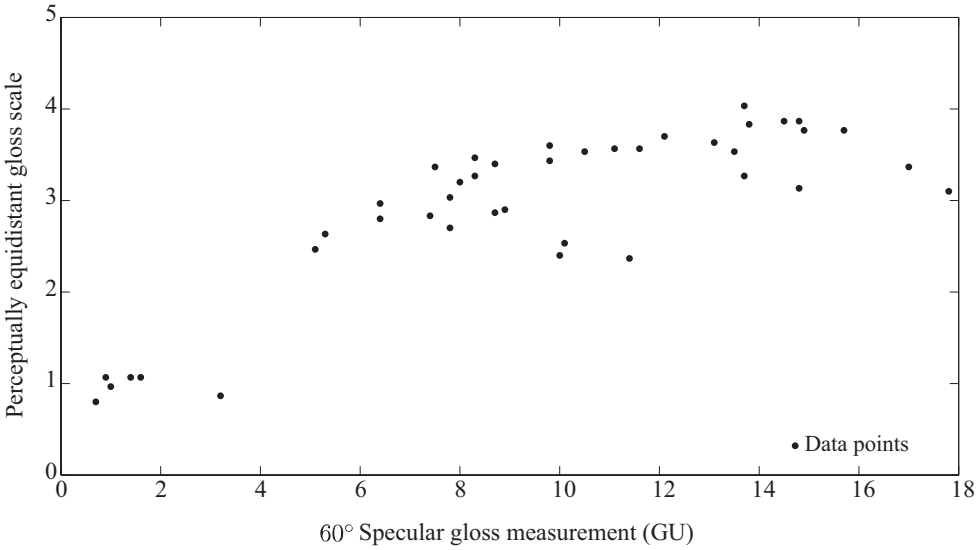

Figure 6.25.: Averaged visual gloss scales vs. 60° specular gloss measurements.

minimum standard deviations were found to be 0.9741 and 0.2211 respectively. As mentioned, Fig. 6.25 shows the data points as the result of averaged perceptual gloss scales vs. gloss measurements at 60° specular angle. We tested 6 different functions for fitting these data points. Table 6.9 lists these functions together with their corresponding equations.

Fitting Function	**Equation**
Linear	$f(x) = ax + b$
Gaussian	$f(x) = ae^{-(\frac{x-b}{c})^2}$
Exponential	$f(x) = ae^{bx}$
Power	$f(x) = ax^b + c$
Polynomial (2^{nd} degree)	$f(x) = ax^2 + bx + c$
Cubic (i.e. Polynomial (3^{rd} degree))	$f(x) = ax^3 + bx^2 + cx + d$

Table 6.9.: Functions used to fit the data points defined by "averaged visual gloss scales" and "60° specular gloss measurements". This table has been taken from [SBU*15].

To evaluate the fitting functions, the coefficients of determination (R^2s) were computed. Table 6.10 indicates how well different functions fit the data points according to their corresponding R^2s. As can be seen, the Polynomial (2^{nd} degree) and Cubic (i.e. Polynomial (3^{rd} degree)) functions represent the best fitting curves equally, with the highest R^2 = 0.8529. Figure 6.26 illustrates the fitted data points using these two functions representing the same curve. Note that the corresponding coefficient "a" for Cubic function (see Table 6.9) is very small (a = -2.965e-05).

As can be seen in this figure, the gloss perception is generally increasing from the lowest to the highest measured gloss values. However, a slightly decreasing trend is visible at almost the end of the curve for the largest measured

Coefficient of Determination (R^2)					
Linear	Gaussian	Exponential	Power	Polynomial (2nd degree)	Cubic (i.e. Polynomial (3rd degree))
0.7010	0.8358	0.6022	0.8047	**0.8529**	**0.8529**

Table 6.10.: Coefficients of determination (R^2s) computed for different fitting functions considering all data points.

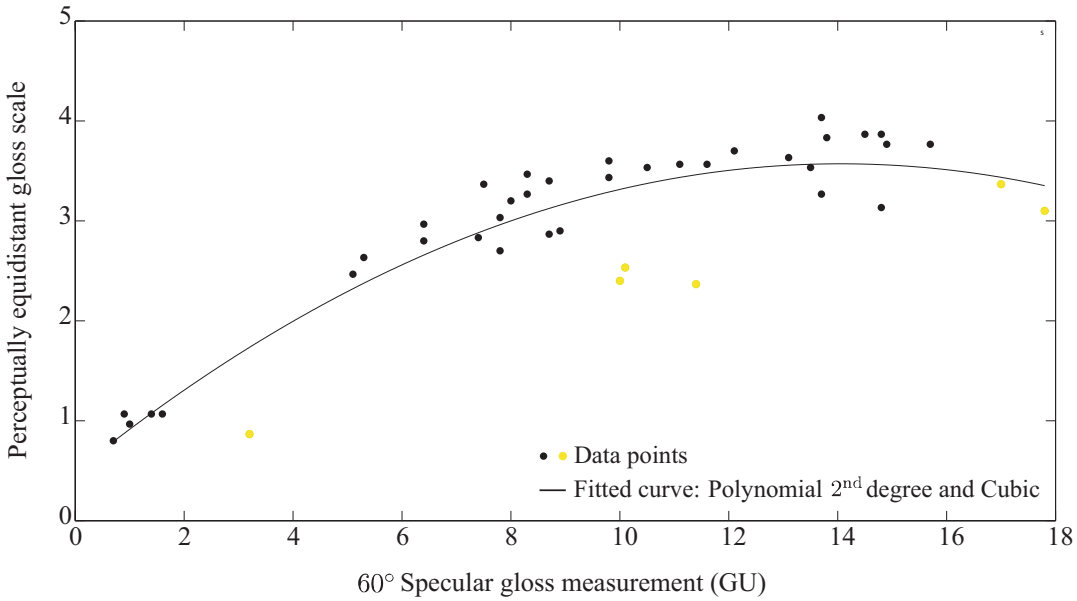

Figure 6.26.: Polynomial 2nd degree and Cubic (i.e. Polynomial 3rd degree) functions used for fitting all data points resulting in the same curve. The yellow dots represent the data points correspond to yellow (Y) samples. This figure has been taken from [SBU14].

gloss values. We believe that this is caused by the yellow (Y) samples which were perceived as less glossy, although their gloss values were larger than the others. This is because specular highlights are less visible on samples with higher lightness in comparison to darker ones. This is an example of the influence of *contrast gloss* (i.e. one of the perceptual gloss dimensions, according to Hunter [HH87]) on overall gloss perception.

In order to have a more accurate transformation from measured gloss values to perceived gloss scales, the color attribute also has to be considered along with the surface glossiness. For this reason, a small study to understand the effect of color on gloss perception was performed, and explained in the next section.

6.2.4.3. Influence of Color on Gloss Perception

To understand the effect of color on perceived surface glossiness, the perceptual gloss scales were averaged across all observers for each sample within each color set (encompassing 6 samples printed with the same colorant combination yet different gloss levels). Thus, 6 averaged perceptual gloss magnitudes were considered for each

color set.

The Polynomial 2nd degree and Cubic (i.e. Polynomial 3rd degree) functions were used for fitting the data points representing averaged visual gloss scales vs. 60° specular gloss measurements for each separate color set. These two functions were utilized because they represented the highest coefficient of determination (R^2) for all data points (i.e. joint-color sets) equally, and approximately equal performance for separate color sets (see Table 6.11).

Figures 6.27 and 6.28 show the fitted curves for separate color sets using these two functions.

	Coefficient of Determination (R^2)					
Color Test Set	**Cubic**	**Polynomial** (2nd degree)	Exponential	Gaussian	Power	Linear
C	**0.99**	**0.99**	0.54	**0.99**	0.79	0.64
M	**0.99**	**0.99**	0.78	0.98	0.96	0.87
Y	**0.96**	**0.96**	0.83	**0.96**	0.94	0.91
K = (C+M+Y)	**0.98**	**0.98**	0.78	**0.98**	0.96	0.90
R = (M+Y)	**0.96**	0.94	0.75	0.92	0.93	0.84
G = (C+Y)	**0.96**	0.94	0.75	0.91	0.93	0.83
B = (C+M)	**0.99**	0.98	0.85	0.97	0.98	0.93
Joint-Color Sets	**0.85**	**0.85**	0.60	0.83	0.80	0.70

Table 6.11.: Coefficients of determination (R^2s) computed for different fitting functions considering separate- and joint-data sets.

As can be seen in Fig. 6.27 and 6.28, almost all of the curves plotted for different color sets using either Polynomial 2nd degree or Cubic function, represent an increasing perceived glossiness trend from the smallest to the largest measured gloss values. The graphs plotted for the red (R) and green (G) color test sets using the Cubic function, show slightly constant behavior from approximately 7 to 11 GU. The cyan (C) curves in both figures represent a decreasing trend at the highest gloss values, from approximately 10 to 15 GU. We do not have any specific explanation for that.

As another result, we noticed that lighter samples, with higher lightness values, were perceived as less glossy than the darker ones. This is probably caused by a smaller luminance contrast between specular and off-specular angles. The corresponding visual gloss attribute is called *contrast gloss*, and is not related to the specular gloss measurements; thus, it is not considered in the measurements conducted via gloss meter.

Eventually, we believe that the influence of color on gloss perception can be explained more precisely using two terms: the *general perceived glossiness trend* and the *perceived gloss magnitudes*. We found that the effect of color on the general perceived glossiness trend is not noticeable since an increasing function of perceived gloss scales and measured gloss values can almost always be noticed, regardless of the samples' color variations, which agrees with the reported result in [JPLD06]. However, lighter samples with larger lightness values are perceived as less glossy than the darker ones, due to the influence of *contrast gloss* on the overall gloss perception. This means that specular highlights have a larger contrast on darker samples, leading to higher overall perceived surface glossiness.

6.2.5. Psychophysical Experiment 3

As mentioned previously, the gloss rank order and gloss scaling psychophysical experiments conducted in Sections 6.2.3 and 6.2.4 were based only on the printed samples of **Group I** (see Section 6.2.1.1). These samples

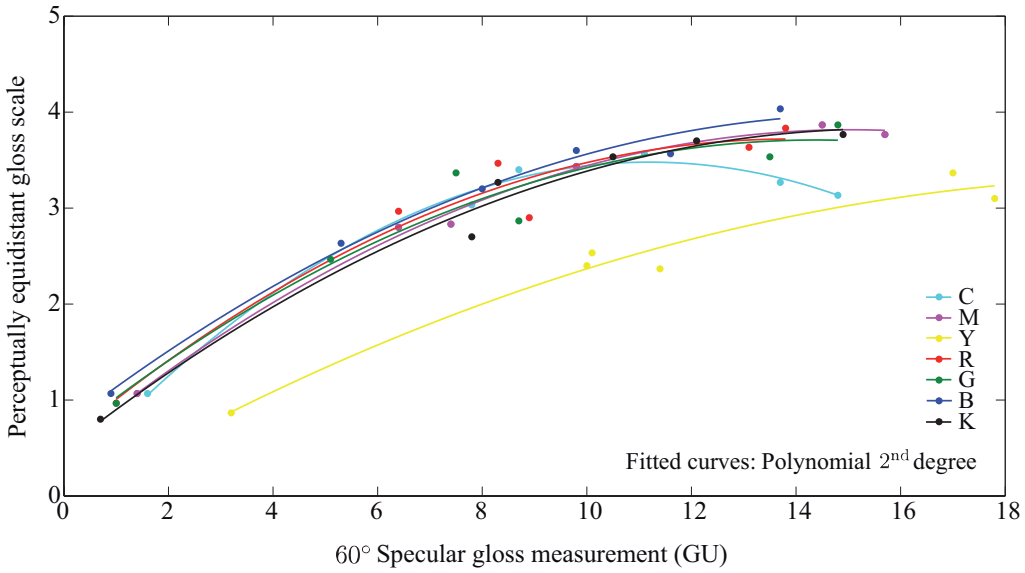

Figure 6.27.: Polynomial 2nd degree function used to fit the data points within separate color sets. This figure has been taken from [SBU14].

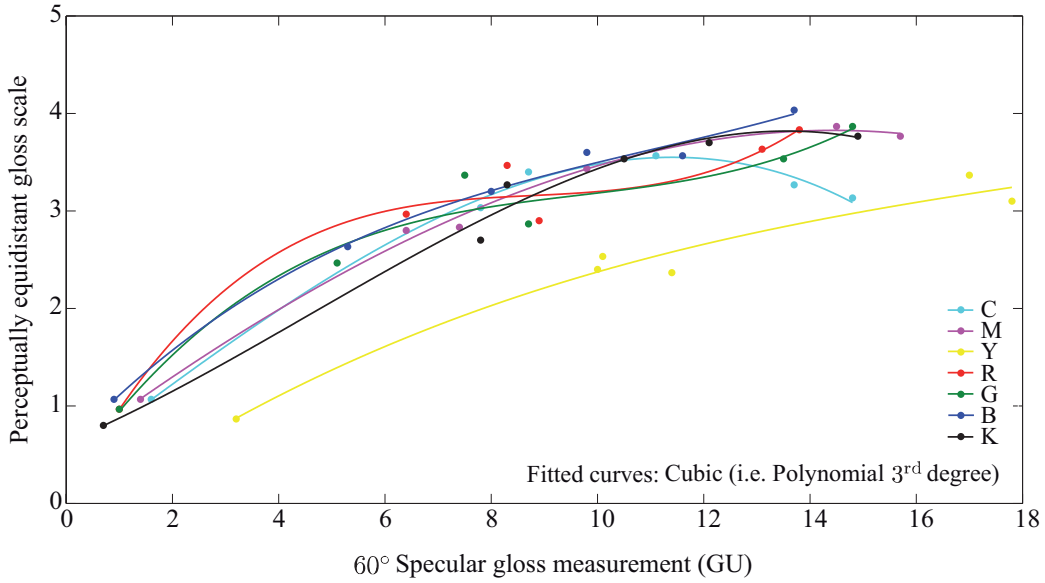

Figure 6.28.: Cubic (i.e. Polynomial 3rd degree) function used to fit the data points within separate color sets.

were printed using the **WWCMY** and **MCMY** print modes explained in Sections 6.1.1.1 and 6.1.1.2. Utilizing these printing strategies, printing color-samples with gloss variations in the range of approximately 0.70 GU

("Very Matt") to 18.10 GU ("Semi Matt") is possible. However, the *Varnish Halftoning* (**VH**) printing strategy described in Section 6.1.2, enables us to print color-samples covering a wider range of gloss values from approximately 13.10 GU ("Semi Matt") to 89.50 GU (almost "High Gloss"). The samples printed via this printing method composed another set denoted by **Group II** (see Section 6.2.1.2).

In this section, we conducted another *gloss scaling* psychophysical experiment and an *indirect gloss rank order* observer study using the samples of **Group II**.

The aims of the experiment and study conducted were:

- To study the validity of gloss meters in terms of sorting surfaces according to their measured gloss values (in a wide gloss range from "Semi Matt" to almost "High Gloss"), in comparison with perceptual gloss ranks and based on the printed flat samples used in this dissertation.
- To investigate the relationship between a perceptually equidistant gloss scale and gloss values measured approximately in an entire gloss range from "Full Matt" to almost "High Gloss".

We selected 7 samples of the NCS Gloss Scale (see Section 6.2.2.2) as the reference samples. Table 6.5 and Fig. 6.19 show the reference samples used in this experiment, together with their gloss values measured at 60° specular angle and the assigned gloss scales from 1 to 7.

For conducting the experiment, 17 color-normal or corrected-to-normal observers (6 female and 11 male) participated in the experiment. Their color-vision was tested prior to the experiment with two tests mentioned in Section 6.2.2.1.

The experimental setup was the same as the previous psychophysical experiments and was described in Section 6.2.2.3. Figure 6.24 also shows the experimental setup.

6.2.5.1. Task: Gloss Scaling

The test samples were given to the observers randomly and one-by-one to avoid the interference of observers' color adaptation on their gloss perception. The observers were asked to compare each given test sample to all reference samples and to give a gloss scale based on similarity to the gloss scale they perceived from a reference sample. For higher observers' flexibility, they were also allowed to give gloss magnitudes in half steps. Thus, they could assign gloss scales to the test samples in the range of 0.5 to 7.5 in steps of 0.5 (i.e. 0.5, 1, 1.5,..., 7,7.5).

In order to examine the reliability of gloss meters, in terms of gloss rankings compared to perceptual gloss rankings (in a wide gloss range), we computed the Spearman's rank correlation coefficient (SRCC) which is explained in more detail in the next section.

6.2.5.2. Spearman's Rank Correlation Coefficient (*SRCC*)

As mentioned in the first psychophysical experiment (see Section 6.2.3), we previously conducted a gloss rank order experiment to understand the rank order correlation between gloss measurements and perceptual gloss magnitudes in the range of "Full Matt" to "Semi Matt"'.

To investigate this correlation in a wider gloss range from "Semi Matt" to almost "High Gloss", we indirectly computed the perceptual gloss ranks from the observers' given gloss scales obtained from the gloss scale psychophysical experiment explained in the previous section. The indirectly computed perceptual gloss ranks for each test sample were averaged across all observers, to obtain a single perceptual gloss rank for any test sample. The measured gloss values – at 20°, 60°, and 85° specular angles – were also sorted in ascending gloss order

from the least glossy to the glossiest sample.

Eventually, the Spearman's rank correlation coefficients (SRCCs) were computed between the indirectly averaged perceptual gloss ranks and the ranked gloss measurements for 20°, 60°, and 85° specular angles. Table 6.12 shows the separately computed SRCCs for different color sets.

Color Test Set		C	M	Y	K	W	R	G	B	CMY
SRCC	**20°**	0.90	0.94	0.94	0.82	1.00	1.00	0.94	1.00	1.00
	60°	0.84	0.94	0.94	0.82	1.00	1.00	0.94	1.00	1.00
	85°	0.84	0.94	0.94	0.94	1.00	1.00	0.94	1.00	1.00

Table 6.12.: Spearman's rank correlation coefficients (SRCCs) between the instrumental and averaged perceptual gloss ranks considering a wide range of gloss values from "Semi Matt" to almost "High Gloss". This table has been taken from [SBU*15].

As can be seen in Table 6.12, very high correlations were found between the instrumental and averaged perceptual gloss ranks for all color sets, covering a wide range of gloss values, from "Semi Matt" to almost "High Gloss". Therefore, we can deduce that the gloss meters are reliable in terms of ranking printed flat surfaces (with almost homogeneous surface topographies and isotropic BRDFs) according to their measured gloss values, in comparison with the corresponding perceived gloss magnitudes. Please note that this conclusion is based on the samples printed by common printing systems with absorption inks.

6.2.5.3. Coefficient of Determination (R^2)

To investigate the relationship between specular gloss measurements (in a wide range of gloss values) and a perceptually-equidistant gloss scale, we combined the printed samples of **Group I** and **Group II** (see Sections 6.2.1.1 and 6.2.1.2) to cover a wide range of gloss values from "Very Matt" to almost "High Gloss", i.e. almost the entire gloss range. The whole set was composed of 96 samples = 42 samples of **Group I** + 54 samples of **Group II** (see Table 6.3 and Fig. 6.16).

Figure 6.29 represents the data points of both groups as the result of averaged perceptual gloss scales (across all observers) and 60° specular gloss measurements. In order to find the aforementioned relationship, we tested the functions listed in Table 6.9.

For each fitting function, we computed the corresponding coefficient of determination (R^2) for three cases (data-sets): 1. samples of **Group I**; 2. samples of **Group II**; and 3. both groups of samples (**Group I** and **II**).

Based on the calculated R^2 values, we found that the Cubic, Polynomial (2^{nd} degree) and Power functions can be considered the best fitting curves (among the ones we used in this experiment) for relating gloss measurements to a perceptually-equidistant gloss scale, considering all three cases. Their performances were approximately equal to the maximum of 0.05 difference between their coefficients of determination (R^2s). Table 6.13 shows the achieved R^2 values based on fitting the three aforementioned data-sets using these three functions.

In literature, it has been shown that the relationship between gloss measurements and gloss perception in the entire gloss range is nonlinear. Obein et al. [OKV04] confirmed this nonlinearity and divided the entire gloss range into three parts: 1. matt, 2. intermediate, and 3. high gloss. They found steeper slopes at two extremes of gloss range (matt and high gloss regions). This means that the gloss perception of the human observer is more sensitive to samples with low and high levels of glossiness. Similarly, Obein et al. [OLKV03] showed that the aforementioned relationship can be described by a three-part linear function. In another study, Billmeyer

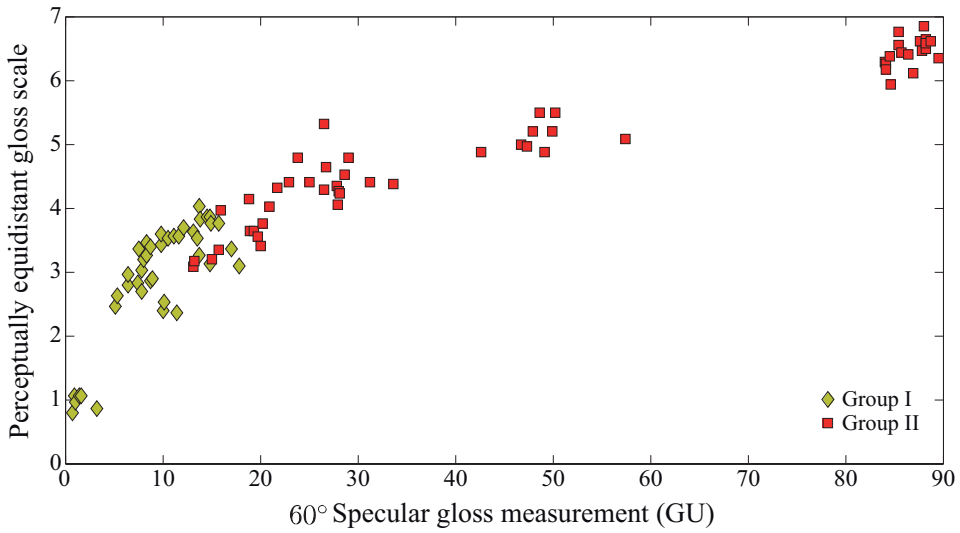

Figure 6.29.: The data-sets of **Group I** and **II**.

Data-Set	**Coefficient of Determination** (R^2)		
	Polynomial (2nd degree)	Cubic	Power
Group I	**0.85**	**0.85**	0.83
Group II	0.93	**0.94**	0.93
Group I and **II**	0.90	0.93	**0.95**

Table 6.13.: The coefficients of determination (R^2s) computed for three data-sets by fitting Polynomial (2nd degree), Cubic, and Power functions. This table has been taken from [SBU*15].

and Q'Donnell [BJO87] explained this relationship via a cubic function. Ji et al. [JPLD06] also confirmed the validity of both functions with a higher correlation, using the cubic curve. It should be noted that the data-set used in [OKV04], [OLKV03], and [BJO87] were all neutral samples, while a combination of neutral and color patches was utilized in [JPLD06].

According to our results (see Table 6.13), the Polynomial (2nd degree) and Cubic functions give equally the best result in terms of fitting the data-set of **Group I**, with the highest $R^2 = 0.85$. On the other hand, the Cubic function can be considered the best choice for fitting the data points of **Group II** with the highest $R^2 = 0.94$. However, the samples of both groups together (**Group I** and **II**: representing almost the entire gloss range) can be fitted via the Power function with the highest $R^2 = 0.95$. Figure 6.30 shows all averaged data points of both groups fitted via the Power function. In this figure, all of the data points (samples) are considered together regardless of their colors (colorant combinations). The parameters of the fitted Power function (see Table 6.9) are: a = 2.9950, b = 0.2300, and c = -1.9820.

Therefore, according to our results, the relationship between specular gloss measurements and a perceptually-equidistant gloss scale in almost the entire gloss range from "Very Matt" to approximately "High Gloss" can be modeled well via the Power function, with an exponent of less than 1, which is in accordance with *Stevens'*

Power Law [Ste61]. This indicates that the gloss perception is very similar to the light intensity perception. Ng et al. [NZM*03] also showed that (for the black samples used in their experiment) the relationship between gloss measurements and perceptual Gloss Just Noticeable Difference (G-JND) can be explained by the *Power Law*.

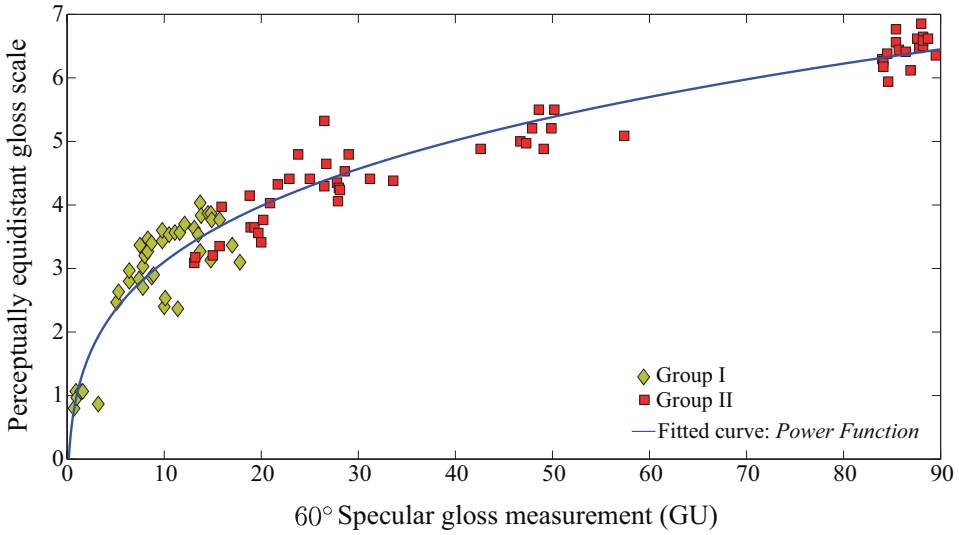

Figure 6.30.: Relationship between specular gloss measurements and a perceptually-equidistant gloss scale in almost the entire gloss range. The Power function was used to fit all data points within **Group I** and **II**. This figure has been taken from [SBU*15].

Figure 6.31 shows different graphs fitted by the Power function to separate color sets: C, M, Y, K, W, R = (M+Y), G = (C+Y), B = (C+M), and CMY = (C+M+Y). Because there were no samples with W and CMY colors within the first group (**Group I**), only the corresponding samples of **Group II** were considered for these two colors. As can be seen in this figure, the lighter samples (Y and W) were perceived as less glossy than the darker ones. As we previously mentioned in Section 6.2.4.3, we believe that this was due to the influence of *contrast gloss* on overall gloss perception. In other word, because specular gloss highlights have greater contrast on darker samples, these samples are perceived as glossier than lighter samples.

6.2.6. Psychophysical Experiment 4

Although some attempts have been carried out previously to investigate the effect of surface texture on the perceived level of surface gloss and vice versa, using display-based images, (to our knowledge) this interrelation has not been investigated using real printed samples with variations in texture types, texture elevations and gloss levels. The aim of conducting this psychophysical experiment is:

- To investigate the interrelation between gloss and texture perception of 2.5D-printed samples.

In this experiment, only samples of **Group III** (see Section 6.2.1.3) with two texture types ("Bumpy" ellipsoids and macroscopic "Facet"s), each type printed in 6 different texture levels and 5 variations of surface glossiness, were used. In total, 15 color-normal or corrected-to-normal observers (6 female and 9 male) participated in the experiment. The experiment was composed of two tasks (A and B) explained in two subsequent sections.

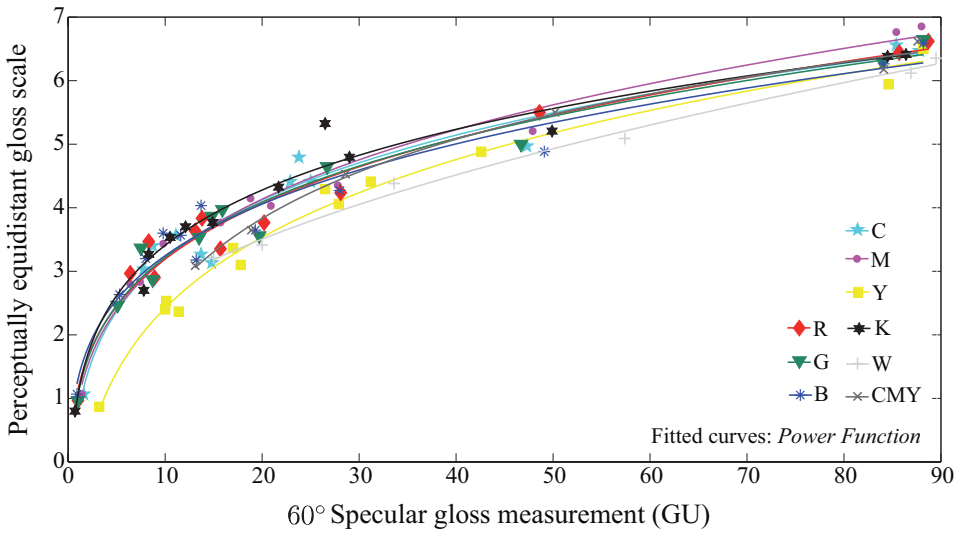

Figure 6.31.: Relationship between specular gloss measurements and a perceptually-equidistant gloss scale in almost the entire gloss range. The Power function was used to fit the data points belonging to different color sets within **Group I** and **II** separately. This figure has been taken from [SBU*15].

6.2.6.1. Task A: Gloss Scaling

In order to investigate the influence of macroscopic surface texture on the perceived gloss level, a gloss scaling task was performed. Six samples of the NCS Gloss Scale (see Section 6.2.2.2) from "Matt" to "High Gloss" (i.e. 6 to 95 GU) were used as reference samples in this task. Gloss scales from 1 to 6 were assigned to this reference samples in order of ascending gloss. All 60 textured samples of **Group III** were given to the observers one-by-one and in a random order in two separate sets of "Bumpy" and "Facet" texture types. The observers were asked to compare each test sample to all NCS Gloss Scale reference samples, and to assign a gloss scale to each of them based on a similar gloss scale perceived from a reference sample. For more flexibility, observers were allowed to give gloss scales also in 0.5 steps, i.e. 0.5, 1,..., 6, 6.5. Tilting the reference and test samples in small viewing angles was also allowed. Figure 6.32 shows the gloss scaling experiment performed using 2.5D textured samples.

6.2.6.2. Task B: Texture Ranking and Scaling

In order to investigate the influence of surface glossiness on the perceived level of texture, the texture ranking and scaling task was performed. In this task, firstly, the 2.5D textured reference samples (see Section 6.2.2.2), with minimal surface glossiness (generated by 0% varnish deposition) and six variations in texture elevation, were given to the observers in a random order. The observers were asked to rank the reference samples from 1 to 6 in ascending order according to their perceived levels of surface texture.

Secondly, all 30 "Facet" texture type samples of **Group III** (see Section 6.2.1.3) were given to the observers in a random order and one-by-one. They were asked to compare each test sample to the texture scale of reference samples made for the experiment, and to assign a texture level to each of the test samples based on a similar

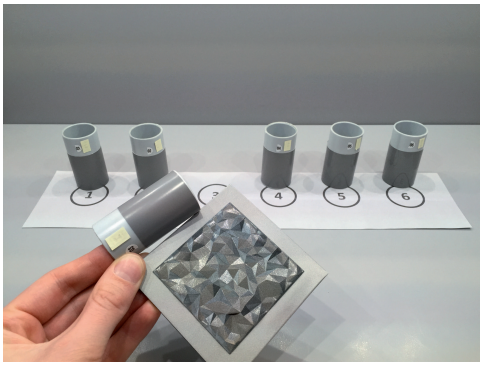

Figure 6.32.: Gloss scaling psychophysical experiment using texture- and gloss-varying 2.5D-printed test samples.

texture scale perceived from a reference sample. For more flexibility, assignment of texture scales in 0.5 steps was also allowed, i.e. 0.5, 1,..., 6, 6.5.

This task was repeated for the second time for 2.5D textured reference samples (see Section 6.2.2.2) with maximum glossiness level (generated by 40% varnish deposition).

It should be noted that due to the time restriction necessary in conducting psychophysical experiments, only the samples printed with the "Facet" texture type were used in this task. Figure 6.33 shows the texture rank order and scaling task.

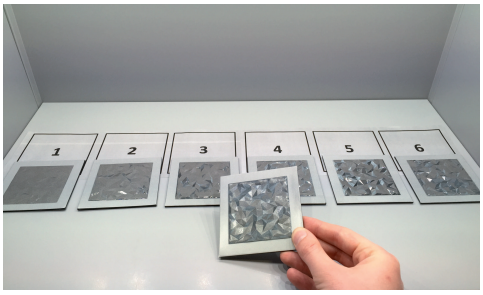

Figure 6.33.: Texture rank order and scaling psychophysical experiment using 2.5D-printed samples with the "Facet" texture type and different variations in gloss and texture levels.

6.2.6.3. Influence of Macroscopic Surface Texture on Perceived Gloss Level

In order to investigate the influence of macroscopic surface texture on perceived gloss level, the perceptual gloss scales given by observers to each textured-sample ("Bumpy" and "Facet" texture types), were extracted from Task A and averaged across all 15 participants. The averaged perceptual gloss scales together with the corresponding standard deviations vs. macroscopic texture levels, with respect to the texture height, are plotted in Fig. 6.34, for the "Bumpy" and "Facet" texture type samples separately.

The averaged perceptual gloss scales corresponding to patches with identical gloss levels (varnish coverages) but

different texture levels (texture elevations), were fitted by a second order polynomial curve in accordance with related studies [HLM08] and [QCSD14]. Thus, five curves were plotted, according to five different gloss levels, for each texture type.

As can be seen in Fig. 6.34, the type of texture influenced the observers' visual perception of surface gloss level so that the "Bumpy" samples were perceived as slightly glossier than the "Facet"s, when the maximum perceived levels of surface glossiness were compared. This can be explained by the fact that specular highlights are generally more visible on "Bumpy" patches than on the "Facet" samples. In "Bumpy" samples, each bump (printed ellipsoid) covers a wide variety of surface normals and consequently it almost always produces specular highlights independently of the sample's orientation. But, the texture of samples printed with the "Facet" texture type, covers only a few surface normal orientations and therefore can produce fewer specular highlights. However, this is not always the case, especially for samples with average perceived gloss scales below 4.5.

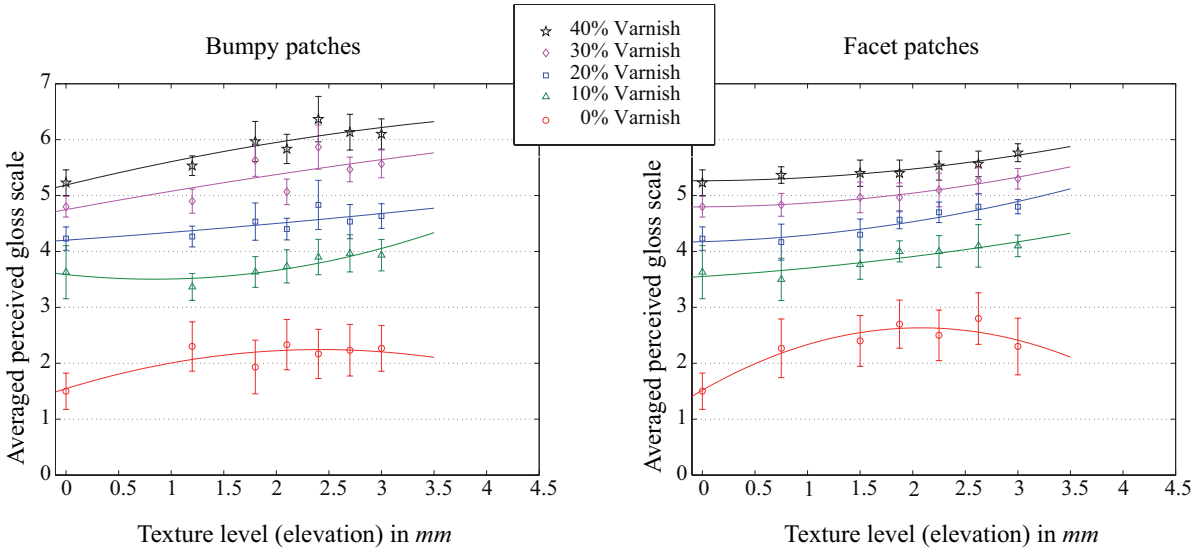

Figure 6.34.: Influence of surface macroscopic texture ("Bumpy" and "Facet" texture types) on perceived gloss level. For a better demonstration, the standard deviations were multiplied by a factor of 0.5.

Moreover, a slight influence of surface texture elevation on the perceived gloss level was observed (see Fig.6.34), indicating that surfaces are generally perceived as glossier when the texture level increases. This is in accordance with related studies [HLM08] and [QCSD14] using display-based images. However, for both the "Bumpy" and "Facet" samples printed with 0% varnish coverage – representing matt appearances – the plotted graphs dropped when the texture elevation increased to a certain level, showing a similarly non-monotonic result to that reported by Qi et al. [QCSD14] previously. In the display-based experiment conducted by Qi et al. [QCSD14], the observers were asked to judge the glossiness of simulated surfaces varying in roughness levels. According to this experiment, Qi and co-workers reported that although increasing the surface mesoscale roughness generally increases the perceived gloss level, the perception of surface glossiness drops when a certain level of surface texture is reached. This can be explained by the fact that specular highlights may not be clearly visible on surfaces with complicated texture (e.g. "Facet" samples used in our experiment), when a certain level of surface texture (complexity) is reached. Another reason might be related to the limited illumination/viewing geometry

provided in the experimental condition, which has a greater effect in the case of display-based experiments, due to the rendering process.

6.2.6.4. Influence of Printed Gloss on Perceived Texture Level

As mentioned previously, the aim of Task B, explained in Section 6.2.6.2, was to investigate the effect of printed gloss on perceived texture level. Figure 6.35 shows the perceived texture scales of samples printed with different levels of gloss (generated by varnish deposition in the range of [0,40] percent area coverage in steps of 10%), and an identical texture level. In this figure, each ellipse shows the number of observers who agreed on a specific perceived level of texture. According to our results and as can be seen in this figure, a large variation between observers' judgments of the perceived texture levels was found. Moreover, no significant influence of the surface gloss level on the perceived texture level was observed, indicating texture constancy regardless of glossiness level. This is, however, in contrast to related studies [HLM08] and [QCSD14] in which the influence of surface gloss on the perceived surface texture is defined by a monotonically increasing function, showing that samples with higher glossiness appearance are generally perceived as more textured.

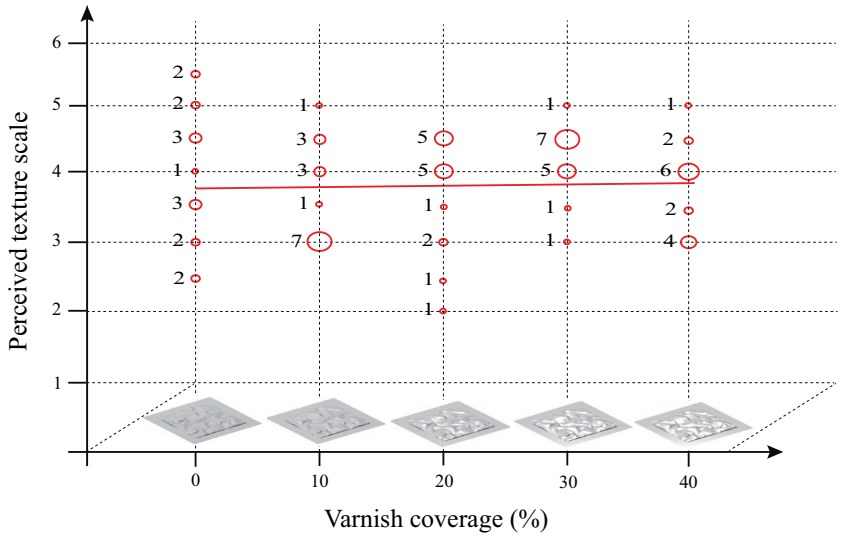

Figure 6.35.: Perceived texture scale vs. printed gloss level. In this figure, five "Facet" type samples with an identical texture level, but in five different gloss levels – generated with varnish deposition – were used. A large variation between observers' judgments on perceived texture levels was observed. The influence of printed gloss on perceived texture level was found to be negligible.

A possible reason for the different results obtained in our experiment from those reported in previous studies [HLM08] and [QCSD14], is the difference between two different types of experiments: one used real 2.5D-printed samples (our experiment), and the others used display-based simulated and static images ([HLM08] and [QCSD14]). In general, in experiments with conditions which are more similar to real world situations, observers can acquire more information (e.g. BRDF and 3D depth information by stereo vision); consequently, more accurate judgments are may be possible in these cases.

6.3. Summary

In this chapter, we studied the following topics:

- Printing flat gloss-variant color samples using the same amount of ink area coverage to avoid gloss-differential and bronzing artifacts and to control the surface glossiness locally.
- Testing the validity of instrumental devices (gloss meters) in terms of ranking gloss values measured from flat samples with almost homogeneous appearance, compared to perceptual gloss ranks.
- Finding the relationship between instrumental gloss measurements and perceptual gloss magnitudes based on color-printed flat samples with almost homogeneous appearance.
- Investigating the effect of printed gloss on color.
- Investigating the effect of printed color on gloss perception.
- Investigating the interrelation between perceived gloss and texture levels of 2.5D samples printed in two texture types and different variations of gloss levels and texture elevations.

In order to print samples with different gloss levels, three printing strategies were proposed and denoted by **WWCMY**, **MCMY**, and *Varnish Halftoning* (**VH**). Using 2.5D printing systems capable of multi-layer and multi-pass printing, three groups of color samples (**Group I**, **II**, and **III**) were printed. The first set of samples (**Group I**) – printed via **WWCMY** and **MCMY** print modes – covered gloss values between 0.70 and 18.10 GU, representing a gloss range from "Very Matt" to "Semi Matt". The second set of samples (**Group II**) – printed using the *Varnish Halftoning* (**VH**) printing strategy – covered another range of gloss values from 13.10 to 89.5 GU, representing a gloss range from "Semi Matt" to almost "High Gloss". The gloss values were measured at the 60° specular angle. The samples of **Group III** were also printed using the *Varnish Halftoning* (**VH**) printing strategy. In contrast to flat samples of **Group I** and **II**, the samples of **Group III** were printed in two texture types and different texture heights.

Considering the samples of **Group I** and **II**, printing gloss-variant color samples which span almost the entire gloss-range is possible, independent of the amount of ink deposited, which means bronzing and gloss-differential artifacts can be avoided.

We conducted four psychophysical experiments based on gloss and texture ranking and scaling tasks, using the samples of the aforementioned three groups. According to the computed Spearman's rank correlation coefficients (SRCCs) between the instrumental and perceptual gloss ranks, we confirmed the reliability of gloss meters in terms of gloss measurements from printed flat samples with almost homogeneous appearances and isotropic BRDFs.

We found that the relationship between instrumental gloss measurements and perceptual gloss magnitudes can be described via the Polynomial (2^{nd} degree), Cubic, and Power functions with almost equal performance. The Polynomial (2^{nd} degree) and Cubic (according to [JPLD06, OLKV03, BJO87, OKV04]) functions showed the best results for the lower gloss range, from "Very Matt" to "Semi Matt" equally. The Cubic function (according to [JPLD06,OLKV03,BJO87,OKV04]) was found to be the best fitting curve for the upper part of the gloss range, from "Semi Matt" to almost "High Gloss". However, the Power function led to the best result when considering approximately the entire gloss range from "Very Matt" to almost "High Gloss", which is in accordance with *Stevens' Power Law* [Ste61]. This confirms the result found in [NZM*03], based on the relationship between gloss measurements and perceptual Gloss Just Noticeable Differences (G-JNDs) and extends it to color-printed patches.

We found varnish to have a small influence on the sample's color. Thus, for critical printing applications where a very accurate reproduction is required, color and gloss cannot be treated separately. In these cases, the interaction

between color and gloss has to be taken into account using separation methods.

In our opinion, the effect of color on gloss perception can be better explained using two terms: the general *perceived glossiness trend* and the *perceived gloss magnitude*. We realized that color does not have a noticeable influence on the general perceived glossiness trend so that an increasing function of perceived gloss levels and measured gloss values can almost always be noticed regardless of the sample's underlying color. However, lighter samples are perceived as less glossy than darker ones in general. This is because specular gloss highlights have lower contrast on lighter samples, which shows the influence of *contrast gloss* on overall gloss perception.

According to a psychophysical experiment conducted using 2.5D textured samples (**Group III**), a slight influence of printed texture type and texture elevation on the perceived gloss level was observed. No noticeable influence of printed gloss on perceived texture level was found, indicating *texture constancy* regardless of different printed gloss levels.

7. Summary and Conclusion

In a comprehensive printing workflow, reproduction of appearance attributes such as color, gloss, opacity (translucency or transparency), and texture must be taken into account for accurate printing, especially for reproduction of 2.5D and 3D objects. Such a printing workflow is not yet available. However, different attempts to investigate the reproduction of the aforementioned appearance attributes separately, have been carried out. Among this research, the most effort has been expended on color reproduction. In this dissertation, the reproduction of color and gloss appearance attributes are addressed as two separate topics: *spectral and specular reproduction*.

In the printing workflows that are used nowadays, accurate reproduction of colors is important only for a predefined illuminant (i.e. an illuminant that the reproduction is adjusted to; e.g. daylight). Therefore, due to metamerism, color-mismatches may occur when the printout and the original are compared under another illuminant (e.g. tungsten light). This printing workflow is known as a *metameric printing workflow*. Although this printing workflow is useful and sufficient for many applications, for some special cases, such as artwork (e.g. painting and cultural heritage) reproduction, security printing, accurate industrial color communication and so on, when accurate color reproduction of an original under a variety of illuminants (e.g. daylight, tungsten light, museum light, etc.) is required, using metameric reproduction can lead to satisfactory results only by chance. Therefore, in these cases, another printing workflow known as the *spectral printing workflow*, must be used. In this workflow, printing beyond color, i.e. reproduction of spectral raw data (reflectances in the visible wavelength range) rather than reproduction of colorimetric values (colors) under only a predefined illuminant, is taken into account. The aim of spectral reproduction is to achieve an illuminant-invariant match between the original and reproduction. This is an ideal goal; however, colorimetric inaccuracies across considered illuminants are expected. Spectral reproduction is discussed as the first focused topic in this dissertation (see Chapters 2, 3, and 4).

In a spectral printing workflow, due to the limitations of the printing systems now extant (even multi-channel (multi-colorant) printers), reproduction of all reflectances is not possible. Therefore, non-reproducible spectra must be mapped into the printable reflectances which define the printer spectral gamut, $\mathcal{G}$. This process is called *spectral gamut mapping*. In the next stage, appropriate printer colorant combinations must be selected in order to print the gamut-mapped reflectances. This process is called *separation*. In this dissertation, for answering the first research question defined in Section 1.2, an approach called *Spatio-Spectral Gamut Mapping and Separation* SSGMS [SU15a] was proposed, which combines the spectral gamut mapping and separation stages in a spectral printing workflow. This approach is an improvement on the *Paramer Mismatch-Based Spectral Gamut Mapping* PMSGM [UB11] and *Spatially Resolved Joint Spectral Gamut Mapping and Separation* SGMS [SU13] methods, as it minimizes their associated *banding* and *smearing* artifacts.

The infrastructure of each of these three methods is based on a multi-illuminant framework composed of a hierarchy of application-dependent illuminants $I_1, ..., I_n$, sorted from most to least important in an underlying application. The input to this framework is a spectral image R rendered to n colorimetric images $L_1, ..., L_n$ for all illuminants. Since our aim in spectral reproduction is to be as good as metameric reproduction for the first illuminant and to be superior to the metameric reproduction for the remaining illuminants, a traditional metameric gamut mapping is performed for L_1, considering the printer metameric gamut, G, defined for the first illuminant I_1. This results in a gamut-mapped image called $\widehat{L_1}$. The remaining gamut mappings are performed in paramer-mismatch gamuts $\rho(p_0)$s, computed individually for each image pixel, p_0, from the corresponding parameric set

$\tau(p_0)$. Each parameric set $\tau(p_0)$ is composed of printable colorant combinations, resulting in paramers under I_1 and non-paramers under the rest of the illuminants. Gamut mappings within these smaller gamuts (ρs) ensure unnoticeable color changes for the gamut-mapped image $\widehat{L_1}$.

Unlike the pixel-wise and semi-spatial strategies used in the PMSGM [UB11] and SGMS [SU13] methods for gamut mappings within paramer-mismatch gamuts, both the *colorimetric* and *spatial* content of the original image is considered within local 3×3 spatial windows of surrounding neighboring pixels of each image pixel p_0. An optimization process is performed by traversing the image from the top-left to the bottom-right pixel. The aim of employing this optimization process is to select a colorant combination from each parameric set $\tau(p_0)$ so that it minimizes a cost function composed of two parts: *colorimetric* and *spatial*. The purpose of the colorimetric stage of the cost function is to ensure colorimetric accuracy across all considered illuminants and to preserve metameric and parameric edges (edges appearing under one illuminant, while not visible under another illumination condition.). The spatial stage enables avoidance of banding and smearing artifacts within smooth image regions. A locally adaptive trade-off between the colorimetric and spatial stages of the cost function, results in local dominance of one of these two parts. As a result of the optimization process, a *separation image* S is generated, containing the chosen printable colorant combinations for all image pixels. This image is then further processed (ink limited and halftoned) to control the printer and, eventually, to generate the spectral print.

In order to test the proposed SSGMS method, 11 spectral images were used: A cutout of the METACOW image [FJ04], 8 natural images taken from the Foster database [FANF06], and two paintings. According to the experiments conducted based on the spectral images used, the separation images generated by applying the proposed SSGMS method led to almost artifact-free spectral reproductions for natural scenes and paintings, and mild artifacts for the completely noise-free and artificial METACOW image [FJ04].

In order to answer the last three research questions defined in Section 1.2, which are related to the second focused topic (see Chapters 5 and 6), three printing strategies were proposed. Using these printing strategies, controlling and printing gloss effects locally in a wide range of gloss values, independent of the amount of ink deposited, is feasible. This helps to avoid gloss-related artifacts such as *gloss-differential* and *bronzing*.

We studied the relationship between measured gloss values and visually perceived gloss magnitudes of colored and flat samples printed using the aforementioned printing strategies, by conducting three psychophysical experiments. Understanding this relationship is important for obtaining a perceptually-meaningful gloss reproduction. As a result of these experiments, we found that this relationship can be explained by a *Power function* according to *Stevens' Power Law*, considering almost the entire gloss range.

Moreover, we conducted another psychophysical experiment, in order to investigate the interrelation between perceived surface gloss and texture, using 2.5D samples printed in two texture types and different variations in gloss and texture levels. According to the results of this experiment, texture type and texture elevation influence perceived gloss level slightly. No noticeable influence of printed gloss on perceived texture level was found, indicating texture constancy regardless of different gloss levels.

8. Contribution and Outlook

8.1. Contribution

Since the research conducted in this dissertation is considered a joint work between six junior and senior researchers (see Table 8.1), here I summarize my main contributions to the two focused topics: 1. Spectral reproduction (specifically spectral gamut mapping), 2. Specular (gloss) printing.

First Topic

As previously mentioned, we proposed an approach called SSGMS [SU15a] for the purpose of spectral gamut mapping and separation. For developing this method, I computed all of the printable colorant combinations (printer colorant space Ω) together with their corresponding colorimetric values for all considered application-dependent illuminants. This data enables rapid determination of the parameric sets (τs) via quick access to the lists of colorimetric values during the program runtime.

I came up with the idea of initializing the separation image S, which enabled us to consider a complete 3×3 spatial window of pre-processed neighbors of each image pixel p_0 (except the bordering pixels). This makes it possible to avoid the smearing artifacts associated with the SGMS [SU13] method.

I implemented the colorimetric and spatial stages of the cost function related to the proposed SSGMS [SU15a] approach, in C++.

I tested the proposed SSGMS [SU15a] approach, the SGMS [SU13] method (the initial version of SSGMS), and also the PMSGM [UB11] gamut mapping strategy using 11 spectral images, and compared the results obtained in terms of visible artifacts and preservation of metameric edges. In order to compute the colorimetric inaccuracy as well as the increased computational time imposed by the spatial stage of the cost function used in the SSGMS method, I specifically compared this method to the PMSGM approach and evaluated the results obtained considering two illuminants: CIED65 and CIEA.

I presented a simple strategy for generating artificial targets to find printable metamers using any printing system. Using the results achieved, I generated and printed spectral print samples using two printing systems: HP Designjet Z3100 and Canon iPF6450.

Second Topic

In the scope of spectral (gloss) reproduction as the second research topic of this dissertation, I printed the color-samples varying in gloss levels by the *Varnish Halftoning* (**VH**) strategy during my secondment at Océ Print Logic Technologies SA., Creteil, France, using an Océ Arizona 480 GT printer.

I measured the color and gloss values of all samples printed with different printing strategies: **MCMY**, **WWCMY**, and **VH**.

I designed the (rank order and gloss scaling) psychophysical experiments conducted in order to investigate the

relationship between measured gloss values and perceived gloss magnitudes using color-printed samples used in this dissertation.

For conducting the gloss scaling psychophysical experiments, reference samples of equidistant steps in terms of visual gloss perception were required. Thus, I chose the reference samples from the NCS Gloss Scale product.

The data points obtained as the result of gloss measurements and perceptual gloss scales given by the observers, had to be fitted via different functions in order to investigate the relationship between gloss measurements and visual gloss perception. Therefore, I chose the fitting functions listed in table 6.9.

I extracted the required data from the psychophysical experiments conducted and gloss measurements, to compute e.g. Coefficients of Determination (R^2s) and Spearman's Rank Correlation Coefficients (*SRCC*s).

From the conducted experiments and computations, I made the final evaluations and conclusions in terms of the gloss measurement-perception relationship considering the samples used, the effect of varnish on color, the influence of gloss on perceived color, etc.

Junior or Senior Researcher	**Affiliation**
Sepideh Samadzadegan	Technische Universität Darmstadt, Germany.
Teun Baar	Océ Print Logic Technologies SA., Creteil, France. Institut Mines-Télécom Télécom ParisTech, CNRS LTCI Paris, France.
Jana Blahová	VoxVil AB, Örnsköldsvik, Sweden. Technische Universität Darmstadt, Germany (previous affiliation).
Dr. Philipp Urban	Fraunhofer Institute for Computer Graphics Research IGD, Darmstadt, Germany. Technische Universität Darmstadt, Germany (previous affiliation).
Dr. Maria V. Ortiz Segovia	Océ Print Logic Technologies SA., Creteil, France.
Dr. Hans Brettel	Institut Mines-Télécom Télécom ParisTech, CNRS LTCI Paris, France.

Table 8.1.: Junior and senior researchers contributed to the research carried out in this dissertation.

8.2. Outlook

In order to expand the research conducted in this dissertation, potential future research is summarized here as outlooks, separately for each topic.

First Topic

As mentioned in Section 4.2.3.3, the weighting parameters of the proposed SSGMS [SU15a] method were adjusted suboptimally by inspecting the generated separation images and the printouts using a cutout of the META-COW [FJ04] image visually. To improve this method, these parameters should be adjusted optimally using a more comprehensive strategy.

Using a method (e.g. based on edge detection) that enables the SSGMS approach to decide upon the necessity of the segmentation process and also the required number of clusters for each rendered image (under a specific illuminant) automatically is considered to be another extension to the research conducted.

As mentioned in Section 4.2.2.2, in the SSGMS approach, a small amount of noise added to the image rendered for the first illuminant prior to gamut mapping, may improve the final result. To improve this method, one could come up with a strategy (e.g. based on the image spatial frequencies) that enables the SSGMS approach to decide upon the necessity of the noise addition part and the amount of noise required, automatically.

Note that the research conducted is based on academic requirements. For industrial applications, developing methods for performance-optimized spectral gamut mapping and separation, including spectral lookup tables for spectral profiles, is required.

Second Topic

As mentioned in Sections 6.2.1.1 and 6.2.1.2, the samples printed using the **MCMY**, **WWCMY**, and **VH** printing strategies may suffer from banding and orange peel artifacts. Investigating other printing strategies or improving those proposed, so that they lead to printouts with more homogeneous appearance, is therefore suggested as an extension to the second research topic in this dissertation.

For printing local gloss effects, we presented a color-gloss model in Section 6.1.3 containing two printing modes: **MCMY** and **WWCMY**. Using these printing modes, printing gloss values in the range of approximately 0.70 to 18.10 GU is possible. Embedding the *Varnish Halftoning* (**VH**) printing strategy in this model leads to printing local gloss effects in a wider range of gloss values, roughly from 13.10 to 89.50 GU.

According to the experiments conducted, we realized that surface glossiness has little influence on perceived color; however, even this small influence cannot be neglected for critical printing applications where very accurate color and gloss reproduction is desirable. For these cases, investigating the interaction between color and gloss for developing color-gloss gamut mapping algorithms, is required.

Based on the related research conducted on gloss perception, the colors and textures of objects influence their perceived glossiness and vice versa. Since most of these studies use display-based computer simulated objects, investigating the interactions, instrumental and perceptual relationships between color, gloss, and texture using real color-, gloss-, and texture-variant 2.5D/3D prints by conducting appropriate psychophysical experiments is considered another interesting extension to the research conducted in this dissertation.

Bibliography

[And63] ANDERSON T. W.: Asymptotic theory for principal component analysis. *The Annals of Mathematical Statistics 34*, 1 (1963), 122–148. 56

[AST11] ASTM/E12.03: *Standard Test Methods for Measurement of Gloss of High-Gloss Surfaces by Abridged Goniophotometry*. Tech. rep., American Society for Testing and Materials, West Conshohocken, PA., USA., 2011. 97

[AST12] ASTM/E12.03: *Standard Test Methods for Instrumental Measurement of Distinctness-of-Image Gloss of Coating Surfaces*. Tech. rep., American Society for Testing and Materials, West Conshohocken, PA., USA., 2012. 97

[AST13] ASTM/D20.40: *Standard Test Method for Specular Gloss of Plastic Films and Solid Plastics*. Tech. rep., American Society for Testing and Materials, West Conshohocken, PA., USA., 2013. 96

[AST14] ASTM/E12.03: *Standard Test Method for Specular Gloss*. Tech. rep., American Society for Testing and Materials, West Conshohocken, PA., USA., 2014. 96, 98

[BA03] BAQAI F. A., ALLEBACH J. P.: Halftoning via direct binary search using analytical and stochastic printer models. *IEEE Trans Image Process. 12*, 1 (January 2003). 116

[Bal99] BALASUBRAMANIAN R.: Optimization of the spectral neugebauer model for printer characterization. *Journal of Electronic Imaging 8*, 2 (1999), 156–166. 52

[Bar96] BARBER C. B.: The quickhull algorithm for convex hulls. *ACM Transactions on Mathematical Software (TOMS) 22*, 4 (Dec 1996), 469–483. 56

[BB83] BERNS R. S., BILLMEYER F. W.: Proposed indices of metamerism with constant chromatic adaptation. *Color Research & Application 8*, 3 (1983), 186–189. 64

[BBH08] BUGNON T., BRICHON M., HERSCH R. D.: Simplified ink spreading equations for cmyk halftone prints. In *Proc. SPIE-IS&T Color Imaging XIII: Processing, Hardcopy, and Applications* (San Jose, CA, USA., 2008), vol. 6807. 52

[BdEW01] BALA R., DEQUEIROZ R., ESCHBACH R., WU W.: Gamut mapping to preserve spatial luminance variations. *Journal of Imaging Science and Technology (JIST)*, 5 (Sep 2001), 436–443. 45

[BDW81] BARTELL F. O., DERENIAK E. L., WOLFE W. L.: The theory and measurement of bidirectional reflectance distribution function (brdf) and bidirectional transmittance distribution function (btdf). In *Proc. SPIE: Radiation Scattering in Optical Systems* (1981), vol. 0257. 35

[Ber00] BERNS R. S.: *Billmeyer and Saltzman's: Principles of Color Technology*, 3 ed. John Wiley & Sons, Inc, New York, 2000. 37, 38, 39, 40, 42, 48, 58

[BF97] BRAUN G. J., FAIRCHILD M. D.: Techniques for gamut surface definition and visualization. In *IS&T/SID, 5th Color and Imaging Conference* (Scottsdale Ariz., 1997), vol. 6, pp. 147–152. 45

[BF03] B.ZHOU, FANG X.: Improving mid-tone quality of variable-coefficient error diffusion using threshold modulation. *ACM Transactions on Graphics (TOG) - Proceedings of ACM SIGGRAPH 22*, 3 (2003), 437–444. 92

[BFH05] BAKKE A. M., FARUP I., HARDEBERG J. Y.: Multispectral gamut mapping and visualization: a first attempt. In *SPIE 5667, Color Imaging X: Processing, Hardcopy, and Applications* (San Jose, California, USA, 2005), pp. 193–200. 55, 56, 57, 58

[BJO87] BILLMEYER-JR F. W., O'DONNELL F. X. D.: Visual gloss scaling and multidimensional scaling analysis of painted specimens. *Color Research & Application 12*, 6 (1987), 315–326. 104, 105, 140, 146

[Bra03] BRAINARD D. H.: Color appearance and color difference specification. In *The Science of Color*, Shevell S. K., (Ed.), 2nd ed. Elsevier, 2003, ch. 5. 118

[BSB*14] BAAR T., SAMADZADEGAN S., BRETTEL H., URBAN P., SEGOVIA M. V. O.: Printing gloss effects in a 2.5D system. In *SPIE/IS&T Electronic Imaging Conference* (San Francisco, California, USA., 2014). 109, 111, 112, 113, 114, 115, 119, 130, 131, 132

[BSBB06] BONNIER N., SCHMITT F., BRETTEL H., BERCHE S.: Evaluation of spatial gamut mapping algorithms. In *IS&T/SID, 14th Color and Imaging Conference* (Scottsdale, Ariz. USA., 2006), vol. 6, pp. 56–61. 63

[CBT04] CHEN Y., BERNS R. S., TAPLIN L. A.: Six color printer characterization using an optimized cellular yule-nielsen spectral neugebauer model. *Journal of Imaging Science and Technology (JIST) 48*, 6 (2004), 519–528. 52

[CBTI03] CHEN Y., BERNS R. S., TAPLIN L. A., IMAI F. H.: A multi-ink color-separation algorithm maximizing color constancy. In *IS&T/SID, 11th Color and Imaging Conference* (Scottsdale, Arizona, USA., 2003), pp. 277–281. 64

[CIE95] CIE: *Industrial Colour-Difference Evaluation*. Tech. Rep. 116, CIE Central Bureau, Vienna, Austria, 1995. 64

[CIE01] CIE: *Improvement to Industrial Colour-Difference Evaluation*. Tech. Rep. 142, CIE Central Bureau, Vienna, Austria, 2001. 55, 64

[CK10] CHITADE A. Z., KATIYAR S. K.: Colour based image segmentation using k-means clustering. *International Journal of Engineering Science and Technology 2*, 10 (2010), 5319–5325. 78

[CL99] CHOLEWO T. J., LOVE S.: Gamut boundary determination using alpha-shapes. In *IS&T/SID, 7th Color and Imaging Conference* (Scottsdale Ariz., 1999), pp. 200–204. 45

[Coh01] COHEN J.: *Visual Color and Color Mixture: The Fundamental Color Space*. University of Illinois Press, 2001. 58

[Dan92] DANNEMILLER J. L.: Spectral reflectance of natural objects: how many basis functions are necessary? *Journal of the Optical Society of America A (JOSA A) 9*, 4 (1992), 507–515. 53, 56

[DIN82] DIN: *Reflectometer as a means for gloss assessment of plane surfaces of paint coatings and plastics*. Tech. rep., Deutsches Institut für Normung/German institute for standardisation, 1982. 96

[DNH99] DALAL E. N., NATALE-HOFFMAN K. M.: The Effect of Gloss on Color. *Color Research & Application 24*, 5 (1999), 369–376. 100

[DR06] DERHAK M. W., ROSEN M. R.: Spectral Colorimetry using LabPQR: An Interim Connection Space. *Journal of Imaging Science and Technology (JIST) 50*, 1 (2006). 43, 49, 53, 58

[EE99] EHRENSTEIN W. H., EHRENSTEIN A.: Psychophysical methods. In *Modern Techniques in Neuroscience Research*, Windhorst U., Johansson H., (Eds.). Springer Berlin Heidelberg, 1999, ch. 43. 98, 99, 100

[Fai05] FAIRCHILD M. D.: *Color Appearance Models*, 2 ed. John Wiley & Sons, Ltd, West Sussex, England, 2005. 37

[FANF06] FOSTER D. H., AMANO K., NASCIMENTO S. M. C., FOSTER M. J.: Frequency of metamerism in natural scenes. *Journal of the Optical Society of America A 23*, 10 (2006), 2359–2372. 81, 82, 83, 85, 89, 150

[Far43] FARNSWORTH D.: The farnsworth-munsell 100-hue and dichotomous tests for color vision. *Journal of the Optical Society of America (JOSA) 33*, 10 (1943), 568–574. 126, 127

[FFTR13] FORES A., FERWERDA J., TASTL I., RECKER J.: Perceiving Gloss in Surfaces and Images. In *Color and Imaging Conference* (Albuquerque, New Mexico, USA, 2013). 96, 106, 116

[FJ04] FAIRCHILD M. D., JOHNSON G. M.: METACOW: A Public-Domain, High-Resolution, Fully-Digital, Noise-Free, Metameric, Extended-Dynamic-Range, Spectral Test Target for Imaging System Analysis and Simulation. In *IS&T/SID, 12th Color Imaging Conference* (Scottsdale Ariz., USA., 2004), pp. 239–245. 68, 69, 70, 72, 78, 79, 81, 82, 83, 84, 85, 89, 150, 152

[Fle12] FLEMING R. W.: Human perception: Visual heuristics in the perception of glossiness. *Current Biology (Curr Biol.) 22*, 20 (October 2012), R865–R866. 101, 102, 104

[Fle14] FLEMING R. W.: Visual perception of materials and their properties. *Vision Research 94* (January 2014), 62–75. 102, 104

[FPG01] FERWERDA J. A., PELLACINI F., GREENBERG D. P.: A psychophysically-based model of surface gloss perception. In *SPIE, Human Vision and Electronic Imaging VI* (San Jose, CA, USA., 2001), vol. 4299. 96, 103, 104

[FTA04] FLEMING R. W., TORRALBA A., ADELSON E. H.: Specular reflections and the perception of shape. *Journal of Vision 4* (September 2004), 798–820. 100

[Ges84] GESCHEIDER G. A.: *Psychophysics: method, theory, and application*, 2nd ed. Psychology Press, 1984. 99, 100

[Har02] HARDEBERG J. Y.: On the spectral dimensionality of object colours. In *IS&T, Conference on Colour in Graphics, Imaging, and Vision (CGIV)* (Poitiers, France, 2002), vol. 6, pp. 480–485. 53, 56

[HB95] HUNG P., BERNS R. S.: Determination of constant hue loci for a CRT gamut and their predictions using color appearance spaces. *Color Research & Application 20*, 5 (October 1995), 285–295. 63, 66

[HC05] HERSCH R. D., CRETE F.: Improving the Yule-Nielsen modified Neugebauer model by dot surface coverages depending on the ink superposition conditions. In *Proc. SPIE-IS&T Color Imaging X: Processing, Hardcopy, and Applications* (San Jose, CA, USA., 2005), vol. 5667. 52

[HH87] HUNTER R. S., HAROLD R. W.: *The Measurement of Appearance*. John Wiley & Sons, 1987. 95, 97, 98, 100, 103, 121, 122, 135

[HH14] HÉBERT M., HERSCH R. D.: Review of spectral reflectance models for halftone prints: Principles, calibration, and prediction accuracy. *Color Research & Application* (2014). 52

[HLM08] HO Y.-X., LANDY M. S., MALONEY L. T.: Conjoint measurement of gloss and surface texture. *A journal of the Association for Psychological Science (Psychol Sci.) 19*, 2 (February 2008), 196–204. 100, 124, 125, 144, 145

[Hod05] HODGSON A.: The use of gloss effects from inkjet printing for brand identification, personalisation and security. In *IS&T. International Conference on Digital Production Printing and Industrial Applications* (Amsterdam, Netherlands., 2005), pp. 108–109. 110

[HS01] HANEISHI H., SAKUDA Y.: Representing gamut of spectral reflectance by a polyhedron in high dimensional space. In *The 3rd International Conference on Multispectral Color Science (MCS'01)* (2001), pp. 5–8. 56

[Hut99] HUTCHINGS J. B.: *Food Color and Appearance*, 2nd ed. Springer, 1999. 34

[Ing14] INGERSOLL L. R.: A means to measure the glare of paper. In *Electr. World* (1914), vol. 63, pp. 645–647. 95

[IRB02] IMAI F. H., ROSEN M. R., BERNS R. S.: Comparative study of metrics for spectral match quality. In *The First European Conference on Colour Graphics, Imaging, and Vision (CGIV)* (Poitiers, France, 2002), vol. 1, pp. 492–496. 52, 55

[Ish17] ISHIHARA S.: *Tests for colour-blindness*. Tokyo, Japan, 1917. 126, 127

[ISO10] ISO/TC79/SC2: *Anodizing of aluminium and its alloys – Measurement of specular reflectance and specular gloss of anodic oxidation coatings at angles of 20 degrees, 45 degrees, 60 degrees or 85 degrees*. Tech. rep., International Organization for Standardization (ISO), 2010. 96

[ISO14a] ISO/TC35/SC9: *Paints and varnishes – Determination of gloss value at 20 degrees, 60 degrees and 85 degrees*. Tech. rep., International Organization for Standardization (ISO), 2014. 96

[ISO14b] ISO/TC35/SC9: *Paints and varnishes – Determination of haze on paint films at 20 degrees*. Tech. rep., International Organization for Standardization (ISO), 2014. 97

[ITHM96] IMAI F. H., TSUMURA N., HANEISHI H., MIYAKE Y.: Principal component analysis of skin color and its application to colorimetric color reproduction on crt display and hardcopy. *Journal of Imaging Science and Technology (JIST)*, 5 (1996), 422–430. 56

[JIS97] JIS: *Specular glossiness – Methods of measurement*. Tech. rep., Japanese Industrial Standards Committee, 1997. 96

[JPLD06] JI W., POINTER M. R., LUO R. M., DAKIN J.: Gloss as an aspect of the measurement of appearance. *JOSA A 23*, 1 (2006), 22–33. 98, 99, 104, 105, 106, 107, 136, 140, 146

[Kan99] KANG H. R.: *Digital Color Halftoning*. SPIE Press, 1999. 46

[Keh13] KEHREN K.: *Optical Properties and Visual Appearance of Printed Special Effect Colors*. PhD thesis, Technische Universität Darmstadt, Darmstadt, Germany, 2013. 100

[Kip01] KIPPHAN H.: *Handbook of Print Media: Technologies and Production Methods*. Springer-Verlag New York Inc, 2001. 34

[KTH*99] KAWAGUCHI T., TSUMURA N., HANEISHI H., KOUZAKI M., MIYAKE Y.: Vector Error Diffusion Method for Spectral Color Reproduction. In *IS&T/PIC* (Savannah, Georgia, USA., 1999), pp. 394–397. 56

[LA08] LAU D. L., ARCE G. R.: *Modern Digital Halftoning*, 2 ed. CRC Press, 2008. 46

[LCR01] LUO M. R., CUI G., RIGG B.: The development of the cie 2000 colour-difference formula: Ciede2000. *Color Research & Application 26*, 5 (2001), 340–350. 60

[Lee05] LEE H.-C.: *Introduction to Color Imaging Science*. Cambridge University Press, New York, NY, USA., 2005. 35, 36

[LHPD12] LELOUP F. B., HANSELAER P., POINTER M. R., DUTRÉ P.: Integration of Multiple Cues for Visual Gloss Evaluation. In *Predicting Perceptions: The 3rd International Conference on Appearance* (Edinburgh, UK, 2012), pp. 52–55. 103

[LPDH11] LELOUP F. B., POINTER M. R., DUTRÉ P., HANSELAER P.: Luminance-based specular gloss characterization. *JOSA A 28*, 6 (2011), 1322–1330. 100

[LU12] LISSNER I., URBAN P.: Towards a unified color space for perception-based image processing. *Image Processing, IEEE Transactions on 21*, 3 (2012), 1153–1168. 39, 42, 73, 80, 87

[LU14] LEMOAN S., URBAN P.: A new connection space for low-dimensional spectral color management. In *SPIE/IS&T Electronic Imaging Conference* (San Francisco, California, USA, 2014). 49, 53

[Mah96] MAHY M.: Gamut calculation of color reproduction devices. In *IS&T/SID, 4th Color and Imaging Conference* (Scottsdale Ariz., 1996), vol. 6, pp. 145–150. 45

[Mah97] MAHY M.: Calculation of color gamuts based on the Neugebauer model. *Color Research & Application 22*, 6 (Dec 1997), 365–374. 45

[Mah98] MAHY M. F.: Insight into the solutions of the Neugebauer equations. In *SPIE* (San Jose, CA., 1998), vol. 3300, pp. 76–85. 45

[McC01] MCCANN J. J.: Color gamut mapping using spatial comparisons. In *SPIE, Color Imaging: Device-Independent Color, Color Hardcopy, and Graphic Arts VI* (San Jose, CA., 2001), vol. 4300, pp. 126–130. 45

[MKA12] MARLOW P. J., KIM J., ANDERSON B. L.: The perception and misperception of specular surface reflectance. *Current Biology (Curr Biol.) 22*, 20 (October 2012), 1909–1913. 100, 101, 102, 104

[ML00] MOROVIČ J., LUO M. R.: Calculating medium and image gamut boundaries for gamut mapping. *Color Research & Application 25*, 6 (Dec 2000), 394–401. 45

[ML01] MOROVIČ J., LUO M. R.: The fundamentals of gamut mapping: A survey. *Journal of Imaging Science and Technology 45*, 3 (2001), 283–290. 63

[Mor08] MOROVIČ J.: *Color Gamut Mapping*. John Wiley & Sons, 2008. 44, 56, 59, 63

[MvV03] MIKULA M., ČEPPAN M., VAŠKO K.: Gloss and goniocolorimetry of printed materials. *Color Research & Application 28*, 5 (2003), 335–342. 100

[MW03] MOROVIČ J., WANG Y.: A multi-resolution, full-colour spatial gamut mapping algorithm. In *IS&T/SID, 11th Color and Imaging Conference* (Scottsdale, Ariz., 2003), pp. 282–287. 45

[NT00] NADAL M. E., THOMPSON E. A.: New primary standard for specular gloss measurements. *Journal of Coatings Technology 72*, 911 (2000), 61–66. 97

[NTO04] NORMAN J. F., TODD J. T., ORBAN G. A.: Perception of three-dimensional shape from specular highlights, deformations of shading, and other types of visual information. *Psychol Sci. 15*, 8 (2004), 565–70. 100

[NZM*03] NG Y., ZEISE E., MASHTARE D., KESSLER J., WANG J.: Standardization of Perceptual based Gloss and Gloss Uniformity for Printing Systems (INCITS W1.1). In *PICS Conference* (Rochester, NY, USA, 2003), pp. 88–93. 98, 107, 110, 141, 146

[OKV04] OBEIN G., KNOBLAUCH K., VIÉNOT F.: Difference scaling of gloss: Nonlinearity, binocularity, and constancy. *Journal of Vision 4*, 9 (2004), 711–720. 104, 139, 140, 146

[OLKV03] OBEIN G., LEROUX T., KNOBLAUCH K., VIÉNOT F.: Visually relevant gloss parameters. In *11th International Metrology Congress* (Toulon, France., 2003), pp. 20–24. 104, 105, 139, 140, 146

[OR05] OHTA N., ROBERTSON A.: *Colorimetry: Fundamentals and Applications*. John Wiley & Sons, Ltd, 2005. 38, 39, 42

[Ost01] OSTROMOUKHOV V.: A simple and efficient error-diffusion algorithm. In *ACM SIGGRAPH* (Los Angeles, CA, USA., 2001), pp. 567–572. 92

[PHJ89] PARKKINEN J. P. S., HALLIKAINEN J., JAASKELAINEN T.: Characteristic spectra of munsell colors. *Journal of the Optical Society of America A (JOSA A) 6*, 2 (1989), 318–322. 53, 56

[PMJ14] PAPAS M., MESA K., JENSEN H. W.: A physically-based bsdf for modeling the appearance of paper. In *Eurographics Symposium on Rendering (EGSR)* (2014), vol. 33. 35

[QCSD14] QI L., CHANTLER M. J., SIEBERT J. P., DONG J.: Why do rough surfaces appear glossy? *J. Opt. Soc. Am. A 31*, 5 (2014), 935–943. 144, 145

[RBH10] ROSSIER R., BUGNON T., HERSCH R.: Introducing ink spreading within the cellular yule-nielsen modified neugebauer model. In *IS&T/SID, 18th Color and Imaging Conference* (San Antonio, Texas, USA., 2010), pp. 295–300. 52

[RD06] ROSEN M., DERHAK M.: Spectral Gamuts and Spectral Gamut Mapping. In *Spectral Imaging: 8th International Symposium on Multispectral Color Science* (San Jose, CA, 2006), SPIE. 49, 53, 59, 60

[SB02] SHARMA G., BALA R. (Eds.): *Digital Color Imaging Handbook*. CRC Press, Inc., Boca Raton, FL, USA, 2002. 39

[SBU14] SAMADZADEGAN S., BLAHOVÁ J., URBAN P.: Color-Printed Gloss: Relating Measurements to Perception. In *IS&T/SID, 22nd Color and Imaging Conference* (Boston, Massachusetts, USA., 2014), pp. 207–211. 109, 132, 133, 135, 137

[SBU*15] SAMADZADEGAN S., BAAR T., URBAN P., SEGOVIA M. M. V. O., BLAHOVÁ J.: Controlling colour-printed gloss by varnish-halftones. In *SPIE/IS&T Electronic Imaging Conference* (San Francisco, California, USA., 2015). 109, 117, 118, 123, 127, 129, 134, 139, 140, 141, 142

[Sne62] SNELLEN H.: *Probebuchstaben zur Bestimmung der Sehschärfe*. 1862. 126, 127

[SPGH14] SHRESTHA R., PILLAY R., GEORGE S., HARDEBERG J. Y.: Quality evaluation in spectral imaging - quality factors and metrics. *Journal of the International Colour Association 12* (2014), 22–35. 55

[SPM08] SILVENNOINEN R., PEIPONEN K. E., MYLLER K.: *Specular Gloss*. Elsevier Science, 2008. 98

[Ste61] STEVENS S. S.: To honor fechner and repeal his law. *Science 133*, 3446 (Jan 1961), 80–86. 39, 141, 146

[SU13] SAMADZADEGAN S., URBAN P.: Spatially Resolved Joint Spectral Gamut Mapping and Separation. In *IS&T/SID, 21st Color and Imaging Conference* (Albuquerque, New Mexico, USA., 2013), pp. 2–7. 71, 72, 73, 74, 75, 80, 82, 83, 88, 93, 94, 149, 150, 151

[SU15a] SAMADZADEGAN S., URBAN P.: Spatio-spectral gamut mapping and separation. *Journal of Imaging Science & Technology (JIST) 59*, 4 (July 2015), 40402–1–40402–12. 71, 72, 73, 79, 80, 81, 82, 83, 84, 85, 86, 87, 88, 89, 93, 149, 151, 152

[SU15b] SAMADZADEGAN S., URBAN P.: Spatio-Spectral Gamut Mapping and Separation. In *IS&T/SID, 23rd Color and Imaging Conference* (Darmstadt, Germany, 2015). 71

[SWD05] SHARMA G., WU W., DALAL E. N.: The ciede2000 color-difference formula: Implementation notes, supplementary test data, and mathematical observations. *Color Research & Application 30*, 1 (Feb 2005), 21–30. 42, 63

[TB98] TZENG D.-Y., BERNS R. S.: Spectral-based ink selection for multiple-ink printing I. colorant estimation of original objects. In *IS&T/SID* (Scottsdale Ariz. USA., 1998), pp. 106–111. 52

[TB99] TZENG D.-Y., BERNS R. S.: Spectral-based ink selection for multiple-ink printing II. optimal ink selection. In *IS&T/SID* (Scottsdale Ariz. USA., 1999), pp. 182–187. 52

[TB00] TZENG D.-Y., BERNS R. S.: Spectral-Based Six-Color Separation Minimizing Metamerism. In *IS&T/SID* (Scottsdale Ariz., 2000), pp. 342–347. 80

[TB01] TAPLIN L. A., BERNS R. S.: Spectral color reproduction based on six-color inkjet output system. In *IS&T/SID, 9th Color and Imaging Conference* (Scottsdale Ariz., 2001), pp. 209–213. 52

[Tor58] TORGERSON W. S.: *Theory and Methods of Scaling*. John Wiley & Sons, Inc., New York, USA., 1958. 103

[TRB07] TSUTSUMI S., ROSEN M. R., BERNS R. S.: Spectral Gamut Mapping using LabPQR. *Journal of Imaging Science and Technology (JIST) 51*, 6 (2007), 473–485. 49, 53, 59, 60, 61, 62

[UB11] URBAN P., BERNS R. S.: Paramer Mismatch-based Spectral Gamut Mapping. *IEEE Transactions on Image Processing 20*, 6 (2011), 1599–1610. 66, 67, 68, 69, 71, 72, 73, 74, 75, 77, 78, 80, 82, 83, 84, 85, 86, 88, 89, 93, 94, 149, 150

[Uli87] ULICHNEY R.: *Digital Halftoning*. The MIT Press, 1987. 46

[Urb05] URBAN P.: *Metamere und multispektrale Methoden zur Reproduktion farbiger Vorlagen*. PhD thesis, Technische Universität Hamburg-Harburg, Germany, 2005. 62

[Urb07] URBAN P.: Reproduktion von multispektralbildern mit autotypischer farbmischung. In *13th Workshop Farbbildverarbeitung* (Koblenz, Germany, 2007), pp. 31–42. 52

[URB08] URBAN P., ROSEN M. R., BERNS R. S.: Spectral Gamut Mapping Framework Based on Human Color Vision. In *CGIV* (Barcelona, Spain, 2008), pp. 548–553. 62, 64, 65, 69

[Urb09] URBAN P.: Spectral-based image reproduction workflow - from capture to print. In *Jahrbuch der Druckingenieure*. 2009, pp. 83–91. 52

[URR02] URBAN P., ROLF-RAINER G.: Gamut boundary determination by sampling an inverse printer model. In *IS&T's NIP18* (San Diego, Calif., 2002), vol. 18, pp. 778–781. 45

[USD13] URBAN P., STAHL S., DÖRSAM E.: Image display-printing (desktop, commercial). In *Academic Press Library in Signal Processing: Image, Video Processing and Analysis, Hardware, Audio, Acoustic and Speech Processing*, Theodoridis S., (Ed.), vol. 4. Elsevier, 2013, ch. 5. 33, 34, 43, 44, 45, 46, 47, 52

[Vig85] VIGGIANO J. A. S.: The Color of Halftone Tints. In *TAGA Proceedings* (1985), pp. 647–661. 52, 63, 76, 80

[Vig90] VIGGIANO J. A. S.: Modeling the Color of Multi-color Halftones. In *TAGA Proceedings* (1990), pp. 44–62. 52, 63, 76, 80

[Vig04] VIGGIANO J. A. S.: Metrics for evaluating spectral matches: A quantitative comparison. In *IS&T, The Second European Conference on Colour in Graphics, Imaging, and Vision (CGIV)* (Aachen, Germany, 2004), pp. 286–291. 52

[VLD07] VANGORP P., LAURIJSSEN J., DUTRÉ P.: The influence of shape on the perception of material reflectance. *ACM Transactions on Graphics 26*, 77 (July 2007). 100

[vT94] VAN TRIGT C.: Metameric blacks and estimating reflectance. *Journal of The Optical Society of America A (JOSA A) 11*, 3 (1994), 1003–1024. 58

[War92] WARD G. J.: Measuring and modeling anisotropic reflection. In *SIGGRAPH 92 Proceedings of the 19th annual conference on Computer graphics and interactive techniques* (New York, NY, USA., 1992), vol. 26, pp. 265–272. 103

[WB00] WYBLE D. R., BERNS R. S.: A critical review of spectral models applied to binary color printing. *Color Research & Application 25*, 1 (February 2000), 4–19. 52

[WFEM10] WENDT G., FAUL F., EKROLL V., MAUSFELD R.: Disparity, motion, and color information improve gloss constancy performance. *J Vis. 10*, 9 (2010). 100

[XB08] XIAO B., BRAINARD D. H.: Surface gloss and color perception of 3d objects. *Visual Neuroscience (Vis Neurosci.) 25*, 3 (2008), 371–85. 100

[YC51] YULE J. A. C., COLT R. S.: Colorimetric Investigations in Multicolor Printing. In *TAGA Proceedings* (1951), pp. 77–82. 52, 63, 76, 80

[YN51] YULE J. A. C., NIELSEN W. J.: The penetration of light into paper and its effect on halftone reproduction. In *Tech. Assn. Graphic Arts* (1951), vol. 4, pp. 65–76. 52, 63, 76, 80

[ZS07] ZOLLIKER P., SIMON K.: Retaining local image information in gamut mapping algorithms. *IEEE Transactions on Image Processing 16*, 3 (Apr 2007), 664–672. 45

[ZWL*12] ZHANG X., WANG Q., LI J., YANG P., YU J.: The interim connection space based on human color vision for spectral color reproduction. *Journal of the Optical Society of America A (Opt. Soc. Am. A) 29*, 6 (June 2012), 1027–1034. 49, 53